Charles University in Prague

Faculty of Science

Developmental and Cell Biology

Mgr. Lucie Kohoutová

Characteristics of novel protein interactions of gamma-tubulin and their roles with microtubules and in cell division

Ph.D. Thesis

Supervisor: Doc. RNDr. Pavla Binarová, CSc.

Academy of Sciences of the Czech Republic

Institute of Microbiology, v. v. i.

Laboratory of Functional Cytology

Prague, 2014

Prohlášení:

Prohlašuji, že jsem závěrečnou práci zpracovala samostatně a že jsem uvedla všechny použité informační zdroje a literaturu. Tato práce ani její podstatná část nebyla předložena k získání jiného nebo stejného akademického titulu.

V Praze dne 10. 12. 2014

Mgr. Lucie Kohoutová

Prohlášení:

Jménem ostatních spoluautorů publikací, které tvoří základ disertační práce Mgr. Lucie Kohoutové, potvrzuji, že podíl autorky na jejich přípravě je popsaný v komentářích k jednotlivým publikacím pravdivě.

V Praze dne 10. 12. 2014

Doc. RNDr. Pavla Binarová, CSc.

My acknowledgement follows in Czech:

V první řadě chci poděkovat své školitelce Doc. RNDr. Pavle Binarové, CSc. za možnost vypracování disertační práce v její laboratoři. V neposlední řadě patří můj dík i celému týmu této laboratoře a dalším spolupracovníkům, se kterými jsem se měla možnost setkat. Za soustavnou podporu děkuji své rodině a příteli Martinovi.

TABLE OF CONTENTS

ABBREVIATIONS

APC	adenomatous polyposis coli
ATM	ataxia-telangiectasia-mutated
ATP	adenosine triphosphate
ATR	ataxia-telangiectasia-mutated and Rad3-related
BRCA1	breast cancer 1, early onset
CaMV	cauliflower mosaic virus
CDK5RAP2	CDK5 regulatory subunit-associated protein 2
CLASP	cytoplasmic linker-protein-associated protein
CRA	CT11-RanBPM
Crm1	chromosome region maintenance 1
CTLH	carboxy-terminal to LisH
γ-TuC	γ-tubulin complex
γ-TuRC	γ-tubulin ring complex
γ-TuSC	γ-tubulin small complex
DAPI	4',6-diamidino-2-phenylindole
DP	dimerization partner of E2F
dsDNA	double strand deoxyribonucleic acid
EB1	end-binding protein 1
E2F	adenovirus E2 binding transcription factor
EdU	5-ethynyl-2´-deoxyuridine
FRET	Förster resonance energy transfer
GCP	γ-tubulin complex protein
GDP	guanosine-5'-diphosphate
GID	glucose-induced degradation deficient
GTP	guanosine-5'-triphosphate
HURP	hepatocarcinoma upregulated
LC	liquid chromatography
LisH	lissencephaly type-I-like homology
MALDI	matrix-assisted laser desorption/ionization
MAP	microtubule-associated protein
MAPK, MPK	mitogen-activated protein kinase
MS	mass spectrometry
MTOC	microtubule-organizing centre
NSF	N-ethylmaleimide-sensitive factor
PCR	polymerase chain reaction
PPB	pre-prophase band
Ran BP	Ran-binding protein
RanBPM	Ran-binding protein in the microtubule-organizing centre
RanGAP1	RanGTPase-activating protein 1
RB	retinoblastoma protein
RCC1	regulator of chromosome condensation 1
SADB/Brsk1	brain specific kinase 1
SDS-PAGE	sodium dodecylsulphate polyacrylamide gel electrophoresis
SPB	spindle pole body
SPRY	spore lysis A and ryanodine receptor
TPX2	targeting protein for *Xenopus* kinesin-like protein 2
TUNEL	terminal deoxynucleotidyl transferase-dUTP nick-end labelling
WT	wild type

ABSTRACT

Spatial and temporal regulation of microtubule nucleation and dynamics is required for formation of specific microtubular arrays that react to internal and external signals and change accordingly. Microtubules are nucleated from microtubule-organizing centres such as centrosomes in animal cells or spindle pole bodies in fungi. All higher plants lack centrosomes and thus present a model for study of acentrosomal cell division and microtubule nucleation and organization.

γ-Tubulin is a conserved protein from tubulin superfamily with a central role in microtubule nucleation. It also regulates microtubule dynamics and organization including mitotic spindle positioning. Moreover, γ-tubulin functions in cell cycle regulation, checkpoints control, regulation of transcription, and coordination of late mitotic events.

We aimed to characterize protein interactions of γ-tubulin and their functions in *Arabidopsis*.

We identified *Arabidopsis* homologue of putative centrososomal protein RanBPM. Our data showed that AtRanBPM is a member of CTLH complexes. Our finding of CTLH complexes in plants confirmed their conservation in eukaryotic cells.

We found that NITRILASE1 is a cell cycle regulator in *Arabidopsis* that is important for maintenance of genome stability and proper cell division.

We studied a role of AtTPX2, *Arabidopsis* homologue of TPX2 protein, in microtubule nucleation and organization. We showed that Ran-dependent importin pathway regulates AtTPX2 protein in acentrosomal plant cells. AtTPX2 enhanced an ability of nuclear envelope and chromatin to promote microtubule nucleation.

We characterized MAPK kinase MPK6 functions with microtubules. We found novel interactions of MPK6 with proteins of microtubule nucleation machinery and microtubule plus end complexes. These interactions might be behind function of MPK6 in the cell division revealed in our functional studies of MPK6 mutants in *Arabidopsis*.

We further focused on NSF protein with function in membrane trafficking and fusion and its interaction with γ-tubulin in *Arabidopsis*.

Our data contributed to knowledge of functions of γ-tubulin and its interactors with microtubules and to understanding of regulation of the cell division in acentrosomal plant cells.

SOUHRN

Přesná časová regulace lokalizace nukleace mikrotubulů spolu s regulací jejich dynamiky je nezbytná pro tvorbu mikrotubulárních uspořádání schopných pružně reagovat na vnitřní a vnější signály. Nukleace mikrotubulů probíhá z mikrotubuly organizujících center, u řady živočišných buněk z centrosomů a u kvasinek z pólových tělísek. Buňky vyšších rostlin ztratily centrozómy, a představují tak vhodný model pro výzkum acentrozomálního buněčného dělení a acentrozomální nukleace mikrotubulů a jejich organizace.

γ-Tubulin je konzervovaný protein z tubulinové nadrodiny, který hraje důležitou roli v nukleaci mikrotubulů a reguluje jejich dynamiku a organizaci včetně regulace pozice dělícího vřeténka. γ-Tubulin hraje významnou roli v regulaci buněčného cyklu, jeho kontrolních bodů, v regulaci transkripce a také koordinuje jednotlivé kroky buněčného cyklu v pozdní mitóze.

V této práci jsme chtěli charakterizovat proteinové interakce γ-tubulinu a jejich funkce v buňkách *Arabidopsis*.

Identifikovali jsme homolog domnělého centrozomálního proteinu RanBPM u *Arabidopsis* a dále jsme ukázali jeho přítomnost v CTLH komplexech. Náš nález CTLH komplexů v rostlinách ukazuje na konzervovanost těchto komplexů v eukarotických buňkách.

Zjistili jsme, že NITRILÁZA1 reguluje buněčný cyklus u *Arabidopsis* a je důležitá pro zachování genomové stability a pro správné buněčné dělení.

Studovali jsme roli homologu TPX2 u *Arabidopsis* v nukleaci mikrotubulů a jejich organizaci. Ukázali jsme, že v acentrosomálních buňkách rostlin je AtTPX2 regulován Ran-dependentní importinovou dráhou a že zvyšuje schopnost chromatinu a jaderné membrány nukleovat mikrotubuly.

Charakterizovali jsme funkci MAP kinázy MPK6 s mikrotubuly. Nalezli jsme nové interakce MPK6 s proteiny odpovědnými za nukleaci mikrotubulů a s plus-koncovými mikrotubulárními proteinovými komplexy. Tyto interakce mohou stát za dosud ne zcela vysvětlenou funkcí MPK6 v buněčném dělení naznačenou naší funkční studií MPK6 mutantů *Arabidopsis*.

Dále jsme zkoumali protein NSF zajišťující fúzi membrán a membránový transport a nalezli jeho interakci s γ-tubulinem u *Arabidopsis*.

Naše data přispěla k poznání funkcí γ-tubulinu a jeho interaktorů při organizaci mikrotubulů a dále k poznání regulace buněčného dělení v acentrozomálních buňkách rostlin.

1. INTRODUCTION

Reproduction is an attribute of all living organisms ensuring continuation of species. On a cellular level, regulation of a transition between cycling and quiescence is critical. Cells in multicellular organisms or in colonies need to cooperate and respond to changing environment. Microtubules, a part of cytoskeleton, play a significant role in extracellular and intracellular signalling.

Cytoskeleton, a complex filamentous structure, usually comprises of actin microfilaments, intermediate filaments, and microtubules in eukaryotic cells. Subunits of both actin microfilaments and microtubules are highly conserved in yeast, plants, and animals [1], while components of intermediate filaments have not been found in plants with the exception of nuclear or perinuclear ones [2; 3]. In my thesis, I focus on plant microtubules and on γ-tubulin and its roles in acentrosomal plant cells.

1.1 Microtubules

1.1.1 Microtubules functions

Microtubules ensure many important functions in the eukaryotic cell. As mentioned above, they participate in signal transduction forming a platform for many interactions in the cell [4]. Moreover, microtubules are involved in trafficking of complexes and vesicles and contribute to cell organization through organelle positioning [5]. Besides intracellular movements, in animals, microtubules ensure movements also on whole cell level. Microtubules further contribute to cell polarity and are responsible for shape of the cell [6]. Moreover, microtubules are indispensable for mitotic spindle formation and segregation of chromosomes. In plants, microtubules form not only mitotic spindle but also plant specific structures such as pre-prophase band (PPB) and phragmoplast that ensure the proper cell division [7].

1.1.2 Microtubule composition

Microtubules are hollow cylinders with a diameter of ~ 25 nm; they consist of protofilaments formed by dimers comprising of α-tubulin and β-tubulin (Fig. 1). The tubulin dimers in protofilaments are oriented head to tail, so microtubules are intrinsically polar having their so called plus and minus end. α-Tubulins are exposed at the minus end, while β-tubulins are exposed at the plus end of the microtubule [8].

In vivo, the microtubule normally contains 13 paraxial protofilaments, while *in vitro* number of protofilaments is much wider ranging usually from 10 to 16 protofilaments resulting, except of number 13, in protofilament skewing [8]. It is clear that the number of protofilaments in the microtubule is well regulated *in vivo*, for example through microtubule-organizing centra (MTOCs) [9]. Highly prefered form of microtubule *in vivo* is called a B-lattice consisting of 13 protofilaments [10], where the neighbouring protofilaments are shifted around 0.9 nm lengwise resulting in a 12 nm shift between the first protofilament and the thirteenth one per one turn [11]. As 12 nm corresponds to two and half of the length of the tubulin dimer, there is therefore a "seam" between the two protofilaments, where lateral contacts are heterologous mediated by α-tubulins and β-tubulins, while in the rest of the microtubule protofilaments the contacts are homologous [12] (Fig. 1B, C). The seam makes microtubule further nonsymetric along its longer axis [10].

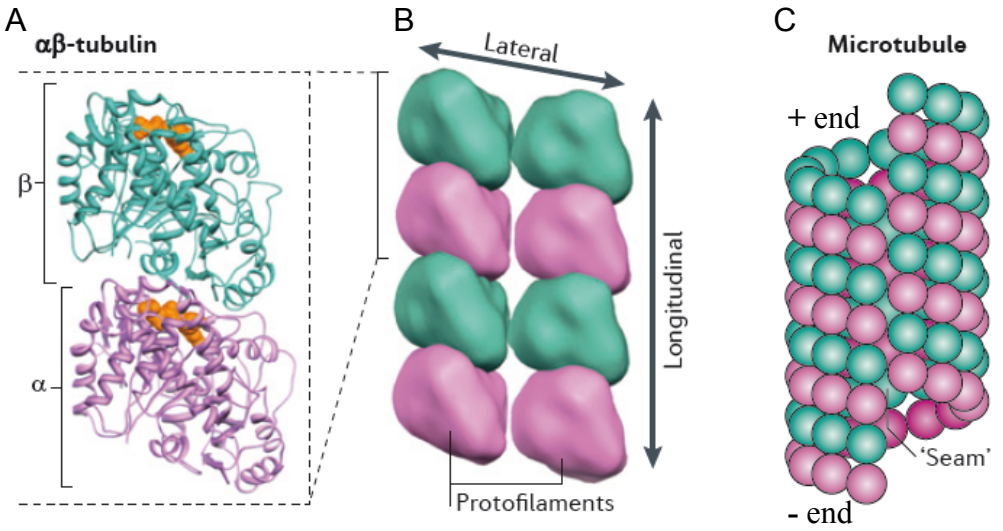

Fig. 1: Microtubule structure

(A) tubulin dimer with bound GTPs (orange); α-tubulin (violet), β-tubulin (green), (B) part of the microtubule with depicted lateral and longitudinal contacts, (C) microtubule with depicted seam and plus and minus end. Adapted from [13].

1.1.3 Microtubule dynamics

Microtubules are highly dynamic structures; they switch between catastrophic depolymerization leading to their shortening and rescue polymerization leading to their growth. Changes between the shortening and the growth are called dynamic instability and are

more frequent at the plus end than at the minus end resulting in more stable minus end [14]. Between catastrophe and rescue there is a relatively short period called pause.

Dynamics at the opposite ends of microtubule often differs as the tubulin dimers are associated to and dissociated from them usually at different rates; at the plus end, the rate of not only adding but also of removing the dimers is higher than at the minus end [15]. If the rate of adding of the dimers is equal to the rate of their removal, microtubule is actually moving by treadmilling with an unchanged length. In plant cells, cortical microtubules often undergo hybrid treadmilling – a movement in a plus end direction caused by a dynamic instability with preferred rescues at the plus end and intermittent slow lost of tubulin dimers from the minus end [16].

The tubulin dimer carries two GTP molecules (Fig. 1A); GTP bound in α-tubulin is nonhydrolyzable; only GTP bound in β-tubulin can be hydrolyzed to GDP after it is built in in the microtubule lattice. Energy from hydrolysis of GTP is not needed for polymerization itself; it is used for destabilization of the lattice [17]. Stabilizing GTP cap is being formed at the plus end if the hydrolysis of GTP bound to β-tubulin in the microtubule is slower than adding of the new tubulin dimer carrying GTP [8]. A minimal density of GTP in the cap seems to be needed for microtubule to continue growing [18].

1.1.4 Regulation of microtubule dynamics and organization

There is a dramatic reorganization of microtubules in the eukaryotic cell during transition from interphase to mitosis; microtubule dynamics increases in mitosis in comparison with interphase [19].

Dynamics and organization of microtubules can be influenced by different isotypes of tubulins used for microtubule formation, by posttranslation modifications of the tubulins or by other proteins or their complexes, which bind the microtubules or their precursors. Moreover, it can be changed by different drugs.

1.1.4.1 Tubulin isotypes

Different tubulin isotypes can be expressed either tissue-specifically or ubiquitously and contribute to different properties of microtubules [20]. Higher plants contain different tubulin isotypes as shown for tobacco [21] or rice [22]. The less conserved part of tubulin molecule is the C-terminus; it is prone to posttranslation modifications, which can set further differences between tubulin isotypes [20].

1.1.4.2 Posttranslation modifications

Posttranslation modifications of tubulins in animals were reviewed recently and this part of the tubulin code was suggested to serve for microtubule associated proteins and motor proteins changing their velocity and processivity or strength of binding [23]. Posttranslational modifications of tubulins occur also in plants. In tobacco cells, acetylation, polyglutamylation, tyrosination, and detyrosination resulting in detyrosinated tubulin or Δ2-tubulin occured for α-tubulin and polyglutamylation also for β-tubulin; stabilizing modifications as acetylation and detyrosination leading to Δ2-tubulin were observed in the pole regions of spindle poles [21]. Posttranslational modifications of tubulins are tissue-specific in maize [24]. Recently, tyrosine nitration was shown to impair microtubule organization in Arabidopsis [25; 26]. According to modelling tyrosine nitration is able to change interaction of α-tubulin with kinesin [25], while it does not change microtubule plus end dynamics itself [26].

1.1.4.3 Microtubule binding proteins

There are many microtubule binding proteins which influence microtubule dynamics and organization including groups of severing proteins, sequestring proteins, capping proteins, and bundling proteins. They are differently bound along the microtubular lattice, or to shorter microtubule intermediates, or to tubulin dimers. In plants, the microtubule-associated proteins were recently reviewed by Hamada [27]. Here, I put focus only on several of them which are related to my work.

EB1 protein interacts autonomously with the microtubule and serves as a mediator, which is able to bind other proteins to the microtubules [18]. In animals, CDK5RAP2 binds through EB1 to the plus end of microtubules and regulates microtubule dynamics by enhancing growth and reducing pauses [28]. Recently, kinetic of EB1 binding to microtubules and direct regulation of microtubule dynamics by EB1 was shown by Maurer et al. [18]. EB1 binds to growing end of microtubule with no respect whether it is plus or minus end and forms comets like pattern. EB1 increases not only growth velocity but also frequency of catastrophes through enhancing maturation of the microtubule. The authors suggested that EB1 might promote formation of GDP lattice of the microtubule through enhancing GTP hydrolysis and/or conformation changes in the lattice. There is a connection between pause time and kinetics of microtubule maturation, which includes at least two kinetic steps catalyzed by EB1 [18].

Plants possess homologues of EB1 protein. There are three EB1 proteins EB1a, b, and c in *Arabidopsis* [29]. EB1c differs most from EB1a and b subgroup [29]. Cell cycle

dependent localization of EB1a-GFP was mapped in *Arabidopsis* [30]. Plant EB1a and EB1b form heterodimers with each other *in vitro*, while EB1c forms homodimers [31]. EB1a-GFP and EB1b-GFP localize on growing plus ends of cortical microtubules and of mitotic arrays. Strikingly, EB1c-GFP protein is localized strongly in nuclei in interphase besides its temporary localization with plus ends of cortical and endoplasmic microtubules. In mitosis, EB1c-GFP is within a whole spindle and later it is present mainly in a midzone of phragmoplast. Mutant *eb1c* showed defects in spindle and phragmoplast alignment in *Arabidopsis*. Moreover, lagging chromosomes were observed in anaphase in tobacco with suppressed expression of EB1c [31].

In *Drosophila* cells, γ-tubulin complexes γ-TuRCs are important for proper localization of EB1 to plus ends of astral microtubules and for stabilization of astral microtubules [32]. Both γ-tubulin and EB1 influenced kinetics of microtubule growth after cold treatment in *Drosophila* [33]. γ-TuRCs regulate dynamics of interphase microtubules stabilizing them through binding to the microtubule lattice; behind this point microtubules do not depolymerize [34]. In fission yeast, stabilization of microtubule bundles was shown through γ-tubulin complexes γ-TuCs bound on minus ends of the microtubules and was independent of nucleation potential of γ-TuCs [35].

Plant kinetochores can stabilize plus ends of kinetochore microtubules [36]. Plant cortical microtubules can be stabilized by bundling and also by their attachment to the cortex [16]. Phospholipase D interacted with microtubules as well as with plasma membrane, so it was suggested as a linker [37]. Later, CLASP was identified as one of molecules responsible for cortex attachment of cortical microtubules [38]; CLASP promotes rescues or pauses in microtubules near to cell edges and therefore helps to form transfacial microtubule bundles and coordinates microtubule organization in plants [39].

Family of MAP65 proteins functions in bundling of plants microtubules. There are nine MAP65 genes in *Arabidopsis* [40]. Recently, it was shown that MAP65-1 reduces stiffness of microtubules as well as of cross-linked microtubules allowing their bending and thus MAP65-1 allows further bundling if two bundles meet [41]. MAP65-1, which prefers antiparallel bundling, allowed bundling under steeper angles than MAP65-4 [41], which is nonselective for polarity of bundles making parallel and antiparallel bundles [42]. MAP65-1 together with CLASP can contribute to overcoming of steep angles of transfacial bundles and it is also important for microtubule organization in spindle midzone [41].

MAP65-4 promotes growth of bundles of microtubules through regulating their dynamic instability without affecting the speed of growth or shortening [42]. In tobacco cells,

MAP65-4 localizes on perinuclear microtubules in prophase and on forming poles of spindle and remained with kinetochore microtubules to anaphase; its role in assembly of bipolar spindle was suggested [42].

MAP65-3 is essential for cytokinesis as it ensures proper phragmoplast formation [43]. MAP65-3 cross-links antiparallel bundles interdigitating in phragmoplast and it is also important for localization of kinesin 12A to the plus ends of the bundles [44].

TPX2 (targeting protein for *Xenopus* kinesin-like protein 2) can load several other proteins to microtubules [45; 46]. TPX2 plays roles in microtubule nucleation and acentrosomal spindle assembly [47], spindle pole organization and centrosomal spindle formation as TPX2 closely cooperates with Ser/Thr kinase Aurora A [45; 46]. In mitotic centrosomal cells, TPX2 influenced Aurora A localization on spindle microtubules; it bound Aurora A independently of activation of Aurora A and it was phosphorylated by Aurora A *in vitro* [46]. Recently, *in vitro* Aurora A was found to be activated either by phosphorylation by other Aurora A molecule or by allosteric change after binding of TPX2 [48]. Furthermore, TPX2 influences activity of Aurora B through its involvement in chromosomal passenger complex [49]. In plant acentrosomal cells, AtTPX2 and Aurora 1 bind to microtubules together in cell cycle dependent manner as described by our laboratory [50]. TPX2 is a putative substrate of ATM kinase [51]. TPX2 forms foci with phosphorylated ATM kinase and with mediator of DNA damage checkpoint 1 in G1 phase after DNA damage, while later even after DNA damage it remains with mitotic spindle; upon DNA damage, TPX2 is expressed reversely with γ-H2AX [52]. Multiple roles for TPX2 in microtubule organization were shown by Schatz and his co-workers who found that besides its ability to nucleate microtubules dependently on importin, TPX2 also bundles microtubules independently of importin [53]. Later nucleation by TPX2 was suggested to be performed in concert with other molecules in acentrosomal system [54].

1.1.4.4 Microtubule binding drugs

In my studies I used taxol and amiprophos methyl to influence dynamics of microtubules. Paclitaxel, an alkaloid from *Taxus baccata*, is used as an anticancer drug. It stabilizes microtubules as it binds to β-tubulin and together with extended loop in α-tubulin it stabilizes lateral contacts between their protofilaments [55; 56].

Amiprophos methyl is a herbicide depolymerizing plant microtubules without an effect on animal microtubules. Amiprophos methyl increases dynamics at microtubule ends. It has a common binding site with oryzalin, another effective depolymerizing agent for plant

microtubules [57], which was later shown to be binding to α-tubulin and suggested to destabilize protofilament interaction [55].

1.2 Microtubule-organizing centres

To fulfill specific needs of the cell, microtubule nucleation, dynamics, and organization has to be properly spatially and temporally regulated.

Microtubule nucleation is a formation of microtubules *de novo*. Microtubules can self-assemble if the concentration of tubulin dimers is higher than the critical concentration [58]. The critical concentration *in vivo* is reduced by microtubule-organizing centres (MTOCs), from which microtubules are nucleated. MTOCs also stabilize an intermediate of forming microtubule [58].

There are two types of MTOCs: discrete and dispersed. Discrete MTOCs are more locally restricted and include centrosomes found in many animal cells, spindle pole bodies (SPBs) in yeasts, and basal bodies [59]. Dispersed MTOCs are localized in the cytoplasm, scattered on membranes, pre-existing microtubules, or with kinetochores. Dispersed MTOCs are present in higher plant cells that do not possess centrosome [60], in oocytes [61], in some differentiated animal cells as muscle, neuronal and epithelial cells, which are equipped with centrosomes, and in fission yeast, which has interphase MTOCs besides its SPB [62]. Microtubule nucleation contributes massively to microtubule organization and is spacially and temporally regulated through localization and activation of MTOCs. γ-Tubulin is ubiqitous and important component of MTOCs.

1.3 γ-Tubulin

1.3.1 γ-Tubulin introduction

γ-Tubulin is a member of tubulin superfamily; it was discovered as a suppressor of β-tubulin mutation in fungus *Aspergillus nidulans* [63] and it has been found in all eukaryotes so far examined. γ-Tubulin is structurally similar to α-tubulin and β-tubulin [64]. γ-Tubulin is conserved among species, the most divergent γ-tubulins are found in *S. cerevisiae* and *C. elegans* [65]. In yeasts, *Aspergillus, Caenorhabditis,* and *Xenopus*, only one gene for γ-tubulin exists, while in *Drosophila*, human, and *Arabidopsis* two genes coding γ-tubulin evolved [59]. Two γ-tubulins perform divergent roles during mouse development due to their different expression but both are able to nucleate microtubules [66]. Two genes encoding γ-tubulin 1 and γ-tubulin 2 in *Arabidopsis* share 95% identity in coding region [67] and were

shown to have highly redundant functions [68]; encoded proteins γ-tubulin 1 and 2 share 98% identity.

1.3.2 Molecular mechanisms of microtubule nucleation

γ-Tubulin is a main nucleator of microtubules in eukaryotes including higher plants [68; 69; 70]. However, even after depletion of both γ-tubulins in *Drosophila*, microtubules are still present in interphase cells, so other mechanisms of microtubule nucleation besides that guided by γ-tubulin are suggested [33]. γ-Tubulin is not essential for nucleation and stabilization of cytoplasmic microtubules in *C. elegans* as after ~ 98% depletion of γ-tubulin these microtubules are still preserved [71]. Microtubules nucleate without γ-tubulin from histon H1 localized on nuclear membranes in tobacco cells and *in vitro* [72; 73]. On the other hand, γ-tubulin is essential for centrosomal aster formation before nuclear envelope breakdown in *C. elegans* [71].

In *Arabidopsis*, loss of γ-tubulin caused by RNAi leads to complete diminishing of microtubules, while milder γ-tubulin downregulation causes impaired recovery of microtubules after their depolymerization [70]; microtubule nucleation is severely impaired also in γ-tubulin T-DNA mutant and mutation in both γ-tubulin genes is lethal [68].

Only very few microtubules nucleated after ~ 95% depletion of γ-tubulin in *Xenopus* egg extract; occasionally formed microtubules were very long; so γ-tubulin was suggested to be responsible for microtubule nucleation [74].

In animal cells equipped with centrosomes, γ-tubulin largely concentrates with centrosomes when microtubule nucleation is needed [75]. Besides its centrosomal localization, γ-tubulin is present in cytoplasm [76], in nuclei [77; 78], and nucleoli [77; 79]. In mitotic cell, γ-tubulin is present in spindle with accumulation on its poles [80; 81]. Complexes of γ-tubulin are also on astral microtubules [32].

Localization of γ-tubulin in acentrosomal plant cells is regulated in a cell cycle specific manner [60; 82; 83]. γ-Tubulin localizes with microtubular arrays; it is present on the cortex in G1 phase with cortical microtubules and in prophase around nuclei [82]. In acentrosomal spindle, γ-tubulin localizes predominantly with kinetochore fibres and is enriched on acentrosomal spindle poles. Furthermore, γ-tubulin is associated with two plant specific microtubular arrays, PPB and phragmoplast in cytokinesis [82]. Our group showed that plant γ-tubulin is present in cytoplasm, with microtubules, with membranes, on kinetochores of chromosomes, and in the nuclei [60; 83].

γ-Tubulin forms complexes with γ-tubulin complex proteins (GCPs). Two molecules of γ-tubulin together with one molecule of each γ-tubulin complex proteins GCP2 and GCP3 form stable γ-tubulin small complex (γ-TuSC) found in all eukaryotes [84]. Structure of γ-TuSC resembling shape of Y was revealed by electron microscopy in combination with FRET technique; γ-tubulin interacts with C-termini of GCPs located down in Y [85]. Later γ-TuSCs were shown to form rings *in vitro* and in presence of fragment of Spc110 protein, an anchoring protein to SPB from budding yeast, also helical filaments, where γ-TuSCs interacted laterally [86]. The rings and filaments formed by γ-TuSCs were able to nucleate microtubules *in vitro*, while γ-TuSC alone not [86]. In *Xenopus*, *Drosophila*, and *Homo sapiens*, γ-TuSCs with additional GCPs proteins form large γ-tubulin ring complexes (γ-TuRCs) which are mainly responsible for nucleation [87; 88; 89]. In *Drosophila*, where other GCPs besides GCP2 and GCP3 are dispensable for viability of whole organism [90], γ-TuSCs are able to nucleate microtubules but γ-TuRCs are 150 times more efficient in the process [88]. γ-Tubulin alone is only a poor nucleator of microtubules *in vitro* [85].

In *Drosophila*, depletion of GCP4 followed by dissociation of γ-TuRC impairs association of γ-TuSCs along spindle microtubules and at midbody while centrosomal localization of γ-TuSCs is preserved [90]. This fact points to specific regulation of the complexes. Interestingly, direct interaction of γ-tubulin with C-terminus of GCP4 was shown *in vitro* and possibility of binding of GCP4–6 instead GCP2 or GCP3 in γ-TuSCs and their possible role in initiation or termination of microtubule nucleation was suggested [91]. While GCPs forming γ-TuSC are usually indespenable for viability through their nucleation functions, other GCPs in γ-TuCs have probably stabilizing role or a role in capture or activation of the complexes [13; 84]. So far, GCP2 to 9 are known [84]. Here, I focus on GCPs in plants.

GCP3 was observed on the cortex of *Arabidopsis* and tobacco [92]. Later GCP2 was shown to position γ-tubulin containing complexes to pre-existing microtubules contributing to microtubule organization in *Arabidopsis* [93]. Authors suggested that interrupted interaction of GCP2 and GCP3 caused wider distribution of nucleation angles and therefore impaired organization of microtubules [93]. Nucleation from GCP2 and GCP3 complexes is highly prefered from the pre-existing cortical microtubules to plasma membrane where the complexes are also sometimes captured [94]. Complexes of GCP2 and GCP3 are recruited from cytoplasm to pre-existing microtubules where they are transiently stabilized. Spatial stabilization can be prolonged by nucleation of a new microtubule from the complexes. If the

new microtubule is cleaved by katanin, GCP2 and GCP3 complexes are probably released for next usage as they were not observed on shortening minus end of the microtubule [94].

Another GCP, GIP1/MOZART1 interacts with GCP3 in yeast two hybrid assay [95] and *in vitro* and colocalizes with GCP3, GCP4, and γ-tubulin in *Arabidopsis* spindle [96]. As only GCP2–GCP6 and γ-tubulin were purified with GIP1, GIP1 was suggested as a component of a subpopulation of γ-TuCs [95]. Observation in *Arabidopsis* plants showed that GIP1-labeled complexes in contrast to only GCP2-labeled complexes are found practically only on pre-existing microtubules where they nucleate microtubules; nucleation occurs more frequently from GIP1-labeled complexes in comparison with only GCP2-labeled complexes [95]. Besides its localization in nucleoplasm and cytoplasm, GIP1 localizes at nuclear envelope close to nuclear pore complexes, on minus ends of perinuclear microtubules, sometimes close to heterochromatin [97]. GIP1 single mutant did not show developmental defects, while double mutant was embryonically lethal [95; 96]. Seedlings of *gip1gip2* knock down showed impaired orientation of spindles, anaphase delay with lagging chromosomes, and enlarged nuclei of irregular shape [96]. Closer inspection of nuclear phenotype of *gip1gip2* knock down mutants revealed invaginated nuclei, with nuclear pore complexes and inner membrane marker AtSUN1 protein clustered at nuclear envelope and with disturbed chromocentra [97]. GIP1 besides its role as a component of γ-TuCs with suggested role in recruiting γ-TuCs to nuclear envelope has a role in nuclear morphology [97].

GCP4 is essential for microtubules organization in interphase as well as in mitosis [98]. After GCP4 downregulation, interphase microtubules are highly bundled with parallelly oriented bundles as branching angle of newly formed microtubules is decreased. Moreover, depletion of GCP4 results in loss of portion of γ-tubulin from spindle and phragmoplast. Kinetochore microtubules are not focused to poles and phragmoplast microtubules are bundled and of different length; cytokinesis is impaired after depletion of GCP4 as showed by presence of cell wall stubs, incomplete cell plates or completely undivided cells [98].

NEDD1 seems to be essential in *Arabidopsis* as it influences organization of microtubules during mitosis, controls position of spindle and its length and also organization of phragmoplast microtubules [99]. Moreover, without NEDD1, microtubules are not nucleated on nuclear envelope of reformed nuclei in cytokinesis. Cell plates are incomplete, branched, or scattered in *nedd1* mutant, while karyokinesis is normal [99]. There are not functional studies on plant GCP5 and GCP6, but they are components of γ-TuCs in *Arabidopsis* [95].

γ-Tubulin forms complexes which differ in size distribution and in their strength of binding properties between animals and plants [60; 88]. High molecular forms of γ-tubulin in plants are still under investigation. γ-Tubulin seems to be mostly part of larger complexes associated with membranes in plants [60; 100]. Plant γ-tubulin was also found in smaller complexes around 750 kDa [100] and it forms soluble small complexes with GCP2 and GCP3 [101].

In addition to GCPs, other factors can tune γ-tubulin nucleation activity.

Augmin complex promoted microtubule nucleation in mitotic spindles in *Drosophila* cells and was suggested to bound γ-TuRC to pre-existing microtubules in the spindle while it did not influence centrosomal localization of γ-tubulin [102]. Augmin complex is also relatively conserved in plants [103; 104].

CDK5RAP2 protein localizes in centrosomes and also in Golgi throughout the interphase to mitosis dependenly on centrosome [105]. CDK5RAP2 through its conserved domain γ-TUNA stimulates microtubule nucleation activity of already assembled γ-TuRCs on centrosomes and in the cytoplasm [106; 107]. CDK5RAP2 has homologues in *Drosophila* centrosomin and *S. pombe* proteins Mto1p and Pcp1p. Similarly to its human counterpart, Mto1p is necessary for cytoplasmic microtubule nucleation in fission yeast [35].

Kinesin-14 Pkl1 from fission yeast regulates γ-TuRC through its direct binding to it [108]. It extracts γ-tubulin from γ-TuRC *in vitro* probably through competitive binding with GCP2 and GCP3 and either retains γ-TuRC nonactive or cause its complete destruction [108]. Kinesin-14 Pkl1 prevents microtubule nucleation *in vivo* resulting in impaired bipolar spindle formation and chromosome separation [109]. It has an antagonist in kinesin-5 which also binds γ-TuRC [109].

1.3.3 Models of microtubule nucleation

There are two models of microtubule nucleation based on γ-tubulin complexes, which differ in type of γ-tubulin contacts with tubulin dimers. Protofilament model prefers a long line of longitudinally connected γ-tubulin molecules, which interacts predominantelly laterally with α- and β-tubulin, while template model prefers γ-tubulin ring similar to animal ones, where γ-tubulin has predominantly longitudinal contacts with α- and β-tubulin [110]. There are experimental evidences for both models [110]. Revision of template model showed that there is seven γ-TuSCs plus three additional γ-tubulin molecules and two molecules of GCP3 homologue responsible for attachment of microtubules to SPBs and for microtubule nucleation in budding yeast [111]. In higher plants, γ-tubulin ring complexes have not been observed so

far. Both strategies using either protofilament or template model might be functional and used dependently on the conditions and/or organism.

1.4 Acentrosomal nucleation

In plant cells that lack centrosomes, microtubules are nucleated from dispersed sites that are positive for γ-tubulin [112]. Acentrosomal nucleation is employed even in cells normally equipped with centrosomes as after centrosomes ablation the cells were still able to nucleate microtubules [113]. Here, I focus on several types of acentrosomal nucleation from dispersed MTOCs.

1.4.1 Nucleation from pre-existing microtubules

Microtubule nucleation from pre-existing microtubules was observed in plants [16], in fission yeast [114], and recently in *Xenopus* egg extract [74] and in human cells [115]. It differs in angles of branching.

In *S. pombe*, microtubules are antiparallel and branching is dependent on Mto2p, which localizes γ-TuCs along existing microtubules and during interphase is needed for microtubule nucleation from other sites than SPB [114].

In *Xenopus* egg extract, TPX2 protein and augmin complex are responsible for branching of microtubules from pre-existing ones usually up to 30° [74]. γ-Tubulin interacts physically with augmin and TPX2; under depletion of TPX2 or augmin, only individual microtubules were formed instead of fan-shaped microtubule structures [74]. γ-Tubulin was suggested to be a main nucleator; augmin either recruits and activates γ-TuRCs allowing microtubule nucleation or stabilizes already formed microtubules in spindle [116].

In human cells after augmin depletion, number of microtubules in spindle decreased, while number of microtubules around centrosome did not change [115]. Using electron tomography and 3D modelling on fixed cells, connections between some of mother and daughter microtubules were found where the branching occured under angles less than 30°. Besides being responsible for spindle mass increase [102], augmin was suggested also in controling polarity of newly formed microtubules [115]. The precise mechanism of binding of augmin to γ-TuRC is still unknown.

In *Arabidopsis* and tobacco cells, microtubule branching was originally observed under the angle around 42° with γ-tubulin responsible for the nucleation being recruited to pre-existing microtubules from cytoplasmic pool [112]. Later, the angles were measured more precisely using other marker proteins to follow single microtubules; branching was observed

around angle 60° with a presence of fraction of parallel microtubules [117]. Normal branching angles can be distorted if γ-TuC function is impaired [93; 98]. In *ton2* mutant less branched and more parallel microtubules are present, but TON2 protein influences the microtubule arrays without changing the branching angle [118].

1.4.2 Nucleation from membranes

Microtubule nucleation from membranes includes nucleation from nuclear envelope and Golgi apparatus.

γ-Tubulin and GCP3 localizes together at the nuclear envelope of tobacco and Arabidopsis cells [92] and γ-TuSCs are recruited to nuclear envelope of tobacco nuclei [101]. Nucleation of new microtubules did not occur from nuclear envelope in *Arabidopsis* in absence of GCP2 [6].

In higher plants, nuclear envelope increases its microtubule nucleation activity in late G2-phase and is highly used when pre-spindle forms. Plant nucleus directs polarity of newly generated microtubules and regulates orientation of cortical microtubules including microtubules of PPB by forming bidirectional arrays [6].

In animal cells, nucleation from Golgi represents important tool for regulation of cell polarity. Proteins CDK5RAP2, AKAP450, myomegalin, CAP350, and pericentrin, which are found in the centrosome, are also used for microtubule nucleation from Golgi apparatus in animal cells [119]. Proper localization of the process is probably ensured by GM130, a protein present on cis-Golgi [119]. Nucleation from Golgi was at first observed in hepatic cells and γ-tubulin was responsible for the nucleation [120]. In muscle cells microtubules are nucleated from static Golgi elements where γ-tubulin and pericentrin are localized [121]. Also neuronal cells use nucleation from Golgi apparatus that is still dependent on γ-TuRCs [119]. CLASP protein was suggested to be responsible for the stabilization of microtubule organized from Golgi in animal cells [122].

1.4.3 Kinetochore-based nucleation

γ-Tubulin was shown to localize with plant kinetochores in cell cycle specific manner [83; 123]. Microtubule nucleation from kinetochores was observed early in spindle formation and during recovery from depolymerization drug treatment in plants [36; 123; 124]. Kinetochores are suggested as important microtubule nucleation sites during acentrosomal plant spindle formation.

Microtubule nucleation from kinetochores occurs also in *Drosophila* [125]. In mammalian cells, RanGTP accumulates with kinetochores and promote microtubule nucleation; it forms complex with chromosome region maintenance 1 (Crm1) and RanGAP1 which regulates the nucleation; newly nucleated microtubules are then stabilized by hepatocarcinoma upregulated protein (HURP) [126]. Later, γ-TuRCs were shown to be recruited into kinetochores by Nup107-160 complexes; with RanGTP playing a role in activation of the whole complex [127]. RanGTP further releases various mitotic-specific proteins from importin at kinetochores; balanced Crm1 and importin β levels are needed for SUMO-conjugated RanGAP1/RanBP2 recruitment into kinetochores [128]. Besides its role in nuclear transport importin β has a role at kinetochores in mitotic somatic cells [128].

1.4.4 Chromatin-mediated nucleation

Microtubule nucleation in the vicinity of chromatin occurs in a RanGTP-dependent way. Ran nucleotide exchange factor regulator of chromosome condensation 1 (RCC1), which exchanges GDP for GTP in Ran, is bound on chromatin, so in interphase it is present in the nuclei and in mitosis with condensed chromatin [36]. RanGTPase activator protein (RanGAP) and Ran binding proteins (RanBP) are localized in cytoplasm. Those proteins all together ensure gradient of RanGTP decresing with distance from chromatin [36]. In plants, homologue of RCC1 protein was not found but Ran was shown to be able to directly bind histone H3 and H4 [36; 129].

RanGTP causes release of TPX2 from importin α and free TPX2 induces spindle assembly in acentrosomal *Xenopus* egg extract via chromatin mediated-nucleation [47]. In *Drosophila* syncytial embryos, main factor responsible for chromatin-mediated nucleation is HURP; it also functions in a Ran-dependent way [130].

1.5 Microtubular arrays in acentrosomal plant cells

Similarly to other eukaryotes, microtubule organization in plants is influenced by microtubule nucleation in combination with regulation of microtubule dynamics. Microtubules scan the space; dependently on an angle under which they meet, microtubules can form parallel bundles, cross each other, shrink totally or be rescued and form new microtubules [131; 132].

Microtubular arrays change dynamically during the cell cycle in plant cells (Fig. 2) [133]. In interphase, relatively stable cortical microtubules are present on cortex [16]. During late G2 phase, the nucleation from nuclei contributes to formation of PPB which marks a site

of the cell plate formation [7]. Later in prophase, microtubules are nucleated on nuclear envelope and after nuclear envelope breakdown microtubules are reorganized to bipolar mitotic spindle where kinetochore microtubules are attached to chromosomes [36]. During anaphase, chromosomes are separated as kinetochore microtubules shorten and poles are increasing their distance [134]. In telophase, microtubules contribute to building of the structure called phragmoplast, which is formed centrifugally from the center to edges; as vesicles are loaded along its microtubules, cell plate is formed followed later by cell wall formation [7].

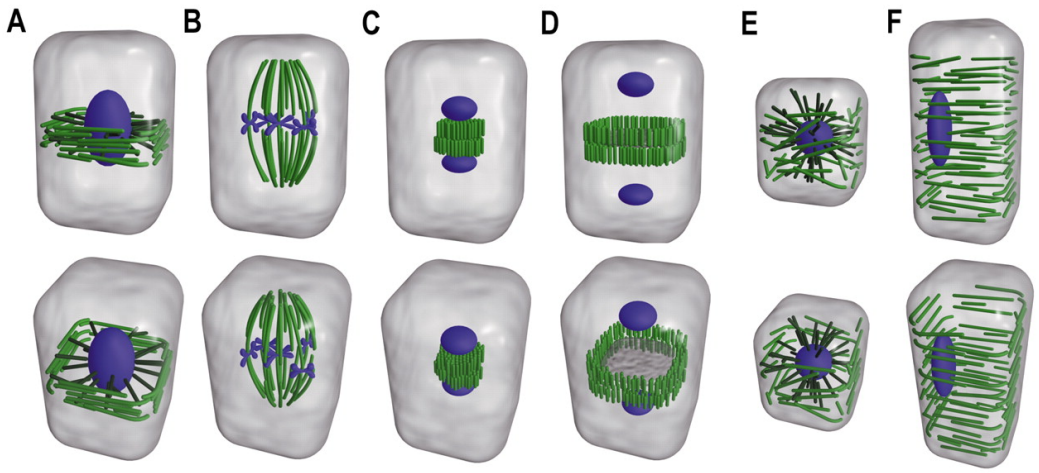

Fig. 2: Plant microtubular arrays during cell cycle

(A) preprophase band, (B) mitotic spindle, (C) young phragmoplast, (D) old phragmoplast with newly formed cell plate, (E) microtubules nucleated from nuclei and at the cortex, (F) interphase cortical microtubules. Microtubules (green), chromatin (blue), cell plate (darker grey). Taken from [133].

1.5.1 Spindle

Bipolar spindle is required for proper segregation of chromosomes to daughter cells. γ-Tubulin is critical for bipolar spindle assembly in *C. elegans* [71]. In *Drosophila*, *Xenopus* egg extract, and animal centrosomal cells, depletion of γ-tubulin increases number of monopolar spindles [33; 81; 116].

γ-TuRC acts in bipolar spindle formation through organization of the microtubule minus ends in animal cells with centrosomes [81]. γ-TuRCs attach microtubules at pole-distal regions of the spindle, then are probably stabilized by nucleation and/or binding to minus end of microtubules and then brought dependently on microtubules by molecular motors to the

spindle poles, where they are incorporated to the centrosome. The transporting rate is regulated also in cell cycle specific manner and drops during entrance to anaphase [81].

Petry et al. suggest that in spindle formation without centrosomes different mechanisms of acentrosomal nucleation are combined: at first chromatin nucleation in random directions is mainly used, then mass of spindle increases due to augmin through branching or bundling and finally, centrosome-like poles are formed to stabilize bipolar structure [116]. Augmin also contributes to spindle bipolarity, but augmin-independent nucleation from acentrosomal poles is able to repair multipolar spindles formed after augmin depletion [116].

Similarly, acentrosomal mechanisms are combined for spindle formation in higher plants. Nucleus plays important role in pre-spindle generation [135]. Later, chromatin nucleation is employed and kinetochores can nucleate and also stabilize the microtubules [36].

Polarity of the spindle is critical for plant morphogenesis as plant cells cannot move due to their rigid cell walls [136]. Accordingly, plant mitotic spindles maintain bipolarity after reduction of γ-tubulin levels; severe depletion of γ-tubulin results in collapse of spindles [68; 70]. In *Arabidopsis*, the most of subunits of augmin complex is conserved with animal ones [104]. Depletion of augmin subunit AUG3 results in spindles with disturbed polarity or with unconverged poles and also influences localization of γ-tubulin in phragmoplasts [103]. Plant specific subunit AUG7 is essential for proper spindle assembly and phragmoplast organization [104].

It was suggested that orientation of plant spindle contributes to the cell plate position [7]. When augmin complex is disfunctional in *aug7* mutants, misoriented spindles lead to misoriented phragmoplasts [104]. Microtubule plus end protein EB1c is responsible for spindle positioning in *Arabidopsis*; null mutant *eb1c* shows impaired orientation of spindles as well as shortened or collapsed spindles; moreover, phragmoplasts are misoriented [31].

Spindle orientation is important as its aberrant orientation is connected with several developmental diseases in human. Recently, γ-TuRC was shown to be important for spindle positioning in *Drosophila* and human cells; EB1 can counteract with this γ-TuRC function although the direct interaction of EB1 and γ-TuRC was not proven [32].

1.5.2 Phragmoplast

Phragmoplast is a plant specific structure important for delivery of vesicles for cell plate formation. Alignment of phragmoplast and site of cell plate formation is supposed to be marked before mitosis by PPB. TONNEAU proteins TON1 [137] and TON2 are needed for the PPB formation [138]. Maintenance of the cell division plain given by PPB is ensured by

different markers and kinesins [139]. PHRAGMOPLAST ORIENTING KINESINs POK1 and POK2 ensure presence of positive cortical division zone markers RanGAP1 [140] and MAP TANGLED [141] at cortical division zone. Another kinesin AtKINUa was found at PPB in dependance on its degradation by proteasome and was suggested for synchronization of chromatin cycle and microtubule array cycle [142].

Phragmoplast contains stable microtubule bundles oriented almost perpendicular to the cell plate and dynamic microtubules oriented obliquely to the cell plate [143]. γ-Tubulin localizes mainly on the stable bundles from which dynamic microtubules are nucleated. While nucleation of new microtubules is similar between leading and trailing edge, microtubule stability is higher at the leading edge of the phragmoplast. There is a movement of dynamic microtubules probably capped by γ-tubulin on their minus ends to distal region of phragmoplast along the stable bundles. MAP65-1 is present more on stable bundles, mainly at the leading edge [143]. The precise regulation of gradient of microtubule stability and depolymerization in phragmoplast is unknown, but MAPK kinase signalling through MAP65-1 and microtubule severing by katanin can be involved [144].

1.6 γ-Tubulin functions besides its role in microtubule nucleation

1.6.1 γ-Tubulin is implicated in coordination of cell cycle, checkpoints control, and in regulation of transcription

γ-Tubulin is an ubiquitous microtubule nucleator with additional roles in regulation of microtubular cytoskeleton organization [69; 81]. Besides its functions with microtubules, γ-tubulin plays roles in various cell cycle-related functions.

Phosphorylation of γ-tubulin on Ser131 by SADB/Brsk1 kinase in human cells regulates centrosome duplication [145].

γ-Tubulin has a role in G1/S restriction checkpoint as it regulates progression of S-phase [78]. γ-Tubulin binds directly to E2F transcription factor competing for its binding site with transcription factor DP; through regulation of E2F transcription activity γ-tubulin regulates expression of other genes [146]. Moreover, γ-tubulin binds through E2F to promoter of its own gene and also to retinoblastoma protein (RB) promoter; both RB and γ-tubulin regulate expression of each other; low levels of both proteins cause apoptosis [147].

γ-Tubulin interacts with Rad51 in nuclei in S-phase and mainly after DNA damage; the role of γ-tubulin in DNA repair by homologous recombination was suggested [77]. Furthermore, γ-tubulin interacts with ATR and with BRCA1 in nuclei and accumulates in

centrosome after DNA damage [148]. DNA damage checkpoint proteins connect DNA damage response and microtubule nucleation machinery through γ-tubulin availability on centrosome [148]. γ-Tubulin was also suggested to regulate function of C53 in DNA damage G2/M checkpoint in human cells [79].

γ-Tubulin functions in spindle assembly checkpoint in *S. pombe* [149]. While spindle assembly checkpoint seems to be normal in *Aspergillus* with mutated γ-tubulin, combination of γ-tubulin mutation with mutated Mad2, Bub1, or Bub3 is lethal [150]. Similarly, in *S. cerevisiae* deletion of checkpoint gene Mad2 in combination with γ-tubulin mutant is lethal [151].

γ-Tubulin is important in coordination of late mitotic events and cytokinesis in fungi *S. pombe* and *A. nidulans* and plant *A. thaliana* [70; 149; 150]. γ-Tubulin inactivates anaphase-promoting complex/cyclosome after mitotic exit in *Aspergillus* [152].

Altogether these data show that γ-tubulin plays multiple cellular roles in coordination of cell cycle, in DNA damage control, and in regulation of transription.

1.6.2 γ-Tubulin is important for cell polarity and membrane processes

Severe morphogenetic defects on root hairs observed in *Arabidopsis* seedlings with depleted γ-tubulin indicated implication of γ-tubulin in cell polarity [70]. In animal cells, cell polarity is ensured also by functional connection between centrosomes and Golgi apparatus as both contributes to microtubule nucleation [119].

γ-Tubulin and other centrosomal proteins form complexes with signalling and microtubule plus end tracking proteins representing linkers between microtubules and membranes [28; 153]. Yeast γ-tubulin was shown to be responsible for assembly of functional complex Kar9-Bim1, homologues of mammalian adenomatous polyposis coli (APC) and EB1, and its loading to astral microtubules having an impact on spindle position and later on cell polarity [154]. In colon epithelial tumor cells, APC forms 20 S and 60 S complexes with γ-tubulin, α-tubulin and IQGAP1 [153].

Moreover, γ-tubulin interacts with proteins in Golgi membranes including protein p115 required for Golgi structure and for late mitotic spindle maintenance [155]. Another protein of Golgi apparatus, GMAP-210, responsible for Golgi ribbon assembly and maintenance, recruits γ-tubulin complexes [156].

Also proteins of membrane trafficking machinery are connected either to γ-tubulin and/or to other centrosomal proteins. GTPase dynamin 2, functioning in vesicle formation and trafficking, interacts directly with γ-tubulin in centrosome and is required for centrosome

cohesion [157]. An adaptor protein PACSIN 2, involved in vesicle transport and membrane dynamics, localizes on centrosome with γ-tubulin and together with γ-tubulin forms putative complexes with dynamin 2; PACSIN 2 is also implicated in regulation of microtubule nucleation [158]. Endocytic adaptor protein ARH associates with γ-tubulin complexes and functions in centrosome assembly and also affects duration of cytokinesis [159]. GAPCenA, a GTPase activating Rab6, is found with cytosolic γ-tubulin and contributes to microtubule nucleation [160]. Protein EV15 with partial homology to GAPCenA, interacts with γ-tubulin and α-tubulin at centrosome [161]. γ-Tubulin is also found in protein complexes of effectors of Rab GTPases on membranes [162; 163].

All these data suggest that γ-tubulin is present in multi-protein complexes with function in membrane and microtubular cytoskeleton interactions.

1.7 Cell cycle

Plants need the proper spatial-temporal regulation of the switch between cycling and quiescence to ensure the right morphogenesis during their development. In plants, there are two niches of stem cells which divide during the whole life of the plant localized in root and shoot meristems [164].

The basic regulators of the cell cycle are highly conserved between animals and plants but plants evolved also some unique mechanisms mirroring their specific needs in resisting harsh conditions without possibility to escape [165].

There are several checkpoints controlling the cell cycle to prevent cell division in cells with defect of chromosomes duplication or distribution. Cells arrested by the checkpoint control either undergo reparation or are destroyed in senescence process or programmed cell death. As higher plant cells cannot move, damaged cells undergoing massively programmed cell death would cause severe damage of plant body. Therefore instead of the programmed cell death higher plant cells often undergo endoreduplication.

1.7.1 Endoreduplication versus endomitosis

Endoreduplication also known as endocycle or endoreplication includes several S phases together with G phases but without mitosis and results in higher DNA content with unsepareted chromosomes. Endoreduplication goes along with differentiation in plant development [166; 167] but it is also a consequence of external stresses [168].

Endomitosis ommits part of nuclear division and cytokinesis leading to higher DNA content but with separated chromosomes. In plants, endomitosis naturally occurs in nutritive cells [168].

1.7.2 Regulation of γ-tubulin during cell cycle and in response to external signalling

In budding yeast, γ-tubulin is phosphorylated by Cdk1 *in vivo* as shown in phosphoproteomic study on isolated SPB; phosphorylation was detected on six sites of γ-tubulin in mitotic phase and on two sites in G1 phase [151] including Tyr445 which phosphorylation influences number of microtubules and their organization [169]. Phosphorylation on Ser360 is important for dynamic of spindle organization as mutation of Ser360 to Asp causes mitotic delay and improper separation of spindle poles; in combination with EB1 deletion, this mutation is lethal [151]. Tandem affinity immunopurification through γ-tubulin and GCP2 homologue revealed five phosphorylation sites on γ-tubulin [170]. Phosphorylation sites Ser74, Ser100, and Ser360 are essential for growth through their influence on both cytoplasmic and nuclear microtubules. Phospho-mimicking mutants show delay in spindle formation and cells built only shorter bipolar spindles and later arrest in metaphase with unsegregated chromosomes, while spindle positioning is not significantly affected. *In vitro*, Ser74 is phosphorylated by polo-like kinase Cdc5 [170]. Microtubule nucleation and organization can be regulated also through phosphorylation of other γ-TuCs components or their adaptors [151; 170]. Budding yeast adaptor Spc110 is phosphorylated in cell-cycle dependent manner and allows assembly of γ-TuSCs, which then nucleates microtubules [171]. Human γ-tubulin expressed in *E. coli* is *in vitr*o phosphorylated by Cdk1-cyclin B on Ser80 and Thr196 [172]. Protein phosphatase 4, which interacts with γ-tubulin and GCP2 from human cells, was suggested to be involved in regulation of microtubule nucleation through Cdk1-cyclin B activation which inhibits protein phosphatase 4 and causes prolonged phosphorylation of γ-tubulin [172].

Regulation of γ-tubulin phosphorylation in *Drosophila* is controlled through Wee1 kinase, a negative regulator of cyclin dependent kinase, but precise mechanism is unknown [173].

Previously mentioned phosphorylation of γ-tubulin on Ser131 is responsible for translocation of γ-tubulin to centrosome where it negatively influences number of astral microtubules [145]. Phosphorylation of γ-tubulin on Ser131 might facilitate access of SADB/Brsk1 to Ser385 of γ-tubulin which phosphorylation leads to γ-tubulin relocation to

chromatin in nucleus and consequently allows its regulation of S-phase through E2F described above [78].

Several phosphorylation sites including above mentioned Ser131, Thr196, Ser360, and Tyr445 are conserved in *Arabidopsis* γ-tubulin.

γ-Tubulin forms complexes with several kinases in animal cells including phosphoinositide 3-kinase and Src family kinase Fyn [163]. γ-Tubulin localization to centrosomes and subsequently microtubule nucleation is influenced by integrins and Src kinase through MAP kinase signalling [174].

1.8 MAP kinase signalling and cytoskeleton

In plants, MAP kinases react not only to abiotic and biotic stresses but are also involved in regulation of plant development [175; 176].

MAP kinases are part of a cascade consisting of two other kinases. The first kinase in the cascade, MAPKK kinase, can be activated after different stimuli. Its activation leads to activation of the second kinase in the cascade, MAPK kinase, by which the MAP kinase is finally activated and MAP kinase can then phosphorylate its substrates. The numbers of MAP kinase signalling pathway members clearly shows that at least one MAPK kinase has more than one MAP kinase as its substrate [177]. Specificity of MAP kinases signalling is ensured by spatial and temporal regulation of the pathway members that is controlled also by scaffolds and adaptor proteins [178].

Besides their role in regulation of transcription, MAP kinases regulate cytoskeleton organization [179].

Phosphorylation of tobacco MAP65-1 by MAP kinase results in less bundled microtubules decreasing microtubule stability; it promotes phragmoplast expansion [180]. *Arabidopsis* MPK6 and MPK4 phosphorylate AtMAP65-1 *in vitro* [181]. MAP65-1 appeared to be phosphorylated after MPK6 and MPK3 activation also in *Arabidopsis* seedlings [182]. Nitration is an important posttranslation modification of tubulins which can regulate organization of microtubules [26]. MPK6 regulates activity of nitrate reductase 2, which produces nitric oxide [183].

MAP kinases play a role in plant morphogenesis by regulation of cytokinesis [179; 184]. *Arabidopsis* MAP kinase MPK4 is involved in regulation of cytokinesis as its mutant shows impaired cytokinesis manifested by binucleated and multinucleated cells, cell wall stubs, and incomplete cell plates [185].

Arabidopsis MAP kinase MPK6 plays roles in regulation of cell proliferation and differentiation. Together with MPK3, MPK6 is important for maintaining of cell proliferation in ovule development [186], for cell proliferation and later for differentiation in anther development [187], and for proper differentiation of cells in stomatal development [188]. Recently, MPK6 was suggested to be a repressor of cell proliferation [189].

In animal cells, MAP kinases ERK1 and ERK2 localize to MTOCs on poles as well as in the cytoplasm [190] and interact with microtubules [191]. Lee et al. suggested that MAPK can regulate γ-tubulin dynamics and is important for centrosome assembly and microtubule organization in mouse oocytes [192]. Changed localization of phosphorylated MAP kinase and of γ-tubulin after microtubule stabilization in pig oocytes suggested that localization of the kinase is important in regulation of microtubules [193].

2. AIMS OF THE STUDY

A long-term goal of the Laboratory of Functional Cytology is characterization of γ-tubulin and its complexes and their role in acentrosomal plant cells. Besides functions in microtubule nucleation and organization, we focus on non-canonical roles of γ-tubulin in cell cycle regulation, DNA repair and γ-tubulin interactions with membranes.

Specific aims of the Ph.D. thesis were:

1) Biochemical characterization of RanBPM complexes in acentrosomal *Arabidopsis* cells
2) Functional analysis of *Arabidopsis* NITRILASE1; particularly an identification of its role in the cell cycle and plant development
3) Understanding of AtTPX2 interaction with importin and γ-tubulin and a role of AtTPX2 in microtubule nucleation and organization in acentrosomal *Arabidopsis* cells
4) Elucidation of MAP kinase MPK6 function with microtubules and γ-tubulin in *Arabidopsis*
5) Characterization of interaction of γ-tubulin and NSF in *Arabidopsis*

3. COMMENTS ON PRESENTED PUBLICATIONS

3.1 Interactions of an Arabidopsis RanBPM homologue with LisH-CTLH domain proteins revealed high conservation of CTLH complexes in eukaryotes

Eva Tomaštíková, Věra Cenklová, Lucie Kohoutová, Beáta Petrovská, Lenka Váchová, Petr Halada, Gabriela Kočárová, and Pavla Binarová; BMC Plant Biology (2012), 12:83 1-14

RanBPM (Ran-binding protein in MTOC) was reported as one of centrosomal proteins in human cells involved in microtubule nucleation and its interaction with γ-tubulin was suggested [194]. However, later it was shown that microtubule nucleation is performed only by truncated version of RanBPM; presence of the full-length version of RanBPM in centrosome was not confirmed [195].

Full-length RanBPM forms 670 kDa-complex [195]. The 20S complex called CTLH in mammalian cells consists of several proteins containing LisH/CTLH motif and of armadillo-repeat proteins [196]. In budding yeast, there is a complex formed by homologuous proteins called GID [197]. GID complex plays role in glucose-induced ubiquitination of some gluconeogenic enzymes and their consequent proteasome-dependent degradation [197]. For mammalian CTLH complex, similar roles were suggested as CTLH works in proteasome-dependent degradation and endosome/lysosome-dependent degradation of proteins [198].

Nowadays, RanBPM is known as a scaffold protein having lots of different interaction partners [199]. Besides the members of CTLH complexes, RanBPM interacts with several receptors, other members of signalling pathways, proteins involved in cell cycle regulation and apoptosis. RanBPM plays role in stabilization of proteins, regulation of the cell cycle and apoptosis, and transriptional activities through signal transduction [199].

We found Arabidopsis homologue of RanBPM annotated as an uncharacterized protein and we aimed to get insight into its possible functions with γ-tubulin and in microtubule nucleation.

Cellular distribution of AtRanBPM showed that it is mainly cytoplasmic protein present in a form of large complexes. We further showed presence of AtRanBPM in the complexes of 230 – 500 kDa by native electrophoresis. After immunopurification of the complexes of AtRanBPM, we identified by MALDI-MS and LC-MALDI MS/MS among

AtRanBPM interactors proteins containing LisH and CRA domains; LisH, CRA and RING-U-box domains and a transducin/WD40 repeats. Several of them have their counterparts in mammals and yeast. Furthermore, we confirmed AtRanBPM as a cytoplasmic protein accumulating in the perinuclear area with a weak signal in the nuclei by microscopy *in vivo* and *in situ*. Expression level of AtRanBPM in dividing cells and stationary cells did not differ much. Neither immunoprecipitation nor immunofluorescence showed interaction of AtRanBPM with γ-tubulin; therefore AtRanBPM role in nucleation is improbable. In this sense, AtRanBPM did not behave as truncated version of RanBPM in mammalian cells.

Our findings contributed to knowledge of the conservation of CTLH complexes among yeast, mammals, and plants. The function of CTLH complexes in plants is still not fully understood but our data suggest that homologues of TWA1, MAEA, Rmnd5, and RanBPM form core complex, while other proteins ensure interaction with proteins in signalling and other pathways as suggested by Francis [200].

Methods and tools used in this study:
Molecular cloning of AtRanBPM
Preparation of stably transformed cell cultures and plants of *Arabidopsis thaliana*
In silico analyses, database searches
Biochemical analyses (differential centrifugation, native electrophoresis, immunopurification, SDS-PAGE, immunoblotting, silver staining)
MALDI-MS, LC-MALDI MS/MS analyses
Immunofluorescence
Epifluorescence and confocal microscopical analyses

In this project, I performed biochemical analyses, immunopurifications of AtRanBPM complexes, and characterization of the complexes by native electrophoreses. Furthermore, I contributed by confocal microscopical images of subcellular distribution of AtRanBPM in cells and roots of Arabidopsis. I also prepared the respective figures and texts for the manuscript.

3.2 NITRILASE1 regulates the exit from proliferation, genome stability and plant development

Anna Doskočilová[#], Lucie Kohoutová[#], Jindřich Volc, Hana Kourová, Oldřich Benada, Jana Chumová, Ondřej Plíhal, Beáta Petrovská, Petr Halada, László Bögre, and Pavla Binarová;
New Phytologist (2013), 198(3): 685–698 [#]These authors contributed equally to this article.

Animal nitrilase 1 is a negative regulator of proliferation and cell cycle progression cooperating with FHIT, a well-known tumour supressor [201]. Furthermore, nitrilase 1 overexpression results in higher level of apoptosis in animal cells [202]. Plant NITRILASE1 forms aggregates after wounding as an early event in programmed cell death [203]. As only limited data on molecular characteristics and possible functions of plant NITRILASE1 besides its enzymatic activities were published at the time of our study, we focused on NITRILASE1 and its putative functions in cell cycle regulation.

In *Arabidopsis*, there are four genes for nitrilases. NITRILASE1 is most homologous to animal nitrilase 1. We followed localization of NITRILASE1-GFP *in vivo* and of endogenous NITRILASE1 *in situ* by immunofluorescence. In dividing interphase cells, NITRILASE1 localized mainly in cytoplasm and around the nuclei, while in differentiated cells it became predominantly nuclear, so its localization changed with the state of the cell. Moreover, NITRILASE1 was found in the spindle area and phragmoplast area. We further confirmed its interaction with microtubules by spin down experiment where NITRILASE1 was pelleted with polymerized plant microtubules *in vitro* and by enrichment of GFP-NITRILASE1 signal on microtubules *in vivo* after taxol treatment. After microtubule depolymerization, NITRILASE1 signal became dispersed in the cytoplasm and unlike γ-tubulin hardly any signal of NITRILASE1 was found on microtubule kinetochore stubs. This indicated other role for NITRILASE1 with microtubules than in microtubule nucleation, capturing, or stabilization.

Mutants in NITRILASE1 did not show any morphological phenotypes under physiological conditions [204]. Therefore we prepared dsRNA construct for downregulating NITRILASE1-3 (NIT-RNAi) in *Arabidopsis*. Downregulation of NITRILASE1-3 was confirmed by quantitative real time PCR and correlated with strength of phenotype of NIT-RNAi plants. The phenotypes of NIT-RNAi plants ranged from milder to stronger ones; first true leaves if they developed were small and thick and in the strongest phenotypes only disorgenized calli-like structures were formed at the shoot apex instead of true leaves.

Development of main roots of NIT-RNAi plants was affected; meristematic zones of roots were shortened, malformated, with irregular cell files.

NITRILASE1-3 downregulation resulted in massive genome instability. DNA content of cells from malformated NIT-RNAi leaves measured by flow cytometry was highly increased (up to 32C) in comparison with wild type (WT). Elevated DNA content of NIT-RNAi calli-like structures was not caused by endoreduplication as indicated by increased average number of chromocentra in NIT-RNAi plants. Furthermore, distribution of chromocentra in NIT-RNAi cells was much wider than in WT; this corresponded with a lack of distinct peaks for DNA content distribution measured by flow cytometry. Moreover, highly increased number of chromosomes was observed in NIT-RNAi cells from prophase to anaphase. Interestingly, these highly polyploid cells still continued dividing.

Moreover, in cultured cells overproducing NITRILASE1, growth was slowed down and there was also an increased level of programmed cell death in comparison with WT culture. The slower growth of cultured cells overproducing NITRILASE1 was confirmed by lower fresh mass weight, lower mitotic index, lower amount of cells with G2/M-phase DNA content showed by flow cytometry, and two- to three-fold lowered amount of cells in S-phase detected by EdU labelling compared to WT. We also detected programmed cell death through dsDNA breaks by TUNEL assay. It was elevated in cells overproducing NITRILASE1 in comparison with WT and became more prominent with the time.

Furthermore, we found that NITRILASE1-3 are required for proper cytokinesis as their downregulation lead to aberrant cell divisions. Among cytokinetic defects present in 74 % of cotyledon stomata were undivided rounded guard mother cells, guard mother cells with incomplete cell plate, or single guard cells. Stomata with aberrant cytokinesis were also observed in hypocotyls and true leaves. Moreover, there were pavement cells with cell wall stubs, cells with highly enlarged nuclei caused probably by fusion of nuclei as well as binuclear cells still capable to enter S-phase. Cells with enlarged nuclei or binuclear cells were present also in NIT-RNAi roots; the amount of proliferating cells detected by Edu labelling was increased compared to WT.

Altogether our data showed that NITRILASE1 serves as a negative regulator of the cell cycle and is required for exit from cell cycle and entry into differentiation and for regular cytokinesis. Plant NITRILASE1 is an important player in maintenance of genome stability and the function is conserved in animals and plants.

Methods and tools used in this study:

Molecular cloning of Arabidopsis NITRILASE1 and preparation of dsRNA construct for downregulation of NITRILASE1-3

Preparation of stably transformed cell cultures and plants of *Arabidopsis thaliana*

Biochemical analyses (differential centrifugation, gel permeation chromatography, blue native electrophoresis, immunopurification, microtubule spin down experiments, SDS-PAGE, immunoblotting, silver staining)

MALDI-MS/MS analyses

Drug treatments

Immunofluorescence

Epifluorescence and confocal microscopical analyses

Electron microscopy analyses (negative staining and immunogold labelling)

Quantitative real-time PCR

Cell cycle analyses (EdU assay, chromocentra counting, flow cytometry)

Programmed cell death analyses (TUNEL assay)

My task in this study was focused on phenotype analyses of NIT-RNAi plants and NITRILASE1 overexpressing cultured cells. I analysed cell cycle mainly by flow cytometry, chromocentra counting, and Edu assays analyses. Further, I performed epifluorescence and confocal microscopy of labeled cells and plants and of cells and plants in vivo. I contributed to the manuscript writing, figures preparation and revisions.

3.3 Overexpressed TPX2 causes ectopic formation of microtubular arrays in the nuclei of acentrosomal plant cells

Beáta Petrovská[#], Hana Jeřábková[#], Lucie Kohoutová[#], Věra Cenklová, Žaneta Pochylová, Zuzana Gelová, Gabriela Kočárová, Lenka Váchová, Michaela Kurejová, Eva Tomaštíková, and Pavla Binarová; Journal of Experimental Botany (2013), 64(14):4575-4587 [#]These authors contributed equally to this article.

TPX2 protein (targeting protein for Xenopus kinesin-like protein 2) plays many various roles. TPX2 targets other proteins to microtubules; is involved in microtubule organization and in centrosomal and acentrosomal microtubule nucleation and has a role in DNA damage [205]. TPX2 functions in plants are only partially characterized. We focused on a role of AtTPX2 in microtubule nucleation and organization with the aim to get further insight into mechanisms of acentrosomal microtubule nucleation and organization.

We transformed *Arabidopsis* cells with 35S::AtTPX2-GFP construct. AtTPX2-GFP signal appeared as dots and patches. Later thick fibres and fibrillar structures were observed in the nuclei and in the vicinity of the nuclei in cells overexpressing AtTPX2-GFP as confirmed by 3D reconstructions of cells *in vivo* as well as of immunostained cells. Based on immunofluorescence staining with anti-α-tubulin and anti-actin antibodies, we concluded that the observed fibres represent nuclear and perinuclear ectopic microtubular arrays decorated by AtTPX2-GFP. The arrays were stable as shown by their persistence in cells overexpressing AtTPX2-GFP after microtubule depolymerizing drug treatment.

We showed that importin α physically interacted with AtTPX2-GFP as it was co-purified with AtTPX2-GFP from *Arabidopsis* extract. We also examined the interaction *in situ* by immunofluorescence. When only AtTPX2-GFP dots and patches were present, importin was localized mainly in the nuclei and on the nuclear envelope, and also with some of the dots and patches; later importin signal largely diminished from the nucleus and became restricted to the perinuclear and nuclear microtubular fibres. Ran signal was elevated in nuclei with the dots and patches above the level of untransformed cells and its signal weakened during the formation of fibres. Our data suggest involvement of the Ran-dependent importin pathway in TPX2-mediated formation of microtubular arrays.

We observed γ-tubulin colocalized with the AtTPX2-GFP decorated fibres in a patchy pattern. However, we were not able to co-purify γ-tubulin with AtTPX2-GFP. Absence of γ-tubulin in AtTPX2-GFP immunoprecipitate could be caused by its very low amount in the

complex which can be further decreased by a high instability of plant TPX2 itself resulting in AtTPX2 degradation during purification. Recently, Petry et al. showed physical interaction of TPX2 together with γ-tubulin and augmin in *Xenopus* egg extracts [74].

As AtTPX2 binds Aurora 1 kinase [50], we tested if the formation of the arrays is dependent on Aurora 1 binding or its activity. Using Aurora kinase inhibitor ZM447439 and also a construct of AtTPX2 lacking both Aurora kinase binding sites, we proved that the formation of the ectopic microtubules was independent of Aurora kinase 1 activity as well as of its binding to AtTPX2.

On the contrary to animal cells where microtubules decorated by TPX2 were observed in apoptotic cells [206] the fibres decorated by AtTPX2 were not found in *Arabidopsis* cells undergoing programmed cell death in our experiments. We further showed that the formation of the ectopic microtubule arrays was independent of mitotic signalling and occurred in interphase cells.

In conclusion, we showed that AtTPX2-GFP overexpression enhances an ability of the chromatin and nuclear envelope to nucleate microtubules in plant cells where centrosomes are absent. The formation of ectopic microtubule arrays decorated by AtTPX2-GFP was independent of Aurora 1 kinase. Our data on copurification and colocalization of plant importin with AtTPX2-GFP and observation of Ran gradient during fibre formation altogether suggest that Ran-dependent importin pathway regulates TPX2-mediated formation and organization of microtubules in plants.

Methods and tools used in this study:
Molecular cloning of full length AtTPX2 and its truncated version and of AtAurora1
Preparation of stably transformed cell cultures and plants of Arabidopsis thaliana
In silico analyses, database searches
Biochemical analyses (immunopurification, SDS-PAGE, immunoblotting)
Drug treatments
Immunofluorescence
Epifluorescence and confocal microscopical analyses
3D reconstructions
Colocalization analyses
Quantitative real-time PCR analyses
Programmed cell death analyses (Evans blue staining, TUNEL assay)

In this project, I performed confocal microscopy, Imaris 3D reconstructions, and epifluorescence microscopy, and analyzed dynamics of ectopic fibre formation. I performed immunopurifications of AtTPX2 complexes with importin and γ-tubulin and analyzed Ran subcellular distribution microscopically. I contributed to the manuscript writing and prepared respective figures.

3.4 The Arabidopsis mitogen-activated protein kinase 6 is associated with γ-tubulin on microtubules, phosphorylates EB1c and maintains spindle orientation under nitric oxide stress

Lucie Kohoutová, Hana Kourová, Szilvia Nagy, Jindřich Volc, Petr Halada, Tamás Mészáros, Irute Meskiene, László Bögre, and Pavla Binarová; New Phytologist (submitted 2014)

MAP kinase MPK6 belongs to the best examined kinases in plants, but still its substrates/interactors are largely uncovered. MPK6 was shown to be implicated in regulation of proliferation and differentiation [188; 189]. It might be also connected to cytoskeleton regulation through MAP65-1 protein, its known target [181].

We showed that a portion of cellular pool of MPK6 pelleted with plant microtubules. We used a commercially available antibody directed against phosphorylated and active ERK1, named p-ERK that was shown to recognize the conserved phosphoepitope on the activation loop of plant MAP kinases. We found that MPKs recognized by p-ERK are highly enriched in microtubular fraction. We confirmed interaction of MPK6 and γ-tubulin in cytoplasmic and in microtubular fractions by immunoprecipitations.

We focused on localization of MPK6 and p-ERK with microtubular arrays in plants. MPK6 and p-ERK signal were present in spindle and phragmoplast area, but they differed in localization with PPB where signal for p-ERK was hardly detectable. We showed that localization of p-ERK followed dynamic localization of γ-tubulin on shortening kinetochore fibres of anaphase spindle and in midzone during anaphase/telophase transition. In spite of the interaction of MPK6 with γ-tubulin, γ-tubulin was not phosphorylated by active MPK6 *in vitro*. Our findings suggest that γ-tubulin is most probably not a substrate of MPK6 but it might function as a scaffold for MPKs signalling in plants.

To shed light on a role of MPK6 with microtubules, we used *Arabidopsis* knock out mutant line *mpk6-2*. When grown in control conditions, mpk6-2 mutants did not show root developmental phenotype. However, under nitrosative stress after NO_2-Tyr treatment, misoriented spindles and phragmoplasts were present in *mpk6-2* lines while in WT the effect of NO_2-Tyr was weaker. Dephosphorylation of three kinases MPK3, MPK4, and MPK6 in plants overexpressing phosphatase AP2C3 resulted in severe division defects; chromosomes congression and segregation were affected and spindles and phragmoplasts were misaligned.

In conclusion, we showed γ-tubulin as a new interactor of MPK6. Functional studies on *Arabidopsis* mutants suggested a role of MPK6 in spindle positioning and cell division and showed that MPK6 is crucial for regulation of microtubule organization under nitrosative stress.

Methods and tools used in this study:
Molecular cloning of EB1c, γ-tubulin, MPK6
Preparation of stably transformed cell cultures of *Arabidopsis thaliana*
Biochemical analyses (immunopurificatiosn, SDS-PAGE, immunoblotting, gel permeation chromatography, microtubule spin down experiments)
In vitro phosphorylation studies
LC-MALDI MS/MS analyses
Drug treatments
Whole mount staining
Immunofluorescence
Epifluorescence and confocal microscopical analyses

In this project, I performed microscopical observations of MPKs, γ-tubulin, and EB1 localizations and evaluated phenotypes of AP2C3 oe plants. I also performed immunopurification experiments. I designed majority of experiments and evaluated data. I contributed substantially to writing and figures preparation.

4. UNPUBLISHED RESULTS

Besides published data (see overview above), I contributed to other projects in the laboratory; their results are under preparation for publishing.

4.1 Characterization of interaction of γ-tubulin and NSF in Arabidopsis

In our proteomic studies of γ-tubulin interactors, we identified several proteins involved in membrane trafficking including NSF (N-ethylmaleimide-sensitive factor) protein, an ATPase belonging to the family of ATPases associated with various cellular activities.

Mammalian NSF has many different molecular interactors including membrane receptors, Rab GTPases, their interactors, and other proteins [207]. In metazoans, NSF forms homo-hexamers, which act in concert with its adaptor protein α-SNAP in disassembly of cis-SNARE complexes recycling them for repeated usage in membrane fusion events [208]. Besides its classical role, NSF is suggested to serve as chaperone in dissociation of various signalling receptor complexes like β_2-adrenergic receptor/β-arrestin1 complex or AMPA receptor/PICK1 complex [209; 210]. NSF is also responsible for disassembly of the complex formed by its adaptor γ-SNAP and Gaf-1/Rip11 protein, a regulator of apical membrane trafficking in polarized epithelial cells, which binds Rab11 GTPase [211]. Mammalian γ-tubulin was found in membrane associated complexes with Gaf-1/Rip11 [162].

In *Arabidopsis*, a large portion of cellular γ-tubulin pool is present with membranes [60], but practically no information is available about proteins interacting with γ-tubulin in these complexes. As our laboratory published previously, processes dependent on proper regulation of membrane trafficking such as cytokinesis, anisotropic growth and polar tip growth are impaired after RNAi depletion of γ-tubulin in *Arabidopsis* plants [70].

In *Arabidopsis*, NSF is encoded by a single gene. Mammalian NSF and soluble NSF attachment protein (α-SNAP) were shown to interact with plant cis-SNARE complexes [212; 213], but no data are available on forms of plant NSF, its interactions and cellular functions. We wanted to characterize plant NSF and examine its functions and its possible link to γ-tubulin and microtubular cytoskeleton.

To confirm the interaction of NSF and γ-tubulin that we found by LC-MALDI MS, we performed immunoprecipitations using affinity purified antibody against plant γ-tubulin. We identified 81 kDa-band corresponding to molecular weight of NSF by MALDI-MS on silver stained gel in immunoprecipitate from detergent-solubilized microsomal fraction (Fig. 3A).

We further immunoblotted the immunoprecipitate with antibody affinity purified on immunogenic peptide that we prepared against peptide from NSF (Fig. 3B).

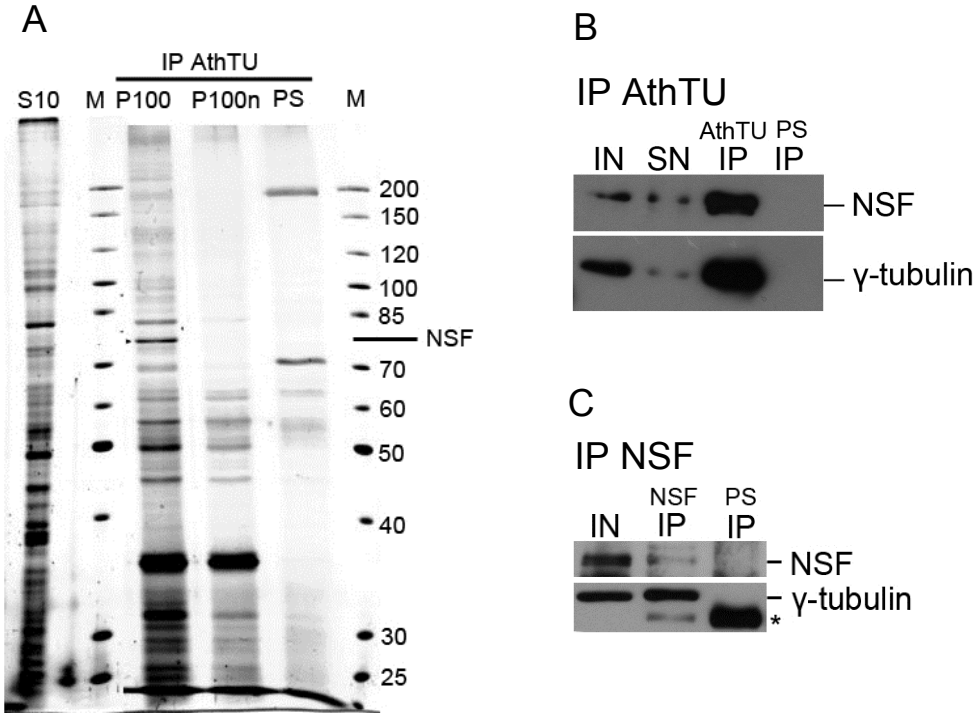

Fig. 3: NSF co-purified with γ-tubulin and vice versa from solubilized microsomal fraction of *Arabidopsis* cell culture

(A) Endogenous NSF was among proteins co-purified with γ-tubulin using antibody AthTU against plant γ-tubulin on silver stained gel. S10 - crude extract, M - markers of molecular weight (kDa), P100 - immunoprecipitate from solubilized microsomal fraction, P100n - immunoprecipitate from microsomal fraction without solubilization, PS - negative control using preimmune serum. (B) Immunoprecipitation with AthTU antibody; IN – solubilized microsomal fraction, SN – supernatant, AthTU IP – immunoprecipitate using AthTU antibody; PS IP - immunoprecipitate using preimmune serum. Western blot probed with anti-NSF antibody and TU-32 antibody for detection of γ-tubulin. (C) Immunoprecipitation with anti-NSF antibody; IN – solubilized microsomal fraction, NSF IP – immunoprecipitate using anti-NSF antibody, PS IP - immunoprecipitate using preimmune serum. Western blots probed with anti-NSF antibody and AthTU antibody, asterisk – IgG.

To validate the interaction of NSF with γ-tubulin further, we performed reciprocal immunopurification experiments from detergent-solubilized microsomal fraction with affinity purified rabbit polyclonal antibodies that we prepared against peptides derived from NSF protein sequence. Antibody recognizing sequence IGKMLNGKDPKIVN in the D1 domain of

NSF was suitable for purification (Fig. 3C), whereas antibody against QPAFGASTDDLERC in the D2 domain did not bind native NSF (data not shown). In conclusion, we found NSF co-purified with γ-tubulin and vice versa from *Arabidopsis* detergent-solubilized microsomal fraction.

Further, we cloned NSF coding sequence from cDNA *Arabidopsis* library, prepared constructs of GFP or RFP-tagged NSF by Gateway cloning [214] and derived stable Arabidopsis cell lines expressing tagged NSF under constitutive 35S CaMV promoter. We confirmed that protein product of N-terminal GFP-NSF fusion had a size ~ 110 kDa corresponding to molecular weight of GFP-NSF molecule. We tested cellular fractions of GFP-NSF expressing culture by GFP immunopurification and showed that γ-tubulin co-purified with GFP-NSF from solubilized microsomal fraction, while in low and high speed supernatants the interaction was undetectable (Fig. 4A). We further performed immunopurification experiments using GFP trap from cell lines expressing GFP-NSF (Fig. 4B) and analyzed proteins co-purified with GFP-NSF by MALDI-MS or LC-MS/MS. γ-Tubulin, 26S proteasome subunits, chaperones and yet uncharacterized receptor kinases and phosphatases were found to be co-purified with NSF.

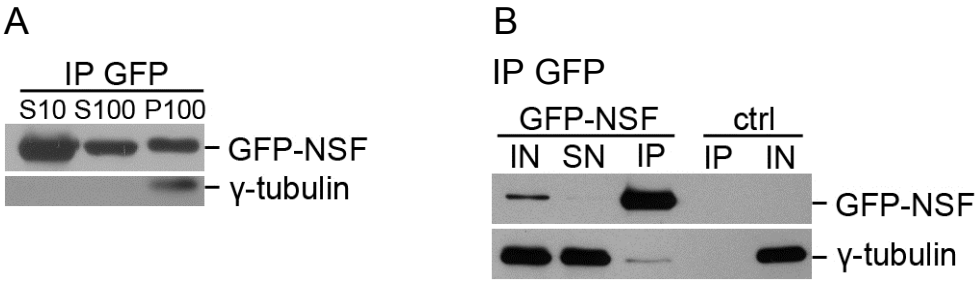

Fig. 4: γ-Tubulin co-purified with GFP-NSF from solubilized microsomal fractions

(A) Immunoprecipitation with anti-GFP antibody from different cellular fractions of GFP-NSF expressing *Arabidopsis* cell culture; S10 – crude extract, S100 – high speed supernatant, P100 – solubilized microsomal fraction. Western blot probed with anti-GFP antibody for detection of GFP-NSF and AthTU antibody. (B) Immunoprecipitation from GFP-NSF expressing *Arabidopsis* cell culture (GFP-NSF) and from WT culture used as a negative control (ctrl). IN - solubilized microsomal fraction P100, SN - supernatant, IP – immunoprecipitate.

To examine dependance of the interaction of NSF and γ-tubulin on ATP, we supplemented extracts with ATP and performed immunopurification experiments. Preliminary

data suggested that under supplementation of extracts with exogenous ATP, smaller amount of GFP-NSF co-purified with γ-tubulin (Fig. 5).

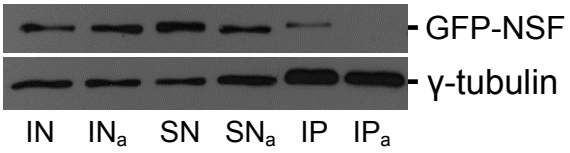

Fig. 5: GFP-NSF co-purified with γ-tubulin dependently on ATP

IN/IN$_a$ – solubilized microsomal fractions without/with exougenous ATP, SN/SN$_a$ – supernatants without/with exougenous ATP, IP/IP$_a$ – immunoprecipitates (using antibody against γ-tubulin) without/with exougenous ATP

To estimate the size of NSF and γ-tubulin complexes, we performed gel permeation chromatography. Position of co-elution of GFP-NSF and γ-tubulin in resolved fractions from detergent-solubilized microsomal pellet P100 suggested presence of high molecular complexes of those proteins (Fig. 6A). Blue native electrophoresis of fractions from gel permeation chromatography (shown for fraction f3) confirmed presence of NSF in high molecular complexes and complexes corresponding to molecular weight of putative hexameres (Fig. 6B).

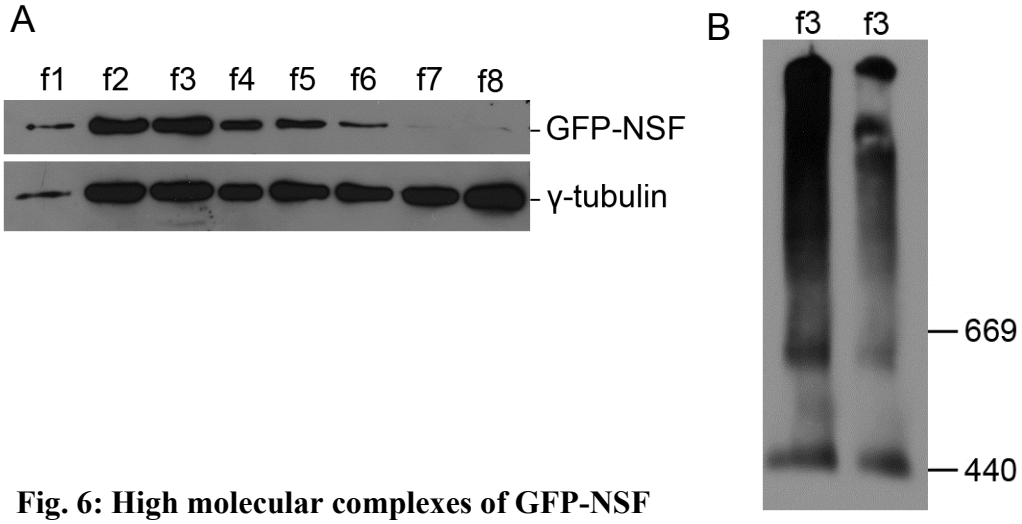

Fig. 6: High molecular complexes of GFP-NSF

(A) GFP-NSF co-eluted with γ-tubulin in gel permeation chromatography in high molecular fractions. Western blot probed with anti-GFP antibody and AthTU antibody. (B) GFP-NSF complexes from fraction 3 from gel permeation chromatography separated by blue native electrophoresis. GFP-NSF is present in high molecular complexes and also in smaller complexes, putative hexamers.

As data about cellular distribution of NSF localization are missing in plants, we performed differential centrifugation to follow it biochemically. We found that endogenous NSF and GFP-NSF were present in low speed pellet, in microsomal fraction and also in supernatants being cytoplasmic as well as present with membranes (Fig. 7).

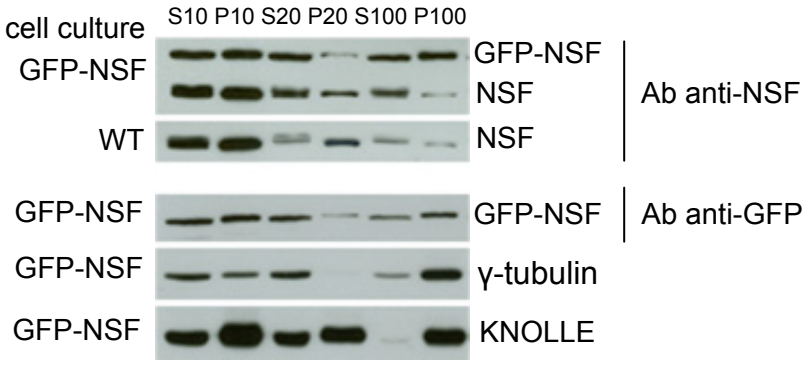

Fig. 7: Subcellular distribution of GFP-NSF and endogenous NSF in *Arabidopsis*
Fractions from differential centrifugation from GFP-NSF expressing cell culture and from WT culture probed with anti-NSF antibody, anti-GFP antibody, antibody against γ-tubulin, and against KNOLLE as a membrane marker. S10/P10 – crude supernatant/pellet, S20/P20 - low speed supernatant/pellet, S100/P100 – high speed supernatant/pellet.

Distribution shown by differential centrifugation was in agreement with our microscopic observations of GFP-NSF in cells with stable expression (Fig. 8A, B). We also cloned GFP-NSF under NSF native promoter and expressed it in *Arabidopsis* cultured cells. Fragments corresponding to the coding sequence of NSF and NSF's putative promoter sequence (~ 2,000 bp upstream CDS) were cloned using Gateway technology to the binary vector pK7m34GW [215]. Both expressed GFP-NSF driven from constitutive 35S CaMV promoter or from native promoter showed similar localization in vicinity of nuclei, under plasma membrane and in cytoplasm (Fig. 8A, B, C). During cytokinesis, GFP-NSF was present mainly in cell plate (Fig. 8B, arrow, 8C, arrows). Cells overexpressing GFP-NSF showed strong signal in cytoplasm and formed numerous small vesicles (Fig. 8D).

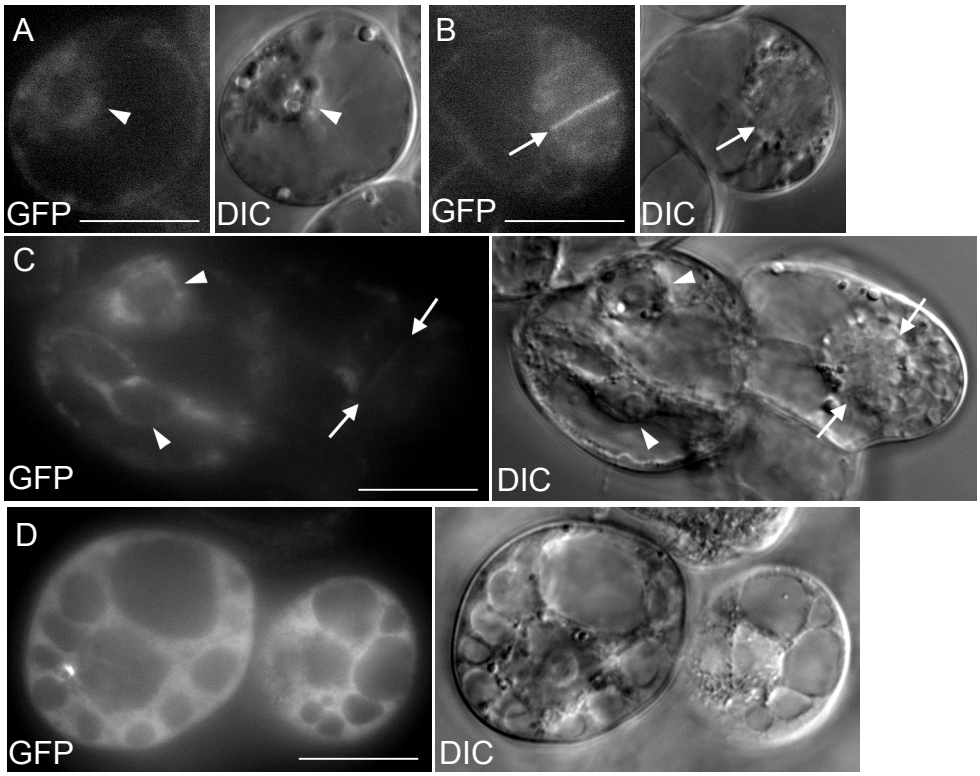

Fig. 8: *In vivo* localization of GFP-NSF in *Arabidopsis* cultured cells

(A, B) Culture with stable expression of GPF-NSF under 35S CaMV promoter. (A) Interphase cell with GFP-NSF around nucleus (arrowhead), under plasma membrane and in cytoplasm. (B) Cell during cytokinesis with GFP-NSF accumulated in cell plate (arrow). (C) Culture with expression of GPF-NSF under NSF native promoter. GFP-NSF around nuclei (arrowheads), under plasma membrane and in cytoplasm in interphase, and in cell plate during cytokinesis (arrows). (D) Culture overexpressing GFP-NSF with numerous vesicles and strong signal of GPF-NSF in cytoplasm. (A-D) Bars 20 μm.

Our immunofluorescence labelling showed that signal for GFP-NSF and endogenous NSF was enriched in spindle and phragmoplast area (Fig. 9, 10). To prove possible association of NSF with microtubules biochemically, we performed taxol driven polymerization of microtubules from plant cell extracts. NSF was pulled down with plant microtubules polymerized *in vitro* by taxol-driven polymerization (Fig. 11).

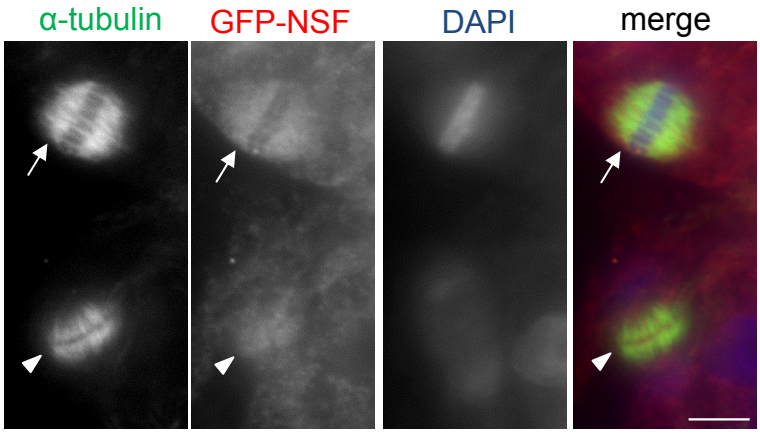

Fig. 9: GFP-NSF is present on microtubular arrays in dividing cells of *Arabidopsis*

Double immunofluorescence of *Arabidopsis* cultured cells; GFP-NSF (red, anti-GFP antibody), α-tubulin (green), chromatin stained by DAPI (blue). GFP-NSF in the area of spindle (arrow) and phragmoplast (arrowhead). Bar 5 μm.

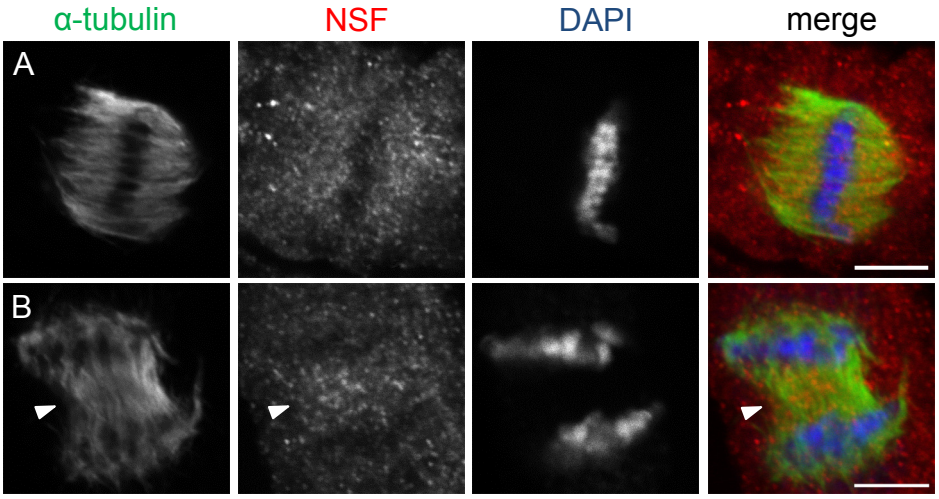

Fig. 10: NSF is present on microtubular arrays in dividing cells of *Arabidopsis*

Double immunofluorescence of *Arabidopsis* cultured cells; endogenous NSF (red), α-tubulin (green), chromatin stained by DAPI (blue). (A) NSF in the area of spindle in metaphase and (B) in young phragmoplast in late anaphase (arrowhead). (A-B) Bar 5 μm.

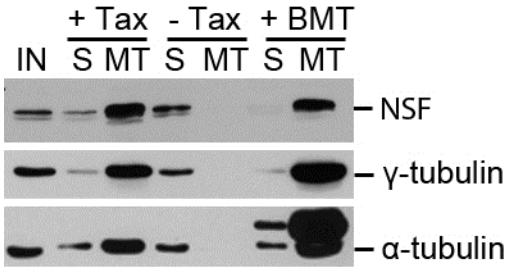

Fig. 11: NSF was pelleted with plant microtubules

NSF was enriched in microtubular pellet after *in vitro* taxol-driven polymerization of plant microtubules; NSF was not more enriched after addition of polymerized animal microtubules. γ-Tubulin was pelleted with plant microtubules and was enriched after the brain microtubules addition. IN – S70, S – supernatant, MT – MT pellet, + Tax/– Tax - taxol added/ommited, + BMT – porcine brain microtubules added besides taxol.

We further examined localization of NSF with γ-tubulin. We co-transformed RFP-NSF to GFP-γ-tubulin culture and followed their localization *in vivo*. GFP-γ-tubulin and RFP-NSF localized together around nuclei, under plasma membrane and in cytoplasm (Fig. 12). Double immunofluorescence localization of NSF and γ-tubulin *in situ* showed their localization in spindle and also in early stages of phragmoplast development where NSF was still not so accumulated in forming cell plate (Fig. 13). Further analyses are needed to characterize NSF colocalization with γ-tubulin in interphase and mitotic cells.

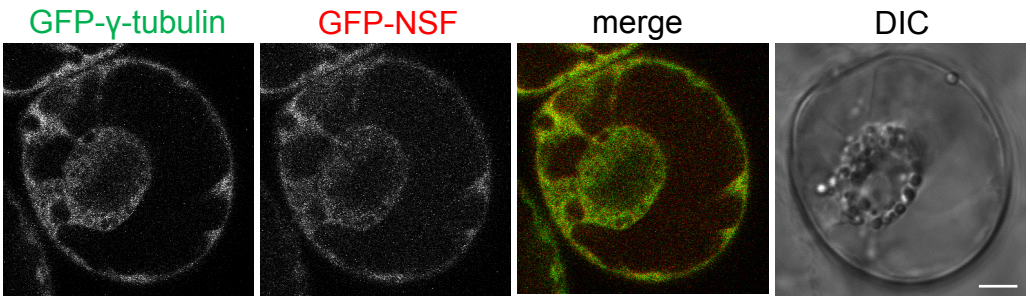

Fig. 12: *In vivo* localization of RFP-NSF and GFP-γ-tubulin in interphase *Arabidopsis* cultured cell

Both proteins were around nuclei, under plasma membrane and in cytoplasm. Bar 5 μm.

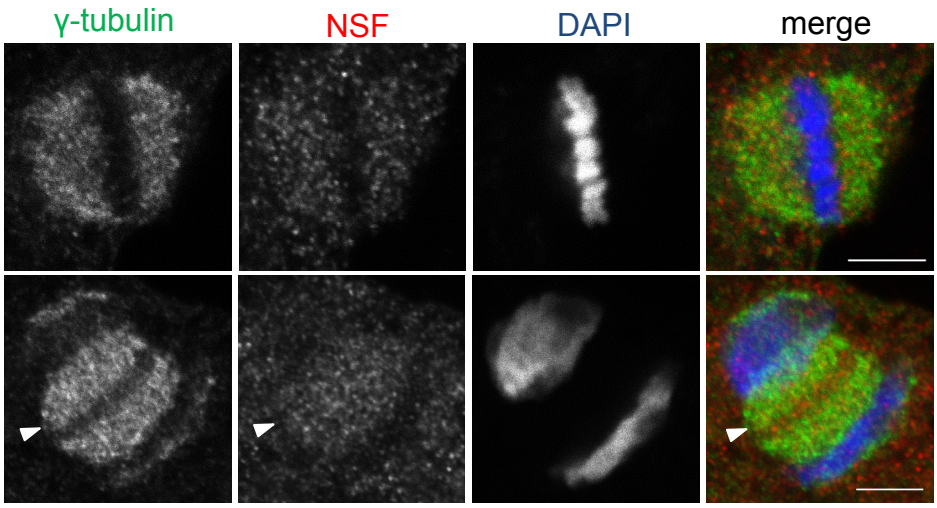

Fig. 13: NSF localized with γ-tubulin in dividing cells of *Arabidopsis*

Double immunofluorescence of *Arabidopsis* cultured cells; endogenous NSF (red), γ-tubulin (green), chromatin stained by DAPI (blue). (A) NSF in the area of the spindle in metaphase and (B) mainly in the area of young phragmoplast in telophase (arrowhead). (A-B) Bar 5 μm.

Arabidopsis seedlings overexpressing GFP-NSF showed gain-of-function phenotype (Fig. 14). Plants overexpressing GFP-NSF had shorter roots than WT plants (Fig. 14A). Trichomes on first true leaves had often two branches instead of three typical for WT (Fig. 14B, arrows). The main roots of plants overexpressing GFP-NSF differentiated ectopic root hairs (Fig. 14C, arrows). Supernumerous small vesicles were visible in cells of division zone of main root, while in some cells large vacuoles were present that abolished central position of nuclei typical for WT (Fig. 14D). Supernumerous vesicles were present in division, expansion and at the beginning of differentiation zone of the root of plants overexpressing GFP-NSF (Fig. 14E, F). All together the data from gain-of-function phenotype suggest that overexpression of NSF resulted in impaired membrane trafficking and therefore cell polarity defects.

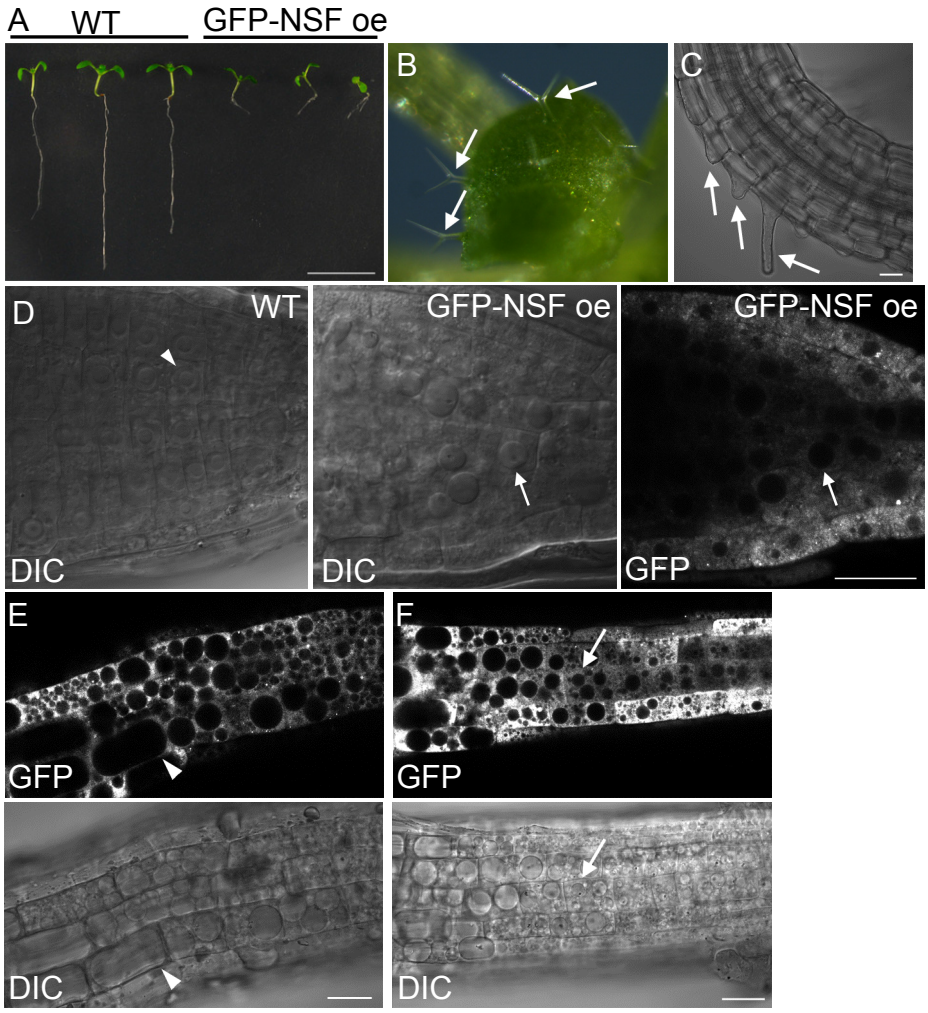

Fig. 14: Phenotype of *Arabidopsis* plants overexpressing GFP-NSF

(A) 13-d-old plants of GFP-NSF oe with shortened roots in comparison with WT. Bar 1 cm. (B) Two-branched trichomes in plant overexpressing GFP-NSF (arrows). (C) Ectopic root hairs in plant overexpressing GFP-NSF (arrows). (D) Nuclei in cell of division zone near to the root tip in WT (arrowhead). Large vesicle in cell of division zone near to the root tip in plant overexpressing GFP-NSF (arrow) and supernumerous small vesicles. (E) Differentiation and expansion zone of root of plant overexpressing GFP-NSF with cells with supernumerous vesicles. Older differentiated cell had already one large vacuole with GFP-NSF still in cytoplasm (arrowhead). (F) Expansion and division zone with cells with smaller and bigger vesicles. The cell with several smaller vesicles (arrow). (C-F) Bar 20 µm.

We further prepared dsRNA constructs to downregulate NSF in *Arabidopsis* plants. For RNAi hairpin under constitutive 35S CaMV promoter, we used ~ 500 bp fragments from N-terminal part of NSF coding sequence; RNAi hairpin construct was prepared by classical cloning of the fragments to vector pHANNIBAL [216]. The whole hairpin excised from pHANNIBAL was then inserted to binary vector pART27 [217] with 35S CaMV promoter (here as 35S NSF-RNAi). We also prepared RNAi hairpin under inducible promoter triggered by dexamethasone to be able to study RNAi phenotype of NSF protein later in plant development especially if NSF would be essential gene as expected and phenotype of plants with NSF-RNAi expressed under 35S CaMV promoter (35S NSF-RNAi plants) would be lethal. We used two different fragments from NSF coding sequence, one near to the N-terminus and the second near to the C-terminus of NSF by PCR and using gateway technology we prepared dsRNA construct for NSF in binary vector pOpOffHyg2 [218] under inducible dexamethasone promoter (here as NSF-RNAi). We transformed dsRNA constructs for NSF downregulation through *Agrobacterium tumefaciens* into *Arabidopsis* plants and selected seedlings from T1 generation. Unfortunately, frequence of transformation for dsRNA construct 35S NSF-RNAi was extremely low.

Arabidopsis NSF-RNAi plants had shortened main roots compared to WT after induction by dexamethasone (Fig. 15A) and died after three weeks post germination. Main roots of NSF-RNAi plants were often bulged with root hairs differentiated near to the root tip (Fig. 15B, arrow). Polar growth of root hairs was impaired; root hairs with two axes (Fig. 15C, arrowheads) and with bulged bases (Fig. 15D, arrows) were observed. Plants 35S NSF-RNAi had also shortened main roots in comparison with WT (Fig. 15E); sometimes there were no true leaves after 16 days post germination although they were normally present in WT (Fig. 15F, arrow). When true leaves of 35S NSF-RNAi plants emerged, trichomes with two or four branches instead of three were often formed (Fig. 15G, H). Strong phenotypes had impaired roots with swollen enlarged cells (Fig. 15I, arrowhead). There were large vesicles in root cells of 35S NSF-RNAi plants in comparison with WT (Fig. 15I, J, arrows). Phenotypes of plants with downregulated NSF suggested that lack of NSF caused impaired cell division and polar growth.

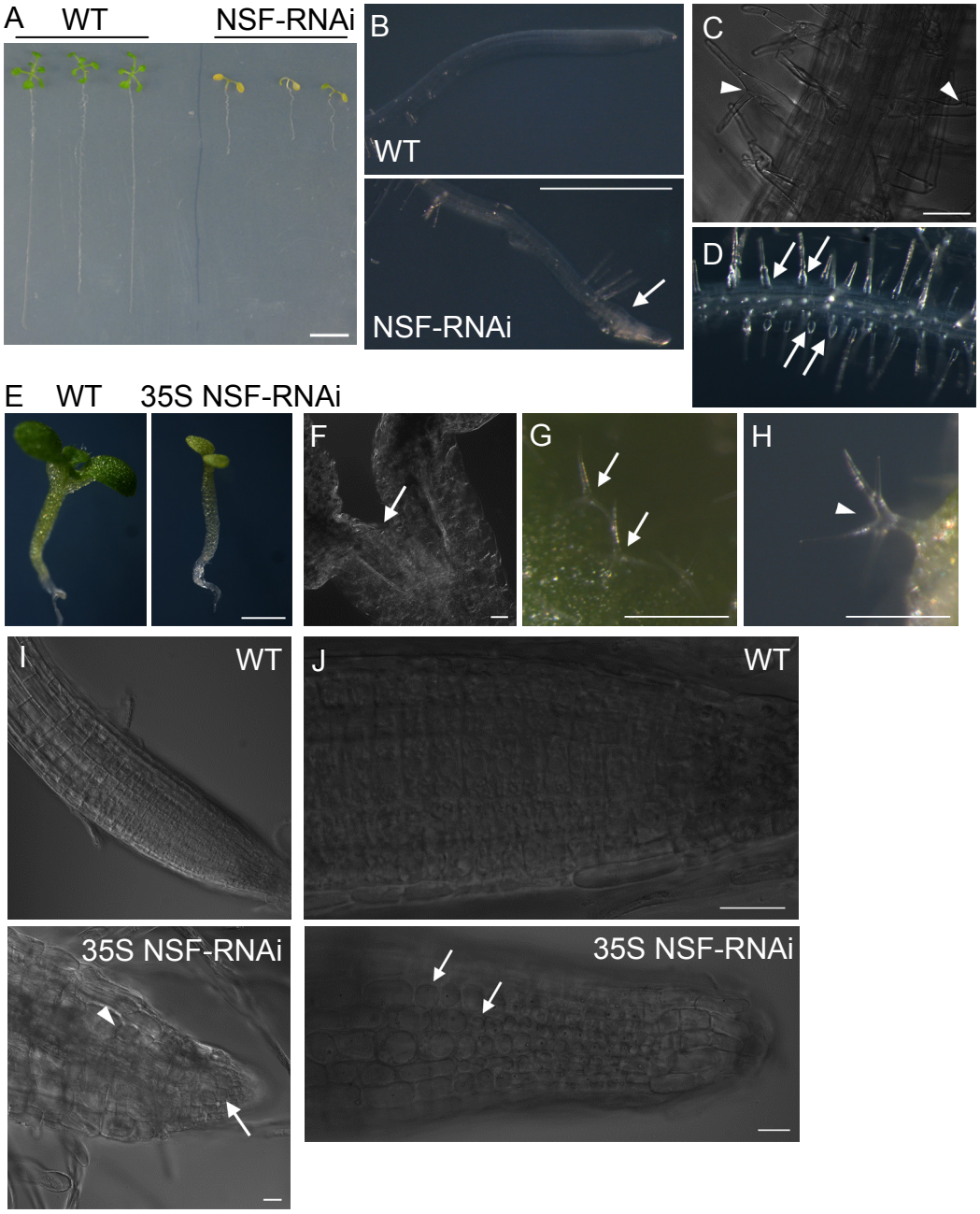

Fig. 15: Phenotype of *Arabidopsis* plants with downregulated NSF

(A-D) Plants with NSF-RNAi under inducible promoter (A) 21-d-old plants NSF-RNAi after 13 days on dexamethasone had shorter roots than WT plants. Bar 1 cm. (B) Bulged root tip of NSF-RNAi plant (arrow); root hairs nearer to the root tip compared to WT plants. Bar 0.5 cm. (C) Two-axed root hairs on main root of NSF-RNAi plant (arrowheads). Bar 50 µm. (D) Bulged bases of root hairs of NSF-RNAi plant (arrows). (E-J) Plants with NSF-RNAi under constitutive 35S CaMV promoter (E) 10-d-old 35S NSF-RNAi in comparison with WT. Bar

1 mm. (F) Shoot apex of 16-d-old 35S NSF-RNAi plant without emerging meristem. Bar 50 μm. (G) Trichomes with two branches (arrows) and (H) four branches (arrowhead) of 35S NSF-RNAi leave. (I) Extremely impaired main root of 10-d-old 35S NSF-RNAi plant with enlarged and swollen cells (arrowhead) and large vesicles (arrow) in comparison with WT main root. Bar 20 μm. (J) Large vesicles in main root of 35S NSF-RNAi (arrows) in comparison with WT. Bars 20 μm.

Further analyses will be performed to show microtubule organization and γ-tubulin localization in plants with downregulated NSF. Furthermore, we will transform GFP-NSF under its native promoter to plants to follow dynamics of NSF in seedlings and its colocalization with γ-tubulin.

We showed biochemically and microscopically that NSF is present on microtubules and with membranes where it probably interacts with γ-tubulin. NSF formed large complexes and also complexes corresponding to its hexamers. Our data suggest an important role of NSF in polar growth and cell division.

In this project I performed cloning, prepared stable lines of Arabidopsis cultured cells and plants. I analysed phenotypes of RNAi plants and gain-of-function plants. I also performed microscopical analyses of NSF localization. I performed immunoprecipitations and blue native electrophoreses. I also contributed to designing of experiments and writing of manuscript under preparation where I will be first author.

5. CONCLUSIONS

Results of this Ph.D. thesis can be summarized as follows:

We found RanBPM homologue in *Arabidopsis thaliana*. We showed that AtRanBPM is present as a member of cytoplasmic complexes of ~ 230 – 500 kDa consisting of several proteins with conserved domains. By identifying the members of the complexes we showed that CTLH complexes are conserved not only between yeast and mammals but also in plants. Our results suggest other than nucleation role for RanBPM homologue in plants. Similarly to other eukaryotes, CTLH complexes might provide a platform for signalling.

We characterized functions of NITRILASE1 as a negative regulator of the cell cycle in *Arabidopsis*. NITRILASE1 is essential for maintenance of genome stability as it is needed for exit from proliferation and entry into differentiation and for proper cytokinesis in the plant cells. Our data suggest that NITRILASE1 function in the cell cycle and programmed cell death is conserved in animals and plants.

Overexpression of AtTPX2-GFP resulted in formation of ectopic microtubular arrays decorated by AtTPX2 in the nuclei and in the perinuclear area in *Arabidopsis* cells. We proved physical interaction of endogenous plant importin and AtTPX2-GFP. Our data suggest involvement of Ran-dependent importin pathway in regulation of TPX2-dependent microtubule formation and/or organization in plants. We propose that AtTPX2 overexpression amplify an ability of chromatin and nuclear envelope to nucleate microtubules in plant acentrosomal cells.

We found that MAP kinase MPK6 is present with microtubules and interacts with γ-tubulin in *Arabidopsis*. The cell cycle specific localization pattern of MPK6 with γ-tubulin suggested their role in anaphase/telophase transition. Functional studies on *Arabidopsis* mutants suggested a role of MPK6 in spindle positioning and cell division and showed that MPK6 is crucial for regulation of microtubule organization under nitrosative stress.

We showed that a portion of NSF protein, AAA ATPase involved in recycling of SNARE complexes, is present with microtubules and with membranes in *Arabidopsis*. Furthermore, we found that NSF interacts with γ-tubulin. Downregulation of NSF and gain-of-function phenotype suggested a role of NSF in cell division and polar growth.

6. REFERENCES

1. Erickson H.P. (2007). Evolution of the cytoskeleton. *Bioessays* 29(7): 668-677.
2. Masuda K., Xu Z.J., Takahashi S., Ito A., Ono M., Nomura K., and Inoue M. (1997). Peripheral framework of carrot cell nucleus contains a novel protein predicted to exhibit a long alpha-helical domain. *Exp Cell Res* 232(1): 173-181.
3. Graumann K. (2014). Evidence for LINC1-SUN associations at the plant nuclear periphery. *PloS one* 9(3): e93406.
4. Gundersen G.G., and Cook T.A. (1999). Microtubules and signal transduction. *Curr Opin Cell Biol* 11(1): 81-94.
5. Brandizzi F., and Wasteneys G.O. (2013). Cytoskeleton-dependent endomembrane organization in plant cells: an emerging role for microtubules. *Plant J: Cell Mol Biol* 75(2): 339-349.
6. Ambrose C., and Wasteneys G.O. (2014). Microtubule Initiation from the Nuclear Surface Controls Cortical Microtubule Growth Polarity and Orientation in Arabidopsis thaliana. *Plant & cell physiology* 55(9): 1636-1645.
7. Rasmussen C.G., Wright A.J., and Muller S. (2013). The role of the cytoskeleton and associated proteins in determination of the plant cell division plane. *Plant J: Cell Mol Biol* 75(2): 258-269.
8. Wade R.H. (2009). On and around microtubules: an overview. *Mol Biotechnol* 43(2): 177-191.
9. Evans L., Mitchison T., and Kirschner M. (1985). Influence of the centrosome on the structure of nucleated microtubules. *J Cell Biol* 100(4): 1185-1191.
10. McIntosh J.R., Morphew M.K., Grissom P.M., Gilbert S.P., and Hoenger A. (2009). Lattice structure of cytoplasmic microtubules in a cultured Mammalian cell. *J Mol Biol* 394(2): 177-182.
11. Amos L., and Klug A. (1974). Arrangement of subunits in flagellar microtubules. *J Cell Sci* 14(3): 523-549.
12. Nogales E., Whittaker M., Milligan R.A., and Downing K.H. (1999). High-resolution model of the microtubule. *Cell* 96(1): 79-88.
13. Kollman J.M., Merdes A., Mourey L., and Agard D.A. (2011). Microtubule nucleation by gamma-tubulin complexes. *Nat Rev Mol Cell Biol* 12(11): 709-721.
14. Horio T., and Hotani H. (1986). Visualization of the dynamic instability of individual microtubules by dark-field microscopy. *Nature* 321(6070): 605-607.
15. Bergen L.G., and Borisy G.G. (1980). Head-to-tail polymerization of microtubules in vitro. Electron microscope analysis of seeded assembly. *J Cell Biol* 84(1): 141-150.
16. Shaw S.L., Kamyar R., and Ehrhardt D.W. (2003). Sustained microtubule treadmilling in Arabidopsis cortical arrays. *Science* 300(5626): 1715-1718.
17. Hyman A.A., Salser S., Drechsel D.N., Unwin N., and Mitchison T.J. (1992). Role of GTP hydrolysis in microtubule dynamics: information from a slowly hydrolyzable analogue, GMPCPP. *Mol Biol Cell* 3(10): 1155-1167.
18. Maurer S.P., Cade N.I., Bohner G., Gustafsson N., Boutant E., and Surrey T. (2014). EB1 accelerates two conformational transitions important for microtubule maturation and dynamics. *Current biology* 24(4): 372-384.
19. Schulze E., and Kirschner M. (1986). Microtubule dynamics in interphase cells. *J Cell Biol* 102(3): 1020-1031.
20. Luduena R.F. (2013). A hypothesis on the origin and evolution of tubulin. *Int Rev Cell Mol Biol* 302: 41-185.
21. Smertenko A., Blume Y., Viklicky V., Opatrny Z., and Draber P. (1997). Post-translational modifications and multiple tubulin isoforms in Nicotiana tabacum L. cells. *Planta* 201(3): 349-358.
22. Yoshikawa M., Yang G., Kawaguchi K., and Komatsu S. (2003). Expression analyses of beta-tubulin isotype genes in rice. *Plant Cell Physiol* 44(11): 1202-1207.

23. Janke C. (2014). The tubulin code: molecular components, readout mechanisms, and functions. *J Cell Biol* 206(4): 461-472.
24. Wang W., Vignani R., Scali M., Sensi E., and Cresti M. (2004). Post-translational modifications of alpha-tubulin in Zea mays L are highly tissue specific. *Planta* 218(3): 460-465.
25. Blume Y.B., Krasylenko Y.A., Demchuk O.M., and Yemets A.I. (2013). Tubulin tyrosine nitration regulates microtubule organization in plant cells. *Frontiers in plant science* 4: 530.
26. Lipka E., and Muller S. (2014). Nitrosative stress triggers microtubule reorganization in Arabidopsis thaliana. *J Exp Botany* 65(15): 4177-4189.
27. Hamada T. (2014). Microtubule organization and microtubule-associated proteins in plant cells. *Int Rev Cell Mol Biol* 312: 1-52.
28. Fong K.W., Hau S.Y., Kho Y.S., Jia Y., He L., and Qi R.Z. (2009). Interaction of CDK5RAP2 with EB1 to track growing microtubule tips and to regulate microtubule dynamics. *Mol Biol Cell* 20(16): 3660-3670.
29. Bisgrove S.R., Lee Y.R., Liu B., Peters N.T., and Kropf D.L. (2008). The microtubule plus-end binding protein EB1 functions in root responses to touch and gravity signals in Arabidopsis. *Plant Cell* 20(2): 396-410.
30. Chan J., Calder G., Fox S., and Lloyd C. (2005). Localization of the microtubule end binding protein EB1 reveals alternative pathways of spindle development in Arabidopsis suspension cells. *Plant Cell* 17(6): 1737-1748.
31. Komaki S., Abe T., Coutuer S., Inze D., Russinova E., and Hashimoto T. (2010). Nuclear-localized subtype of end-binding 1 protein regulates spindle organization in Arabidopsis. *J Cell Sci* 123(Pt 3): 451-459.
32. Bouissou A., Verollet C., de Forges H., Haren L., Bellaiche Y., Perez F., Merdes A., and Raynaud-Messina B. (2014). gamma-Tubulin Ring Complexes and EB1 play antagonistic roles in microtubule dynamics and spindle positioning. *EMBO J* 33(2): 114-128.
33. Rogers G.C., Rusan N.M., Peifer M., and Rogers S.L. (2008). A multicomponent assembly pathway contributes to the formation of acentrosomal microtubule arrays in interphase Drosophila cells. *Mol Biol Cell* 19(7): 3163-3178.
34. Bouissou A., Verollet C., Sousa A., Sampaio P., Wright M., Sunkel C.E., Merdes A., and Raynaud-Messina B. (2009). {gamma}-Tubulin ring complexes regulate microtubule plus end dynamics. *J Cell Biol* 187(3): 327-334.
35. Anders A., and Sawin K.E. (2011). Microtubule stabilization in vivo by nucleation-incompetent gamma-tubulin complex. *J Cell Sci* 124(Pt 8): 1207-1213.
36. Zhang H., and Dawe R.K. (2011). Mechanisms of plant spindle formation. *Chromosome Res* 19(3): 335-344.
37. Gardiner J.C., Harper J.D., Weerakoon N.D., Collings D.A., Ritchie S., Gilroy S., Cyr R.J., and Marc J. (2001). A 90-kD phospholipase D from tobacco binds to microtubules and the plasma membrane. *Plant Cell* 13(9): 2143-2158.
38. Ambrose J.C., and Wasteneys G.O. (2008). CLASP modulates microtubule-cortex interaction during self-organization of acentrosomal microtubules. *Mol Biol Cell* 19(11): 4730-4737.
39. Ambrose C., Allard J.F., Cytrynbaum E.N., and Wasteneys G.O. (2011). A CLASP-modulated cell edge barrier mechanism drives cell-wide cortical microtubule organization in Arabidopsis. *Nature communications* 2: 430.
40. Hussey P.J., Hawkins T.J., Igarashi H., Kaloriti D., and Smertenko A. (2002). The plant cytoskeleton: recent advances in the study of the plant microtubule-associated proteins MAP-65, MAP-190 and the Xenopus MAP215-like protein, MOR1. *Plant Mol Biol* 50(6): 915-924.
41. Portran D., Zoccoler M., Gaillard J., Stoppin-Mellet V., Neumann E., Arnal I., Martiel J.L., and Vantard M. (2013). MAP65/Ase1 promote microtubule flexibility. *Mol Biol Cell* 24(12): 1964-1973.

42. Fache V., Gaillard J., Van Damme D., Geelen D., Neumann E., Stoppin-Mellet V., and Vantard M. (2010). Arabidopsis kinetochore fiber-associated MAP65-4 cross-links microtubules and promotes microtubule bundle elongation. *Plant Cell* 22(11): 3804-3815.
43. Muller S., Smertenko A., Wagner V., Heinrich M., Hussey P.J., and Hauser M.T. (2004). The plant microtubule-associated protein AtMAP65-3/PLE is essential for cytokinetic phragmoplast function. *Curr Biol* 14(5): 412-417.
44. Ho C.M., Hotta T., Guo F., Roberson R.W., Lee Y.R., and Liu B. (2011). Interaction of antiparallel microtubules in the phragmoplast is mediated by the microtubule-associated protein MAP65-3 in Arabidopsis. *Plant Cell* 23(8): 2909-2923.
45. Wittmann T., Boleti H., Antony C., Karsenti E., and Vernos I. (1998). Localization of the kinesin-like protein Xklp2 to spindle poles requires a leucine zipper, a microtubule-associated protein, and dynein. *J Cell Biol* 143(3): 673-685.
46. Kufer T.A., Sillje H.H., Korner R., Gruss O.J., Meraldi P., and Nigg E.A. (2002). Human TPX2 is required for targeting Aurora-A kinase to the spindle. *J Cell Biol* 158(4): 617-623.
47. Gruss O.J., Carazo-Salas R.E., Schatz C.A., Guarguaglini G., Kast J., Wilm M., Le Bot N., Vernos I., Karsenti E., and Mattaj I.W. (2001). Ran Induces Spindle Assembly by Reversing the Inhibitory Effect of Importin alpha on TPX2 Activity. *Cell* 104(1): 83-93.
48. Zorba A., Buosi V., Kutter S., Kern N., Pontiggia F., Cho Y.J., and Kern D. (2014). Molecular mechanism of Aurora A kinase autophosphorylation and its allosteric activation by TPX2. *eLife* 3: e02667.
49. Iyer J., and Tsai M.Y. (2012). A novel role for TPX2 as a scaffold and co-activator protein of the Chromosomal Passenger Complex. *Cellular signalling* 24(8): 1677-1689.
50. Petrovska B., Cenklova V., Pochylova Z., Kourova H., Doskocilova A., Plihal O., Binarova L., and Binarova P. (2012). Plant Aurora kinases play a role in maintenance of primary meristems and control of endoreduplication. *New Phytol* 193(3): 590-604.
51. Matsuoka S., Ballif B.A., Smogorzewska A., McDonald E.R., 3rd, Hurov K.E., Luo J., Bakalarski C.E., Zhao Z., Solimini N., Lerenthal Y., et al. (2007). ATM and ATR substrate analysis reveals extensive protein networks responsive to DNA damage. *Science* 316(5828): 1160-1166.
52. Neumayer G., Helfricht A., Shim S.Y., Le H.T., Lundin C., Belzil C., Chansard M., Yu Y., Lees-Miller S.P., Gruss O.J., et al. (2012). Targeting protein for xenopus kinesin-like protein 2 (TPX2) regulates gamma-histone 2AX (gamma-H2AX) levels upon ionizing radiation. *J Biol Chem* 287(50): 42206-42222.
53. Schatz C.A., Santarella R., Hoenger A., Karsenti E., Mattaj I.W., Gruss O.J., and Carazo-Salas R.E. (2003). Importin alpha-regulated nucleation of microtubules by TPX2. *Embo J* 22(9): 2060-2070.
54. Brunet S., Sardon T., Zimmerman T., Wittmann T., Pepperkok R., Karsenti E., and Vernos I. (2004). Characterization of the TPX2 domains involved in microtubule nucleation and spindle assembly in Xenopus egg extracts. *Mol Biol Cell* 15(12): 5318-5328.
55. Morrissette N.S., Mitra A., Sept D., and Sibley L.D. (2004). Dinitroanilines bind alpha-tubulin to disrupt microtubules. *Mol Biol Cell* 15(4): 1960-1968.
56. Snyder J.P., Nettles J.H., Cornett B., Downing K.H., and Nogales E. (2001). The binding conformation of Taxol in beta-tubulin: a model based on electron crystallographic density. *PNAS* 98(9): 5312-5316.
57. Murthy J.V., Kim H.H., Hanesworth V.R., Hugdahl J.D., and Morejohn L.C. (1994). Competitive Inhibition of High-Affinity Oryzalin Binding to Plant Tubulin by the Phosphoric Amide Herbicide Amiprophos-Methyl. *Plant Physiology* 105(1): 309-320.
58. Hashimoto T. (2013). A ring for all: gamma-tubulin-containing nucleation complexes in acentrosomal plant microtubule arrays. *Current opinion in plant biology* 16(6): 698-703.

59. Wiese C., and Zheng Y. (2006). Microtubule nucleation: gamma-tubulin and beyond. *J Cell Sci* 119(Pt 20): 4143-4153.
60. Drykova D., Cenklova V., Sulimenko V., Volc J., Draber P., and Binarova P. (2003). Plant gamma-tubulin interacts with alphabeta-tubulin dimers and forms membrane-associated complexes. *Plant Cell* 15(2): 465-480.
61. Schatten H., and Sun Q.Y. (2011). Centrosome dynamics during mammalian oocyte maturation with a focus on meiotic spindle formation. *Mol Reprod Dev* 78(10-11): 757-768.
62. Bartolini F., and Gundersen G.G. (2006). Generation of noncentrosomal microtubule arrays. *J Cell Sci* 119(Pt 20): 4155-4163.
63. Oakley C.E., and Oakley B.R. (1989). Identification of gamma-tubulin, a new member of the tubulin superfamily encoded by mipA gene of Aspergillus nidulans. *Nature* 338(6217): 662-664.
64. Aldaz H., Rice L.M., Stearns T., and Agard D.A. (2005). Insights into microtubule nucleation from the crystal structure of human gamma-tubulin. *Nature* 435(7041): 523-527.
65. Oakley B.R. (2000). gamma-Tubulin. *Curr Top Dev Biol* 49: 27-54.
66. Vinopal S., Cernohorska M., Sulimenko V., Sulimenko T., Vosecka V., Flemr M., Draberova E., and Draber P. (2012). gamma-Tubulin 2 nucleates microtubules and is downregulated in mouse early embryogenesis. *PloS one* 7(1): e29919.
67. Liu B., Joshi H.C., Wilson T.J., Silflow C.D., Palevitz B.A., and Snustad D.P. (1994). gamma-Tubulin in Arabidopsis: gene sequence, immunoblot, and immunofluorescence studies. *Plant Cell* 6(2): 303-314.
68. Pastuglia M., Azimzadeh J., Goussot M., Camilleri C., Belcram K., Evrard J.L., Schmit A.C., Guerche P., and Bouchez D. (2006). Gamma-tubulin is essential for microtubule organization and development in Arabidopsis. *Plant Cell* 18(6): 1412-1425.
69. Job D., Valiron O., and Oakley B. (2003). Microtubule nucleation. *Curr Opin Cell Biol* 15(1): 111-117.
70. Binarova P., Cenklova V., Prochazkova J., Doskocilova A., Volc J., Vrlik M., and Bogre L. (2006). Gamma-tubulin is essential for acentrosomal microtubule nucleation and coordination of late mitotic events in Arabidopsis. *Plant Cell* 18(5): 1199-1212.
71. Hannak E., Oegema K., Kirkham M., Gonczy P., Habermann B., and Hyman A.A. (2002). The kinetically dominant assembly pathway for centrosomal asters in Caenorhabditis elegans is gamma-tubulin dependent. *J Cell Biol* 157(4): 591-602.
72. Hotta T., Haraguchi T., and Mizuno K. (2007). A novel function of plant histone H1: microtubule nucleation and continuous plus end association. *Cell Struct Funct* 32(2): 79-87.
73. Nakayama T., Ishii T., Hotta T., and Mizuno K. (2008). Radial microtubule organization by histone H1 on nuclei of cultured tobacco BY-2 cells. *J Biol Chem* 283(24): 16632-16640.
74. Petry S., Groen A.C., Ishihara K., Mitchison T.J., and Vale R.D. (2013). Branching microtubule nucleation in Xenopus egg extracts mediated by augmin and TPX2. *Cell* 152(4): 768-777.
75. Zheng Y., Jung M.K., and Oakley B.R. (1991). Gamma-tubulin is present in Drosophila melanogaster and Homo sapiens and is associated with the centrosome. *Cell* 65(5): 817-823.
76. Moudjou M., Bordes N., Paintrand M., and Bornens M. (1996). gamma-Tubulin in mammalian cells: the centrosomal and the cytosolic forms. *J Cell Sci* 109(Pt 4): 875-887.
77. Lesca C., Germanier M., Raynaud-Messina B., Pichereaux C., Etievant C., Emond S., Burlet-Schiltz O., Monsarrat B., Wright M., and Defais M. (2005). DNA damage induce gamma-tubulin-RAD51 nuclear complexes in mammalian cells. *Oncogene* 24(33): 5165-5172.
78. Eklund G., Lang S., Glindre J., Ehlen A., and Alvarado-Kristensson M. (2014). The nuclear localization of gamma-tubulin is regulated by SadB-mediated phosphorylation. *J Biol Chem* 289(31): 21360-21373.
79. Horejsi B., Vinopal S., Sladkova V., Draberova E., Sulimenko V., Sulimenko T., Vosecka V., Philimonenko A., Hozak P., Katsetos C.D., et al. (2012). Nuclear gamma-tubulin associates with nucleoli and interacts with tumor suppressor protein C53. *J Cell Physiol* 227(1): 367-382.

80. Lajoie-Mazenc I., Tollon Y., Detraves C., Julian M., Moisand A., Gueth-Hallonet C., Debec A., Salles-Passador I., Puget A., Mazarguil H., et al. (1994). Recruitment of antigenic gamma-tubulin during mitosis in animal cells: presence of gamma-tubulin in the mitotic spindle. *J Cell Sci* 107(Pt 10): 2825-2837.
81. Lecland N., and Luders J. (2014). The dynamics of microtubule minus ends in the human mitotic spindle. *Nature cell biology* 16(8): 770-778.
82. Liu B., Marc J., Joshi H.C., and Palevitz B.A. (1993). A gamma-tubulin-related protein associated with the microtubule arrays of higher plants in a cell cycle-dependent manner. *J Cell Sci* 104(Pt 4): 1217-1228.
83. Binarova P., Cenklova V., Hause B., Kubatova E., Lysak M., Dolezel J., Bogre L., and Draber P. (2000). Nuclear gamma-tubulin during acentriolar plant mitosis. *Plant Cell* 12(3): 433-442.
84. Teixido-Travesa N., Roig J., and Luders J. (2012). The where, when and how of microtubule nucleation - one ring to rule them all. *J Cell Sci* 125(Pt 19): 4445-4456.
85. Kollman J.M., Zelter A., Muller E.G., Fox B., Rice L.M., Davis T.N., and Agard D.A. (2008). The structure of the gamma-tubulin small complex: implications of its architecture and flexibility for microtubule nucleation. *Mol Biol Cell* 19(1): 207-215.
86. Kollman J.M., Polka J.K., Zelter A., Davis T.N., and Agard D.A. (2010). Microtubule nucleating gamma-TuSC assembles structures with 13-fold microtubule-like symmetry. *Nature* 466(7308): 879-882.
87. Zheng Y., Wong M.L., Alberts B., and Mitchison T. (1995). Nucleation of microtubule assembly by a gamma-tubulin-containing ring complex. *Nature* 378(6557): 578-583.
88. Oegema K., Wiese C., Martin O.C., Milligan R.A., Iwamatsu A., Mitchison T.J., and Zheng Y. (1999). Characterization of two related Drosophila gamma-tubulin complexes that differ in their ability to nucleate microtubules. *J Cell Biol* 144(4): 721-733.
89. Murphy S.M., Preble A.M., Patel U.K., O'Connell K.L., Dias D.P., Moritz M., Agard D., Stults J.T., and Stearns T. (2001). GCP5 and GCP6: two new members of the human gamma-tubulin complex. *Mol Biol Cell* 12(11): 3340-3352.
90. Verollet C., Colombie N., Daubon T., Bourbon H.M., Wright M., and Raynaud-Messina B. (2006). Drosophila melanogaster gamma-TuRC is dispensable for targeting gamma-tubulin to the centrosome and microtubule nucleation. *J Cell Biol* 172(4): 517-528.
91. Guillet V., Knibiehler M., Gregory-Pauron L., Remy M.H., Chemin C., Raynaud-Messina B., Bon C., Kollman J.M., Agard D.A., Merdes A., et al. (2011). Crystal structure of gamma-tubulin complex protein GCP4 provides insight into microtubule nucleation. *Nat Struct Mol Biol* 18(8): 915-919.
92. Erhardt M., Stoppin-Mellet V., Campagne S., Canaday J., Mutterer J., Fabian T., Sauter M., Muller T., Peter C., Lambert A.M., et al. (2002). The plant Spc98p homologue colocalizes with gamma-tubulin at microtubule nucleation sites and is required for microtubule nucleation. *J Cell Sci* 115(Pt 11): 2423-2431.
93. Nakamura M., and Hashimoto T. (2009). A mutation in the Arabidopsis gamma-tubulin-containing complex causes helical growth and abnormal microtubule branching. *J Cell Sci* 122(Pt 13): 2208-2217.
94. Nakamura M., Ehrhardt D.W., and Hashimoto T. (2010). Microtubule and katanin-dependent dynamics of microtubule nucleation complexes in the acentrosomal Arabidopsis cortical array. *Nat Cell Biol* 12(11): 1064-1070.
95. Nakamura M., Yagi N., Kato T., Fujita S., Kawashima N., Ehrhardt D.W., and Hashimoto T. (2012). Arabidopsis GCP3-interacting protein 1/MOZART 1 is an integral component of the gamma-tubulin-containing microtubule nucleating complex. *Plant J: for cell and molecular biology* 71(2): 216-225.
96. Janski N., Masoud K., Batzenschlager M., Herzog E., Evrard J.L., Houlne G., Bourge M., Chaboute M.E., and Schmit A.C. (2012). The GCP3-interacting proteins GIP1 and GIP2 are

required for gamma-tubulin complex protein localization, spindle integrity, and chromosomal stability. *Plant Cell* 24(3): 1171-1187.
97. Batzenschlager M., Masoud K., Janski N., Houlne G., Herzog E., Evrard J.L., Baumberger N., Erhardt M., Nomine Y., Kieffer B., et al. (2013). The GIP gamma-tubulin complex-associated proteins are involved in nuclear architecture in Arabidopsis thaliana. *Frontiers in plant science* 4: 480.
98. Kong Z., Hotta T., Lee Y.R., Horio T., and Liu B. (2010). The {gamma}-tubulin complex protein GCP4 is required for organizing functional microtubule arrays in Arabidopsis thaliana. *Plant Cell* 22(1): 191-204.
99. Zeng C.J., Lee Y.R., and Liu B. (2009). The WD40 repeat protein NEDD1 functions in microtubule organization during cell division in Arabidopsis thaliana. *Plant Cell* 21(4): 1129-1140.
100. Stoppin-Mellet V., Peter C., and Lambert A.M. (2000). Distribution of gamma-tubulin in higher plant cells: Cytosolic gamma-tubulin is part of high molecular weight complexes. *Plant Biology* 2(3): 290-296.
101. Seltzer V., Janski N., Canaday J., Herzog E., Erhardt M., Evrard J.L., and Schmit A.C. (2007). Arabidopsis GCP2 and GCP3 are part of a soluble gamma-tubulin complex and have nuclear envelope targeting domains. *Plant J* 52(2): 322-331.
102. Goshima G., Mayer M., Zhang N., Stuurman N., and Vale R.D. (2008). Augmin: a protein complex required for centrosome-independent microtubule generation within the spindle. *J Cell Biol* 181(3): 421-429.
103. Ho C.M., Hotta T., Kong Z., Zeng C.J., Sun J., Lee Y.R., and Liu B. (2011). Augmin plays a critical role in organizing the spindle and phragmoplast microtubule arrays in Arabidopsis. *Plant Cell* 23(7): 2606-2618.
104. Hotta T., Kong Z., Ho C.M., Zeng C.J., Horio T., Fong S., Vuong T., Lee Y.R., and Liu B. (2012). Characterization of the Arabidopsis augmin complex uncovers its critical function in the assembly of the acentrosomal spindle and phragmoplast microtubule arrays. *Plant Cell* 24(4): 1494-1509.
105. Wang Z., Wu T., Shi L., Zhang L., Zheng W., Qu J.Y., Niu R., and Qi R.Z. (2010). Conserved motif of CDK5RAP2 mediates its localization to centrosomes and the Golgi complex. *Biol Chem* 285(29): 22658-22665.
106. Fong K.W., Choi Y.K., Rattner J.B., and Qi R.Z. (2008). CDK5RAP2 is a pericentriolar protein that functions in centrosomal attachment of the gamma-tubulin ring complex. *Mol Biol Cell* 19(1): 115-125.
107. Choi Y.K., Liu P., Sze S.K., Dai C., and Qi R.Z. (2010). CDK5RAP2 stimulates microtubule nucleation by the gamma-tubulin ring complex. *J Cell Biol* 191(6): 1089-1095.
108. Olmsted Z.T., Riehlman T.D., Branca C.N., Colliver A.G., Cruz L.O., and Paluh J.L. (2013). Kinesin-14 Pkl1 targets gamma-tubulin for release from the gamma-tubulin ring complex (gamma-TuRC). *Cell cycle* 12(5): 842-848.
109. Olmsted Z.T., Colliver A.G., Riehlman T.D., and Paluh J.L. (2014). Kinesin-14 and kinesin-5 antagonistically regulate microtubule nucleation by gamma-TuRC in yeast and human cells. *Nature communications* 5: 5339.
110. Raynaud-Messina B., and Merdes A. (2007). Gamma-tubulin complexes and microtubule organization. *Curr Opin Cell Biol* 19(1): 24-30.
111. Erlemann S., Neuner A., Gombos L., Gibeaux R., Antony C., and Schiebel E. (2012). An extended gamma-tubulin ring functions as a stable platform in microtubule nucleation. *J Cell Biol* 197(1): 59-74.
112. Murata T., Sonobe S., Baskin T.I., Hyodo S., Hasezawa S., Nagata T., Horio T., and Hasebe M. (2005). Microtubule-dependent microtubule nucleation based on recruitment of gamma-tubulin in higher plants. *Nat Cell Biol* 7(10): 961-968.

113. Khodjakov A., Cole R.W., Oakley B.R., and Rieder C.L. (2000). Centrosome-independent mitotic spindle formation in vertebrates. *Curr Biol* 10(2): 59-67.
114. Janson M.E., Setty T.G., Paoletti A., and Tran P.T. (2005). Efficient formation of bipolar microtubule bundles requires microtubule-bound gamma-tubulin complexes. *J Cell Biol* 169(2): 297-308.
115. Kamasaki T., O'Toole E., Kita S., Osumi M., Usukura J., McIntosh J.R., and Goshima G. (2013). Augmin-dependent microtubule nucleation at microtubule walls in the spindle. *J Cell Biol* 202(1): 25-33.
116. Petry S., Pugieux C., Nedelec F.J., and Vale R.D. (2011). Augmin promotes meiotic spindle formation and bipolarity in Xenopus egg extracts. *PNAS* 108(35): 14473-14478.
117. Chan J., Sambade A., Calder G., and Lloyd C. (2009). Arabidopsis cortical microtubules are initiated along, as well as branching from, existing microtubules. *Plant Cell* 21(8): 2298-2306.
118. Kirik A., Ehrhardt D.W., and Kirik V. (2012). TONNEAU2/FASS regulates the geometry of microtubule nucleation and cortical array organization in interphase Arabidopsis cells. *Plant Cell* 24(3): 1158-1170.
119. Rios R.M. (2014). The centrosome-Golgi apparatus nexus. *Philosophical transactions of the Royal Society of London. Series B, Biological sciences* 369(1650).
120. Chabin-Brion K., Marceiller J., Perez F., Settegrana C., Drechou A., Durand G., and Pous C. (2001). The golgi complex is a microtubule-organizing organelle. *Mol Biol Cell* 12(7): 2047-2060.
121. Oddoux S., Zaal K.J., Tate V., Kenea A., Nandkeolyar S.A., Reid E., Liu W., and Ralston E. (2013). Microtubules that form the stationary lattice of muscle fibers are dynamic and nucleated at Golgi elements. *J Cell Biol* 203(2): 205-213.
122. Efimov A., Kharitonov A., Efimova N., Loncarek J., Miller P.M., Andreyeva N., Gleeson P., Galjart N., Maia A.R., McLeod I.X., et al. (2007). Asymmetric CLASP-dependent nucleation of noncentrosomal microtubules at the trans-Golgi network. *Dev Cell* 12(6): 917-930.
123. Binarova P., Hause B., Dolezel J., and Draber P. (1998). Association of gamma-tubulin with kinetochore/centromeric region of plant chromosomes. *Plant Journal* 14(6): 751-757.
124. Yu H.G., Hiatt E.N., and Dawe R.K. (2000). The plant kinetochore. *Trends in plant science* 5(12): 543-547.
125. Maiato H., Rieder C.L., and Khodjakov A. (2004). Kinetochore-driven formation of kinetochore fibers contributes to spindle assembly during animal mitosis. *J Cell Biol* 167(5): 831-840.
126. Torosantucci L., De Luca M., Guarguaglini G., Lavia P., and Degrassi F. (2008). Localized RanGTP accumulation promotes microtubule nucleation at kinetochores in somatic mammalian cells. *Mol Biol Cell* 19(5): 1873-1882.
127. Mishra R.K., Chakraborty P., Arnaoutov A., Fontoura B.M., and Dasso M. (2010). The Nup107-160 complex and gamma-TuRC regulate microtubule polymerization at kinetochores. *Nat Cell Biol* 12(2): 164-169.
128. Roscioli E., Di Francesco L., Bolognesi A., Giubettini M., Orlando S., Harel A., Schinina M.E., and Lavia P. (2012). Importin-beta negatively regulates multiple aspects of mitosis including RANGAP1 recruitment to kinetochores. *J Cell Biol* 196(4): 435-450.
129. Bilbao-Cortes D., Hetzer M., Langst G., Becker P.B., and Mattaj I.W. (2002). Ran binds to chromatin by two distinct mechanisms. *Current biology* 12(13): 1151-1156.
130. Hayward D., and Wakefield J.G. (2014). Chromatin-mediated microtubule nucleation in Drosophila syncytial embryos. *Communicative & integrative biology* 7: e28512.
131. Dixit R., and Cyr R. (2004). Encounters between dynamic cortical microtubules promote ordering of the cortical array through angle-dependent modifications of microtubule behavior. *Plant Cell* 16(12): 3274-3284.
132. Roll-Mecak A., and Vale R.D. (2006). Making more microtubules by severing: a common theme of noncentrosomal microtubule arrays? *J Cell Biol* 175(6): 849-851.

133. Wasteneys G.O. (2002). Microtubule organization in the green kingdom: chaos or self-order? *J Cell Sci* 115(Pt 7): 1345-1354.
134. Hayashi T., Sano T., Kutsuna N., Kumagai-Sano F., and Hasezawa S. (2007). Contribution of anaphase B to chromosome separation in higher plant cells estimated by image processing. *Plant Cell Physiol* 48(10): 1509-1513.
135. Vos J.W., Pieuchot L., Evrard J.L., Janski N., Bergdoll M., de Ronde D., Perez L.H., Sardon T., Vernos I., and Schmit A.C. (2008). The plant TPX2 protein regulates prospindle assembly before nuclear envelope breakdown. *Plant Cell* 20(10): 2783-2797.
136. Masoud K., Herzog E., Chaboute M.E., and Schmit A.C. (2013). Microtubule nucleation and establishment of the mitotic spindle in vascular plant cells. *Plant J: for cell and molecular biology* 75(2): 245-257.
137. Azimzadeh J., Nacry P., Christodoulidou A., Drevensek S., Camilleri C., Amiour N., Parcy F., Pastuglia M., and Bouchez D. (2008). Arabidopsis TONNEAU1 proteins are essential for preprophase band formation and interact with centrin. *Plant Cell* 20(8): 2146-2159.
138. Camilleri C., Azimzadeh J., Pastuglia M., Bellini C., Grandjean O., and Bouchez D. (2002). The Arabidopsis TONNEAU2 gene encodes a putative novel protein phosphatase 2A regulatory subunit essential for the control of the cortical cytoskeleton. *Plant Cell* 14(4): 833-845.
139. Lipka E., and Muller S. (2012). Potential roles for Kinesins at the cortical division site. *Frontiers in plant science* 3: 158.
140. Xu X.M., Zhao Q., Rodrigo-Peiris T., Brkljacic J., He C.S., Muller S., and Meier I. (2008). RanGAP1 is a continuous marker of the Arabidopsis cell division plane. *PNAS* 105(47): 18637-18642.
141. Walker K.L., Muller S., Moss D., Ehrhardt D.W., and Smith L.G. (2007). Arabidopsis TANGLED identifies the division plane throughout mitosis and cytokinesis. *Curr Biol* 17(21): 1827-1836.
142. Malcos J.L., and Cyr R.J. (2011). An ungrouped plant kinesin accumulates at the preprophase band in a cell cycle-dependent manner. *Cytoskeleton* 68(4): 247-258.
143. Murata T., Sano T., Sasabe M., Nonaka S., Higashiyama T., Hasezawa S., Machida Y., and Hasebe M. (2013). Mechanism of microtubule array expansion in the cytokinetic phragmoplast. *Nature communications* 4: 1967.
144. Horio T., and Murata T. (2014). The role of dynamic instability in microtubule organization. *Frontiers in plant science* 5: 511.
145. Alvarado-Kristensson M., Rodriguez M.J., Silio V., Valpuesta J.M., and Carrera A.C. (2009). SADB phosphorylation of gamma-tubulin regulates centrosome duplication. *Nat Cell Biol* 11(9): 1081-1092.
146. Hoog G., Zarrizi R., von Stedingk K., Jonsson K., and Alvarado-Kristensson M. (2011). Nuclear localization of gamma-tubulin affects E2F transcriptional activity and S-phase progression. *Faseb J* 25(11): 3815-3827.
147. Ehlen A., Rossello C.A., von Stedingk K., Hoog G., Nilsson E., Pettersson H.M., Jirstrom K., and Alvarado-Kristensson M. (2012). Tumors with nonfunctional retinoblastoma protein are killed by reduced gamma-tubulin levels. *J Biol Chem* 287(21): 17241-17247.
148. Zhang S., Hemmerich P., and Grosse F. (2007). Centrosomal localization of DNA damage checkpoint proteins. *J Cell Biochem* 101(2): 451-465.
149. Hendrickson T.W., Yao J., Bhadury S., Corbett A.H., and Joshi H.C. (2001). Conditional Mutations in gamma-Tubulin Reveal Its Involvement in Chromosome Segregation and Cytokinesis. *Mol Biol Cell* 12(8): 2469-2481.
150. Prigozhina N.L., Oakley C.E., Lewis A.M., Nayak T., Osmani S.A., and Oakley B.R. (2004). gamma-tubulin plays an essential role in the coordination of mitotic events. *Mol Biol Cell* 15(3): 1374-1386.

151. Keck J.M., Jones M.H., Wong C.C., Binkley J., Chen D., Jaspersen S.L., Holinger E.P., Xu T., Niepel M., Rout M.P., et al. (2011). A cell cycle phosphoproteome of the yeast centrosome. *Science* 332(6037): 1557-1561.
152. Nayak T., Edgerton-Morgan H., Horio T., Xiong Y., De Souza C.P., Osmani S.A., and Oakley B.R. (2010). Gamma-tubulin regulates the anaphase-promoting complex/cyclosome during interphase. *J Cell Biol* 190(3): 317-330.
153. Mahadevaiyer S., Xu C., and Gumbiner B.M. (2007). Characterization of a 60S complex of the adenomatous polyposis coli tumor suppressor protein. *Biochim Biophys Acta* 1773(2): 120-130.
154. Cuschieri L., Miller R., and Vogel J. (2006). Gamma-tubulin is required for proper recruitment and assembly of Kar9-Bim1 complexes in budding yeast. *Mol Biol Cell* 17(10): 4420-4434.
155. Radulescu A.E., Mukherjee S., and Shields D. (2011). The Golgi protein p115 associates with gamma-tubulin and plays a role in Golgi structure and mitosis progression. *J Biol Chem* 286(24): 21915-21926.
156. Rios R.M., Sanchis A., Tassin A.M., Fedriani C., and Bornens M. (2004). GMAP-210 recruits gamma-tubulin complexes to cis-Golgi membranes and is required for Golgi ribbon formation. *Cell* 118(3): 323-335.
157. Thompson H.M., Cao H., Chen J., Euteneuer U., and McNiven M.A. (2004). Dynamin 2 binds gamma-tubulin and participates in centrosome cohesion. *Nat Cell Biol* 6(4): 335-342.
158. Grimm-Gunter E.M., Milbrandt M., Merkl B., Paulsson M., and Plomann M. (2008). PACSIN proteins bind tubulin and promote microtubule assembly. *Exp Cell Res* 314(10): 1991-2003.
159. Lehtonen S., Shah M., Nielsen R., Iino N., Ryan J.J., Zhou H., and Farquhar M.G. (2008). The endocytic adaptor protein ARH associates with motor and centrosomal proteins and is involved in centrosome assembly and cytokinesis. *Mol Biol Cell* 19(7): 2949-2961.
160. Cuif M.H., Possmayer F., Zander H., Bordes N., Jollivet F., Couedel-Courteille A., Janoueix-Lerosey I., Langsley G., Bornens M., and Goud B. (1999). Characterization of GAPCenA, a GTPase activating protein for Rab6, part of which associates with the centrosome. *Embo J* 18(7): 1772-1782.
161. Faitar S.L., Dabbeekeh J.T., Ranalli T.A., and Cowell J.K. (2005). EVI5 is a novel centrosomal protein that binds to alpha- and gamma-tubulin. *Genomics*.
162. Chen D., Xu W., He P., Medrano E.E., and Whiteheart S.W. (2001). Gaf-1, a gamma -SNAP-binding protein associated with the mitochondria. *J Biol Chem* 276(16): 13127-13135.
163. Macurek L., Draberova E., Richterova V., Sulimenko V., Sulimenko T., Draberova L., Markova V., and Draber P. (2008). Regulation of microtubule nucleation from membranes by complexes of membrane-bound gamma-tubulin with Fyn kinase and phosphoinositide 3-kinase. *Biochem J*.
164. Fulcher N., and Sablowski R. (2009). Hypersensitivity to DNA damage in plant stem cell niches. *PNAS* 106(49): 20984-20988.
165. Komaki S., and Sugimoto K. (2012). Control of the plant cell cycle by developmental and environmental cues. *Plant & cell physiology* 53(6): 953-964.
166. Galbraith D.W., Harkins K.R., and Knapp S. (1991). Systemic Endopolyploidy in Arabidopsis thaliana. *Plant Physiology* 96(3): 985-989.
167. Inagaki S., and Umeda M. (2011). Cell-cycle control and plant development. *Int Rev Cell Mol Biol* 291: 227-261.
168. Matsunaga S., Katagiri Y., Nagashima Y., Sugiyama T., Hasegawa J., Hayashi K., and Sakamoto T. (2013). New insights into the dynamics of plant cell nuclei and chromosomes. *Int Rev Cell Mol Biol* 305: 253-301.
169. Vogel J., Drapkin B., Oomen J., Beach D., Bloom K., and Snyder M. (2001). Phosphorylation of gamma-tubulin regulates microtubule organization in budding yeast. *Dev Cell* 1(5): 621-631.
170. Lin T.C., Gombos L., Neuner A., Sebastian D., Olsen J.V., Hrle A., Benda C., and Schiebel E. (2011). Phosphorylation of the yeast gamma-tubulin Tub4 regulates microtubule function. *PLoS ONE* 6(5): e19700.

171. Lin T.C., Neuner A., Schlosser Y.T., Scharf A.N., Weber L., and Schiebel E. (2014). Cell-cycle dependent phosphorylation of yeast pericentrin regulates gamma-TuSC-mediated microtubule nucleation. *eLife* 3: e02208.
172. Voss M., Campbell K., Saranzewa N., Campbell D.G., Hastie C.J., Peggie M.W., Martin-Granados C., Prescott A.R., and Cohen P.T. (2013). Protein phosphatase 4 is phosphorylated and inactivated by Cdk in response to spindle toxins and interacts with gamma-tubulin. *Cell cycle* 12(17): 2876-2887.
173. Stumpff J., Kellogg D.R., Krohne K.A., and Su T.T. (2005). Drosophila Wee1 interacts with members of the gammaTURC and is required for proper mitotic-spindle morphogenesis and positioning. *Curr Biol* 15(17): 1525-1534.
174. Colello D., Mathew S., Ward R., Pumiglia K., and LaFlamme S.E. (2012). Integrins regulate microtubule nucleating activity of centrosome through mitogen-activated protein kinase/extracellular signal-regulated kinase kinase/extracellular signal-regulated kinase (MEK/ERK) signaling. *J Biol Chem* 287(4): 2520-2530.
175. Mishra N.S., Tuteja R., and Tuteja N. (2006). Signaling through MAP kinase networks in plants. *Archives of biochemistry and biophysics* 452(1): 55-68.
176. Rasmussen M.W., Roux M., Petersen M., and Mundy J. (2012). MAP Kinase Cascades in Arabidopsis Innate Immunity. *Frontiers in plant science* 3: 169.
177. Andreasson E., and Ellis B. (2010). Convergence and specificity in the Arabidopsis MAPK nexus. *Trends in plant science* 15(2): 106-113.
178. Meister M., Tomasovic A., Banning A., and Tikkanen R. (2013). Mitogen-Activated Protein (MAP) Kinase Scaffolding Proteins: A Recount. *International journal of molecular sciences* 14(3): 4854-4884.
179. Sasabe M., and Machida Y. (2012). Regulation of organization and function of microtubules by the mitogen-activated protein kinase cascade during plant cytokinesis. *Cytoskeleton* 69(11): 913-918.
180. Sasabe M., Soyano T., Takahashi Y., Sonobe S., Igarashi H., Itoh T.J., Hidaka M., and Machida Y. (2006). Phosphorylation of NtMAP65-1 by a MAP kinase down-regulates its activity of microtubule bundling and stimulates progression of cytokinesis of tobacco cells. *Genes & development* 20(8): 1004-1014.
181. Smertenko A.P., Chang H.Y., Sonobe S., Fenyk S.I., Weingartner M., Bogre L., and Hussey P.J. (2006). Control of the AtMAP65-1 interaction with microtubules through the cell cycle. *J Cell Sci* 119(Pt 15): 3227-3237.
182. Hoehenwarter W., Thomas M., Nukarinen E., Egelhofer V., Rohrig H., Weckwerth W., Conrath U., and Beckers G.J. (2013). Identification of novel in vivo MAP kinase substrates in Arabidopsis thaliana through use of tandem metal oxide affinity chromatography. *Molecular & cellular proteomics : MCP* 12(2): 369-380.
183. Wang P., Du Y., Li Y., Ren D., and Song C.P. (2010). Hydrogen peroxide-mediated activation of MAP kinase 6 modulates nitric oxide biosynthesis and signal transduction in Arabidopsis. *Plant Cell* 22(9): 2981-2998.
184. Calderini O., Bogre L., Vicente O., Binarova P., Heberle-Bors E., and Wilson C. (1998). A cell cycle regulated MAP kinase with a possible role in cytokinesis in tobacco cells. *J Cell Sci* 111(Pt 20): 3091-3100.
185. Kosetsu K., Matsunaga S., Nakagami H., Colcombet J., Sasabe M., Soyano T., Takahashi Y., Hirt H., and Machida Y. (2010). The MAP kinase MPK4 is required for cytokinesis in Arabidopsis thaliana. *Plant Cell* 22(11): 3778-3790.
186. Wang H., Liu Y., Bruffett K., Lee J., Hause G., Walker J.C., and Zhang S. (2008). Haplo-insufficiency of MPK3 in MPK6 mutant background uncovers a novel function of these two MAPKs in Arabidopsis ovule development. *Plant Cell* 20(3): 602-613.

187. Hord C.L., Sun Y.J., Pillitteri L.J., Torii K.U., Wang H., Zhang S., and Ma H. (2008). Regulation of Arabidopsis early anther development by the mitogen-activated protein kinases, MPK3 and MPK6, and the ERECTA and related receptor-like kinases. *Molecular plant* 1(4): 645-658.
188. Wang H., Ngwenyama N., Liu Y., Walker J.C., and Zhang S. (2007). Stomatal development and patterning are regulated by environmentally responsive mitogen-activated protein kinases in Arabidopsis. *Plant Cell* 19(1): 63-73.
189. Lopez-Bucio J.S., Dubrovsky J.G., Raya-Gonzalez J., Ugartechea-Chirino Y., Lopez-Bucio J., de Luna-Valdez L.A., Ramos-Vega M., Leon P., and Guevara-Garcia A.A. (2014). Arabidopsis thaliana mitogen-activated protein kinase 6 is involved in seed formation and modulation of primary and lateral root development. *J Exp Botany* 65(1): 169-183.
190. Verlhac M.H., de Pennart H., Maro B., Cobb M.H., and Clarke H.J. (1993). MAP kinase becomes stably activated at metaphase and is associated with microtubule-organizing centers during meiotic maturation of mouse oocytes. *Dev Biol* 158(2): 330-340.
191. Reszka A.A., Seger R., Diltz C.D., Krebs E.G., and Fischer E.H. (1995). Association of mitogen-activated protein kinase with the microtubule cytoskeleton. *PNAS* 92(19): 8881-8885.
192. Lee S.E., Kim J.H., and Kim N.H. (2007). Inactivation of MAPK affects centrosome assembly, but not actin filament assembly, in mouse oocytes maturing in vitro. *Mol Reprod Dev* 74(7): 904-911.
193. Sun Q.Y., Lai L., Wu G.M., Park K.W., Day B.N., Prather R.S., and Schatten H. (2001). Microtubule assembly after treatment of pig oocytes with taxol: correlation with chromosomes, gamma-tubulin, and MAP kinase. *Mol Reprod Dev* 60(4): 481-490.
194. Nakamura M., Masuda H., Horii J., Kuma K., Yokoyama N., Ohba T., Nishitani H., Miyata T., Tanaka M., and Nishimoto T. (1998). When overexpressed, a novel centrosomal protein, RanBPM, causes ectopic microtubule nucleation similar to gamma-tubulin. *J Cell Biol* 143(4): 1041-1052.
195. Nishitani H., Hirose E., Uchimura Y., Nakamura M., Umeda M., Nishii K., Mori N., and Nishimoto T. (2001). Full-sized RanBPM cDNA encodes a protein possessing a long stretch of proline and glutamine within the N-terminal region, comprising a large protein complex. *Gene* 272(1-2): 25-33.
196. Kobayashi N., Yang J., Ueda A., Suzuki T., Tomaru K., Takeno M., Okuda K., and Ishigatsubo Y. (2007). RanBPM, Muskelin, p48EMLP, p44CTLH, and the armadillo-repeat proteins ARMC8alpha and ARMC8beta are components of the CTLH complex. *Gene* 396(2): 236-247.
197. Santt O., Pfirrmann T., Braun B., Juretschke J., Kimmig P., Scheel H., Hofmann K., Thumm M., and Wolf D.H. (2008). The yeast GID complex, a novel ubiquitin ligase (E3) involved in the regulation of carbohydrate metabolism. *Mol Biol Cell* 19(8): 3323-3333.
198. Suzuki T., Ueda A., Kobayashi N., Yang J., Tomaru K., Yamamoto M., Takeno M., and Ishigatsubo Y. (2008). Proteasome-dependent degradation of alpha-catenin is regulated by interaction with ARMc8alpha. *The Biochemical journal* 411(3): 581-591.
199. Suresh B., Ramakrishna S., and Baek K.H. (2012). Diverse roles of the scaffolding protein RanBPM. *Drug discovery today* 17(7-8): 379-387.
200. Francis O., Han F., and Adams J.C. (2013). Molecular phylogeny of a RING E3 ubiquitin ligase, conserved in eukaryotic cells and dominated by homologous components, the muskelin/RanBPM/CTLH complex. *PloS one* 8(10): e75217.
201. Zhang H., Hou Y.J., Han S.Y., Zhang E.C., Huebner K., and Zhang J. (2009). Mammalian nitrilase 1 homologue Nit1 is a negative regulator in T cells. *Int Immunol* 21(6): 691-703.
202. Semba S., Han S.Y., Qin H.R., McCorkell K.A., Iliopoulos D., Pekarsky Y., Druck T., Trapasso F., Croce C.M., and Huebner K. (2006). Biological functions of mammalian Nit1, the counterpart of the invertebrate NitFhit Rosetta stone protein, a possible tumor suppressor. *J Biol Chem* 281(38): 28244-28253.

203. Cutler S.R., and Somerville C.R. (2005). Imaging plant cell death: GFP-Nit1 aggregation marks an early step of wound and herbicide induced cell death. *BMC Plant Biol* 5: 4.
204. Normanly J., Grisafi P., Fink G.R., and Bartel B. (1997). Arabidopsis mutants resistant to the auxin effects of indole-3-acetonitrile are defective in the nitrilase encoded by the NIT1 gene. *Plant Cell* 9(10): 1781-1790.
205. Neumayer G., Belzil C., Gruss O.J., and Nguyen M.D. (2014). TPX2: of spindle assembly, DNA damage response, and cancer. *CMLS* 71(16): 3027-3047.
206. Moss D.K., Wilde A., and Lane J.D. (2009). Dynamic release of nuclear RanGTP triggers TPX2-dependent microtubule assembly during the apoptotic execution phase. *J Cell Sci* 122(Pt 5): 644-655.
207. Zhao C., Slevin J.T., and Whiteheart S.W. (2007). Cellular functions of NSF: not just SNAPs and SNAREs. *FEBS letters* 581(11): 2140-2149.
208. Zhao C., Smith E.C., and Whiteheart S.W. (2012). Requirements for the catalytic cycle of the N-ethylmaleimide-Sensitive Factor (NSF). *Biochim Biophys Acta* 1823(1): 159-171.
209. McDonald P.H., Cote N.L., Lin F.T., Premont R.T., Pitcher J.A., and Lefkowitz R.J. (1999). Identification of NSF as a beta-arrestin1-binding protein. Implications for beta2-adrenergic receptor regulation. *J Biol Chem* 274(16): 10677-10680.
210. Hanley J.G., Khatri L., Hanson P.I., and Ziff E.B. (2002). NSF ATPase and alpha-/beta-SNAPs disassemble the AMPA receptor-PICK1 complex. *Neuron* 34(1): 53-67.
211. Tani K., Shibata M., Kawase K., Kawashima H., Hatsuzawa K., Nagahama M., and Tagaya M. (2003). Mapping of functional domains of gamma-SNAP. *J Biol Chem* 278(15): 13531-13538.
212. Bassham D.C., and Raikhel N.V. (1999). The pre-vacuolar t-SNARE AtPEP12p forms a 20S complex that dissociates in the presence of ATP. *Plant J: for cell and molecular biology* 19(5): 599-603.
213. Rancour D.M., Dickey C.E., Park S., and Bednarek S.Y. (2002). Characterization of AtCDC48. Evidence for multiple membrane fusion mechanisms at the plane of cell division in plants. *Plant Physiol* 130(3): 1241-1253.
214. Karimi M., Inze D., and Depicker A. (2002). GATEWAY vectors for Agrobacterium-mediated plant transformation. *Trends Plant Sci* 7(5): 193-195.
215. Karimi M., De Meyer B., and Hilson P. (2005). Modular cloning in plant cells. *Trends Plant Sci* 10(3): 103-105.
216. Wesley S.V., Helliwell C.A., Smith N.A., Wang M.B., Rouse D.T., Liu Q., Gooding P.S., Singh S.P., Abbott D., Stoutjesdijk P.A., et al. (2001). Construct design for efficient, effective and high-throughput gene silencing in plants. *Plant J* 27(6): 581-590.
217. Gleave A.P. (1992). A versatile binary vector system with a T-DNA organisational structure conducive to efficient integration of cloned DNA into the plant genome. *Plant Mol Biol* 20(6): 1203-1207.
218. Wielopolska A., Townley H., Moore I., Waterhouse P., and Helliwell C. (2005). A high-throughput inducible RNAi vector for plants. *Plant Biotechnol J* 3(6): 583-590.

7. PRESENTED PUBLICATIONS

7.1

Tomaštíková, E., Cenklová, V., Kohoutová, L., Petrovská, B., Váchová, L., Halada, P., Kočárová, G., and Binarová, P.; (2012) Interactions of an Arabidopsis RanBPM homologue with LisH-CTLH domain proteins revealed high conservation of CTLH complexes in eukaryotes. BMC Plant Biol,12:83 1-14

BMC Plant Biology

RESEARCH ARTICLE Open Access

Interactions of an *Arabidopsis* RanBPM homologue with LisH-CTLH domain proteins revealed high conservation of CTLH complexes in eukaryotes

Eva Tomaštíková[1], Věra Cenklová[2], Lucie Kohoutová[3], Beáta Petrovská[1], Lenka Váchová[2], Petr Halada[3], Gabriela Kočárová[3] and Pavla Binarová[3*]

Abstract

Background: RanBPM (Ran-binding protein in the microtubule-organizing centre) was originally reported as a centrosome-associated protein in human cells. However, RanBPM protein containing highly conserved SPRY, LisH, CTLH and CRA domains is currently considered as a scaffolding protein with multiple cellular functions. A plant homologue of RanBPM has not yet been characterized.

Results: Based on sequence similarity, we identified a homologue of the human RanBPM in *Arabidopsis thaliana*. AtRanBPM protein has highly conserved SPRY, LisH, CTLH and CRA domains. Cell fractionation showed that endogenous AtRanBPM or expressed GFP-AtRanBPM are mainly cytoplasmic proteins with only a minor portion detectable in microsomal fractions. AtRanBPM was identified predominantly in the form of soluble cytoplasmic complexes ~230 – 500 kDa in size. Immunopurification of AtRanBPM followed by mass spectrometric analysis identified proteins containing LisH and CRA domains; LisH, CRA, RING-U-box domains and a transducin/WD40 repeats in a complex with AtRanBPM. Homologues of identified proteins are known to be components of the C-terminal to the LisH motif (CTLH) complexes in humans and budding yeast. Microscopic analysis of GFP-AtRanBPM *in vivo* and immunofluorescence localization of endogenous AtRanBPM protein in cultured cells and seedlings of *Arabidopsis* showed mainly cytoplasmic and nuclear localization. Absence of colocalization with γ-tubulin was consistent with the biochemical data and suggests another than a centrosomal role of the AtRanBPM protein.

Conclusion: We showed that as yet uncharacterized *Arabidopsis* RanBPM protein physically interacts with LisH-CTLH domain-containing proteins. The newly identified high molecular weight cytoplasmic protein complexes of AtRanBPM showed homology with CTLH types of complexes described in mammals and budding yeast. Although the exact functions of the CTLH complexes in scaffolding of protein degradation, in protein interactions and in signalling from the periphery to the cell centre are not yet fully understood, structural conservation of the complexes across eukaryotes suggests their important biological role.

Keywords: Arabidopsis homologue of RanBPM, CTLH-complex, LisH-CTLH domain proteins

* Correspondence: binarova@biomed.cas.cz
[3]Institute of Microbiology, AS CR, v.v.i., Vídeňská 1083, 142 20, Prague 4, Czech Republic
Full list of author information is available at the end of the article

Background

Ras-related nuclear proteins (Rans) are abundant small GTPases, associated with Ran-specific nuclear GEFs (guanine nucleotide exchange factors), cytoplasmic GAPs (GTPase activating proteins), and with RanBP1 (Ran binding protein 1) that stimulate RanGTP hydrolysis in the cytoplasm [1,2]. The *Arabidopsis* genome contains three genes encoding AtRan [3], two genes encoding AtRanGAP related proteins [4] and three genes for RanBP1 isoforms – RanBP1a, RanBP1b and RanBP1c [3,5]. Plant Ran binding proteins (RanBPs) display significant homology with yeast and mammalian RanBPs, but there is little evidence for their biological function [6,7].

One RanBP in animal cells, RanBPM (RanBP9), was identified in a yeast two-hybrid screen with Ran as a bait. RanBPM comprises four domains – SPRY, LisH, CTLH and CRA and is homologous to the human RanBP10 protein [8]. Although RanBPM and RanBP10 have been shown to bind the Ran protein, they do not contain a consensus Ran-binding sequence [9]. RanBPM was defined as a member of the Scorpin family of proteins (SPRY-containing Ran binding protein) with a unique domain organization [10]. As reviewed in Suresh et al. [11], numerous protein interactions described for the RanBPM protein suggest its multiple roles in the regulation of protein stability, cell cycle regulation and other as yet undefined cellular processes.

RanBPM was reported to be a part of the large CTLH (C-terminal to the LisH motif) complexes [12-14]. CTLH complexes composed of LisH, CTLH and CRA domain containing proteins, transducin/WD40 repeat proteins, and armadillo repeat proteins have been found in mammals and yeast [15,16]. Mammalian and yeast CTLH complexes are structurally conserved but their biological function is still not fully understood. In yeast, the CTLH complex of Gid/Vid proteins plays a role in vacuole and proteasome-dependent fructose-1,6-bisphosphatase degradation [16]. Similarly, it has been suggested that CTLH complexes partake in lysosome and proteasome-dependent proteolysis in mammalian cells [17]. Data on proteins with SPRY, LisH, CTLH or CRA domain-containing proteins in plants are limited. In *Pinus radiata*, the SPRY domain containing protein, SEPR11, is the homologue of a Trithorax-group member and is involved in plant reproduction and development [18]. In *Oryza sativa,* the LisH domain-containing protein, OsLIS-L1 is required for male gametophyte formation and the first internode elongation [19].

Here we provide data on an *Arabidopsis* homologue of RanBPM that belongs to the uncharacterized family of plant SPRY, LisH, CTLH and CRA domain-containing proteins. We used *in silico* analysis, biochemical, proteomic and microscopic analyses *in vivo* and *in situ* to characterize AtRanBPM. We found that the AtRanBPM protein is present predominantly in the form of large cytoplasmic protein complexes that are structurally homologous to the CTLH type of complexes described in mammals and budding yeast.

Results

The Arabidopsis homologue of RanBPM is a SPRY-domain containing protein

By homology search of the *Arabidopsis thaliana* genome, we found a SPRY-domain containing protein AtRanBPM (At1g35470), which is a homologue of the human RanBPM (RanBP9) protein. The *AtRanBPM cDNA* contains a single open reading frame and consists of 467 amino acids. *AtRanBPM* is a member of the HOM002780 gene family that comprises 44 genes in 21 plant species, particularly from the ORTHO002658 subfamily. In *Arabidopsis* there are three paralogues of AtRanBPM (At4g09310, At4g09200, At4g09250**)** and one gene originating from the segmental duplication of chromosome 1 (At4g09340) (Plaza 2.0; A resource for plant comparative genomics, [20]). The products of these genes are described as SPRY domain-containing proteins but their biological roles in plants have not yet been identified.

The AtRanBPM protein is composed of four domains – SPRY, LisH, CTLH and CRA (Figure 1A). SPRY, LisH, CTLH and CRA domain-containing proteins are widely spread across eukaryotes. The protein encoded by *AtRanBPM* is annotated as a protein of unknown function (TAIR; The Arabidopsis Information Resource, [21]). As shown in Figure 1B, AtRanBPM has close homologues in other plant species such as *Ricinus communis* (67% identities, 79% positives), *Vitis vinifera* (66%, 78%), *Populus trichocarpa* (67%, 80%), *Sorghum bicolor* (57%, 74%), *Zea mays* (57%, 74%) and *Oryza sativa Japonica group* (57%, 73%) (Figure 1B, Additional file 1). The *Arabidopsis* RanBPM shows a close identity and similarity to its SPRY, LisH, CTLH and CRA domains with mammalian RanBPM and RanBP10 (Figure 1C, Additional file 2) (WU-BLAST, Basic Local Alignment Search Tool, [22]). However, there is an insertion of about 150 amino acids between the CTLH and CRA domains in human proteins (Figure 1C). A phylogenetic analysis performed using MEGA5 software (MEGA 5.02, Molecular Evolutionary Genetics Analysis, [23]) revealed that *Arabidopsis* RanBPM grouped with homologues from other plant species. The metazoan RanBPM homologues grouped in a separated clade. The *Saccharomyces* homologue, Gid1/Vid30, appears to be ancestral to the plant and metazoan clades (Additional file 3).

SPRY, LisH, CTLH and CRA conserved domains are mainly involved in protein-protein interactions. The SPRY domain (SPla and the RYanodine Receptor) was originally identified as a structural motif in ryanodine receptors [24]. Proteins with SPRY domains are involved in intracellular calcium release, as is the case for ryanodine

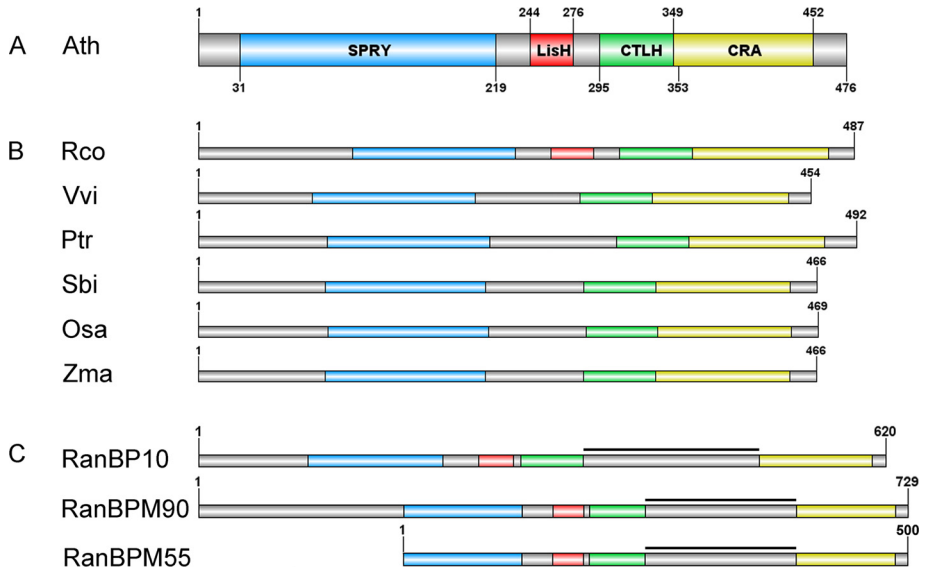

Figure 1 Domain organization of *Arabidopsis* RanBPM protein and its plant and human homologues. A- AtRanBPM protein consists of highly conserved SPRY, LisH, CTLH, and CRA domains. **B**- Comparison of AtRanBPM protein with its closest plant homologues. *Rco – Ricinus communis*, *Vvi – Vitis vinifera*, *Ptr – Populus trichocarpa*, *Sbi – Sorghum bicolor*, *Osa – Oryza sativa*, *Zma – Zea mays*. **C**- Comparison of AtRanBPM protein with its closest human homologues. Bold black lines indicate the 150 amino acids insertion between CTLH and CRA domains present only in human but not in plant RanBPM proteins. RanBPM90 – RanBPM of 90 kDa, RanBPM55 – RanBPM of 55 kDa.

receptors, in RNA metabolism and in regulatory and developmental processes [25]. The LisH domain (Lissencephaly type-1-like homology motif) functions as a stable homodimerization and dimerization motif and its contribution to the dynamics of microtubules has been suggested [26]. Located adjacent to the C-terminus of the LisH domain is a C-terminal to the LisH motif (CTLH) that has a putative α-helical structure with an as yet undescribed function. The CRA domain (CT11-RanBPM) was found to be a motif in the C-terminal part of RanBPM and RanBP10 and represents a protein-protein interaction domain often found in Ran-binding proteins [27].

Putative interaction sites of AtRanBPM were analysed using ELM (The Eukaryotic Linear Motif for functional sites in proteins, [28]) and SUMOsp 2.0 databases (SUMOylation Sites Prediction, [29]) (Figure 2). There are common motifs in the AtRanBPM amino acid sequence, such as phosphorylation consensus sites for phosphoinositide-3-OH kinase related kinases, a protein kinase A phosphorylation site, a mitogen-activated protein kinase phosphorylation site and docking motif, and a putative cyclin recognition site. Further, the AtRanBPM amino acid sequence possesses forkhead-associated phosphopeptide binding domains and a Y-based sorting signal which might act in endosomal and secretory pathways.

Protein expression levels, cellular distribution and molecular forms of AtRanBPM

The AtRanBPM coding sequence [EMBL:AEE31799] was cloned into Gateway-compatible plant binary vectors for N-terminal GFP and C-terminal GFP fusion. *Arabidopsis* cell suspension cultures were transformed according to Mathur et al. [30]. Transformed *Arabidopsis* plants were obtained through the floral-dip method [31].

An antibody against a peptide from the C-terminal part of the AtRanBPM molecule was produced in rabbits and affinity purified using the immunogenic peptide. When cell lines expressing GFP-AtRanBPM were analysed by Western blotting of separated *Arabidopsis* extracts, the antibody recognized a band of 52 kDa, the predicted molecular mass (MW) of AtRanBPM, and a band corresponding to the MW of GFP-AtRanBPM (Figure 3A). Western blot further showed that the protein levels of AtRanBPM were much lower in *Arabidopsis* seedlings than cell cultures. In cultured *Arabidopsis* cells, there was no significant difference in AtRanBPM protein levels between dividing cells and stationary growing non-dividing cells (Figure 3B). Similarly, there was no difference in AtRanBPM protein levels between four, eight and 15 day old *Arabidopsis* seedlings. Our data correspond to those on AtRanBPM expression found in the publically available Affymetrix expression databases, the Arabidopsis eFP browser [32], and the Genevestigator database [33] where AtRanBPM has a constant level of expression in analysed tissues as well as during seedling development.

The cellular distribution of AtRanBPM was analysed using differential centrifugation. As shown in Figure 3C, the majority of the protein was cytoplasmic and only small amounts sedimented either in low speed pellets

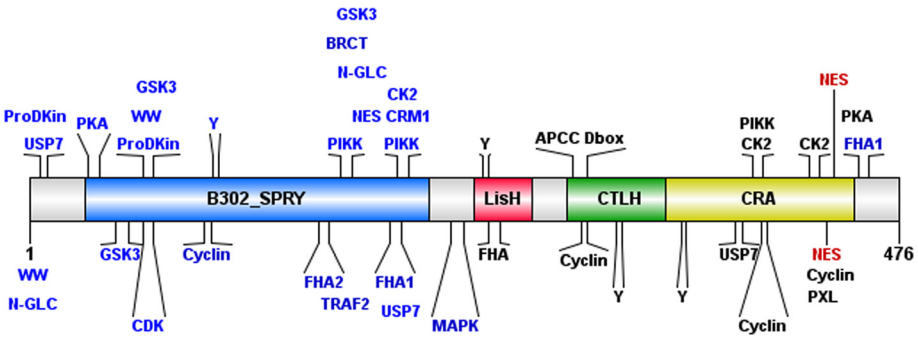

Figure 2 Putative interaction sites and binding motifs in AtRanBPM amino acid sequence. To predict putative interaction sites and binding motifs ELM [28] and SUMOsp 2.0 [29] databases were used.

or in the microsomal pellet (P100). The fact that AtRanBPM was also sedimented from a high-speed cytoplasmic S100 extract to pellet P200 indicated that the protein might be present in the form of higher MW complexes. The separation of S100 high speed extract by native polyacrylamide gel electrophoresis (native PAGE) confirmed cell fractionation data and suggested that AtRanBPM is a component of protein complexes with a molecular mass of around ~230 – 500 kDa (Figure 3D). Further, we immunopurified GFP-AtRanBPM using the GFP trap. Separation of purified GFP-AtRanBPM by native PAGE followed by Western blotting showed the

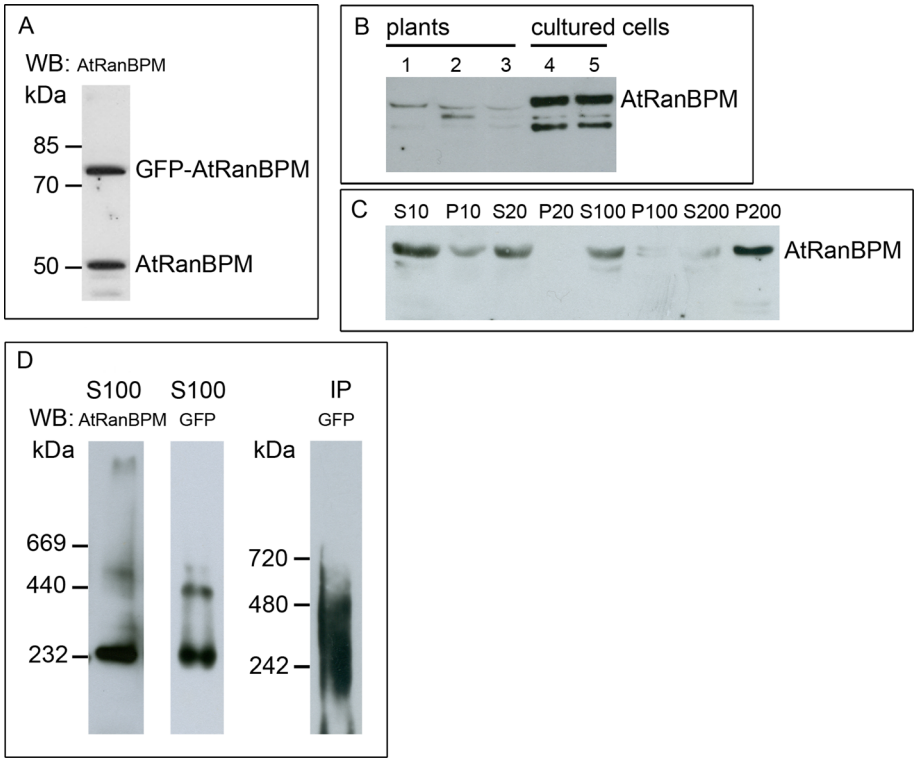

Figure 3 Cellular distribution of AtRanBPM and AtRanBPM complexes. A- The antibody against AtRanBPM recognizes a band of 52 kDa, which corresponds to endogenous AtRanBPM protein, and a band of 80 kDa, which corresponds to expressed GFP-AtRanBPM from cultured cells expressing GFP-AtRanBPM. **B**- Comparison of protein levels of AtRanBPM in *Arabidopsis* seedlings and cultured cells. Lines 1, 2, and 3 – fractions S10 from four-, eight-, and 15-d-old seedlings; lines 4 and 5 – fractions S10 from exponentially growing cultured cells (3 days after subculture) and stationary phase cultured cells (6 days after subculture). Per line, 25 μg of protein content of S10 fraction was loaded. **C**- Distribution of AtRanBPM in the cellular fractions of *Arabidopsis* cultured cells. The majority of the protein was present in cytoplasm (fractions S10, S20, S100), a small amount of the protein was found in pellet P10. AtRanBPM was spun down to high-speed pellet P200 probably in the form of complexes. **D**- GFP-AtRanBPM complexes from high-speed supernatant S100 and from immunoprecipitate (IP) were resolved by non-denaturing PAGE and detected by anti-AtRanBPM antibody or anti-GFP antibody as indicated. For S100 fractions, 15 and 10 μg of protein content was loaded.

presence of complexes of similar size as observed when high-speed supernatant S100 was analysed (Figure 3D). Altogether these data showed that AtRanBPM is present predominantly in the form of large cytoplasmic complexes.

Analysis of AtRanBPM protein complexes by mass spectrometry

To analyse putative interactors of AtRanBPM in the complexes, GFP-AtRanBPM and copurified proteins were separated by SDS-PAGE followed by silver staining, and specific bands were excised and analysed by MALDI-MS (Figure 4A). GFP immunopurification performed in extracts from wild type cell was used as a negative control. Neither AtRanBPM protein nor bands corresponding to the MW of proteins copurified with GFP-AtRanBPM were observed in the negative controls and only background contamination such as HSPs and cytoskeletal proteins were detected by MALDI-MS (Additional file 4). We found that proteins reproducibly copurifying with AtRanBPM belong to CTLH-domain containing proteins including LisH (At1g61150), CRA and U-box (At3g55070, At4g37880), and to the transducin/WD-40 domain-containing proteins At5g08560, and At5g43920 (Table 1, Figure 4B). Alternatively to MALDI-MS, we used LC-MALDI-MS/MS analysis of eluates from the GFP trap to confirm the interaction of GFP-AtRanBPM with the proteins mentioned above.

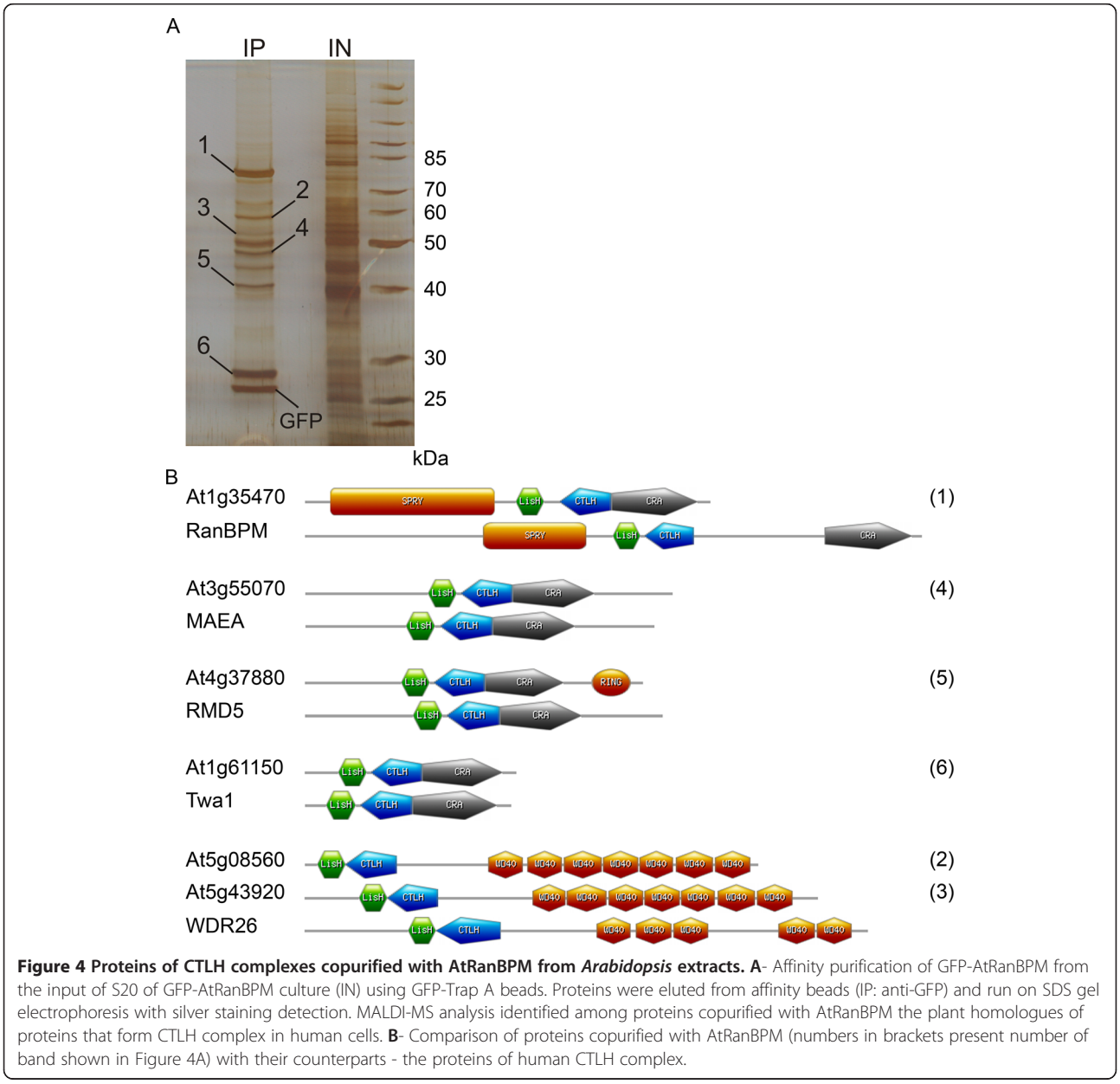

Figure 4 Proteins of CTLH complexes copurified with AtRanBPM from *Arabidopsis* extracts. A- Affinity purification of GFP-AtRanBPM from the input of S20 of GFP-AtRanBPM culture (IN) using GFP-Trap A beads. Proteins were eluted from affinity beads (IP: anti-GFP) and run on SDS gel electrophoresis with silver staining detection. MALDI-MS analysis identified among proteins copurified with AtRanBPM the plant homologues of proteins that form CTLH complex in human cells. **B**- Comparison of proteins copurified with AtRanBPM (numbers in brackets present number of band shown in Figure 4A) with their counterparts - the proteins of human CTLH complex.

Table 1 Proteins copurified with AtRanBPM are members of CTLH complexes

Protein name	AGI number	Band No.	MW [kDa]	No. peptides	Sequence coverage [%]	Aranet/ ATTED-II	Members of CTLH complex in other organisms
AtRanBPM	At1g35470	1	52	17/41	41/60		RanBPM [Q96S59] Gid1/Vid30 [P53076]***
LisH and RanBPM domain-containing protein	At1g61150	6	25	8/26	41/82	-/+	Twa1 [Q9NWU2]**Gid8 [P40208]***
LisH/CRA/RING-U-box domain-containing protein	At3g55070	4	48	10/17	28/31	+/-	MAEA [Q7L5Y9]*Gid9p [P40492]***
LisH/CRA/RING-U-box domain-containing protein	At4g37880	5	44	9/8	32/22	+/-	RMD5 [Q9H871]*Gid2 [Q12508]***
Transducin/WD40 domain-containing protein	At5g08560	2	66	17/14	38/31	+/-	WDR26 [Q9H7D7]
Transducin/WD40 domain-containing protein	At5g43920	3	60	6/4	13/7	+/-	WDR26 [Q9H7D7]

Proteins (for band numbering see Figure 4A) copurified with AtRanBPM protein were identified by both MALDI-MS and LC-MALDI-MS/MS analysis. The values before and after the slash in the columns "No. peptides" and "Sequence coverage" refer to MALDI-MS and LC-MALDI-MS/MS data, respectively. Homologues of human CTLH-complex members reported by Kobayashi et al., [15] (*), proteins in the complex described by Umeda et al. [12] (**), yeast homologues in the Gid complex published by Regelmann et al. [16] (***).

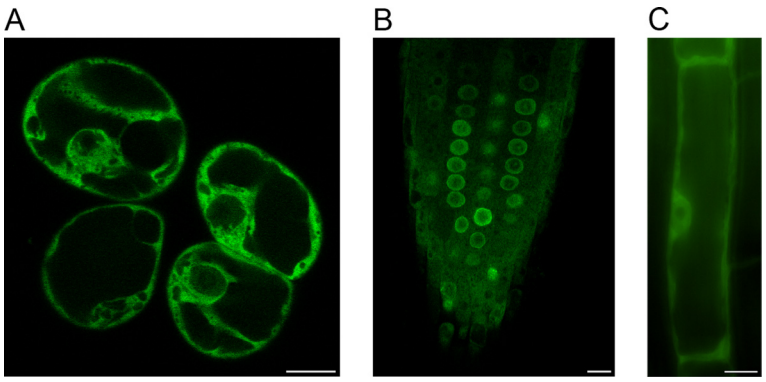

Figure 5 *In vivo* localization of GFP-AtRanBPM in *Arabidopsis* cells and seedlings. A- Localization of GFP-AtRanBPM in *Arabidopsis* suspension culture. The protein is localized in the cytoplasm and in the perinuclear area. Weaker signal is present in nuclei. **B**- Root tip of 8 days old *Arabidopsis* plant. Weak cytoplasmic signal for GFP-AtRanBPM is enriched in the perinuclear area. **C**- Cytoplasmic and perinuclear localization of GFP-AtRanBPM in differentiated cells of root. Bars = 10 μm.

Database search indicated that the proteins copurified with AtRanBPM were homologous to protein components of the human CTLH complex [15]. The CTLH complex is annotated in CORUM (The comprehensive resource for mammalian complexes, [34]) as a complex with a putative function in regulating cell migration, nucleokinesis, chromosome segregation and microtubule dynamics. Components of the CTLH complex are conserved amongst animal species and their presence is predicted for other eukaryotes such as plants and fungi. A relatively lower degree of homology with individual mammalian and plant members of CTLH complexes (Figure 4B, Additional file 5) is due to the fact that part of the molecule separating highly conserved domains contains insertions and deletions of various lengths, differing among plant, mammalian and/or yeast homologues.

The LC-MALDI-MS/MS analysis also identified among proteins copurified with AtRanBPM Armadillo-repeat-containing protein (At3g08947) (Additional file 6). However, the protein was not proven to be a homologue of the human armadillo repeat ARMC8, a member of the CTLH complex [34,35]. Further, Yippee family proteins (At5g53940, At2g40110) and Yippee-like protein (At3g08890) were copurified with AtRanBPM and identified by LC-MALDI-MS/MS (Additional file 6). Yippee-like proteins belong to the YPEL family of proteins whose members have been described as interactors of the human RanBPM [10]. Proteins At5g08560, At5g43920, At3g55070, and At3g37880, copurified with AtRanBPM were predicted to interact within a functional network in the Aranet database (Probabilistic Functional Gene Network for Arabidopsis thaliana, [36]) (Table 1).

Together these data suggest that plant AtRanBPM protein, like its yeast and mammalian homologues, is a component of a cytoplasmic multiprotein complex where it interacts with LisH-CTLH domain-containing proteins and armadillo-repeat-containing proteins.

In vivo localization of GFP-AtRanBPM and AtRanBPM immunofluorescence labelling in Arabidopsis cultured cells and seedlings

In cultured cells of *Arabidopsis,* the GFP-AtRanBPM signal was localized in the cytoplasm and in the perinuclear area of interphase cells, with a weaker signal detected in nuclei (Figure 5A). We observed no gain-of-function phenotype of *Arabidopsis* seedlings expressing GFP-AtRanBPM from Gateway vectors. Similarly to cultured cells, the GFP-AtRanBPM signal was localized in the cytoplasm, in nuclei and accumulated in the vicinity of nuclei in dividing zone of roots (Figure 5B). In differentiated root cells, GFP-AtRanBPM was cytoplasmic and in the perinuclear area (Figure 5C, Additional file 7). C-terminal GFP fusions showed a similar localization pattern when expressed transiently in cultured cells of *Arabidopsis* (Additional file 8).

Immunofluorescence analyses showed that the AtRanBPM protein was distributed patchily in the cytoplasm and nuclei; in non-dividing cells it accumulated in the perinuclear region and in dividing cells, the signal was slightly enriched in the area of the mitotic spindle and the phragmoplast (Figure 6A). Further we compared localization of the endogenous protein and GFP-AtRanBPM by double labelling with anti-AtRanBPM and anti-GFP antibodies. We confirmed a similar localization pattern for AtRanBPM and expressed AtRanBPM with a cytoplasmic signal slightly enriched in the perinuclear area and a weaker nuclear signal (Figure 6B).

To determine whether the AtRanBPM protein plays a role in microtubule organization like the truncated version of human RanBPM [37], we studied the colocalization of AtRanBPM with the centrosomal protein, γ-tubulin. In acentrosomal plant cells, γ-tubulin is present with dispersed sites of microtubule nucleation in the cytoplasm, with nuclei, and on membranes and microtubules [38]. We found that the *Arabidopsis* homologue

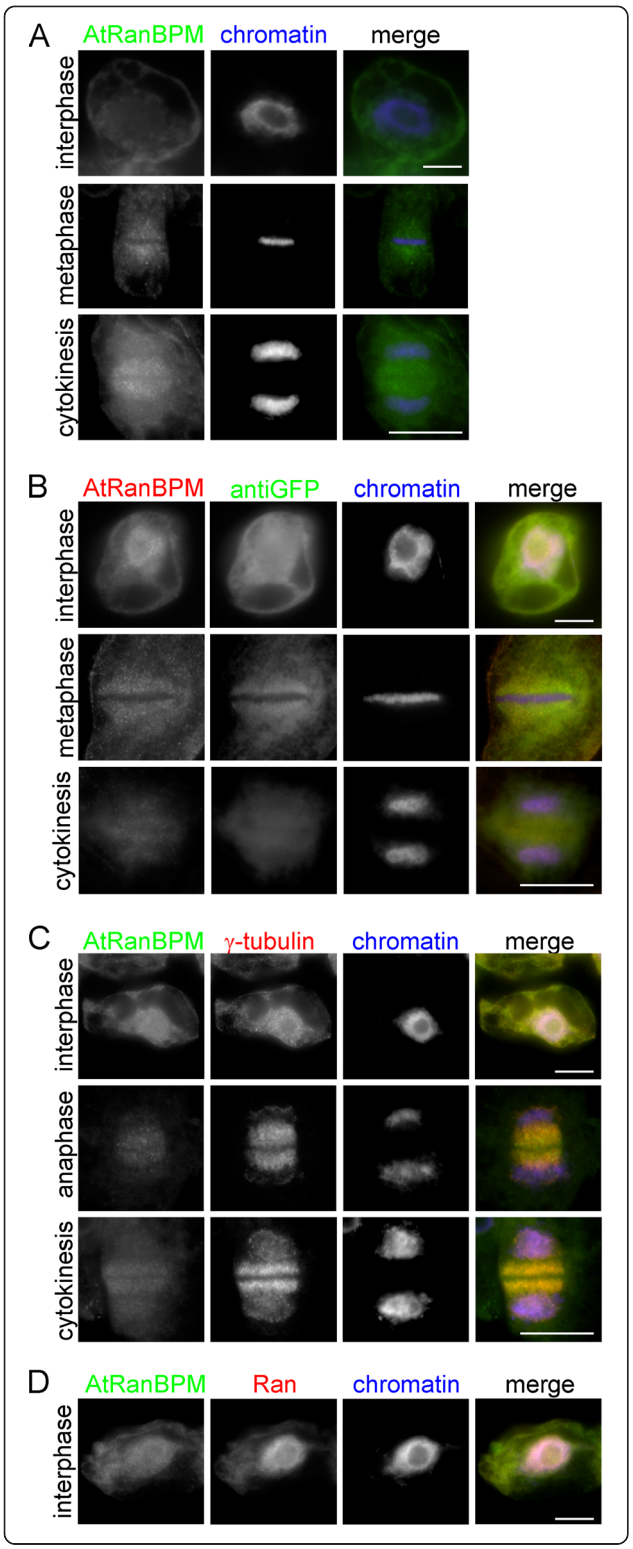

Figure 6 Immunolocalization of AtRanBPM in *Arabidopsis* cultured cells. A- Immunolocalization of endogenous AtRanBPM with affinity purified anti-AtRanBPM antibody. Signal for AtRanBPM was cytoplasmic with slight accumulation in the vicinity of nuclei and in dividing cells with slight enrichment in spindle and phragmoplast area. (AtRanBPM – green, chromatin – blue). **B**- Double immunofluorescence analysis of cells expressing GFP-AtRanBPM confirmed similar localization pattern for expressed GFP protein and for endogenous AtRanBPM protein (Figure 6A) (GFP-AtRanBPM – green, endogenous AtRanBPM – red, chromatin – blue). **C**- Double immunofluorescence analysis of AtRanBPM (green) and γ-tubulin (red) did not confirm colocalization of both proteins in interphase and in dividing cells. **D**- Double immunofluorescence of AtRanBPM (green) and Ran (red). Only a small portion of AtRanBPM is localized in nuclei compared to intensive nuclear signal for Ran protein. Bars = 10 μm.

AtRanBPM did not colocalize with γ-tubulin-positive sites either present with the nuclear envelope or on microtubular arrays (Figure 6C).

As a portion of RanBPM was reported to be associated with the Ran protein in mammalian cells [14] we performed double immunofluorescence labelling of AtRanBPM and Ran protein. In cultured cells of *Arabidopsis*, Ran was localized in the cytoplasm and in nuclei but only a small fraction of AtRanBPM colocalized with nuclear Ran.

Discussion

RanBPM protein was first characterized in human cells as a centrosomal protein involved in microtubule nucleation which colocalized with γ-tubulin at centrosomes and at ectopic nucleation sites [37]. The data on RanBPM initiated an investigation of the role of the RanGTPase pathway and its role in chromatin-mediated microtubule nucleation and spindle assembly [39]. However, later it was found that antibody against the 55 kDa form of RanBPM that was characterized by Nakamura et al. [37] did not recognize the full length 90 kDa RanBPM protein. The truncated form of RanBPM (55 kDa) was shown to be an incorrectly translated product of the *RanBPM* gene and moreover, only the truncated version but not the whole RanBPM molecule was active in microtubule nucleation [14]. The complete RanBPM molecule thus does not show the same properties as the truncated version and it was depicted as a scaffold protein that links and modulates interactions between cell surface receptors and their intracellular signalling pathways [11,40]. The molecular mass of plant AtRanBPM (52 kDa) corresponds to that of the truncated RanBPM rather than to the whole human RanBPM molecule. However, the reason for the apparent discrepancy in size of the full length human and plant RanBPM molecules is an insertion of 150 amino acids between CTLH and CRA domains in the plant protein and the presence of a long stretch of proline and glutamine residues on the N-terminal part of human RanBPM molecule.

We found that AtRanBPM maintained the properties of the full length RanBPM of mammals: (i) while the truncated version of human RanBPM is present in

centrosomal and ectopic microtubule nucleation sites [37], AtRanBPM protein in acentrosomal plant cells did not colocalize with microtubule nucleation sites positive for γ-tubulin; (ii) proteins of the γ-tubulin nucleating machinery were not identified by MALDI-MS or LC-MALDI-MS/MS among proteins interacting with AtRanBPM, nor were they found in coexpression databases and a biological role of AtRanBPM other than in processes relating to centrosomes and microtubules was thus suggested; (iii) the presence of highly conserved SPRY, LisH, CTLH and CRA domains in AtRanBPM indicated its function in mediating multiple protein interactions that were described for the whole molecule of human RanBPM [12,14,15].

AtRanBPM protein was not specifically enriched with microtubules in dividing cells or localized in putative microtubule nucleation sites. Subcellular localization of AtRanBPM corresponded to published data on the subcellular localization of the whole RanBPM molecule in mammalian cells [14,41,42]. Since a weak nuclear signal, observed for human RanBPM was suggested to be a consequence of over-expression of its tagged version [40], we analysed by immunofluorescence the nuclear localization for endogenous AtRanBPM protein. A smaller portion of AtRanBPM was present in nuclei and the possibility that the nuclear signal observed for GFP-AtRanBPM or AtRanBPM-GFP resulted from over expression of GFP fusions was thus excluded. We observed only partial colocalization of Ran and AtRanBPM in nuclei. It would be interesting to address the question whether transport of the AtRanBPM complex between nucleus, perinuclear area and cytoplasm might be regulated by a weak interaction between AtRanBPM and Ran as it was suggested for mammalian RanBPM [14]. Heterogeneity in the localization of mammalian RanBPM might depend on interacting proteins [15]. Conserved domains of RanBPM protein are responsible for interactions and complex formations with a physiologically divergent group of proteins. As reviewed by Suresh et al. [11], RanBPM is a modulator/protein stabilizer, a regulator of transcriptional activity, and has cell cycle and neurological functions. RanBPM interacts with a wide range of receptors [43], acts as a scaffolding protein [44,45], and is involved in signal transduction pathways [44,46], and the apoptotic pathways [47]. Plant homologues of *RanBPM* belong to genes with unknown functions. We found that the product of *AtRanBPM* is predominantly a cytoplasmic protein that is a part of protein complexes with a molecular mass of approximately 230 – 500 kDa. A large protein complex of RanBPM was described by Nishitani et al. [14] and Ideguchi et al. [13]. Later the complex was designated as a CTLH complex [15]. Five from eleven CTLH domain-containing proteins that were identified in databases were described as being a part of the CTLH complex and an interaction within the complex via LisH-CTLH domains was suggested [15]. In *Saccharomyces cerevisiae* all four CTLH domain-containing proteins present in the genome are part of the CTLH-like complex Gid. The Gid complex is suggested to be involved in proteasome-dependent glucose-induced degradation of fructose-1,6-bisphosphatase [16,48]. There are twenty one CTLH-domain containing proteins encoded in the *Arabidopsis* genome and of these, six proteins were identified in our experiments to form CTLH-like complexes with AtRanBPM protein. Though we identified the same spectrum of AtRanBPM interacting proteins in several independent experiments it cannot be ruled out that the members of CTLH complexes exist and remain to be identified. We found that the antibody raised against a peptide from the AtRanBPM sequence did not work in immunopurification experiments. The immunopurifications performed with a panel of antibodies against the AtRanBPM protein might help to disclose the presence of other putative members of plant CTLH complexes. Alternatively, immunopurification of the CTLH complex or pull down experiments via proteins that copurified with AtRanBPM might extend our knowledge of the composition and protein interactions of newly identified CTLH complexes.

All the members of the CTLH complexes that we identified belong to yet uncharacterized plant LisH-CTLH domain-containing proteins. Protein At1g61150 is a homologue of the human Twa1 protein found in yeast by two-hybrid analysis to interact with RanBPM [12]. LisH, CRA, and RING/U-box domain-containing proteins of unknown function (At3g55070, At4g37880), copurified with AtRanBPM, are homologous to human MAEA and RMD5, respectively, that are members of the CTLH complex annotated by Kobayashi et al. [15]. Similarly, LisH and CTLH domain-containing proteins such as RanBP10 or the WD repeat domain 26 (WDR26), were suggested to be putative members of the CTLH complex [15]. We found that uncharacterized *Arabidopsis* transducin/WD-40 domain-containing proteins At5g08560 and At5g43920 which copurified with AtRanBPM, are homologues of human WDR26 protein and thus belong to components of the plant CTLH complex. Corresponding to our microscopic data on cytoplasmic and nuclear localizations of AtRanBPM, the members of the human CTLH complex, proteins RanBPM, RMD5, WDR26, Twa1, and MAEA, were shown to have predominantly cytoplasmic and a weaker nuclear localization [12,15,49].

A component of the human CTLH complex, the armadillo repeat-containing protein ARMC8, when exogenously expressed, upregulates the proteolytic degradation of ectopically expressed α-catenin, and thus was

suggested to play an important role in the ubiquitin-independent and proteasome-dependent degradation of α-catenin [35]. α-Catenin is known to function as a link protein between cadherins and actin-containing filaments of the cytoskeleton [50]; thus a complex might regulate molecular adhesion. We identified Armadillo-repeat-containing protein (At3g08947) among proteins copurified with AtRanBPM but its homology with armadillo repeat ARMC8, a member of the human CTLH complex, was not proven. However, we found that expression of copurified protein At4g37880, a homologue of RMD5 protein, correlated strongly with expression of the armadillo repeat-containing protein At3g01400, one of the homologues of ARMC8, and with expression of the plant adhesion molecule RabGAP/TBC domain-containing protein At3g02460 (ATTED-II, [51]). It is tempting to speculate whether similar function in connecting external signals in adhesion with the cell centre analogous to the cadherin and catenin pathway in animals might exist for plant CTLH complexes. However, further experimental data are needed to prove this hypothetical function of the CTLH complexes in plants.

Besides copurification with CTLH complex proteins, we found that plant AtRanBPM interacts with Yippee proteins (At5g53940, At2g40110) and Yippee-like protein (At3g08890). It was shown in human cells that RanBPM binds members of YPEL (Yippee like) family of proteins involved in a cell division-related functions [10]. Our data showed that binding with Yippee proteins might present one of the AtRanBPM multiple protein interactions in plant cells too.

Conclusions

RanBPM protein was shown to have numerous apparently functionally unrelated protein interactors, including membrane receptors, cytoplasmic and nuclear proteins [12,15]. This suggests its role in a variety of cellular processes. Our biochemical and proteomic studies showed that AtRanBPM is a component of plant homologues of CTLH complexes. The fact that CTLH complexes are present in mammals, yeast and in plants suggests their structural conservation in evolution. CTLH complexes thus might represent a module with important but not fully understood biological functions.

Methods

Plant material

Arabidopsis thaliana (*L.*) *Heynh*. plants, ecotype Columbia were used. Sterilized seeds were sown and stratified at 4 °C for 2 days, then grown under 8 h of light, 16 h of darkness at 20 °C and after 4 weeks, under 16 h of light and 8 h of darkness. Seeds were cultivated on half-strength Murashige and Skoog (MS) medium (Duchefa), supplemented with 0.25 mM MES, 1% saccharose and 1% phytoagar. Transformed seedlings were selected as described in Harrison et al. [52]. *Arabidopsis thaliana* suspension cultures were cultured as described in Drykova et al. [38].

Molecular cloning of AtRanBPM

AtRanBPM coding sequence [EMBL:AEE31799] was obtained by PCR amplification using *Arabidopsis thaliana* cDNA as template and Platinum Pfx DNA Polymerase (Invitrogen). The PCR primers with *attB* sites (underlined) were designed according to the manufacturer's intruction, forward 5' – GGGGACAAGTTTGTACAAAAAAGCAGGCTTCATGAACTCTTCACCACCACCG – 3', reverse 5' – GGGGACCACTTTGTACAAGAAAGCTGGGTCTTAGTCTCCATTCAGTGACCGCCTTTC – 3' for N-terminal GFP fusion and for C-terminal GFP fusion forward 5' – GGGGACAAGTTTGTACAAAAAAGCAGGCTTCATGAACTCTTCACCACCACCG – 3', reverse 5' – GGGGACCACTTTGTACAAGAAAGCTGGGTCTTAGTCTCCATTCAGTGACCGCCTTTC – 3´. PCR products were isolated using QIAquick gel extraction kit (Qiagen) and afterwards cloned by Gateway technology (Invitrogen). Gateway binary vectors pK7WGF2,0 for N-terminal GFP fusion, pMDC43 for C-terminal GFP fusion [53] were used.

Stable transformation of cell suspension cultures and plants

Arabidopsis suspension cultures of Landsberg erecta ecotype stably expressing GFP-AtRanBPM or transiently expressing AtRanBPM-GFP were prepared according to the protocol of Mathur et al. [30]. Arabidopsis plants Landsberg erecta ecotype were transformed by the floral-dip method [31].

Preparation of protein extracts and its fractionation by differential centrifugation

Cultured suspension cells or seedlings of *Arabidopsis thaliana* were ground in liquid nitrogen and thawed in extraction buffer in ratio 1:1 weight to volume. Extraction buffer was 50 mM Na-Hepes, pH 7.5, 75 mM NaCl, 1 mM $MgCl_2$, 1 mM EGTA, 1 mM DTT supplemented with inhibitors of proteases and phosphatases according to Drykova et al. [38] with increased concentration of 4-(2-aminoethyl)benzenesulfonyl fluoride hydrochloride to 2 mM and β-glycerophosphate to 60 mM. Crude extracts were centrifuged at 10,000 *g* for 10 min at 4 °C; obtained supernatants S10 were subsequently centrifuged at 20,000 *g* for 0.5 h at 4 °C to gain supernatants S20 and pellets P20. Supernatants S20 were then centrifuged at 100,000 *g* for 1 h at 4 °C when S100 were needed. Supernatants S100 were centrifuged at 200,000 *g* for 1.5 h at 4 °C to gain supernatants S200 and pellets P200 when needed. For differential centrifugation, pellets were

resuspended in a volume of extraction buffer equal to the volume of the corresponding supernatants; equal sample volumes were loaded on SDS-PAGE gel.

Immunoprecipitation of GFP-AtRanBPM

Cell extracts S20 (~ 4 mg protein/mL) were used directly or solubilized by 1% NP-40 (Calbiochem) for 1 h at 4 °C. Immunoprecipitations of GFP-AtRanBPM protein were then performed using GFP-Trap_A (ChromoTek) according to the manufactures' instructions. GFP immunopurification from extracts S20 of wild type Ler *Arabidopsis* culture was used as a negative control.

Protein digestion and mass spectrometry

The analysed protein bands were cut out of the Ag-stained SDS-PAGE gels, trypsin-digested and the proteins were identified by peptide mass mapping as described elsewhere [54]. Alternatively, eluates from the GFP trap were denatured in 8 M urea and digested overnight using trypsin. After desalting the resulting peptides were separated using the Ultimate HPLC system (LC Packings) on a Magic C18AQ column. The eluent from the column was spotted directly onto PAC-target using a ProteineerFC spotting device (Bruker Daltonics). Automatic MALDI MS/MS analyses were performed on an Ultraflex III TOF/TOF (Bruker Daltonics) and the proteins were identified by searching MS/MS spectra against *A. thaliana* subset of NCBI database using the in-house Mascot program (Matrixscience). The high resolution MALDI spectra were acquired on an APEX-Qe 9.4 T FTMS instrument (Bruker Daltonics).

Electrophoresis and immunoblotting

Protein samples after addition of appropriate sample buffer were separated either on 10% SDS-PAGE gels [55] or on 3-10% non-denaturing PAGE gels as described previously in Drykova et al. [38]. Proteins were transferred onto 0.45 μm polyvinylidene fluoride membranes (Millipore) by wet electroblotting and immunodetected with appropriate antibody. Anti-AtRanBPM antibody was designed against peptide of AtRanBPM amino acid sequence (CSTNPNKKDVQRS), raised in rabbits and purified with immunogenic peptide coupled to protein A sepharose beads (GeneScript) and used in dilution 1:100 for Western blotting from non-denaturating PAGE, 1:300-1:500 for Western blotting from SDS-PAGE. Anti-GFP ab290 (Abcam) was diluted 1:2,000. Secondary anti-Rabbit IgG ECL Antibody, HRP Conjugated (GE Healthcare) was diluted 1:10,000; Super Signal West Pico Chemiluminiscent Substrate (Thermal Scientific) was used according to manufacturer's instructions. Alternatively, SDS-PAGE gels were stained with silver, and the selected protein bands analysed by MALDI-MS.

Immunofluorescence

Arabidopsis thaliana suspension cultures were fixed for 30 min using 3.7% paraformaldehyde and processed for immunofluorescence labelling according to Binarová et al. [56]. Primary antibodies used: mouse anti-α-tubulin monoclonal antibody DM1A (Sigma) diluted 1:500, mouse monoclonal anti-γ-tubulin TU-32 (kindly provided by Pavel Dráber, IMG, Prague, Czech Republic) diluted 1:10, mouse anti-GFP antibody (Abcam) diluted 1:1,000, and mouse antibody against human Ran protein (BD Transduction Laboratories) diluted 1:1,000. Anti-AtRanBPM antibody was used in a dilution 1:1,000, anti-rabbit or anti-mouse secondary antibodies DyLight 488 or DyLight 549 (Jackson Immuno Research Laboratories) were diluted 1:250. DNA was stained with DAPI.

Microscopy

Microscopical analysis was performed on an IX81 motorized inverted research microscope CellR (Olympus) equipped with DSU (Disk Scanning Unit) and digital monochrome CCD camera CCD-ORCA/ER. To avoid filter crosstalk, fluorescence was detected using HQ 480/40 exciter and HQ 510/560 emitter filter cubes for DyLight 488 and HQ 545/30 exciter and HQ 610/75 emitter filter cubes for DyLight 549 (both AHF AnalysenTechnique). Confocal images were taken on Olympus FluoView FV1000 based on IX81 microscope using PLAPO 100x/1.45 and UPLSAPO 60x/1.35 objectives. GFP was excited by 473 nm solid state laser and its emission was detected from 485 to 545 nm. Images were processed and analysed using CellR and FV10-ASW (Olympus). Adobe Photoshop 7.0 was used for preparation of figures.

Database search

To identify putative domains, SMART (Simple Modular Architecture Research Tool, [57], http://smart.embl-heidelberg.de/) and Pfam ([58], http://pfam.sanger.ac.uk/) databases were used. Multiple sequence alignment was performed by ClustalX2 [59] and evaluation of similarity and identity was done by WU-BLAST (Basic Local Alignment Search Tool, [22], http://www.ebi.ac.uk/Tools/sss/wublast/). Schematic drawings of protein structure were prepared in DOG (Domain Graph, [60]) and MyDomains (Prosite, http://prosite.expasy.org/cgi-bin/prosite/mydomains/). Search for putative interaction sites in AtRanBPM amino acid sequence was done in ELM (The eukaryotic linear motif resource for functional sites in proteins, [28], http://elm.eu.org/) and SumoSP 2.0 (Sumoylation sites prediction [29], http://sumosp.biocuckoo.org/). Phylogenetic relationships were analysed in MEGA 5.02 (Molecular evolutionary genetic analysis, [23]). Genes with similar expression pattern to AtRanBPM were identified in publically available databases ATTED-II ([51], http://atted.jp/) and AraNet ([36], http://www.functionalnet.org/aranet/).

Putative interactors were analysed by Arabidopsis eFP browser ([32], http://bar.utoronto.ca/efp/cgi-bin/efpWeb.cgi) and Genevestigator ([33], https://www.genevestigator.com/gv/plant.jsp). The information and phylogenetic relationships of human CTLH complex with similar complexes from other species were found in CORUM ([34], http://mips.helmholtz-muenchen.de/genre/proj/corum/).

Additional files

Additional file 1: Multiple sequence alignment of AtRanBPM plant homologues. Sequence alignment of *Arabidopsis* RanBPM with *Ricinus communis*, *Vitis vinifera*, *Populus trichocarpa*, *Sorghum bicolor*, *Oryza sativa* and *Zea mays* homologues. Alignment was done using ClustalX2 software [59]. Sequence data of this alignment can be found at accession numbers [Swiss-Prot:F4HYD7] for At1g35470, [Swiss-Prot:B9S762] for *R. communis*, [Swiss-Prot:F6HWC3] for *V. vinifera*, [Swiss-Prot:B9MWC1] for *P. trichocarpa*, [Swiss-Prot:C5XUT1] for *S. bicolor*, [Swiss-Prot:Q6ZI83] for *O. sativa*, [Swiss-Prot:B6UAR9] for *Z. mays*.

Additional file 2: Identities and similarities of conserved domains between Arabidopsis RanBPM and its human homologues. Sequence alignment was done for conserved domains SPRY (A), LisH (B), CTLH (C) and CRA (D) of full-sized 90 kDa form (RanBPM_90) and 55 kDa form (RanBPM_55) of human RanBPM protein, and RanBP10 with *Arabidopsis* RanBPM using ClustalX2 software [59]. Sequence data of this alignment can be found at accession numbers [Swiss-Prot:Q6VN20] for RanBP10, [Swiss-Prot:Q96S59] for 90 kDa RanBPM and [EMBL:BAA23216] for 55 kDa RanBPM. The sequence of the SPRY domain was encountered from the 99 amino acids in AtRanBPM sequence. E- Levels of identities and similarities in amino acid composition of conserved domains between AtRanBPM and its human homologues RanBPM and RanBP10.

Additional file 3: Phylogenetic analysis of AtRanBPM and its homologues from other eukaryotic species. The tree was constructed by the neighbor-joining method with the MEGA 5.05 software [23]. Branch numbers represent the percentage of bootstrap values in 1000 sampling replicates. The protein accession numbers are [Swiss-prot:F4HYD7] for AtRanBPM At1g35470, [Swiss-prot: Q9SMS1] At4g09340 (segmental genome duplication of chromosome 1), [Swiss-Prot:B9S762] for *R. communis*, [Swiss-Prot:F6HWC3] for *V. vinifera*, [Swiss-Prot:B9MWC1] for *P. trichocarpa*, [Swiss-Prot:C5XUT1] for *S. bicolor*, [Swiss-Prot:Q6ZI83] for *O. sativa*, [Swiss-Prot:B6UAR9] for *Z. mays*, [Swiss-prot: Q6VN20] for human RanBP10, [Swiss-prot: A3KMV8] for RanBP10 from *Bos taurus*, [Swiss-prot: B5LX41] for RanBP10 from *Felis catus*, [Swiss-prot: Q6VN19] for RanBP10 from *Mus musculus*, [Swiss-prot: Q1LUS8] for RanBP10 from *Danio rerio*, [Swiss-prot: Q9PTY5] for RanBP9 from *Xenopus laevis*, [Swiss-prot: Q96S59] for human RanBP9, [Swiss-prot: P69566] for RanBP9 from *Mus musculus*, [Swiss-prot: Q4Z8K6] for RanBP9/10 from *Drosophila melanogaster* and [Swiss-prot: P53076] for Gid1/Vid30 homologue from *Saccharomyces cerevisiae*. Distance bars are given bottom left and bootstrap values are indicated at the nodes.

Additional file 4: Immunopurification of GFP-AtRanBPM protein. Immunopurification of GFP-AtRanBPM from extracts of GFP-AtRanBPM expressing cell cultures (IP GFP-RanBPM). GFP immunopurification from extracts of wild type Ler *Arabidopsis* cells (IP WT) was used as a negative control. A- Proteins were silver stained after separation on SDS-PAGE. Bands corresponding to MW similar of the proteins copurified with GFP-AtRanBPM (IP GFP-RanBPM) were not present in the negative control (IP WT). B- Signal for AtRanBPM was absent in the negative control (IP WT) after detection with anti-AtRanBPM antibody on Western blots. C- Proteins identified by MALDI-MS in negative control (IP WT in A) were background contamination.

Additional file 5: Identities and similarities between proteins copurifying with AtRanBPM and human CTLH complex members. Identities and similarities between *Arabidopsis* and human proteins were analysed in WU-BLAST.

Additional file 6: Additional proteins copurified with AtRanBPM. The proteins were identified by LC-MALDI-MS/MS and the identity of the matched peptides was confirmed by high-resolution MALDI-FTMS with mass accuracy below 1 ppm.

Additional file 7: GFP-AtRanBPM in *Arabidopsis* root cells. AtRanBPM-GFP signal is dynamic and moving with the cytoplasmic stream.

Additional file 8: Cellular localization of C-terminal GFP and N-terminal GFP AtRanBPM fusion proteins. Cells of *Arabidopsis* expressing C-terminal GFP AtRanBPM (AtRanBPM-GFP) showed weak cytoplasmic and nuclear signal and accumulation of perinuclear GFP signal similarly as observed for N-terminal GFP AtRanBPM (GFP-AtRanBPM).

Abbreviations

CRA: CT11-RanBPM; CTLH: C-terminal to LisH; GAP: GTPase activating protein; GEF: Guanine nucleotide exchange factor; GFP: Green fluorescent protein; Gid/Vid proteins: Glucose-induced degradation/vacuole-induced degradation proteins; LC: Liquid chromatography; LisH: Lissencephaly type-1-like homology; RanBP: Ran binding protein; RanBP1: Ran binding protein1; RanBPM: Ran binding protein in microtubule organizing centre; SPRY: SPIa and Ryanodine receptor; Scorpin family: SPRY-containing Ran binding protein family.

Competing interests

The authors declare that they have no competing interests.

Acknowledgements

We thank Dr. Tomáš Takáč for preliminary confocal analyses. This work was supported by grants 204/07/1169, 204/09/P155, and P501/12/2333 from the Grant Agency of the Czech Republic, grant No. CZ.1.05/2.1.00/01.0007 Centre of the Region Haná for Biotechnological and Agricultural Research for ET and BP, IGA UP PrF/2012/001 for ET, grants LC06034 and LC545 from Ministry of Education, Youth and Sports of Czech Republic, and grant IAA500200719 from Grant Agency of the Czech Academy of the Sciences.

Author details

[1]Centre of the Region Haná for Biotechnological and Agricultural Research, Institute of Experimental Botany AS CR, v.v.i., Sokolovská 6, Olomouc 772 00, Czech Republic. [2]Institute of Experimental Botany, AS CR, v.v.i., Sokolovská 6, 772 00, Olomouc, Czech Republic. [3]Institute of Microbiology, AS CR, v.v.i., Vídeňská 1083, 142 20, Prague 4, Czech Republic.

Authors' contributions

ET performed databases search, *in vivo* microscopical analyses and wrote the manuscript. VC carried out immunolocalization and microscopy, and participated in writing the manuscript. LK performed biochemical analysis, isolation of protein complexes and confocal microscopy, BP performed cloning and together with LV, created stably transformed cell lines and plants of *Arabidopsis thaliana*, and performed *in vivo* microscopical analyses. PH performed proteomic analyses. GK undertook immunopurification of protein complexes. PB designed and coordinated experimental plans, and wrote the manuscript. All authors read and approved the final manuscript.

Received: 20 December 2011 Accepted: 7 June 2012
Published: 7 June 2012

References

1. Vetter IR, Wittinghofer A: **The guanine nucleotide-binding switch in three dimensions.** *Science* 2001, **294:**1299–1304.
2. Weis K: **Nucleocytoplasmic transport: cargo trafficking across the border.** *Curr Opin Cell Biol* 2002, **14:**328–335.
3. Haizel T, Merkle T, Pay A, Fejes E, Nagy F: **Characterization of proteins that interact with the GTP-bound form of the regulatory GTPase Ran in Arabidopsis.** *Plant J* 1997, **11:**93–103.

4. Pay A, Resch K, Frohnmeyer H, Fejes E, Nagy F, Nick P: **Plant RanGAPs are localized at the nuclear envelope in interphase and associated with microtubules in mitotic cells.** *Plant J* 2002, **30:**699–709.
5. Kim SH, Roux SJ: **An Arabidopsis Ran-binding protein, AtRanBP1c, is a co-activator of Ran GTPase-activating protein and requires the C-terminus for its cytoplasmic localization.** *Planta* 2003, **216:**1047–1052.
6. Baloğlu MC, Zakharov FN, Öktem HA, Yücel AM: **Molecular cloning, characterization, and expression analysis of a gene encoding a Ran binding protein (RanBP) in Cucumis melo L.** *Turk J Biol* 2011, **35:**387–397.
7. Cho HK, Park JA, Pai HS: **Physiological function of NbRanBP1 in Nicotiana benthamiana.** *Mol Cells* 2008, **26:**270–277.
8. Wang D, Li Z, Schoen SR, Messing EM, Wu G: **A novel MET-interacting protein shares high sequence similarity with RanBPM, but fails to stimulate MET-induced Ras/Erk signaling.** *Biochem Biophys Res Commun* 2004, **313:**320–326.
9. Dansereau D, Lasko P: **RanBPM regulates cell shape, arrangement, and capacity of the female germline stem cell niche in Drosophila melanogaster.** *J Cell Biol* 2008, **182:**963–977.
10. Hosono K, Noda S, Shimizu A, Nakanishi N, Ohtsubo M, Shimizu N, Minoshima S: **YPEL5 protein of the YPEL gene family is involved in the cell cycle progression by interacting with two distinct proteins RanBPM and RanBP10.** *Genomics* 2010, **96:**102–111.
11. Suresh B, Ramakrishna S, Baek KH: **Diverse roles of the scaffolding protein RanBPM.** *Drug Discov Today* 2012, **17:**379–387.
12. Umeda M, Nishitani H, Nishimoto T: **A novel nuclear protein, Twa1, and Muskelin comprise a complex with RanBPM.** *Gene* 2003, **303:**47–54.
13. Ideguchi H, Ueda A, Tanaka M, Yang J, Tsuji T, Ohno S, Hagiwara E, Aoki A, Ishigatsubo Y: **Structural and functional characterization of the USP11 deubiquitinating enzyme, which interacts with the RanGTP-associated protein RanBPM.** *J Biochem* 2002, **367:**87–95.
14. Nishitani H, Hirose E, Uchimura Y, Nakamura M, Umeda M, Nishii K, Mori N, Nishimoto T: **Full-sized RanBPM cDNA encodes a protein possessing a long stretch of proline and glutamine within the N-terminal region, comprising a large protein complex.** *Gene* 2001, **272:**25–33.
15. Kobayashi N, Yang J, Ueda A, Suzuki T, Tomaru K, Takeno M, Okuda K, Ishigatsubo Y: **RanBPM, Muskelin, p48EMLP, p44CTLH, and the armadillo-repeat proteins ARMC8α and ARMC8β are components of the CTLH complex.** *Gene* 2007, **396:**236–247.
16. Regelmann J, Schutz T, Josupeit FS, Horak J, Rose M, Entian K, Thumm M, Wolf DH: **Catabolite Degradation of Fructose-1, 6-bisphosphatase in the Yeast Saccharomyces cerevisiae: A Genome-wide Screen Identifies Eight Novel GID Genes and Indicates the Existence of Two Degradation Pathways.** *Mol Biol Cell* 2003, **14:**1652–1663.
17. Tomaru K, Ueda A, Suzuki T, Kobayashi N, Yang J, Yamamoto M, Takeno M, Kaneko T, Ishigatsubo Y: **Armadillo Repeat Containing 8alpha Binds to HRS and Promotes HRS Interaction with Ubiquitinated Proteins.** *Open Biochem J* 2010, **4:**1–8.
18. Aquea F, Matte JP, Gutiérrez F, Rico S, Lamprecht M, Sánchez C, Arce-Johnson P: **Molecular characterization of a Trithorax-group homologue gene from Pinus radiata.** *Plant Cell Rep* 2009, **28:**1531–1538.
19. Gao X, Chen Z, Zhang J, Li X, Chen G, Li X, Wu C: **OsLIS-L1 encoding a lissencephaly type-1-like protein with WD40 repeats is required for plant height and male gametophyte formation in rice.** *Planta* 2012, **354:**713–727.
20. Proost S, Van Bel M, Sterck L, Billiau K, Van Parys T, Van de Peer Y, Vandepoele K: **PLAZA: a comparative genomics resource to study gene and genome evolution in plants.** *Plant Cell* 2009, **21:**3718–3731.
21. Swarbreck D, Wilks C, Lamesch P, Berardini TZ, Garcia-Hernandez M, Foerster H, Li D, Meyer T, Muller R, Ploetz L, Radenbaugh A, Singh S, Swing V, Tissier C, Zhang P, Huala E: **The Arabidopsis Information Resource (TAIR): gene structure and function annotation.** *Nucleic Acids Res* 2008, **36:**D1009–14.
22. Lopez R: **WU-Blast2 server at the European Bioinformatics Institute.** *Nucleic Acids Res* 2003, **31:**3795–3798.
23. Tamura K, Peterson D, Peterson N, Stecher G, Nei M, Kumar S: **MEGA5: Molecular Evolutionary Genetics Analysis using Maximum Likelihood, Evolutionary Distance, and Maximum Parsimony Methods.** *Mol Biol Evol* 2011, **28:**2731–2739.
24. Ponting C, Schultz J, Bork P: **SPRY domains in ryanodine receptors (Ca2 + -release channels).** *Trends Biochem Sci* 1997, **5:**2–3.
25. Rhodes D, de Bono B, Trowsdale J: **Relationship between SPRY and B30.2 protein domains. Evolution of a component of immune defence?** *Immunology* 2005, **116:**411–417.
26. Emes RD, Ponting CP: **A new sequence motif linking lissencephaly, Treacher Collins and oral-facial-digital type 1 syndromes, microtubule dynamics and cell migration.** *Hum Mol Genet* 2001, **10:**2813–2820.
27. Menon RP, Gibson TJ, Pastore A: **The C Terminus of Fragile X Mental Retardation Protein Interacts with the Multi-domain Ran-binding Protein in the Microtubule-organising Centre.** *J Mol Biol* 2004, 43–53.
28. Puntervoll P: **ELM server: a new resource for investigating short functional sites in modular eukaryotic proteins.** *Nucleic Acids Res* 2003, **31:**3625–3630.
29. Ren J, Gao X, Jin C, Zhu M, Wang X, Shaw A, Wen L, Yao X, Xue Y: **Systematic study of protein sumoylation: Development of a site-specific predictor of SUMOsp 2.0.** *Proteomics* 2009, **9:**3409–3412.
30. Mathur J, Csaba K: **Establishment and Maintenance of Cell Suspension Cultures**. In *Methods in Molecular Biology. Volume 82. Arabidopsis protocols*. Edited by Martinéz-Zapater J, Salinas J. Totowa: Humana Press; 1997:27–30.
31. Clough SJ, Bent F: **Floral dip: a simplified method for Agrobacterium-mediated transformation of Arabidopsis thaliana.** *Plant J* 1998, **16:**735–743.
32. Winter D, Vinegar B, Nahal H, Ammar R, Wilson GV, Provart NJ: **An "Electronic Fluorescent Pictograph" browser for exploring and analyzing large-scale biological data sets.** *PLoS One* 2007, **2:**e718.
33. Hruz T, Laule O, Szabo G, Wessendorp F, Bleuler S, Oertle L, Widmayer P, Gruissem W, Zimmermann P: **Genevestigator v3: a reference expression database for the meta-analysis of transcriptomes.** *Advances in bioinformatics* 2008, **2008:**420747.
34. Ruepp A, Waegele B, Lechner M, Brauner B, Dunger-Kaltenbach I, Fobo G, Frishman G, Montrone C, Mewes HW: **CORUM: the comprehensive resource of mammalian protein complexes-2009.** *Nucleic Acids Res* 2010, **38:**D497–501.
35. Suzuki T, Ueda A, Kobayashi N, Yang J, Tomaru K, Yamamoto M, Takeno M, Ishigatsubo Y: **Proteasome-dependent degradation of alpha-catenin is regulated by interaction with ARMc8alpha.** *J Biochem* 2008, **411:**581–591.
36. Lee I: **Ambaru Bi, Thakkar P, Marcotte EM, Rhee SY: Rational association of genes with traits using a genome-scale gene network for Arabidopsis thaliana.** *Nature Biotechnol* 2010, **28:**149–156.
37. Nakamura M, Masuda H, Horii J, Kuma KI, Yokoyama N, Ohba T, Nishitani H, Miyata T, Tanaka M, Nishimoto T: **When overexpressed, a novel centrosomal protein, RanBPM, causes ectopic microtubule nucleation similar to gamma-tubulin.** *J Cell Biol* 1998, **143:**1041–1052.
38. Dryková D, Cenklová V, Sulimenko V, Volc J, Dráber P, Binarová P: **Plant gamma-Tubulin Interacts with alpha-Tubulin Dimers and Forms Membrane-Associated Complexes.** *Plant Cell* 2003, **15:**465–480.
39. Heald R, Weis K: **Spindles get the Ran around.** *Cell* 2000, **8924:**1–4.
40. Murrin LC, Talbot JN: **RanBPM, a scaffolding protein in the immune and nervous systems.** *J Neuroimmune Pharm* 2007, **2:**290–295.
41. Zou Y, Lim S, Lee K, Deng X, Friedman E, Chem JB: **Serine/Threonine Kinase Mirk/Dyrk1B Is an Inhibitor of Epithelial Cell Migration and Is Negatively Regulated by the Met Adaptor Ran-binding Protein M.** *J Biol Chem* 2003, **278:**49573–49581.
42. Denti S, Sirri A, Cheli A, Rogge L, Innamorati G, Putignano S, Fabbri M, Pardi R, Bianchi E: **RanBPM Is a Phosphoprotein That Associates with the Plasma Membrane and Interacts with the Integrin LFA-1.** *J Biol Chem* 2004, **279:**13027–13034.
43. Poirier MB, Laflamme L, Langlois MF: **Identification and characterization of RanBPM, a novel coactivator of thyroid hormone receptors.** *J Mol Endocrinol* 2006, **36:**313–325.
44. Talbot JN, Skifter DA, Bianchi E, Monaghan DT, Toews ML, Murrin LC, Myron LT: **Neuroscience Letters Regulation of mu opioid receptor internalization by the scaffold protein RanBPM.** *Neurosci Lett* 2009, **466:**154–158.
45. Puverel S, Barrick C, Dolci S, Coppola V, Tessarollo L: **RanBPM is essential for mouse spermatogenesis and oogenesis.** *Development* 2011, **138:**2511–2521.
46. Cheng L, Lemmon S, Lemmon V: **RanBPM is an L1-interacting protein that regulates L1-mediated mitogen-activated protein kinase activation.** *J Neurochem* 2005, **94:**1102–1110.

47. Atabakhsh E, Bryce DM, Lefebvre KJ, Schild-Poulter C: **RanBPM has proapoptotic activities that regulate cell death pathways in response to DNA damage.** *Mol Cancer Res* 2009, **7:**1962–1972.
48. Santt O, Pfirrmann T, Braun B, Juretschke J, Kimmig P, Scheel H, Hofmann K, Thumm M, Wolf DH: **The Yeast GID Complex, a Novel Ubiquitin Ligase (E3) Involved in the Regulation of Carbohydrate Metabolism.** *Mol Biol Cell* 2008, **19:**3323–3333.
49. Zhu Y, Wang Y, Xia C, Li D, Li Y, Zeng W, Yuan W, Liu H, Zhu C, Wu X, Liu M: **WDR26: a novel Gbeta-like protein, suppresses MAPK signaling pathway.** *J Cell Biochem* 2004, **93:**579–87.
50. Kobielak A, Pasolli HA, Fuchs E: **Mammalian formin-1 participates in adherens junctions and polymerization of linear actin cables.** *Nature Cell Biol* 2004, **6:**21–30.
51. Obayashi T, Nishida K, Kasahara K, Kinoshita K: **ATTED-II updates: condition-specific gene coexpression to extend coexpression analyses and applications to a broad range of flowering plants.** *Plant Cell Physiol* 2011, **52:**213–219.
52. Harrison SJ, Mott EK, Parsley K, Aspinall S, Gray JC, Cottage A: **A rapid and robust method of identifying transformed Arabidopsis thaliana seedlings following floral dip transformation.** *Plant Methods* 2006, **2:**19–25.
53. Karimi M, Inzé D, Depicker A: **GATEWAY vectors for Agrobacterium-mediated plant transformation.** *Trends Plant Sci* 2002, **7:**193–195.
54. Halada P, Man P, Grebenova D, Hrkal Z, Havlicek V: **Identification of HL60 proteins affected by 5-aminolevulinic acid-based photodynamic therapy using mass spectrometric approach.** *Collect Czech Chem Commun* 2001, **66:**1720–1728.
55. Laemmli UK: **Cleavage of structural proteins during the assembly of the head of bacteriophage T4.** *Nature* 1970, **227:**680–685.
56. Binarová P, Cenklová V, Procházková J, Doskočilová A, Volc J, Vrlík M, Bogre L: **gamma-Tubulin Is Essential for Acentrosomal Microtubule Nucleation and Coordination of Late Mitotic Events in Arabidopsis.** *Plant Cell* 2006, **18:**1199–1212.
57. Letunic I, Doerks T, Bork P: **SMART 7: recent updates to the protein domain annotation resource.** *Nucleic Acids Res* 2011, **:**1–4.
58. Finn RD, Tate J, Mistry J, Coggill PC, Sammut SJ, Hotz HR, Ceric G, Forslund K, Eddy SR, Sonnhammer EL, Bateman A: **The Pfam protein families database.** *Nucleic Acids Res* 2008, **36:**D281–8.
59. Larkin M, Blackshields G, Brown NP, Chenna R, McGettigan P, McWilliam H, Valentin F, Wallace IM, Wilm A, Lopez R, Thompson JD, Gibson TJ, Higgins DG: **Clustal W and Clustal X version 2.0.** *Bioinformatics* 2007, **23:**2947–2958.
60. Xao X, Xue Y: **DOG 1.0: illustrator of protein domain structures.** *Cell Res* 2009, **19:**271–273.

doi:10.1186/1471-2229-12-83
Cite this article as: Tomaštíková *et al.*: Interactions of an *Arabidopsis* RanBPM homologue with LisH-CTLH domain proteins revealed high conservation of CTLH complexes in eukaryotes. *BMC Plant Biology* 2012 **12**:83.

7.1.1 Supplementary data

Tomaštíková, E., Cenklová, V., Kohoutová, L., Petrovská, B., Váchová, L., Halada, P., Kočárová, G., and Binarová, P.; (2012) Interactions of an Arabidopsis RanBPM homologue with LisH-CTLH domain proteins revealed high conservation of CTLH complexes in eukaryotes. BMC Plant Biol,12:83 1-14

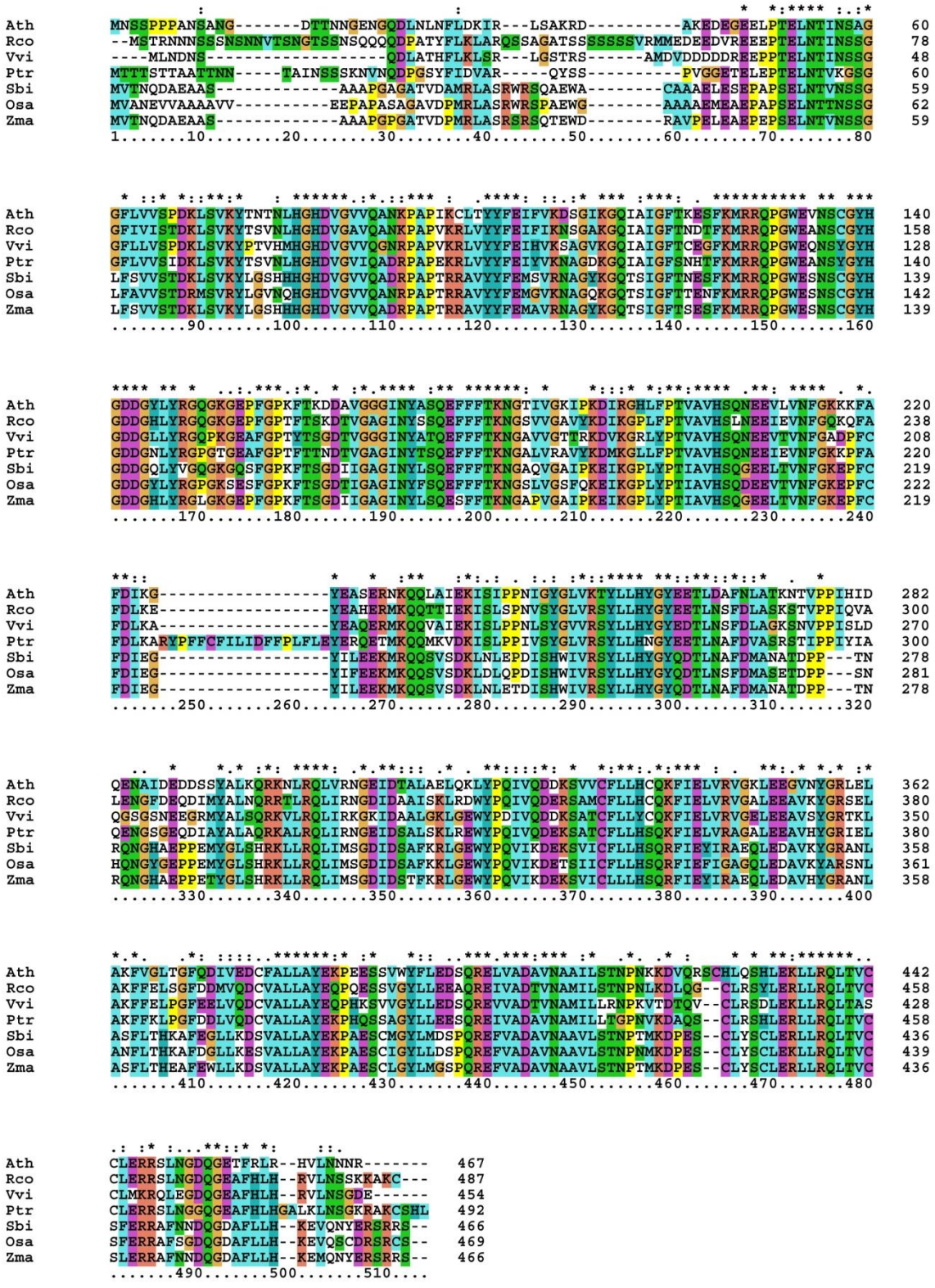

Additional file 1: **Multiple sequence alignment of AtRanBPM plant homologues**. Sequence alignment of *Arabidopsis* RanBPM with *Ricinus communis*, *Vitis vinifera*, *Populus trichocarpa*, *Sorghum bicolor*, *Oryza sativa* and *Zea mays* homologues. Alignment was done using ClustalX2 software (Larkin et al., 2007). Sequence data of this alignment can be found at accession numbers [Swiss-Prot:F4HYD7] for At1g35470, [Swiss-Prot:B9S762] for *R.*

communis, [Swiss-Prot:F6HWC3] for *V. vinifera*, [Swiss-Prot:B9MWC1] for *P. trichocarpa*, [Swiss-Prot:C5XUT1] for *S. bicolor*, [Swiss-Prot:Q6ZI83] for *O. sativa*, [Swiss-prot:B6UAR9] for *Z. mays*.

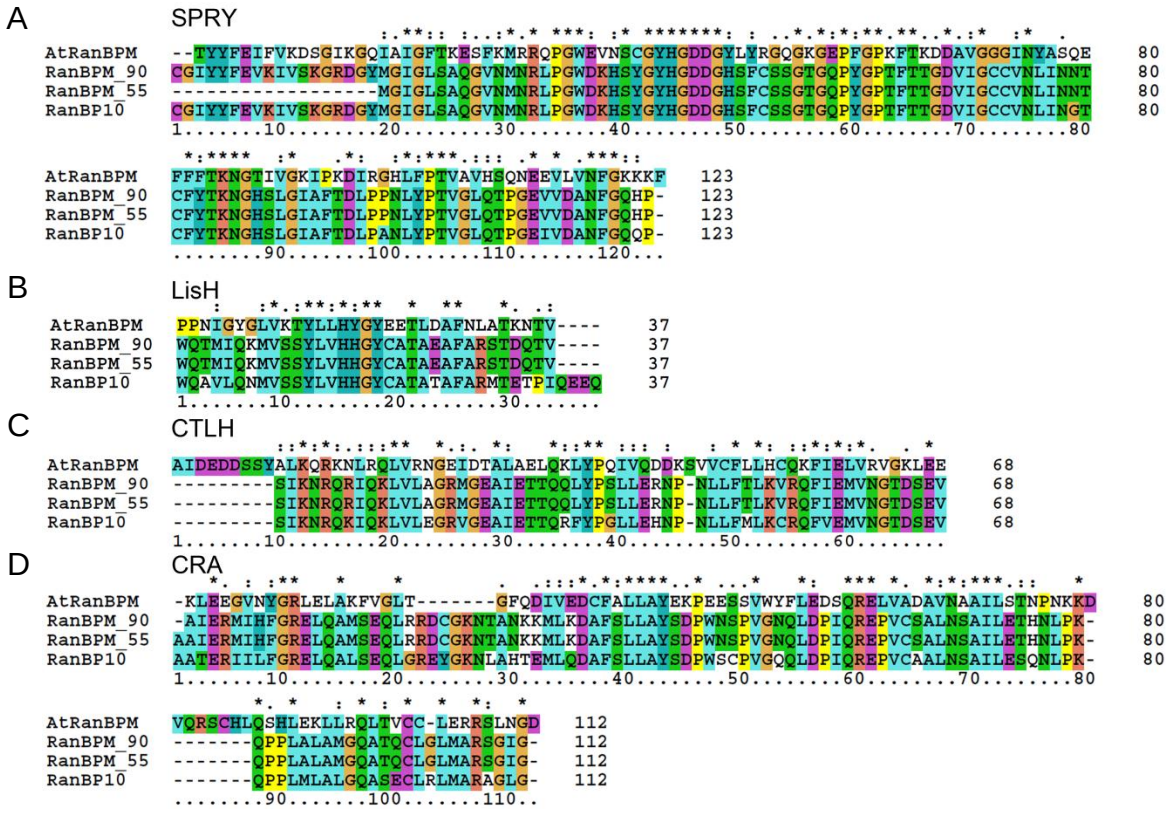

E

	RanBPM		RanBP10	
	Identities [%]	Similarities [%]	Identities [%]	Similarities [%]
SPRY	40,0	58,3	39,7	58,7
LisH	46,2	69,2	43,5	65,2
CTLH	30,8	67,3	28,8	59,2
CRA	43,8	62,5	41,9	62,8

Additional file 2: **Identities and similarities of conserved domains between *Arabidopsis* RanBPM and its human homologues**. Sequence alignment was done for conserved domains SPRY (A), LisH (B), CTLH (C) and CRA (D) of full-sized 90 kDa form (RanBPM_90) and 55 kDa form (RanBPM_55) of human RanBPM protein, and RanBP10 with *Arabidopsis* RanBPM using ClustalX2 software [58]. Sequence data of this alignment can be found at accession numbers [Swiss-Prot:Q6VN20] for RanBP10, [Swiss-Prot:Q96S59] for 90 kDa RanBPM and [EMBL:BAA23216] for 55 kDa RanBPM. Sequence of SPRY domain was encountered from the 99 amino acid in AtRanBPM sequence. E- Levels of identities and

similarities in amino acid composition of conserved domains between AtRanBPM and its human homologues RanBPM and RanBP10.

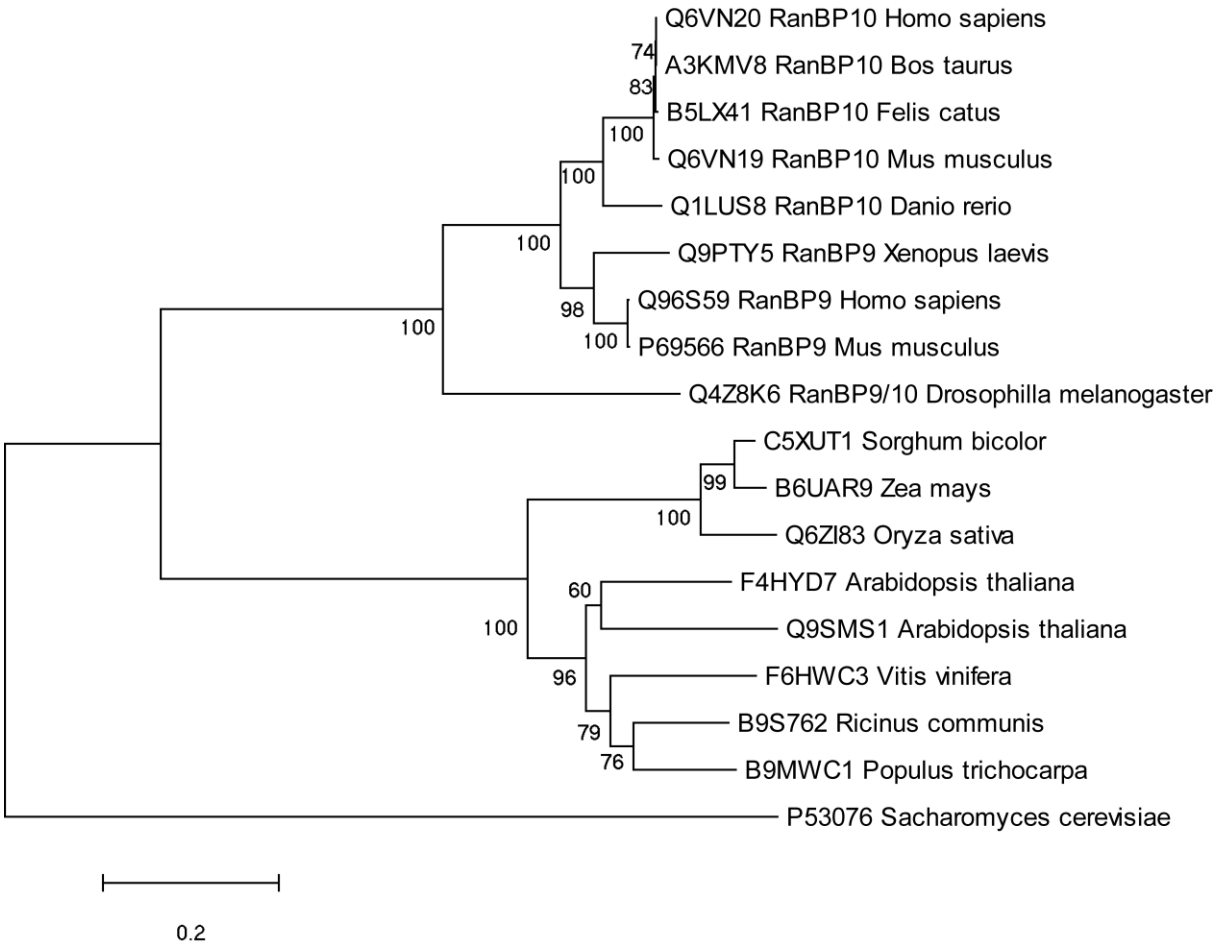

Additional file 3: Phylogenetic analysis of AtRanBPM and its homologues from other eukaryotic species. The tree was constructed by the neighbor-joining method with the MEGA 5.05 program. Branch numbers represent the percentage of bootstrap values in 1000 sampling replicates. The protein accession numbers are [Swiss-prot:F4HYD7] for AtRanBPM At1g35470, [Swiss-prot: Q9SMS1] At4g09340 (segmental genome duplication of chromosome 1), [Swiss-Prot:B9S762] for *R. communis*, [Swiss-Prot:F6HWC3] for *V. vinifera*, [Swiss-Prot:B9MWC1] for *P. trichocarpa*, [Swiss-Prot:C5XUT1] for *S. bicolor*, [Swiss-Prot:Q6ZI83] for *O. sativa*, [Swiss-Prot:B6UAR9] for *Z. mays*, [Swiss-prot: Q6VN20] for human RanBP10, [Swiss-prot: A3KMV8] for RanBP10 from *Bos taurus*, [Swiss-prot: B5LX41] for RanBP10 from *Felis catus*, [Swiss-prot: Q6VN19] for RanBP10 from *Mus musculus*, [Swiss-prot: Q1LUS8] for RanBP10 from *Danio rerio*, [Swiss-prot: Q9PTY5] for RanBP9 from *Xenopus laevis*, [Swiss-prot: Q96S59] for human RanBP9, [Swiss-prot: P69566] for RanBP9 from *Mus musculus*, [Swiss-prot: Q4Z8K6] for RanBP9/10 from *Drosophilla melanogaster* and [Swiss-prot: P53076] for Gid1/Vid30 homologue from *Sacharomyces cerevisiae*. Distance bars are given bottom left and bootstrap values are indicated at the nodes.

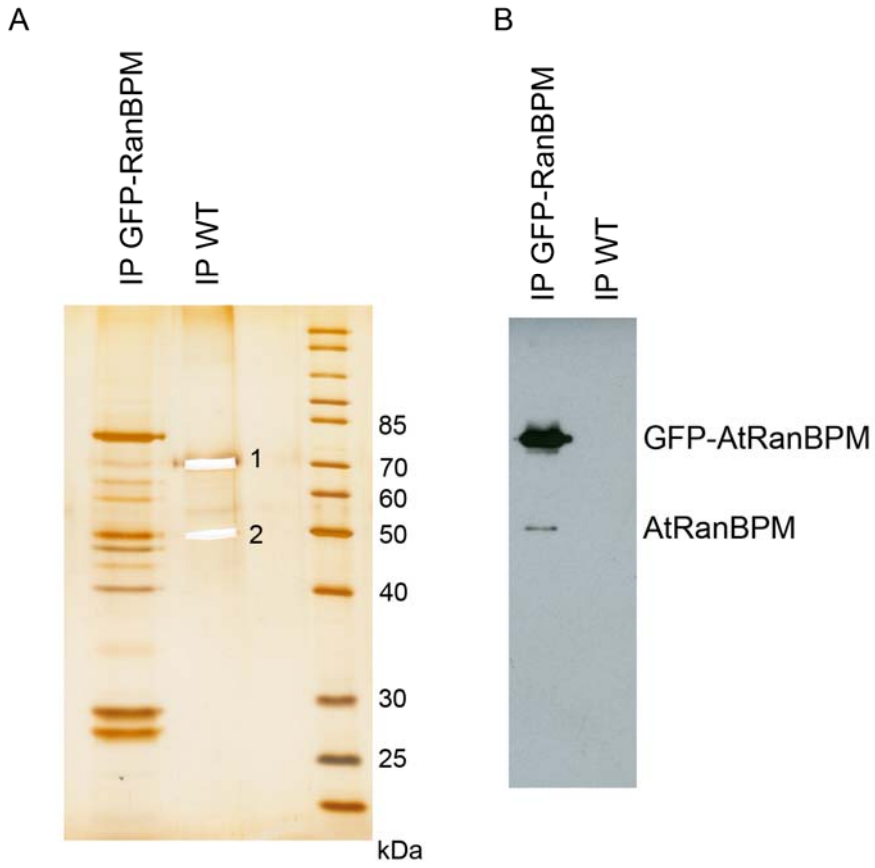

C

	Protein name	DTB No.	MW [kDa]	No. peptides	Sequence coverage [%]	MSMS confirmation
1	Protein S100-A8	S10A8_HUMAN	11	2	11	LLETECPQYIR
1	Actin, cytoplasmic 1	ACTB_HUMAN	42	4	17	SYELPDGQVITIGNER
1	Keratin, type II cytoskeletal 1	K2C1_HUMAN	66	4	12	No
1	Keratin, type I cytoskeletal 14	K1C14_HUMAN	51	1	1	IRDWYQR

Additional file 4: Immunopurification of GFP-AtRanBPM protein.
Immunopurification of GFP-AtRanBPM from extracts of GFP-AtRanBPM expressing cell cultures (IP GFP-RanBPM). GFP immunopurification from extracts of wild type Ler *Arabidopsis* cells (IP WT) was used as a negative control. A- Proteins were silver stained after separation on SDS-PAGE. Bands corresponding to MW similar of the proteins copurified with GFP-AtRanBPM (IP GFP-RanBPM) were not present in the negative control (IP WT). B- Signal for AtRanBPM was absent in the negative control (IP WT) after detection with anti-AtRanBPM antibody on Western blots. C- Proteins identified by MALDI-MS in negative control (IP WT in A) were background contamination.

Arabidopsis - human	**At1g35470 - RanBPM**	**At3g55070 - MAEA**	**At4g37880 - RMD5**	**At1g61150 - Twa1**	**At5g08560 - WDR26**	**At5g43920 - WDR26**
Identities [%]	31	36	37	42	39	40
Similarities [%]	50	58	59	63	59	58

Additional file 5: Identities and similarities between proteins copurifying with AtRanBPM and human CTLH complex members. Identities and similarities between *Arabidopsis* and human proteins were analyzed in WU-BLAST.

Protein name	AGI number	MW [kDa]	No. peptides	Sequence coverage [%]	Mascot score
LisH/CRA domains containing protein	At1g06060	25	1	4	32
Yippee family protein	At5g53940	15	1	9	71
Yippee-like protein	At3g08890	12	1	17	56
Yippee family protein	At2g40110	15	1	9	47
Armadillo/beta-catenin-like repeat-containing protein	At3g08947	97	4	5	120

Additional file 6: **Additional proteins copurified with AtRanBPM.** The proteins were identified by LC-MALDI-MS/MS and the identity of the matched peptides was confirmed by high-resolution MALDI-FTMS with mass accuracy below 1 ppm.

Additional file 7: GFP-AtRanBPM in *Arabidopsis* root cells.
AtRanBPM-GFP signal is dynamic and moving with the cytoplasmic stream.
(http://www.ncbi.nlm.nih.gov/pmc/articles/PMC3464593/)

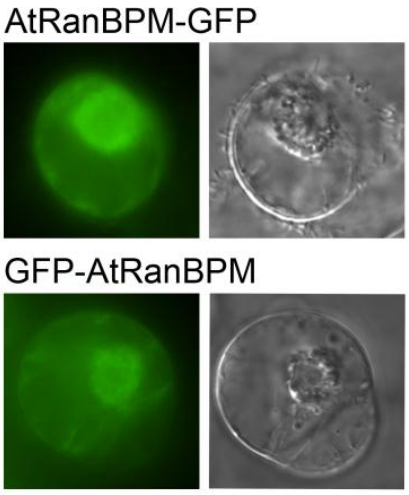

Additional file 8: Cellular localization of C-terminal GFP and N-terminal GFP AtRanBPM fusion proteins.

Cells of *Arabidopsis* expressing C-terminal GFP AtRanBPM (AtRanBPM-GFP) showed weak cytoplasmic and nuclear signal and accumulation of perinuclear GFP signal similarly as observed for N-terminal GFP AtRanBPM (GFP-AtRanBPM).

7.2

Doskočilová, A.[#], Kohoutová, L.[#], Volc, J., Kourová, H., Benada, O., Chumová, J., Plíhal, O., Petrovská, B., Halada, P., Bögre, L., and Binarová, P.; (2013) NITRILASE1 regulates the exit from proliferation, genome stability and plant development. New Phytol, 198(3):685-98

[#]These authors contributed equally to this article.

New Phytologist

Research

NITRILASE1 regulates the exit from proliferation, genome stability and plant development

Anna Doskočilová[1]*, Lucie Kohoutová[1]*, Jindřich Volc[1], Hana Kourová[1], Oldřich Benada[1], Jana Chumová[1], Ondřej Plíhal[1], Beáta Petrovská[2], Petr Halada[1], László Bögre[3] and Pavla Binarová[1]

[1]Institute of Microbiology AS CR, v. v. i., Vídeňská 1083, 142 20, Prague 4, Czech Republic; [2]Centre of the Region Haná for Biotechnological and Agricultural Research, Institute of Experimental Botany AS CR, v. v. i., Sokolovská 6, 772 00, Olomouc, Czech Republic; [3]Plant Molecular Sciences, Centre for Systems and Synthetic Biology, School of Biological Sciences, Royal Holloway, University of London, Egham, Surrey, TW20 0EX, UK

Author for correspondence:
Pavla Binarová
Tel: +42 0296442 130
Email: binarova@biomed.cas.cz

Received: *20 November 2012*
Accepted: *9 January 2013*

New Phytologist (2013) **198:** 685–698
doi: 10.1111/nph.12185

Key words: Arabidopsis, cell cycle, cytokinesis, filaments, microtubules, NITRILASE 1, polyploidy, programmed cell death.

Summary

- Nitrilases are highly conserved proteins with catabolic activity but much less understood functions in cell division and apoptosis. To elucidate the biological functions of Arabidopsis NITRILASE1, we characterized its molecular forms, cellular localization and involvement in cell proliferation and plant development.
- We performed biochemical and mass spectrometry analyses of NITRILASE1 complexes, electron microscopy of nitrilase polymers, imaging of developmental and cellular distribution, silencing and overexpression of nitrilases to study their functions.
- We found that NITRILASE1 has an intrinsic ability to form filaments. GFP-NITRILASE1 was abundant in proliferating cells, distributed in cytoplasm, in the perinuclear area and associated with microtubules. As cells exited proliferation and entered differentiation, GFP-NITRILASE1 became predominantly nuclear. Nitrilase silencing dose-dependently compromised plant growth, led to loss of tissue organization and sustained proliferation. Cytokinesis was frequently aborted, leading to enlarged polyploid cells. In reverse, independently transformed cell lines overexpressing GFP-NITRILASE1 showed slow growth and increased rate of programmed cell death.
- Altogether, our data suggest that NITRILASE1 homologues regulate the exit from cell cycle and entry into differentiation and simultaneously are required for cytokinesis. These functions are essential to maintain normal ploidy, genome stability and tissue organization.

Introduction

There is a rapid expansion of sequenced genomes spanning all the kingdoms, yet hundreds of conserved proteins exist for which general biochemical activities are known but biological functions are only predicted. Nitrilases, members of the C-N hydrolase superfamily catalyzing hydrolysis of nitriles into carboxylic acids and ammonia, are on the top of this list of 'conserved hypotheticals' (Galperin & Koonin, 2004). In Arabidopsis, there are four nitrilases NITRILASE1–4, of which NITRILASE1 (NIT1) shows the highest homology to animal and bacterial nitrilases. Following the plant nomenclature, animal orthologues are named NITRILASE1 (NIT1).

In the family of *Brassicaceae*, NIT1 has an enzymatic function in cyanide detoxification and catabolism of cyanogenic glycosides (Vorwerk *et al.*, 2001). NIT1 was also connected to the tryptophan-mediated alternative pathway of auxin biosynthesis from indole-3-acetonitrile (Michalczuk *et al.*, 1992). However, more recently it has been shown that NIT1 homologues have only very low activity on an indole-3-acetonitrile substrate (Agerbirk *et al.*, 2008). Therefore, the most accepted enzymatic functions for nitrilases in plants are in detoxification and nitrogen recycling, while their importance for auxin biosynthesis seems to be minor (Piotrowski, 2008).

There is accumulating evidence for a biological role of nitrilases beyond their enzymatic functions (Huebner *et al.*, 2011). Bacterial and fungal nitrilases have an ability to assemble into filaments *in vitro* (Thuku *et al.*, 2007; Kaplan *et al.*, 2011). In Arabidopsis leaves, the GFP fusion of NIT1 was observed as aggregated foci in the vicinity of the nuclei after wounding or herbicide treatment during the early steps of plant programmed cell death (PCD; Cutler & Somerville, 2005). NIT1 was also implicated in PCD in animal cells (Semba *et al.*, 2006; Sun *et al.*, 2009). In addition, *NIT1* in animal cells is a tumour suppressor gene; it was shown to negatively regulate T-cell proliferation (Zhang *et al.*, 2009). Curiously, in some organisms, in *Drosophila melanogaster* and in *Caenorhabditis elegans*, NIT1 forms a translational fusion with the FRAGIL HISTIDIN TRIAD (FHIT)

*These authors contributed equally to this work.

protein, suggesting that these proteins function together (Pekarsky *et al.*, 1998). *FHIT* is a well-characterized tumour suppressor gene inducing apoptosis and inhibiting tumorogenesis (Wali, 2010). In other organisms, for example in mouse, NIT1 and FHIT are encoded by separate genes, but the expression and function of *NIT1* and *FHIT* overlap. Moreover, the silencing of either *FHIT*, or *NIT1* in mouse, resulted in increased susceptibility to forestomach tumour and decreased apoptosis, induced by DNA damage (Semba *et al.*, 2006). While tumour suppressor functions of *FHIT* are well understood in animal cells, the mode of action and the biological function of *NIT1*, either in cooperation with or independent of *FHIT*, is much less clear (Huebner *et al.*, 2011).

Here, we provide evidence that in Arabidopsis NIT1 is present in high-molecular-mass polymers and forms filamentous structures similar to bacterial and fungal nitrilases. In agreement with the report of Cutler & Somerville (2005), we confirmed the aggregation of NIT1 at perinuclear locations upon induction of PCD and, in addition, we found that overproduction of NIT1 resulted in a reduced cell growth rate and higher levels of PCD. Downregulation of NIT1 homologues, NIT1–3 with RNAi silencing showed that these Arabidopsis nitrilases are important for cell cycle exit during differentiation, for normal cytokinesis and for maintaining regular ploidy levels and genome integrity. Nitrilases belong to a growing number of enzymes with function in biological processes distinct from their metabolic function. As shown by our data, Arabidopsis NIT1–3 are implicated in processes regulating cell proliferation and differentiation.

Material and Methods

Plant material and cell cultures

Arabidopsis thaliana cell suspension cultures of Columbia (Col) and Landsberg erecta (Ler) were grown under continuous darkness at 25°C as described (Drykova *et al.*, 2003). Seedlings of *Arabidopsis thaliana* (L.) Heynh. ecotype Columbia – Columbia lines expressing PM GFP marker (Cutler *et al.*, 2000) – were grown on half-strength MS agar plates as described (Binarova *et al.*, 2006).

Molecular methods

The complete coding region of *Arabidopsis NIT1* was cloned using Gateway^{R} technology. Vectors for 35S CaMV promoter driven expression for N- and C-terminal GFP fusions and for Multisite Gateway cloning of N-terminal GFP fusion of NIT1 under its native promoter were purchased from Ghent University (Ghent, Belgium). (For details, see Supporting Information Methods S1.) The constructs were transformed into *Agrobacterium tumefaciens* strain GV3101 which has been used for several independent transformations of Arabidopsis cultured cells and plants (Clough & Bent, 1998; Davis *et al.*, 2009). Seedlings were selected on kanamycin (50 μg ml^{-1}) medium. T1 transformants carrying GFP constructs had no discernible abnormalities, and we obtained T2 and T3 generations.

In order to produce a silencing RNAi construct, we cloned the 335 bp fragment of the *NIT1* sequence of the central conserved part of the NIT1 molecule into the pHANNIBAL vector to produce an inverted repeat and then this NIT-RNAi cassette was transferred into the binary vector pART27 (CSIRO Plant Industry, Clayton South, Australia). (For details and primers, see Methods S1.) With the NIT-RNAi construct we performed 15 independent transformations with Columbia, GFP-MAP4 and PM GFP Columbia plants. After 7 d of kanamycin selection resistant seedlings were transferred onto nonselective media. Phenotype was analysed in 6- to 19-d-old seedlings; transformants with the empty pART27 vector were used as the controls. The NIT-RNAi plants with phenotypes could not reach maturity and produce seeds. Therefore, we characterized > 200 of the independent transformants with phenotype in the T1 generation.

Quantitative real-time RT-PCR (Q RT-PCR) analyses were performed following MIQE recommendations (Bustin *et al.*, 2009) using methods described before (Petrovska *et al.*, 2012). (Primers are described in Methods S1.)

Protein methods

Protein extracts were prepared from cultured cells and seedlings as described before (Drykova *et al.*, 2003). (For details of differential centrifugation, see Methods S1.)

Custom polyclonal rabbit antibody (GenScript) for the NIT1 was raised against the C-terminal sequence DIARAKLYFDSVGHYSRPDV (aa 299–318) of the NIT1 molecule, affinity purified on peptide and used in dilution of 1 : 100 to 1 : 1000.

Gel filtrations were carried out from re-solubilized P100 on Superose 6 10/300 GL column (GE Healthcare Bio-Sciences, Uppsala, Sweden) according to Doskocilova *et al.* (2011).

Co-immunoprecipitation was performed using GFP-Trap_A (ChromoTek, Planegg-Martinsried, Germany) according to the manufacturer's instructions.

Protein identifications by MALDI mass spectrometry were performed from excised silver-stained protein bands as described (Halada *et al.*, 2001). Mass spectra were acquired on Ultraflex III instrument (Bruker Daltonics, Billerica, MA, USA) and searched against SwissProt 2011_04 database using the in-house Mascot search engine.

The microtubule spin-down experiments were performed as described previously (Binarova *et al.*, 2006). Three independent experiments were conducted; representative Western blots are shown.

Microscopy

For immunogold labelling and electron microscopy, 5-μl samples were applied directly onto glow-discharged activated Formvar/carbon coated nickel grids for 30 s and fixed in 4% PFA and 0.1% glutaraldehyde in PBS (pH 7.4) for 10 min. (For details of the immunogold labelling and negative staining, see Methods S1). The grids were examined using a Philips CM100 electron microscope at 80 kV and a magnification of ×46 000. Digital images were

recorded using a MegaViewII (Olympus, Tokyo, Japan) slow scan camera at a magnification of ×64 000 giving the digital resolution of *c.* 1 nm per pixel.

Immunofluorescence labelling was performed as described (Drykova *et al.*, 2003) using anti-NIT1 (1 : 100), anti-α-tubulin (1 : 2000) and anti-γ-tubulin TU-32 antibodies (1 : 6). Drugs were diluted in DMSO and used in working concentrations of: 5 μM for amiprophosmethyl (APM, A0185, Duchefa Biochemie, Haarlem, Netherlands), 10 μM for taxol (Paclitaxel, Sigma T7402), and 10 μg ml^{-1} for aphidicolin (Sigma, A0781) and applied as indicated.

Fluorescence microscopy and live cell imaging was performed using the Olympus IX-81 inverted microscope with Olympus DSU – Disc Scanning Confocal Unit and Olympus IX-81 FV-1000 confocal microscope (Olympus); images were taken and analysed as described previously (Doskocilova *et al.*, 2011).

Cell cycle analysis

EdU staining of replicating cells was performed using Click-iT EdU Alexa Fluor 488 HCS Assay (Molecular Probes, Eugene, OR, USA) based on methods modified from Vanstraelen *et al.* (2009). Mitotic index was determined after Carnoy's fixation and 0.45% lacto-propionic-orcein staining. To determine the growth curve of the *Arabidopsis* cell suspension, 5 ml of cultured cells were sedimented and cells were weighed.

For TUNEL assay, cells were fixed by 3.7% paraformaldehyde, attached to poly-L-lysine slides, and permeabilised (0.1% Triton X-100 in 0.1% sodium citrate for 10 min). The labelling reaction was carried out according to the manufacturer's protocol (Roche 12156792910) and the DNA was stained by DAPI. For PCD induction, 2 mM acetylsalicylic acid (ASA, Sigma A6810) treatment for 3–4 h was applied.

For chromocentra counting cells were fixed in an ethanol:acetic acid mixture (v/v 3 : 1) at room temperature for 1 h then macerated in 0.1 M HCl for 10 min at 37°C, rinsed in water, squeezed in 45% acetic acid at 45°C, and stained with 2 μg ml^{-1} DAPI for 10 min in the dark.

Flow cytometry sample preparation was performed using Partec CyStain UV precise P kit (Partec, Munster, Germany). Measurements were performed on a BD LSRII (BD Biosciences, Franklin Lakes, NJ, USA) with a solid state laser (excitation 405 nm) and 450/50 band pass filter. Forward scatter and side scatter were taken at 488 nm. Data were evaluated in FlowJo (Tree Star, Ashland, OR, USA). (For full details of the materials and methods, see Methods S1.) Whenever possible, at least three independent experiments were performed.

Results

NIT1 is present in high-molecular-mass forms that were identified by EM as filamentous structures

Nitrilases are self-polymerizing proteins, as shown for recombinantly expressed bacterial protein *in vitro* (Thuku *et al.*, 2007). Aggregation of Arabidopsis NIT1-GFP was observed in early stages of PCD by Cutler & Somerville (2005), but high-molecular-mass forms of plant nitrilases were not characterized. There are four genes encoding nitrilases in the *Arabidopsis thaliana* genome (Fig. S1a). *NIT1*, *NIT2* and *NIT3* (referred to as *NIT1* homologues) code for proteins sharing high amino acid similarities (84–90%), while their similarity with NIT4 is lower (66–68%). There are orthologues of NIT1 in bacteria, fungi, and animals (Fig. S1b). In order to study the biochemical properties of the protein and its cellular distribution, we prepared antibody against a peptide derived from the C-terminus of NIT1. On Western blots of crude extracts of *Arabidopsis* cultured cells and seedlings, the affinity purified antibody detected a band of *c.* 38 kDa, corresponding to the calculated NIT1 molecular mass (Fig. S2). We also prepared NIT1 C- and N-terminal GFP fusion constructs under the control of the CaMV 35S promoter (p35S::NIT1-GFP and p35S::GFP-NIT1) as well as a NIT1 N-terminal GFP fusion under the control of NIT1 promoter (pNIT1::GFP-NIT1). We transformed *Arabidopsis* cultured cells and plants using these constructs. The NIT1 GFP fusion proteins had the expected 65 kDa molecular mass detected on Western blots as a single band (Figs 1b, S2).

In order to learn about NIT1 molecular forms, we used differential centrifugation. Differential centrifugation from crude cellular extracts showed that endogenous NIT1 remained in the

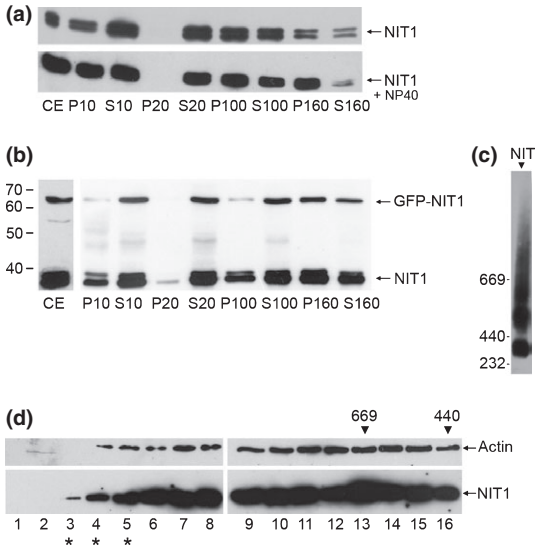

Fig. 1 Subcellular distribution and molecular forms of NIT1. (a) Differential centrifugation was carried out from *Arabidopsis thaliana* cultured cells without or with detergent treatment or (b) from cells transformed with pNIT1::GFP-NIT1. Pellets were resuspended to the volume of corresponding supernatants and equal sample volumes from the fractions were loaded on SDS-PAGE. Antibody against NIT1 was used for detection of endogenous NIT1 and GFP-NIT1 on Western blot. Crude extract (CE); pellet (P); supernatant (S). (c) GFP-NIT1 was immunopurified from microsomal pellet P100 with GFP antibody, loaded on BN-PAGE, blotted and detected with NIT1 antibody. Protein complexes showed a broad range of molecular masses separated by BN-PAGE. (d) Fractions from gel filtration of P100 were Western blotted and immunostained with antibodies against NIT1 and actin. Fractions used for EM analysis are marked with asterisks.

supernatant (S100) and a portion of it was pelleted to the microsomal fraction at 100 000 ***g*** (P100). At 160 000 ***g*** a further fraction of NIT1 was pelleted from the S100 (P160). The fact that NIT1 was sedimented to high-speed pellets also when differential centrifugation was performed with the nonionic detergent NP-40 suggested that higher molecular forms of NIT1 were not membrane-bound (Fig. 1a). Differential centrifugation performed from extracts of cells transformed with pNIT1::GFP-NIT1 construct showed a similar distribution of GFP-NIT1 to the endogenous NIT1 (Fig. 1b).

The presence of NIT1 in large molecular assemblies was also indicated by the broad range of molecular masses of the immunopurified GFP-NIT1 separated under native conditions by blue native PAGE (Fig. 1c). Similarly, gel filtration chromatography of the re-solubilized microsomal P100 pellets also showed a broad size distribution of NIT1 with no significant maxima, ranging from the column void volume at > 2 MDa through to fractions of *c.* 440-kDa-oligomeric forms (Fig. 1d). We conclude that NIT1 exists both as soluble and high-molecular-mass forms.

In order to analyse the composition of the high-molecular-mass forms of NIT1, we immunopurified the complex through the GFP tag and identified the proteins from SDS PAGE silver stained gels by MALDI-MS (Fig. S3). Together with GFP-NIT1, we found untagged endogenous NIT1 and NIT2 in almost equimolar amounts, suggesting that the large molecular mass forms are assemblies of NIT1 and NIT2.

Next we analysed the high-molecular-mass fractions from gel filtration enriched for NIT1, based on Western blot detection (Fig. 1d, asterisks), by electron microscopy (EM). Negative stain EM revealed highly ordered linear filaments of variable lengths (Fig. 2a). These polymers, of up to 200 nm or occasionally longer, exhibited helical substructures, strongly resembling the earlier described filaments of recombinant bacterial nitrilase assembled *in vitro* (Thuku *et al.*, 2007). Closer inspection and measurements of several independent preparations demonstrated that the Arabidopsis putative nitrilase filaments have a uniform diameter of 12 ± 2 nm (mean ± SD, $n = 356$). To confirm the identity of filaments, we performed immunogold labelling of the samples from gel filtration with anti-NIT1 antibody. As shown in Fig. 2(b), the 12 ± 2 nm-diameter filamentous structures were specifically decorated by the anti-NIT1 antibody and secondary antibody coupled with gold particles. NIT1 labelling was preferentially associated with more open parts of the filaments (Fig. 2b, inset III), probably due to better accessibility of the epitope. Taken together, our biochemical analysis revealed the high-molecular-mass assemblies of *Arabidopsis* nitrilases that were visualized by EM as filamentous assemblies.

NIT1 is present in cytoplasm, with microtubular arrays and in the area of cell plate

We confirmed the stress-induced aggregation of NIT1 in the vicinity of nuclei described by Cutler & Somerville (2005). However, we also noticed microtubular localization in untreated proliferating cells, which we characterized further in Arabidopsis cultured cells by double-immunofluorescence labelling with affinity purified antibody against NIT1 and anti-α-tubulin antibody (Fig. 3a), or in cells transformed with pNIT1::GFP-NIT1 construct (Fig. 3b). NIT1 was mostly present in the cytoplasm, but in mitotic cells it localized with microtubules. A weak signal was associated with the preprophase band of cortical microtubules; in metaphase, NIT1 was enriched in the spindle area, and during cytokinesis NIT1 was present in the phragmoplast area and in the area of cell plate formation (Fig. 3a).

GFP-NIT1, expressed under its own promoter in several stable cultured Arabidopsis cell lines showed similar localization patterns *in vivo* as observed for endogenous NIT1 protein visualized by immunofluorescence (Fig. 3b). In interphase, the signals for GFP-NIT1 were present in the cytoplasm, in the vicinity of the

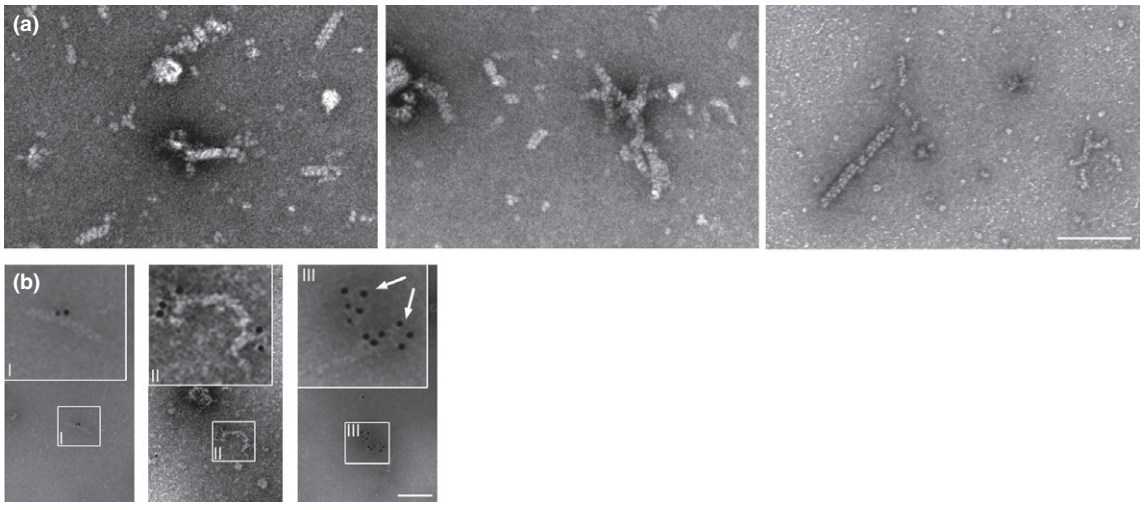

Fig. 2 NIT1 is present in form of linear polymers. Gel filtration fractions marked with asterisks in Fig. 1(d) were negatively stained (a) or immunogold labelled (b). EM showed linear polymers of NIT1. NIT1 filaments with loose structure were more heavily decorated with gold particles (inset III, arrows) compared to compact filaments (inset I and II). Bars, 100 nm.

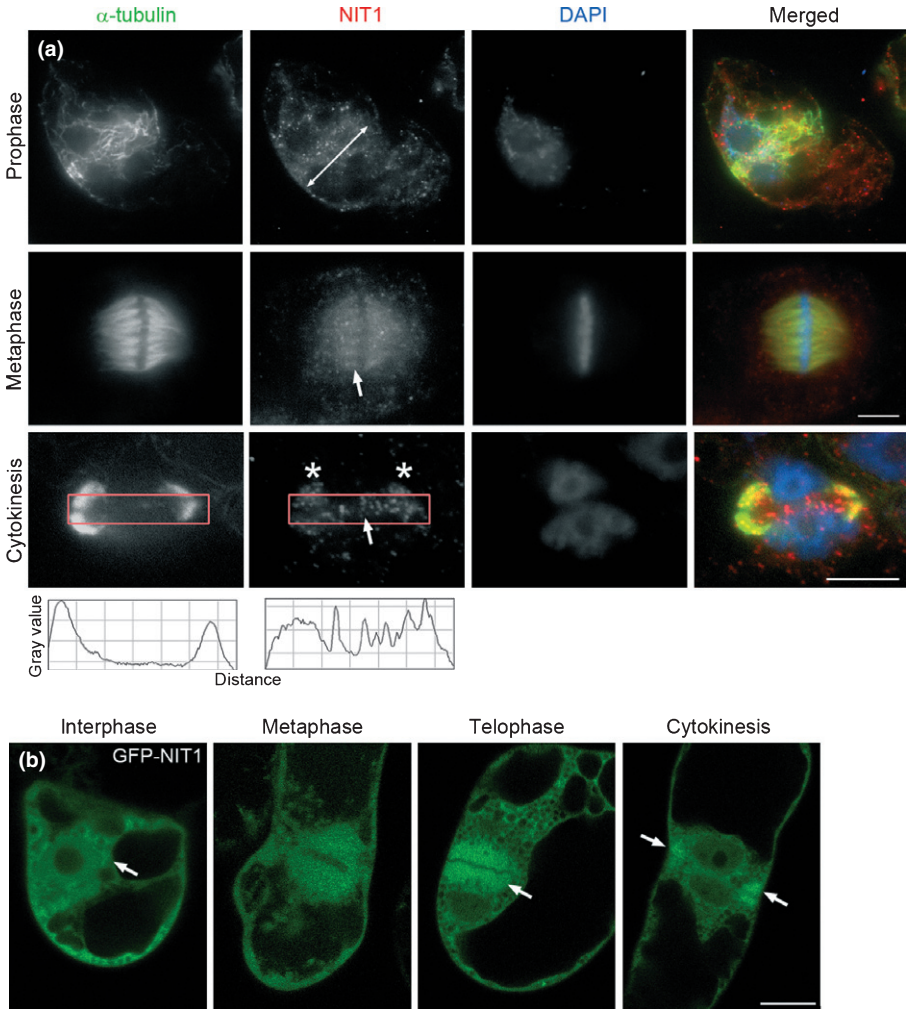

Fig. 3 Localization of NIT1 and GFP-NIT1 in cultured *Arabidopsis* cells. (a) Double immunofluorescence labelling of *Arabidopsis* cultured cells: NIT1 (red), α-tubulin (green), DNA stained by DAPI (blue). In prophase, the area of preprophase band microtubules (bifacial arrow) was positive for NIT1 signal. Kinetochore microtubular fibres of metaphase spindle were decorated with NIT1 (arrow). In cytokinesis, NIT1 was present in the area of phragmoplast. The plots show that NIT1 was present with microtubules of the phragmoplast (asterisks) and in the area of the forming cell plate (arrow). (b) Representative images of GFP-NIT1 expressed under its own promoter show interphase, metaphase, telophase and cytokinesis. In interphase, GFP-NIT1 accumulated in the vicinity of nuclear membrane (arrow). In metaphase, GFP-NIT1 signal was present with mitotic spindle and later in cytokinesis, GFP-NIT1 signal was present in the phragmoplast area (arrows). Bars, 10 μm.

nuclei and weakly in the nuclei. A portion of GFP-NIT1 signal was localized with the mitotic spindle and was enriched with the phragmoplast during cytokinesis. When expression was driven from the 35S CaMV promoter, the GFP signal was stronger, particularly in the cytoplasm (Videos S1, S2). However, the enrichment of 35SGFP-NIT1 with mitotic spindle and cytokinetic apparatus was comparable to that observed for GFP-NIT1 expressed from its own promoter.

The microtubule associated NIT1 signal was enriched in taxol-treated cells (Fig. 4a). To confirm the association of NIT1 with microtubules, we performed a co-sedimentation assay with taxol-induced polymerization of microtubules from high-speed S70 supernatant (Drykova *et al.*, 2003). As shown in Fig. 4(b), NIT1 was detected with pelleted plant microtubules in the presence of taxol, but not in negative controls without taxol. However, unlike γ-tubulin that became further enriched in the pellet by the addition of taxol-stabilized brain microtubules (Drykova *et al.*, 2003), the portion of NIT1 pelleted in the presence or absence of taxol-stabilized brain microtubules remained approximately the same. Next we depolymerized microtubules with amiprophos methyl (APM), which led to the dispersion of NIT1 in the cytosol (Fig. 4c). As we showed previously, the remnants of kinetochore microtubules left after APM treatment are abundantly decorated with γ-tubulin (Binarova *et al.*, 2000), but hardly any NIT1 signal could be detected with the kinetochore microtubular stubs. Our data showed that a portion of NIT1 protein was associated with microtubules but not with sites of microtubule nucleation (Drykova *et al.*, 2003).

NIT1 is abundant in proliferating cells

Signal for GFP-NIT1 under the control of its native promoter was observed predominantly in the meristematic zone of primary roots and in developing young leaves (Fig. 5a). In proliferating cells the GFP-NIT1 signal was diffusely present in the cytoplasm (Figs 5c, S4a). As in cultured cells (Fig. 3a,b) it was somewhat enriched with mitotic microtubules (Fig. 5b). As cells exit proliferation, the nuclear signal became stronger in cells at the expansion and differentiation zones of roots (Figs 5c,d, S4b).

Silencing NITRILASE1–3 expression leads to compromised differentiation and continued cell proliferation

The *nit1–3* mutant allele was originally identified based on its resistance to auxin (Normanly *et al.*, 1997), but later it was shown that IAA synthesis rates and concentrations were similar to

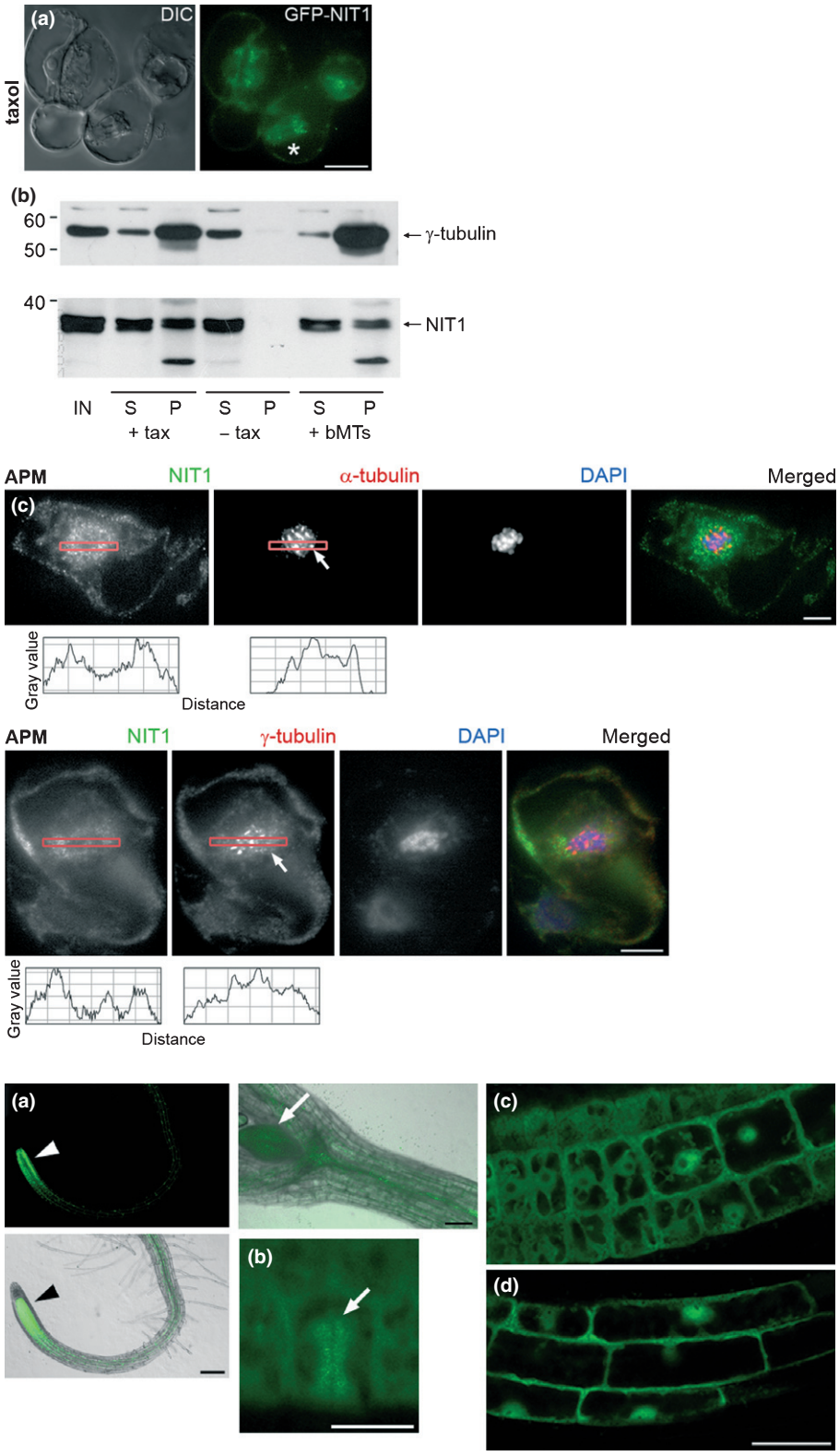

Fig. 4 Localization of GFP-NIT1 and NIT1 in microtubule-targeting drug treated cells of *Arabidopsis*. (a) Localization of GFP-NIT1 with taxol-stabilized microtubules after 3 h of taxol treatment (asterisk). (b) Co-sedimentation of NIT1 with taxol-stabilized microtubules. Western blots show microtubule spin-down assay. Microtubules were prepared from *Arabidopsis* extract S70 (IN) by taxol-induced polymerization and analysed with antibodies against NIT1 and γ-tubulin. S/P + Tax, supernatant/pellet after taxol treatment; S/P – Tax, supernatant/pellet without taxol treatment; S/P + bMTs, supernatant/pellet with added taxol-polymerized brain microtubules. (c) Double immunofluorescence labelling of *Arabidopsis* cell culture after microtubule depolymerization (2 h treatment with APM). NIT1 (green), α-tubulin (red), γ-tubulin (red), DNA stained by DAPI (blue). Microtubule stubs (arrows) were heavily decorated with γ-tubulin but almost no signal was observed for NIT1 (plot analysis of signal intensities). Bars (a,c), 20 μm.

Fig. 5 Localization of GFP-NIT1 driven by its own promoter in 7-d-old *Arabidopsis* seedlings. (a) Representative images of GFP-NIT1 signal in the main root (arrowheads) and developing young leaves (arrow). GFP-NIT1 signal was enriched with microtubules as shown for phragmoplast (b, arrow). (c) Division and expansion zone, (d) differentiation zone of the main root. Cytoplasmic GFP-NIT1 signal in the division zone became more nuclear in cells of expansion and differentiation zone (d). Bars: (a) 100 μm; (b) 20 μm; (c, d), 20 μm.

wild-type (Ljung *et al.*, 2005). *NIT1–3* are members of a small gene family with overlapping expression pattern and possibly redundant functions. To gain insights into nitrilase function, we downregulated *NIT1–3* expression in *Arabidopsis* plants using a dsRNA interference construct composed of a hairpin with inverted repeats, corresponding to a 335-bp fragment of the central part of the NIT1 molecule with significant sequence similarities to NIT1–3 homologues (NIT-RNAi). Several independent transformations were performed with the NIT-RNAi construct alongside an empty vector pART27 using the *Arabidopsis* ecotype

Columbia, an *Arabidopsis* line expressing the GFP marker for tubulin (GFP-MAP4; Marc *et al.*, 1998) and GFP marker for plasmatic membrane (Cutler *et al.*, 2000). Independent of the genetic backgrounds, and the transformation events, the T1-independent transformants with NIT-RNAi showed similar phenotypes ranging from milder to severe reduction of leaf and root growth (Fig. 6a,b). The phenotypes were not observed in plants transformed with empty vector. When the first true leaves of NIT-RNAi plants developed they were small and thick (arrows in Fig. 6c), abaxial polarity and tissue organization was gradually lost and leaves turned into disorganized structures (asterisk in Fig. 6c). In the strongest cases, callus-like structures were formed at the shoot apex instead of true leaves from the very beginning (arrowhead in Fig. 6c). NIT-RNAi plants with reduced levels of *NIT1–3* expression could not reach maturity and produce seeds and therefore we could only analyse seedlings in the T1 generation. To link the developmental abnormalities to the transformation with the NIT-RNAi construct, we counted the frequency of T1-independent transformants showing the phenotype obtained from independent transformations carried out at different times. We found that the phenotype always occurred with a frequency ranging from 30% to 60%, while with the empty vector this was 0%.

We determined by quantitative RT-PCR the reduction of *NIT1–4* expression in *c.* 60 independent NIT-RNAi T1 transformants showing the characteristic phenotypes. There was *c.* 80% reduction in three of the nitrilases, *NIT1–3* in the NIT-RNAi transformants compared to the controls (Fig. S5a). To correlate the strength of phenotypes with the reduction of *NIT1* expression, we analysed independent T1 NIT-RNAi transformants with phenotypes ranging from milder to severe abnormalities in true leaf differentiation and compared the *NIT1* expression levels to that of wild-type controls. The reduction of *NIT1* expression in the NIT-RNAi lines correlated with the severity of the observed phenotypes (Fig. S5b). Furthermore, similar developmental defects were not found in plants transformed with other unrelated dsRNA constructs, such as NodGS (Doskocilova *et al.*, 2011) or γ-tubulin (Binarova *et al.*, 2006) suggesting that the phenotypes we observed are specific for the NIT-RNAi construct and are the result of the silencing of *NIT1–3* expression.

Exit from cell proliferation is impaired when NITRILASE1–3 are silenced and cells became highly polyploid

In order to further analyse the leaf developmental defects, we microscopically inspected the first true leaves of 6–19-d-old seedlings from at least 100 independent NIT-RNAi seedlings with developmental abnormalities that were labelled with DAPI to stain nuclei. All of these plants showed similar type of defects at the cellular level; typical examples are shown in Fig. 7. Cells of young leaves of NIT-RNAi plants became large with grossly enlarged nuclei in comparison to the control. Also the regular line of marginal cells was disrupted and replaced by protrusions from highly enlarged cells (Fig. 7a). The enlarged cells of young malformated leaves of NIT-RNAi plants retained a high nuclei to cytoplasm volume ratio, typical for cells of meristem and leaf primordial, and did not become vacuolated. Correspondingly, cells with giant nuclei remained mitotically active. We observed all stages of mitosis from prophase to anaphase with a highly increased number of chromosomes, ranging from 20 to 60, instead of the regular diploid number of 10 in wild type (Fig. 7b,c). This suggested that the increased nuclei size did not arise through the process of endoreduplication (repeated S-phases) but likely through abnormal cell division.

In order to confirm the increased ploidy, we analysed DNA content by flow cytometry. We collected newly emerging leaves 3–4 and older leaves 1–2 from seedlings 16 d post germination from WT plants and the malformed leaves from NIT-RNAi seedlings at the same age. In wild-type control seedlings, cells of leaves 1–2 have entered endoreduplication and increased DNA content up to 8C while cells of the newly emerging leaves 3–4 were still diploid with 2C and 4C DNA content. By contrast, as shown in Fig. 7(d), for the malformed leaves of 16-d-old NIT-RNAi a grossly increased DNA content up to 32C and an almost complete lack of 2C DNA level were observed. To prove that the increased DNA content measured by flow cytometry in NIT-RNAi leaves is caused by polyploidy and not by increased level of endoreduplication, which naturally occurs in plant cells during development, we counted chromocentra. The chromocentra are formed by heterochromatin aggregates corresponding to mitotic centromeres (Fransz *et al.*, 2002). The average number of

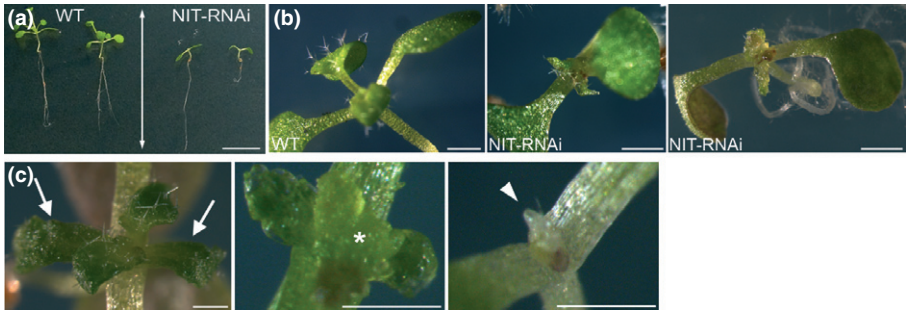

Fig. 6 Developmental abnormalities of T1 transformants of *Arabidopsis* NIT-RNAi plants. (a) 19-d-old independent T1 transformants with NIT-RNAi showing severe growth defects. (b) Representative images of aerial parts of 12-d-old Columbia wild type (WT), 12-d-old Columbia NIT-RNAi and 14-d-old Columbia PM NIT-RNAi plants. (c) Gradual loss of true leaf differentiation in NIT-RNAi T1 transformants: malformated true leaves of milder phenotype (arrows), leaves turning to disorganized structures (asterisk) and calli-like structures instead of the first true leaves in the strongest phenotypes (arrowhead). Bars: (a) 1 cm; (b) 1 mm; (c) 0.5 mm.

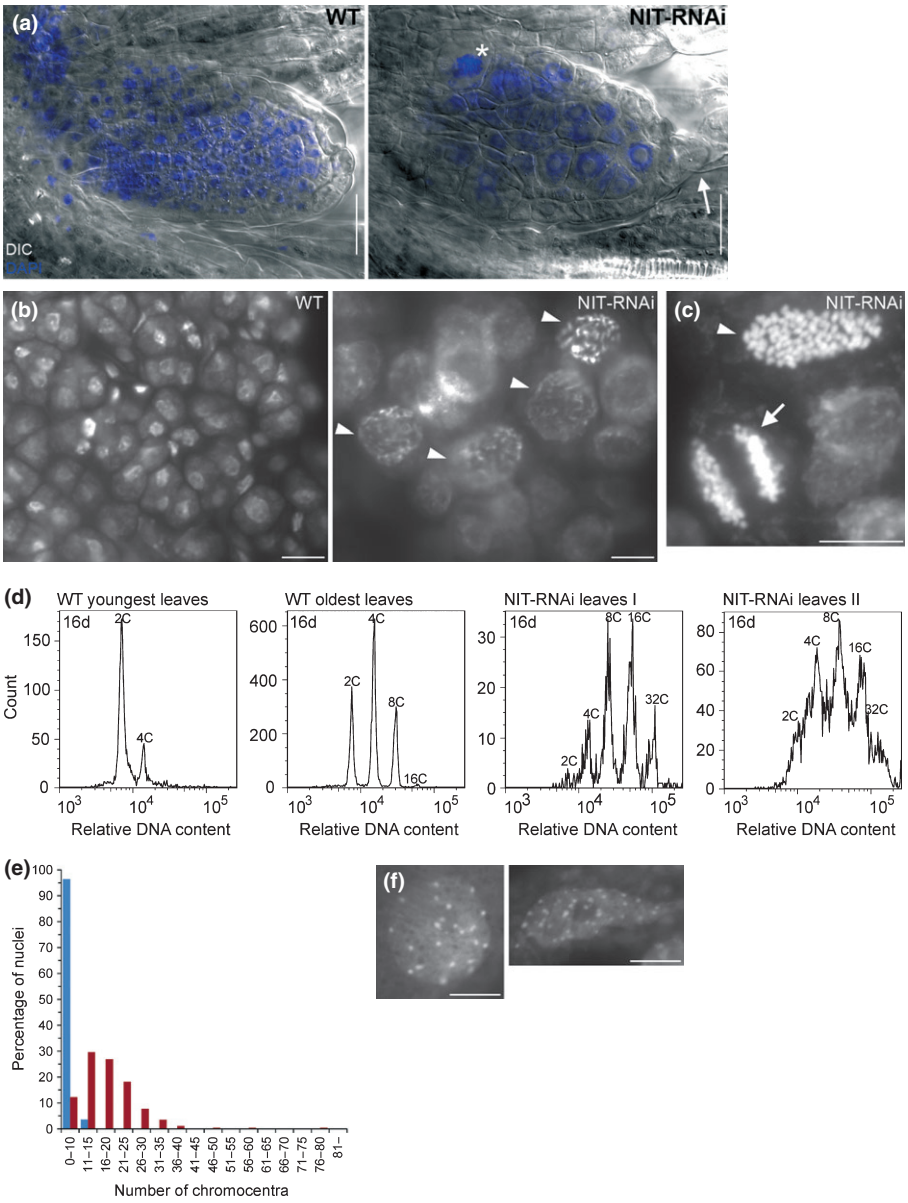

Fig. 7 Cells became highly polyploid in malformed leaves and calli-like structures of T1 NIT-RNAi transformants. (a) Representative image of the first true leaf of 6-d-old NIT-RNAi seedling. DNA stained by DAPI (blue). The cells had enlarged nuclei and leaf structure lacked regular margin cells (arrow). Cells with enlarged nuclei still underwent cell division (asterisk). (b) Representative image of leaves from a 14-d-old T1 transformant of NIT-RNAi plant. DNA stained with DAPI. Nuclei were grossly enlarged (arrowheads) in comparison to the control. Highly polyploid cells were at various stages of mitosis; prophase (b,c arrowheads) and anaphase (c, arrow). (d) Representative flow cytometry data from T1 transformants of NIT-RNAi plants. Youngest leaves (leaves 3, 4) of 16-d-old control WT (2C and 4C DNA levels) and oldest leaves (leaves 1, 2) of WT with 2C, 4C and 8C DNA levels are shown for comparison. Examples of flow data obtained from malformated leaves of the milder phenotype (NIT-RNAi leaves I) and the stronger phenotype (NIT-RNAi leaves II). Vertical axes represent number of nuclei; horizontal axes represent relative DNA content in logarithmic scale. (e) Distribution of number of nuclei with given number of chromocentra in interphase cells of WT (blue bars) and NIT-RNAi (red bars) leaves. (f) Interphase nuclei with high number of chromocentra (e.g. 22 and 38) of NIT-RNAi plants. Bars: (a) 20 μm; (b,c,f) 10 μm.

chromocentra in NIT-RNAi plants was 18.1 ± 8.0 ($n = 287$) compared to 8.2 ± 1.4 ($n = 224$) in control plants. In addition, in cells of NIT-RNAi leaves there is a broad variation in chromocentra number (6–79; Fig. 7e,f), which also corresponds with the lack of distinct peaks in the flow cytometry measurements, and indicates high genome instability in the NIT-RNAi plants. The mitotic figures and the counting of chromocentra firmly established that increased DNA content in the NIT-RNAi cells is not the consequence of elevated levels of endoreduplication.

Taken together, our data show that nitrilases are required to repress the entry into proliferation and in their absence cells become largely polyploid.

NITRILASE1–3 is required for cytokinesis

As polyploid cells often show cytokinetic failure, we searched for cytokinetic defects. Although the cotyledons of NIT-RNAi seedlings had no morphological abnormalities (Fig. 6b), closer inspection revealed that 74% of stomata were aberrant (Fig. 8a). Cytokinetic defects of stomata in cotyledons were early signs of the NIT-RNAi phenotype in T1-independent transformants (Fig. 8b). Round-shaped undivided mother guard cells, single guard cells, cells with aborted cell wall stubs – all indicating defective cytokinesis – were observed in cotyledons of NIT-RNAi seedlings. Abortive cytokinesis of stomata was also present in hypocotyls of NIT-RNAi seedlings (Fig. 8b). In true leaves with milder phenotypes, stomata were present, but both the stomata and pavement cells had extremely frequent cytokinetic defects (Fig. 8c). Hallmarks of aberrant cytokinesis, such as cell wall stubs, enlarged nuclei, fusion of nuclei or binuclear cells, were all abundant (Fig. 8c–e). Binuclear cells remained in the cell cycle and were capable to enter into S-phase, as revealed by positive labelling of replicating nuclei after a 3 h pulse in EdU assay (Fig. 8d). Although *c.* 100 independent NIT-RNAi T1

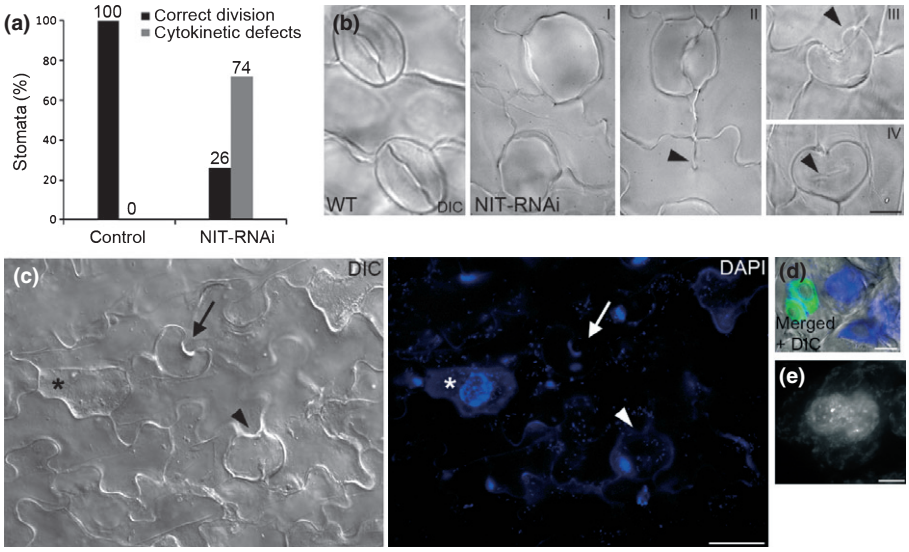

Fig. 8 Cytokinetic defects in NIT-RNAi plants. (a) Percentage of aberrant stomata in cotyledons is plotted, $n = 152$ for both WT and NIT-RNAi plants in Columbia background. (b) Representative images from CLSM of cotyledons (I–III) and hypocotyl (IV) of NIT-RNAi plants revealed strong defects in stomata last symmetric division in comparison to WT plants. Stomata without central pore (I), with incomplete cell plate (IV) or a single guard cell (III). Cell wall stubs were seen also in pavement cells (II). (c) Cytokinetic defects observed in pavement cells of the first true leaves: incomplete stomata with one guard cell (arrow), stomata with incomplete cell wall (arrowhead) and cells with giant nuclei (asterisk). (d) Leaf pavement cells with S-phase labelling of binuclear cell by EdU (EdU Alexa 488 (green); DNA stained by DAPI (blue) and (e) with fused nuclei (DAPI). Bars: (b,d,e) 10 μm; (c) 20 μm.

transformants were evaluated, we did not observe clustering of stomata, indicating that the cytokinesis but not cell lineage patterning during stomata development was affected in NIT-RNAi plants.

Although developmental abnormalities were more prominent in aerial parts, root development was also affected by silenced *NIT1–3* expression (Fig. S6). At the elongation zone, where normally cells exit the cell cycle, in NIT-RNAi, a large proportion of cells still remained in proliferation. The abnormally enlarged nuclei were detected by EdU labelling to go through DNA synthesis (Fig. S6a). In comparison to WT roots, the meristematic zone of primary roots of NIT-RNAi seedlings was markedly shortened and malformed; there were irregular cell files with cells having enlarged nuclei or two nuclei, suggesting defects in cytokinesis also in root cells (arrowheads in Fig. S6b).

Overexpression of NIT1 results in the suppression of cell growth and increased rate of PCD

We aimed to study the effect of overexpression of GFP-NIT1 driven by the 35S promoter, but among 20 independent transformants we could not obtain lines with significant overexpression, and plants expressing GFP-NIT1 at comparable levels to wild-type had no discernible phenotypic effects (Fig. S2). This indicates that the expression of *NIT1* in plants is tightly regulated. Contrary to moderate expressions found in the plants, we could obtain lines with high GFP-NIT1 expression in cultured *Arabidopsis* cells transformed with the p35::GFP-NIT1 construct (Fig. S2).

The effect of GFP-NIT1 overproduction on growth and division was analysed in three independent transformed cell lines. To determine whether the entry into S-phase is affected by higher NIT1 levels, we applied a 3 h pulse labelling of EdU immediately after subculture of stationary grown cells. As shown in Fig. 9(a), the proportion of cells labelled for S-phase during the first 3 h after subculture was reduced two- to three-fold in the GFP-NIT1 overexpression line as compared to the control. Reduced entry and pass through S-phase in GFP-NIT1 overexpressing lines was confirmed also by flow cytometry. We found a lower proportion of cells with G2 DNA content 24 h after subculture in 35S::GFP-NIT1 overexpression lines as compared to control (Fig. 9b). The lower number of cells progressing through the cell cycle within 24 h after subculture corresponded to the lower mitotic index (Fig. 9c). Furthermore, the growth rate of the overexpression lines determined by measuring fresh cell mass was lower compared to control (Fig. 9d).

NIT1 is implicated in PCD both in animal and plant cells (Cutler & Somerville, 2005; Zhang *et al.*, 2009). Clustering of GFP-NIT1 in early PCD of Arabidopsis was described by Cutler & Somerville (2005). To confirm whether GFP-NIT1 behaves similarly in our experiments, we used acetylsalicylic acid (ASA). ASA-induced PCD in Arabidopsis cell cultures as shown by Garcia-Heredia *et al.* (2008) and by us (Fig. S7). Immunofluorescence labelling of endogenous protein or confocal microscopy imaging of GFP-NIT1 *in vivo* showed a patchy signal for NIT1 accumulated in the perinuclear area or even penetrated into the nuclei in ASA-treated cells. Accumulation of GFP-NIT1 in perinuclear area and in nuclei was observed also after aphidicolin induced replication stress (Fig. S8).

We further addressed whether the overexpression of GFP-NIT1 alters the frequency of PCD measured by the DNA double-strand breaks through the TUNEL assay. As shown in Fig. 9(e), the number of TUNEL-positive cells was higher in 35S::GFP-NIT1 lines compared to wild-type. The difference between cells entering PCD became more prominent with time

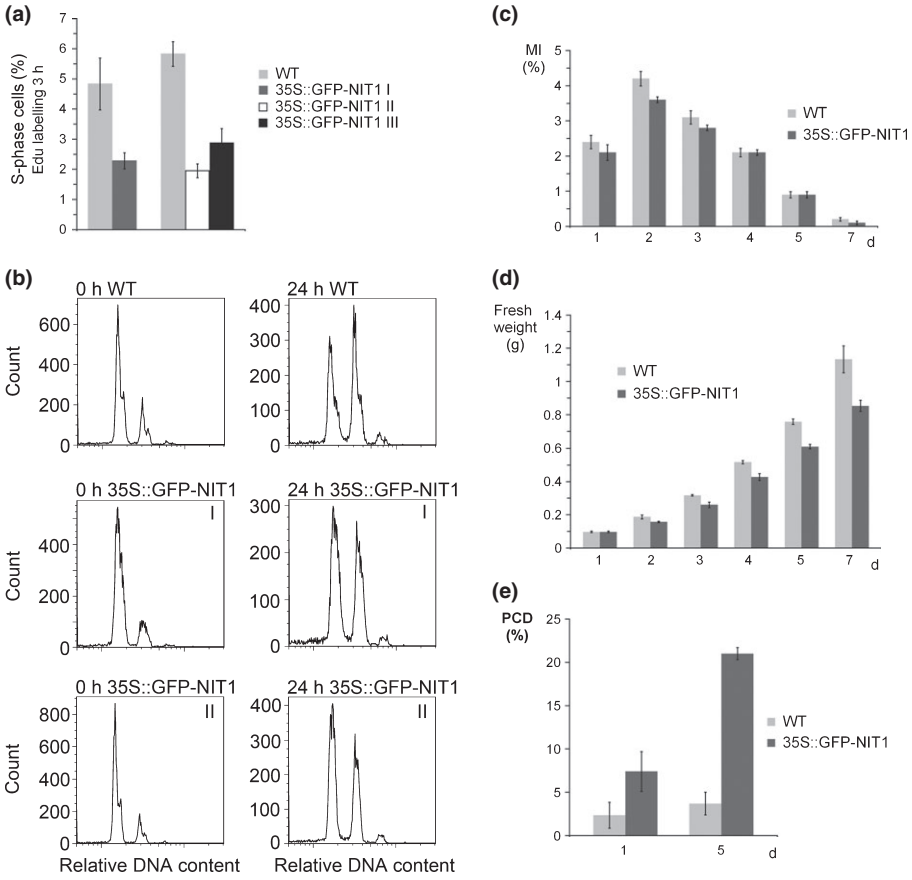

Fig. 9 Overexpression of GFP-NIT1 affected cell growth and resulted in increased PCD in *Arabidopsis* cultured cells. (a) Number of cells progressing through S-phase was reduced in 35S::GFP-NIT1 overexpressing cell lines compared to the controls. 3 h EdU pulse was applied during first 3 h after subculture from stationary culture. Bars represent ± SD. (b) Representative DNA content histograms of WT and two independent 35S::GFP-NIT1 overexpressing lines measured by flow cytometry at time points 0 and 24 h after subculture from stationary phase culture. Vertical axes: number of nuclei, horizontal axes: relative DNA content in logarithmic scale. (c) Mitotic index in time course of growth period of 7 d. Bars represent SD. (d) Cell fresh mass values were lower for 35S::GFP-NIT1 overexpressing cells compared to WT cells. Bars represent ± SD. (e) The level of PCD measured by TUNEL assay in 35S::GFP-NIT1 cells was higher compared to WT. Bars represent ± SD.

after subculture, being 7.4% and 20.9% for the 35S::GFP-NIT1 overexpression cultures, compared to 2.3% and 3.7% for control cultures on the first and fifth day after subculture, respectively.

Altogether, our data suggest that in Arabidopsis overproduction of GFP-NIT1 led to the reduction in cell proliferation and an increased level of PCD.

FHIT expression parallels *NIT1* levels in NIT-RNAi and 35S::GFP-NIT1 overexpression lines

Because in animals *NIT1* functions closely together with the *FHIT* tumour suppressor gene (Semba *et al.*, 2006), we searched for the *Arabidopsis* orthologue of *FHIT* and found a gene *At5 g58240* with 50% identity within the protein coding region (Fig. S9). The *Arabidopsis* gene is annotated as nucleoside phosphoramidase and adenylylsulfatase (*TAIR*; http://www.arabidopsis.org). In agreement, the animal FHIT is also involved in purine metabolism. *FHIT* is co-expressed with *NIT1* in animal cells (Sun *et al.*, 2009). Therefore, we tested *FHIT* expression together with expression of *NIT1* in silenced NIT-RNAi seedlings. As shown in Fig. S10, *FHIT* expression was reduced in NIT-RNAi seedlings while in cell culture with GFP-NIT1 overexpression it was elevated compared to the control. These data indicate that as in animal cells, Arabidopsis NIT1 might function together with FHIT.

In order to analyse further the deregulated cell proliferation we also determined the expression of *CDKA;1* and *CDKB1;1* genes by Q-RT-PCR and found both to be upregulated in the NIT-RNAi plants compared to wild-type (Fig. S10c).

Discussion

Although NIT1 homologues are described as metabolic enzymes involved in glucosinolate catabolism in Arabidopsis or in *Brassica rapa* (Janowitz *et al.*, 2009), a function in early PCD was suggested by Cutler & Somerville (2005). We demonstrated that in *Arabidopsis thaliana* extracts NIT1 assembled into filaments forming a broad range of molecular masses and lengths. Similar filaments are formed *in vitro* from recombinantly expressed bacterial and fungal nitrilases. However, for this to happen, the *Rhodococcus rhodochrous* and *Aspergillus niger* nitrilases have to be posttranslationally modified; C-terminally cleaved to enable stable arrangement of helices (Thuku *et al.*, 2007; Kaplan *et al.*, 2011). The corresponding C-terminal part is missing in the *Arabidopsis* NIT1-3 sequences (Fig. S11), suggesting that in *Arabidopsis* these protein molecules have an intrinsic property to assemble into filamentous polymers. The evolutionarily conserved filament-forming capacity assigns the NIT1 proteins to the expanding group of metabolic filament-forming enzymes that evolved other functions besides their catalytic activities (Ingerson-Mahar *et al.*, 2010; Noree *et al.*, 2010). The functions of these NIT1 filaments are as yet unknown. NIT1 aggregation precedes the occurrence of PCD hallmarks in Arabidopsis (Cutler & Somerville, 2005). We confirmed these findings of Cutler and

Somerville with our GFP-NIT1 fusion in cell culture treated with a PCD-inducing drug, and moreover, we found that overexpression of GFP-NIT1 increased the frequency of PCD. Overexpression of *NIT1* in animal cells also elevates apoptosis and suppresses cell division (Semba *et al.*, 2006). It would be interesting to find out whether animal NIT1 homologue preserves the filament-forming capability of bacterial and plant nitrilases and whether translocation and agregation of NIT1 occurs during animal apoptosis.

We characterized the developmental regulation of *NIT1* expression and its subcellular localization by imaging pNIT1::GFP-NIT1 transformants and by immunofluorescence with NIT1-specific antibodies that we produced. We found that in proliferating cells of root meristem, young leaves or cultured cells, NIT1 is mostly cytoplasmic, but a small portion appears to be associated with microtubular structures. We further confirmed microtubular association with spin down of taxol-stabilized plant microtubules. However, several lines of evidence suggest that the role of NIT1 in proliferation and differentiation is unlikely to be executed via the nucleation and organization of microtubules: (1) unlike γ-tubulin, NIT1 is not associated with microtubule stubs after APM-induced MT depolymerization, (2) aberrant metaphase chromosome alignment and separation of chromatids in anaphase are typical when microtubule function is disturbed; however, these were not evident in dividing polyploid cells with NIT-RNAi silencing, suggesting the presence of functional microtubular arrays. It is more likely that microtubules might provide a signalling platform for transiently associated portion of NIT1 cellular pool.

An important clue on possible NIT1 functions in animal cells came from the realization that in *Drosophila melanogaster* and in *Caenorhabditis elegans*, *NIT1* is fused to *FHIT*, an important tumour suppressor gene (Pekarsky *et al.*, 1998). However, in vertebrates, these two proteins are encoded by two separate genes. The *NIT1* and *FHIT* genes are also at separate genome locations in *Arabidopsis,* where FHIT was characterized for its dinucleoside triphosphate hydrolase and phosphodiesterase activities (Guranowski *et al.*, 2008). The involvement of NIT1 and FHIT in a common pathway is indicated by their overlapping expression and their common functions in the regulation of cell proliferation and apoptosis in animal cells (Semba *et al.*, 2006; Sun *et al.*, 2009; Zhang *et al.*, 2009). Furthermore, in animals, FHIT plays a role in oxidative stress and DNA damage response; its inactivation contributes to the accumulation of abnormal checkpoint phenotypes during cancer development. In *Arabidopsis* cells FHIT might also operate in a common pathway with NIT1, as suggested by our finding of their coordinated expression. Our proteomics analysis of NIT1 interactors did not identify FHIT; this is consistent with a failure to show physical interaction of NIT1 and FHIT in human cells (Huebner & Croce, 2001). Interestingly, in human cells FHIT is associated *in vitro* with microtubules, and the association is required for the tumour suppressor activity of FHIT but most likely does not regulate microtubular nucleation (Chaudhuri *et al.*, 1999). Thus, similar to what we proposed for NIT1, microtubules might provide a signalling platform also for FHIT.

Animal cells with defective nuclear division, or polyploidy, withdraw permanently from the cell cycle due to strong checkpoint controls, and enter apoptosis. NIT1 either alone or together with the tumour suppressor FHIT is suggested to be involved in these checkpoints to function as a repressor of the cell cycle and as a switch to apoptosis (Zhang *et al.*, 2009). In agreement, the level of *NIT1* expression is significantly reduced in tumours (Sun *et al.*, 2009), and kidney cells deficient for NIT1 show hyperproliferation (Semba *et al.*, 2006). In our experiments, the checkpoint control was abrogated in NIT-RNAi plants that failed to exit proliferation during differentiation, carried on cycling and became highly polyploid. Although the checkpoint control of the cell division in plant meristematic cells was suggested to be weaker in comparison to animals (Castellano & Sablowski, 2008), our data suggest that the role of plant NIT1 in the cell cycle checkpoints is conserved. Meristematic cells respond to DNA damage by ATM/ATR dependent PCD, despite the absence of plant homologues of key transducers and executioners of the ATM/ATR activated PCD pathway (Fulcher & Sablowski, 2009). Both NIT1 and FHIT are suggested to play a role in DNA damage-induced apoptosis in animals (Zhang *et al.*, 2009). It would be interesting to know whether NIT1 and possibly also FHIT play a conserved role in the process also in plants, as suggested by accumulation of NIT1 in perinuclear area during early phases of apoptosis and during aphidicolin-induced replication stress. Progression through S-phase was shown to be specifically sensitive to levels of NIT1 in our experiments being elevated or reduced upon dowregulation and overproduction of NIT1.

The Arabidopsis NIT1 protein was predicted to be ubiquitylated (Maor *et al.*, 2007), which was confirmed later using several experimental approaches (Igawa *et al.*, 2009; Saracco *et al.*, 2009). Interaction of human NIT1 with RAD23 protein was found with yeast two hybrid assay (BioGrid, Stark *et al.*, 2006). Rad23 is involved both in animals and plants in DNA repair and proteasomal protein degradation. In *Arabidopsis*, RAD23 interacts with the 26S receptor, RPN10, functioning in the delivery of ubiquitin-conjugating enzyme substrates to 26S proteasome (Farmer *et al.*, 2010). Interestingly, in human cells FHIT interacts with the ubiquitin-conjugating enzyme, hUBC9 (Shi *et al.*, 2000). Significance of these interactions for possible function of NIT1/FHIT in 26S proteasome degradation pathway or in proteasome-independent ubiquitylation driven signalling in processes such as DNA repair, replication, signal transduction and cell division, needs to be determined.

Cell division and differentiation are coordinated in distinct zones of the meristems to maintain meristem function. This appears to be disturbed by the silencing of *NIT1–3*, leading to severe developmental defects both in the root and aerial parts of the seedlings, including sustained proliferation and failure to exit into differentiation, as indicated also by the S-phase EdU labelling at the transition zone of root meristem to elongation growth. However, overexpression of GFP-NIT1 reduced the entry into S-phase and cell proliferation. Particularly leaf development was affected by *NIT1–3* silencing, which was in severe cases manifested as a complete lack of cellular differentiation and tissue organization. Expression of *CDKA;1* and *CDKB1;2* was elevated

in NIT-RNAi seedlings, where proliferating unorganized calli-like structures emerged at the flanks of the meristem instead of leaves. The A and B2-type CDKs were shown to be required not only for cell cycle progression, but also for reprogramming development and meristem organization (Andersen *et al.*, 2008; Gaamouche *et al.*, 2010). Further research is required to address whether and how NIT1–3 function in negative regulation of cell proliferation interplays with the cell cycle regulators during development.

For cells to become polyploid, the sustained proliferation has to be accompanied by abortive cytokinesis. Severe cytokinetic defects were unusually frequent in the NIT-RNAi plants in all organs we have studied and our data pointed to an important but so far uncharacterized function of nitrilases in cytokinesis. Similar to NIT1 silencing, mutation of the destruction box in mitotic B1-type cyclins and its compromised degradation also leads to cytokinetic defects and polyploidization (Weingartner *et al.*, 2004). NIT1 was shown to be ubiquitylated (Igawa *et al.*, 2009; Saracco *et al.*, 2009). As discussed above, association of NIT1 with microtubules and accumulation in the area of cell plate formation is likely to reflect a signalling function rather than function in microtubule nucleation. In plants, a cytokinetic MAPK signalling pathway that associates with mitotic microtubules was characterized (Bogre *et al.*, 1999). Interestingly, this cytokinesis-regulating pathway is multifunctional and just as NIT1, also responds and regulates stress responses.

In summary, we have shown that Arabidopsis NIT1 belongs to growing number of metabolic enzymes with filament-forming capacity. It is likely that different developmental, cellular and stress signals such as wounding, might modulate aggregation of high molecular forms of nitrilases, which in turn could provide platforms for molecular interactions in regulation of cellular processes. Furthermore, we show that NIT1 has a role in repression of proliferation both in conjunction with developmental cues and possibly in response to cell cycle checkpoints. Thus, NIT1 might regulate cell division and differentiation in balance with apoptosis. Another independent function of NIT1 is to ensure correct cytokinesis; compromising NIT1 function resulted to continued proliferation and aberrant cytokinesis leading to immensely polyploid and aneuploid cells. Formation of polyploids and aneuploids are major evolutionary driving forces within the plant kingdom (Doyle *et al.*, 2008). Thus, NIT1 is a largely important multifunctional protein to safeguard plant development, genome integrity and could have important impacts on plant evolution.

Acknowledgements

This work was supported by grant from the Grant Agency of the Czech Republic (P501/12/2333). B.P. was supported by the Centre of the Region Haná for Biotechnological and Agricultural Research (NCZ.1.05/2.1.00/01.0007). We thank Gabriela Kočárová and Jan Svoboda for technical assistance, the CSIRO Plant Industry, Australia for vectors pHANNIBAL and pART27, and Richard Cyr (Pennsylvania State University, USA) for the GFP-MAP4 vector.

References

Agerbirk N, Warwick SI, Hansen PR, Olsen CE. 2008. Sinapis phylogeny and evolution of glucosinolates and specific nitrile degrading enzymes. *Phytochemistry* **69**: 2937–2949.

Andersen SU, Buechel S, Zhao Z, Ljung K, Novak O, Busch W, Schuster C, Lohmann JU. 2008. Requirement of B2-type cyclin-dependent kinases for meristem integrity in *Arabidopsis thaliana*. *Plant Cell* **20**: 88–100.

Binarova P, Cenklova V, Hause B, Kubatova E, Lysak M, Dolezel J, Bogre L, Draber P. 2000. Nuclear gamma-tubulin during acentriolar plant mitosis. *Plant Cell* **12**: 433–442.

Binarova P, Cenklova V, Prochazkova J, Doskocilova A, Volc J, Vrlik M, Bogre L. 2006. Gamma-tubulin is essential for acentrosomal microtubule nucleation and coordination of late mitotic events in Arabidopsis. *Plant Cell* **18**: 1199–1212.

Bogre L, Calderini O, Binarova P, Mattauch M, Till S, Kiegerl S, Jonak C, Pollaschek C, Barker P, Huskisson NS *et al.* 1999. A MAP kinase is activated late in plant mitosis and becomes localized to the plane of cell division. *Plant Cell* **11**: 101–113.

Bustin SA, Benes V, Garson JA, Hellemans J, Huggett J, Kubista M, Mueller R, Nolan T, Pfaffl MW, Shipley GL *et al.* 2009. The MIQE guidelines: minimum information for publication of quantitative real-time PCR experiments. *Clinical Chemistry* **55**: 611–622.

Castellano MM, Sablowski R. 2008. Phosducin-Like Protein 3 is required for microtubule-dependent steps of cell division but not for meristem growth in Arabidopsis. *Plant Cell* **20**: 969–981.

Chaudhuri AR, Khan IA, Prasad V, Robinson AK, Luduena RF, Barnes LD. 1999. The tumor suppressor protein Fhit. A novel interaction with tubulin. *Journal of Biological Chemistry* **274**: 24 378–24 382.

Clough SJ, Bent AF. 1998. Floral dip: a simplified method for Agrobacterium-mediated transformation of *Arabidopsis thaliana*. *Plant Journal* **16**: 735–743.

Cutler SR, Ehrhardt DW, Griffitts JS, Somerville CR. 2000. Random GFP: cDNA fusions enable visualization of subcellular structures in cells of Arabidopsis at a high frequency. *Proceedings of the National Academy of Sciences, USA* **97**: 3718–3723.

Cutler SR, Somerville CR. 2005. Imaging plant cell death: GFP-Nit1 aggregation marks an early step of wound and herbicide induced cell death. *BMC Plant Biology* **5**: 4.

Davis AM, Hall A, Millar AJ, Darrah C, Davis SJ. 2009. Protocol: streamlined sub-protocols for floral-dip transformation and selection of transformants in *Arabidopsis thaliana*. *Plant Methods* **5**: 3.

Doskocilova A, Plihal O, Volc J, Chumova J, Kourova H, Halada P, Petrovska B, Binarova P. 2011. A nodulin/glutamine synthetase-like fusion protein is implicated in the regulation of root morphogenesis and in signalling triggered by flagellin. *Planta* **234**: 459–476.

Doyle JJ, Flagel LE, Paterson AH, Rapp RA, Soltis DE, Soltis PS, Wendel JF. 2008. Evolutionary genetics of genome merger and doubling in plants. *Annual Review of Genetics* **42**: 443–461.

Drykova D, Cenklova V, Sulimenko V, Volc J, Draber P, Binarova P. 2003. Plant gamma-tubulin interacts with alphabeta-tubulin dimers and forms membrane-associated complexes. *Plant Cell* **15**: 465–480.

Farmer LM, Book AJ, Lee KH, Lin YL, Fu H, Vierstra RD. 2010. The RAD23 family provides an essential connection between the 26S proteasome and ubiquitylated proteins in Arabidopsis. *Plant Cell* **22**: 124–142.

Fransz P, De Jong JH, Lysak M, Castiglione MR, Schubert I. 2002. Interphase chromosomes in Arabidopsis are organized as well defined chromocenters from which euchromatin loops emanate. *Proceedings of the National Academy of Sciences, USA* **99**: 14 584–14 589.

Fulcher N, Sablowski R. 2009. Hypersensitivity to DNA damage in plant stem cell niches. *Proceedings of the National Academy of Sciences, USA* **106**: 20 984–20 988.

Gaamouche T, Manes CL, Kwiatkowska D, Berckmans B, Koumproglou R, Maes S, Beeckman T, Vernoux T, Doonan JH, Traas J *et al.* 2010. Cyclin-dependent kinase activity maintains the shoot apical meristem cells in an undifferentiated state. *Plant Journal* **64**: 26–37.

Galperin MY, Koonin EV. 2004. 'Conserved hypothetical' proteins: prioritization of targets for experimental study. *Nucleic Acids Research* **32**: 5452–5463.

Garcia-Heredia JM, Hervas M, De la Rosa MA, Navarro JA. 2008. Acetylsalicylic acid induces programmed cell death in Arabidopsis cell cultures. *Planta* **228**: 89–97.

Guranowski A, Wojdyla AM, Pietrowska-Borek M, Bieganowski P, Khurs EN, Cliff MJ, Blackburn GM, Blaziak D, Stec WJ. 2008. Fhit proteins can also recognize substrates other than dinucleoside polyphosphates. *FEBS Letters* **582**: 3152–3158.

Halada P, Man P, Grebenova D, Hrkal Z, Havlicek V. 2001. Identification of HL60 proteins affected by 5-aminolevulinic acid-based photodynamic therapy using mass spectrometric approach. *Collection of Czechoslovak Chemical Communications* **66**: 1720–1728.

Huebner K, Croce CM. 2001. FRA3B and other common fragile sites: the weakest links. *Nature Reviews Cancer* **1**: 214–221.

Huebner K, Saldivar JC, Sun J, Shibata H, Druck T. 2011. Hits, Fhits and Nits: beyond enzymatic function. *Advances in Enzyme Regulation* **51**: 208–217.

Igawa T, Fujiwara M, Takahashi H, Sawasaki T, Endo Y, Seki M, Shinozaki K, Fukao Y, Yanagawa Y. 2009. Isolation and identification of ubiquitin-related proteins from Arabidopsis seedlings. *Journal of Experimental Botany* **60**: 3067–3073.

Ingerson-Mahar M, Briegel A, Werner JN, Jensen GJ, Gitai Z. 2010. The metabolic enzyme CTP synthase forms cytoskeletal filaments. *Nature Cell Biology* **12**: 739–746.

Janowitz T, Trompetter I, Piotrowski M. 2009. Evolution of nitrilases in glucosinolate-containing plants. *Phytochemistry* **70**: 1680–1686.

Kaplan O, Bezouska K, Plihal O, Ettrich R, Kulik N, Vanek O, Kavan D, Benada O, Malandra A, Sveda O *et al.* 2011. Heterologous expression, purification and characterization of nitrilase from *Aspergillus niger* K10. *BMC Biotechnology* **11**: 2.

Ljung K, Hull AK, Celenza J, Yamada M, Estelle M, Normanly J, Sandberg G. 2005. Sites and regulation of auxin biosynthesis in Arabidopsis root. *Plant Cell* **17**: 1090–1104.

Maor R, Jones A, Nuhse TS, Studholme DJ, Peck SC, Shirasu K. 2007. Multidimensional protein identification technology (MudPIT) analysis of ubiquitinated proteins in plants. *Molecular and Cellular Proteomics* **6**: 601–610.

Marc J, Granger CL, Brincat J, Fisher DD, Kao T, McCubbin AG, Cyr RJ. 1998. A GFP-MAP4 reporter gene for visualizing cortical microtubule rearrangements in living epidermal cells. *Plant Cell* **10**: 1927–1940.

Michalczuk L, Ribnicky DM, Cooke TJ, Cohen JD. 1992. Regulation of indole-3-acetic acid biosynthetic pathways in carrot cell cultures. *Plant Physiology* **100**: 1346–1353.

Noree C, Sato BK, Broyer RM, Wilhelm JE. 2010. Identification of novel filament-forming proteins in *Saccharomyces cerevisiae* and *Drosophila melanogaster*. *Journal of Cell Biology* **190**: 541–551.

Normanly J, Grisalfi P, Fink G, Bartel B. 1997. Arabidopsis mutants resistant to the auxin effects of indole-3-acetonitrile are defective in the nitrilase encoded by the *NIT1* gene. *Plant Cell* **9**: 1781–1790.

Pekarsky Y, Campiglio M, Siprashvili Z, Druck T, Sedkov Y, Tillib S, Draganescu A, Wermuth P, Rothman JH, Huebner K *et al.* 1998. Nitrilase and Fhit homologs are encoded as fusion proteins in *Drosophila melanogaster* and *Caenorhabditis elegans*. *Proceedings of the National Academy of Sciences, USA* **95**: 8744–8749.

Petrovska B, Cenklova V, Pochylova Z, Kourova H, Doskocilova A, Plihal O, Binarova L, Binarova P. 2012. Plant Aurora kinases play a role in maintenance of primary meristems and control of endoreduplication. *New Phytologist* **193**: 590–604.

Piotrowski M. 2008. Primary or secondary? Versatile nitrilases in plant metabolism. *Phytochemistry* **69**: 2655–2667.

Saracco SA, Hansson M, Scalf M, Walker JM, Smith LM, Vierstra RD. 2009. Tandem affinity purification and mass spectrometric analysis of ubiquitylated proteins in Arabidopsis. *Plant Journal* **59**: 344–358.

Semba S, Han SY, Qin HR, McCorkell KA, Iliopoulos D, Pekarsky Y, Druck T, Trapasso F, Croce CM, Huebner K. 2006. Biological functions of mammalian Nit1, the counterpart of the invertebrate NitFhit Rosetta stone protein, a possible tumor suppressor. *Journal of Biological Chemistry* **281**: 28 244–28 253.

Shi Y, Zou M, Farid NR, Paterson MC. 2000. Association of FHIT (fragile histidine triad), a candidate tumour suppressor gene, with the ubiquitin-conjugating enzyme hUBC9. *Biochem Journal* **352**(Pt 2): 443–448.

Stark C, Breitkreutz BJ, Reguly T, Boucher L, Breitkreutz A, Tyers M. 2006. BioGRID: a general repository for interaction datasets. *Nucleic Acids Research* **34**: D535–D539.

Sun J, Okumura H, Yearsley M, Frankel W, Fong LY, Druck T, Huebner K. 2009. Nit1 and Fhit tumor suppressor activities are additive. *Journal of Cellular Biochemistry* **107**: 1097–1106.

Thuku RN, Weber BW, Varsani A, Sewell BT. 2007. Post-translational cleavage of recombinantly expressed nitrilase from *Rhodococcus rhodochrous* J1 yields a stable, active helical form. *FEBS Journal* **274**: 2099–2108.

Vanstraelen M, Baloban M, Da Ines O, Cultrone A, Lammens T, Boudolf V, Brown SC, De Veylder L, Mergaert P, Kondorosi E. 2009. APC/C-CCS52A complexes control meristem maintenance in the Arabidopsis root. *Proceedings of the National Academy of Sciences, USA* **106**: 11 806–11 811.

Vorwerk S, Biernacki S, Hillebrand H, Janzik I, Muller A, Weiler EW, Piotrowski M. 2001. Enzymatic characterization of the recombinant *Arabidopsis thaliana* nitrilase subfamily encoded by the NIT2/NIT1/NIT3-gene cluster. *Planta* **212**: 508–516.

Wali A. 2010. FHIT: doubts are clear now. *ScientificWorldJournal* **10**: 1142–1151.

Weingartner M, Criqui MC, Meszaros T, Binarova P, Schmit AC, Helfer A, Derevier A, Erhardt M, Bogre L, Genschik P. 2004. Expression of a nondegradable cyclin B1 affects plant development and leads to endomitosis by inhibiting the formation of a phragmoplast. *Plant Cell* **16**: 643–657.

Zhang H, Hou YJ, Han SY, Zhang EC, Huebner K, Zhang J. 2009. Mammalian nitrilase 1 homologue Nit1 is a negative regulator in T cells. *International Immunology* **21**: 691–703.

Supporting Information

Additional supporting information may be found in the online version of this article.

Fig. S1 Multiple sequence alignments of *Arabidopsis* NIT1–4 and of nitrilases from various organisms.

Fig. S2 Overproduction of GFP-NIT1 in cultured cells and seedlings.

Fig. S3 Silver stained SDS-PAGE and MALDI-MS data of proteins co-immunopurified with GFP-NIT1 from re-suspended P100 fraction.

Fig. S4 Expression of GFP-NIT1 driven by its own promoter in *Arabidopsis* seedling root.

Fig. S5 Transcript level of *NIT1, 2, 3* and *4* in NIT-RNAi plants; correlation of transcript levels with strength of the phenotype.

Fig. S6 Root phenotypes of plants with NIT1–3 downregulated by RNAi.

Fig. S7 Induction of programmed cell death (PCD) in *Arabidopsis* cells by acetylsalicylic acid.

Fig. S8 NIT1 localization during induction of PCD by acetylsalicylic acid and during aphidicolin-induced replication stress.

Fig. S9 Sequence alignment of FHIT proteins from *Arabidopsis thaliana* and *Homo sapiens*.

Fig. S10 Co-expression of *NIT1* and *FHIT* in NIT-RNAi plants and cultured cells overexpressing GFP-NIT1 and expression of *CDKA;1* and *CDKB1;2* in NIT-RNAi plants.

Fig. S11 Sequence alignment of *Rhodococcus rhodochrous* J1 nitrilase and *Arabidopsis thaliana* NIT1.

Methods S1 Detailed materials and methods.

Video S1 Mitosis in *Arabidopsis* cultured cell expressing GFP-NIT1 under 35S CaMV promoter.

Video S2 Cytokinesis in *Arabidopsis* cultured cell expressing GFP-NIT1 under 35S CaMV promoter.

Please note: Wiley-Blackwell are not responsible for the content or functionality of any supporting information supplied by the authors. Any queries (other than missing material) should be directed to the *New Phytologist* Central Office.

7.2.1 Supplementary data

Doskočilová, A.[#], Kohoutová, L.[#], Volc, J., Kourová, H., Benada, O., Chumová, J., Plíhal, O., Petrovská, B., Halada, P., Bögre, L., and Binarová, P.; (2013) NITRILASE1 regulates the exit from proliferation, genome stability and plant development. New Phytol, 198(3):685-98

[#]These authors contributed equally to this article.

Supporting Information

Supplementary Materials and Methods

Plant material and cell cultures

Arabidopsis thaliana cell suspension cultures of Columbia (Col) and Landsberg erecta (Ler) were grown under continuous darkness at 25 °C as described (Drykova *et al.*, 2003). Seeds of *Arabidopsis thaliana* (L.) Heynh. ecotype Columbia and Columbia lines expressing PM GFP marker (Cutler *et al.*, 2000) were surface-sterilized and grown on half-strength MS agar plates as described (Binarova *et al.*, 2006).

Molecular methods

The complete coding region of *Arabidopsis* NIT1 was PCR amplified with Platinum Pfx DNA polymerase (Invitrogen) using as a template *A. thaliana* cDNA and cloned using Gateway^{R} technology. We prepared N-terminal and C-terminal GFP fusions (vectors pK7WGF2.0, pK7FWG2.0, respectively; Ghent University) of NIT1 under 35S CaMV promoter (p35S::NIT1-GFP and p35S::GFP-NIT1**)** and N-terminal GFP fusion of NIT1 under its native promoter (pNIT1::GFP-NIT1). The region upstream of NIT1 gene of about 1,500 bp was PCR amplified and the respective entry clones were prepared and cloned into the binary vector; pK7m34GW, using Multisite Gateway system (Ghent University) according to Petrovska *et al*. (2012). Primers used for cloning are described below. The constructs were transformed into *Agrobacterium tumefaciens* strain GV3101 which was used for several independent transformations of *Arabidopsis* cultured cells and *Arabidopsis* plants of Columbia ecotype, using standard methods (Clough & Bent, 1998; Davis *et al.*, 2009). All NIT1 constructs carried kanamycin resistance for plant selection. Seedlings were selected

on kanamycin (50 μg ml^{-1}) medium. T1 transformants carrying GFP constructs had no discernible abnormalities, and we obtained T2 and T3 generations.

To produce a silencing RNAi construct, we cloned the 335 bp fragment of *NIT1* sequence of the central conserved part of the NIT1 molecule into the pHANNIBAL vector to produce an inverted repeat. NIT1 PCR fragments were double digested with XhoI-EcoRI and XbaI-HindIII, and the fragments were used for the two rounds of ligations into the vector pHANNIBAL. Then this NIT-RNAi cassette was transferred into the binary vector pART27 (CSIRO Plant Industry) using NotI restriction site. Primers used for cloning are described below. With the NIT-RNAi construct we performed 15 independent transformations with Columbia, GFP-MAP4, and PM GFP Columbia plants. After seven days of kanamycin selection resistant seedlings were transferred onto non-selective media. Phenotype was analysed in six to 19-day-old seedlings; transformants with the empty pART27 vector were used as the controls. The NIT-RNAi plants with phenotypes could not reach maturity and produce seeds. Therefore we characterised more than 200 of the independent transformants with phenotype in the T1 generation.

Sequence alignment was done by Clustal X (Thompson *et al.*, 1997).

Quantitative real-time RT-PCR (Q RT-PCR) analyses were performed following MIQE recommendations (Bustin *et al.*, 2009) using methods described before (Petrovska *et al.*, 2012). The transcript level of each target gene of control was designated as 1.0. Primers used for Q RT-PCR are described below.

Primers used for NIT1 cloning of N- and C-terminal GFP fusions (FNITN+RNITN, FNITN+RNITC, respectively):

FNITN

5′- GGGGACAAGTTTGTACAAAAAAGCAGGCTTCATGTCTAGTACTAAAGATATGTC AACTG -3′

RNITN

5′- GGGGACCACTTTGTACAAGAAAGCTGGGTCCTATTTGTTTGAGTCATCCTCAGC -3′

RNITC

5′- GGGGACCACTTTGTACAAGAAAGCTGGGTCTATTTTGTTTGAGTCATCCTCAGC -3′

NITN15UTRgwFW01

5′- GGGGACAACTTTGTATAGAAAAGTTGAAAAATGTTTTGGAATGACTAATATTGAC -3′

NITN15UTRgwRE01

5′- GGGGACTGCTTTTTTGTACAAACTTGATCAACTCGAGTCTTTGTTTTTTAC-3′

NITN1MULTIgwFW01

5′-GGGGACAGCTTTCTTGTACAAAGTGGAAATGTCTAGTACTAAAGATATGTCAACTG-3′

NITN1MULTIgwRE01

5′- GGGGACAACTTTGTATAATAAAGTTGGCTATTTGTTTGAGTCATCCTCAGC-3′

Two sets of primers used for NIT-RNAi cloning (restriction sites for XhoI, EcoRI, XbaI, and HindIII are underlined, respectively):

NitRNAi335_FW01 5′- GACTCGAGCGAAGAAGGGCGTGATGAG -3′

NitRNAi335_RE01 5′- TCGAATTCGCAGTTCTGTAGAGGGGC -3′

NitRNAi335_FW02 5′- GATCTAGACGAAGAAGGGCGTGATGAG -3′

NitRNAi335_RE02 5′- TCAAGCTTGCAGTTCTGTAGAGGGGC -3′

Primers used for Q RT-PCR. To ensure specificity of primers, primer pairs were designed to span across two neighboring exons and were detected as a single peak in dissociation curve analysis.

PDF2_FOR 5′- TAACGTGGCCAAAATGATGC - 3′

PDF2_REV 5′- GTTCTCCACAACCGCTTGGT - 3′

qNitrilase1_FOR 5′- TGAGTTTCGGAAGTACCATGC - 3′

qNitrilase1_REV 5′- CACGTCAGCCAATCTTGCTA -3′

qNitrilase2_FOR 5′- CGTGATGAGTTCCGCAAGTA - 3′

qNitrilase2_REV 5′- GTTCTTCCCGGCCAACTC -3 ′

qNitrilase3_FOR 5′- CCGGCCACTTTAGACAAGGCGG -3′

qNitrilase3_REV 5′- GCCGATGAACGCCTCGGGAA -3′

qNitrilase4_FOR 5′- CACATGACGGCGGCTCCACA - 3′

qNitrilase4_REV 5′- TCGCCGGCGGACATGTCAAT - 3′

qFhit_FOR 5′- AAGAATGATGAAATCTATGATGCTCTT - 3′

qFhit_REV 5′- GCTCCTATCAACCCGGTCTT -3′

CDKA;1_FOR 5′- ATCCGTCGGTGTGCTAGTCT -3′

CDKA;1_REV 5′- TCTCAACTTTCTCGTACTGATCCA -3′

CYCB1;2_FOR 5′- TCCTGAAGTTTTGCTTGGTTC -3′

CYCB1;2_REV 5′- TCACCAGGGAAAAGAGCTTG -3′

Protein methods

Protein extracts were prepared from cultured cells and seedlings as described before (Drykova *et al.*, 2003). For differential centrifugation, crude extracts were centrifuged at 10,000*g* for 10 min at 4°C, supernatants (S10) subsequently at 20,000*g* for 0.5 h and resulting S20 at 100,000*g* for 1 h (S100). The obtained S100 were finally spun at 160,000*g* for 1.5 h to yield S160 and the pellet P160. The P160 pellets were resuspended in equal volumes to the pellets in extraction buffer. For non-ionic detergent, 1% NP-40 (Roche Diagnostics) was used.

Custom polyclonal rabbit antibody (GenScript) for the NIT1 was raised against the C-terminal sequence DIARAKLYFDSVGHYSRPDV (aa 299-318) of the NIT1 molecule and was used in dilution of 1:100 to 1:500. γ-Tubulin was detected as described (Doskocilova *et al.*, 2011). Antibody against actin was purchased from ABR (MA1-744) and diluted 1:1,000 for Western blot. Secondary horseradish peroxidase conjugated antibodies; anti-mouse and anti-rabbit were diluted 1:10,000 (Amersham-GE Healthcare).

Gel filtrations were done from re-solubilized P100 on Superose 6 10/300 GL column (GE Healthcare Bio-Sciences) according to Doskocilova *et al.* (2011).

Co-immunoprecipitation was performed using GFP-Trap_A (ChromoTek) according to the manufacturer's instructions.

Protein identifications by MALDI mass spectrometry were performed from excised silver-stained protein bands as described (Halada *et al.*, 2001). Mass spectra were acquired on Ultraflex III instrument (Bruker Daltonics) and searched against SwissProt 2011_04 database using in-house Mascot search engine.

The microtubule spin-down experiments were performed as described previously (Binarova *et al.*, 2006; Doskocilova *et al.*, 2011).

Protein samples were separated on 8% SDS-PAGE or on blue native PAGE (BN-PAGE) (Drykova *et al.,* 2003), transferred onto 0.45 μm PVDF membranes (Immobilon-P, Millipore) by wet electroblotting and detected with appropriate antibody. Supersignal ECL kit (Pierce) was used according to manufacturer's instructions.

Three independent experiments were conducted; representative Western blots are shown.

Microscopy

For negative staining, 5 μl of fresh samples were applied onto glow-discharged activated carbon coated copper grids. After 30 s the grids were negatively stained with 2% (w/v) uranyl acetate in ddH_2O for 30 s.

For immunogold labelling and electron microscopy, 5 μl samples were applied directly onto glow-discharged activated Formvar/carbon coated nickel grids for 30 s and fixed in 4% PFA and 0.1% glutaraldehyde in PBS (pH 7.4) for 10 min. After blocking (1% BSA in PBS plus 0.05% Tween), anti-NIT1 antibody, diluted 1:8 in the blocking buffer, was applied for 2 h. Anti-rabbit antibody conjugated with gold particles (BBInternational) was used. The grids were stained using

2% ammonium molybdate in ddH_2O pH 6.5. The grids were examined in Philips CM100 electron microscope at 80 kV and magnification of 46,000×. Digital images were recorded using MegaViewII slow scan camera at magnification of 64,000× giving the digital resolution of about 1 nm per pixel.

Immunofluorescence labelling was performed as described (Drykova *et al.*, 2003) using anti-NIT1 (1:100), anti-α-tubulin (1:2,000), anti-γ-tubulin TU-32 antibodies (1:6). DyLight 488- and DyLight 549-conjugated anti-mouse and anti-rabbit antibodies (Jackson ImmunoResearch Laboratories) diluted 1:500. Drugs were diluted in DMSO and used in working concentrations of: 5 μM for APM (amiprophos methyl, Duchefa A0185), 10 μM for taxol (Paclitaxel, Sigma T7402), and 10 μg ml^{-1} for aphidicolin (Sigma, A0781) and applied as indicated.

Fluorescence microscopy and live cell imaging was done using the Olympus IX-81 inverted microscope with Olympus DSU - Disc Scanning Confocal Unit with oil immersion objectives 100x/1.4, 60x/1.35 or 40x/1.3 and Olympus IX-81 FV-1000 confocal imaging system; images were taken and analysed as described previously (Doskocilova *et al.*, 2011). Pinhole 80 μm for intensity measurement; U-MNUA2 filter block (Olympus) for DAPI with excitation and emission maximum 440 nm and 500-520 nm, respectively was used. Cell counting and plot profile analyses were performed using ImageJ software (http://rsbweb.nih.gov/ij/). Exposures of seedlings were obtained with digital camera Nikon D300. Figures were prepared using Adobe Photoshop CS4.

Cell cycle analysis

EdU staining of replicating cells was performed using Click-iT EdU Alexa Fluor 488 HCS Assay (Molecular Probes) based on methods modified from Vanstraelen *et al.* (2009). Plants or cultured cells were treated for 1-3 hours with 10 μM EdU, fixed by 3.7% paraformaldehyde in PBS pH 7.4 for 15 min, rinsed by PBS, treated with 0.5% Triton-X-100 in PBS for 25 min, rinsed by PBS and treated with Click-iT reaction cocktail for 30 min, after washing by PBS, samples were stained by 1

μg ml^{-1} DAPI for 10 min. Three independent experiments were performed and at least 2,000 nuclei were counted on each slide.

Mitotic index was determined after Carnoy´s fixation and 0.45% lacto-propionic-orcein staining. Aliquots of the cell culture were collected during the growth period of seven days. To determine the growth curve of *Arabidopsis* cell suspension, 5 ml of cultured cells were sedimented, the medium was aspirated, and cells were weighted. Three independent experiments were performed and 1,000 cells were counted from each sample.

For TUNEL assay, cells were fixed by 3.7% paraformaldehyde with 0.4 M mannitol, washed with PBS, and attached to poly-L-lysine slides. After cell permeabilisation (0.1% Triton X-100 in 0.1% sodium citrate for 10 min), labelling reaction was done according to the manufacturer's protocol (Roche 12156792910) and the DNA was stained by DAPI. For PCD induction, 2 mM acetylsalicylic acid (ASA, Sigma A6810) treatment for 3-4 h was applied. Images of PCD-stained nuclei and DAPI-stained nuclei were obtained microscopically and analysed by ImageJ with the Cell Counter plugin (http://rsbweb.nih.gov/ij/plugins/cell-counter.html). Three independent experiments were performed and 1,000 cells were counted from each sample.

For chromocentra counting cells of callus-like structures or leaves were fixed in ethanol:acetic acid mixture (v/v 3:1) at room temperature for 1 hour then macerated in 0.1 M HCl for 10 min at 37°C, rinsed by water, squeezed in 45% acetic acid at 45°C, and stained by 2 μg ml^{-1} DAPI for 10 min in the dark.

Flow cytometry sample preparation was done using Partec CyStain UV precise P kit (Partec, Munster) to determine DNA content of calli-like structures or leaves of NIT-RNAi plants and of 35S::GFP-NIT1 cultured cells. Calli-like structures or leaves were chopped by razor in Extraction Buffer. Cells of suspension cultures were spun down; the pellets were frozen in liquid nitrogen and resuspended in the Extraction Buffer. Samples were stained by DAPI using Staining Buffer and filtered through 20 μm CellTrics (Partec, Munster). Measurements were performed on a BD LSRII

(BD Biosciences) with a solid state laser (excitation 405 nm) and 450/50 band pass filter. Forward scatter and side scatter were taken at 488 nm. Data were evaluated in FlowJo (Tree Star). Whenever possible, at least three independent experiments were performed; data are shown for one experiment.

Supplementary Figures

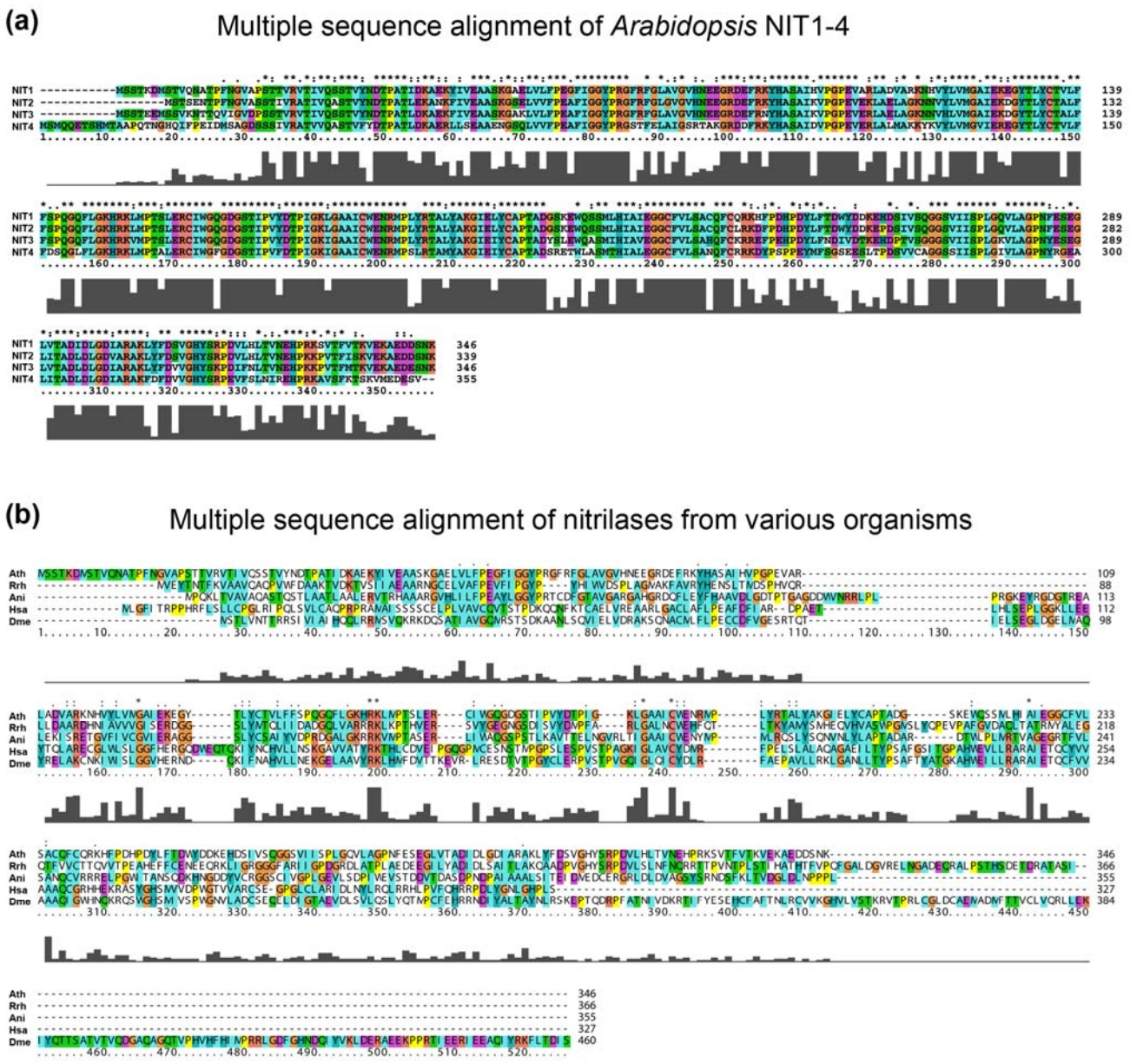

Fig. S1

(a) Multiple sequence alignment of *Arabidopsis* NIT1-4. (b) Multiple sequence alignment of nitrilases from various organisms: *Arabidopsis thaliana* (Ath), *Rhodococcus rhodochrous* J1 (Rrh), *Aspergillus niger* (Ani), *Homo sapiens* (Hsa), and *Drosophila melanogaster* (Dme). The chemical nature of the individual amino acids is color-coded as follows: cyan, A, F, H, I, M, L, V, W, Y; orange, G; yellow, P; magenta, D, E; green, N, Q, S, T; red, K, R; pink, C. Identical amino acids are marked with asterisk, conserved substitutions are marked with colon, and semi-conserved substitutions are marked with dot.

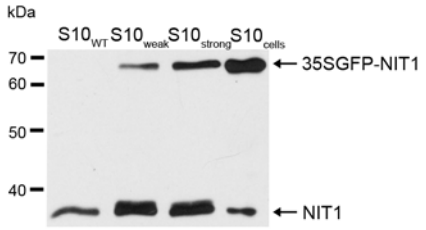

Fig. S2

Overproduction of GFP-NIT1 was higher in cultured cells compared to 35S::GFP-NIT1 over-expressing seedlings. Crude extracts ($S10_{WT}$) were prepared from WT plants, lines expressing 35S::GFP-NIT1 in moderate and strong manner ($S10_{weak}$ and $S10_{strong}$; microscopically selected), and from cell culture over-expressing 35S::GFP-NIT1 ($S10_{cells}$). Western blot detection using anti-NIT1 antibody. Equal amounts of protein were loaded to each lane.

(a)

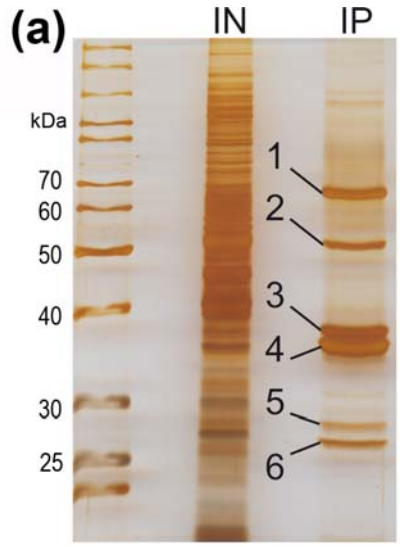

(b)

Band No.	*Protein name*	*UniProt DTB No.*	*MW [kDa]*	*No. peptides*	*Sequence coverage [%]*
1	**Nitrilase 1**	NRL1_ARATH	38	14	48
	Green fluorescent protein	GFP_AEQVI	27	5	26
2	**Elongation factor 1-alpha**	EF1A_ARATH	49	6	20
3	**Nitrilase 2**	NRL2_ARATH	37	9	34
	Elongation factor 1-alpha	EF1A_ARATH	49	7	22
4	**Nitrilase 1**	NRL1_ARATH	38	14	48
5	**Green fluorescent protein**	GFP_AEQVI	27	4	16
6	**Green fluorescent protein**	GFP_AEQVI	27	6	26

Fig. S3

Endogenous NIT1 (band no. 4) and NIT2 (band no. 3) co-purrified with expressed GFP-NIT1 (band no. 1). Silver stained SDS-PAGE (a) and MALDI-MS data (b) of proteins co-immunopurified with GFP-NIT1 from resuspended P100 fraction. IN = input, IP = immunoprecipitated sample.

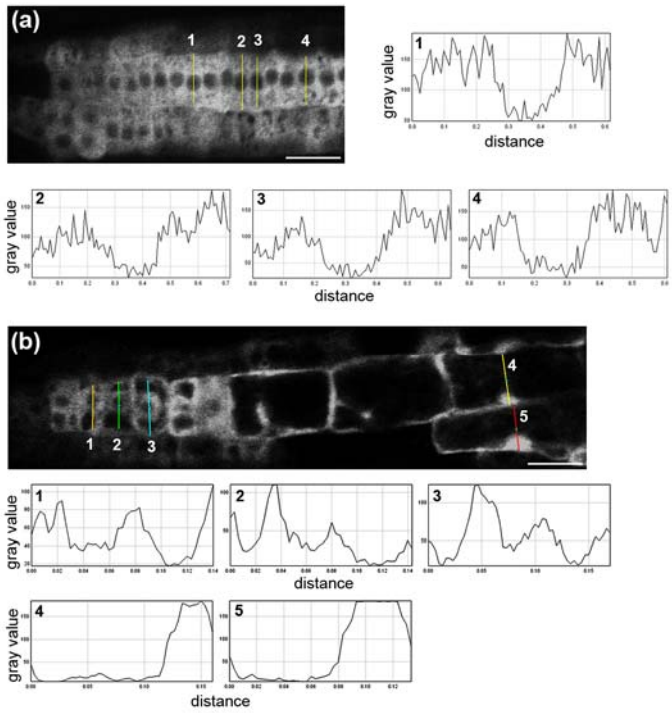

Fig. S4

Expression of GFP-NIT1 driven by its own promoter in root of 7-day-old *Arabidopsis* seedling. (a) Representative image of GFP-NIT1 signal in division zone where it is mainly cytoplasmic. Plots (1-4) show intensity profile. (b) Representative image of GFP-NIT1 signal in expansion and differentiation zone. In cells of expansion and differentiation zone, the signal became nuclear. Plots (1-5) show intensity profile. Bars, (a,b) 20 µm.

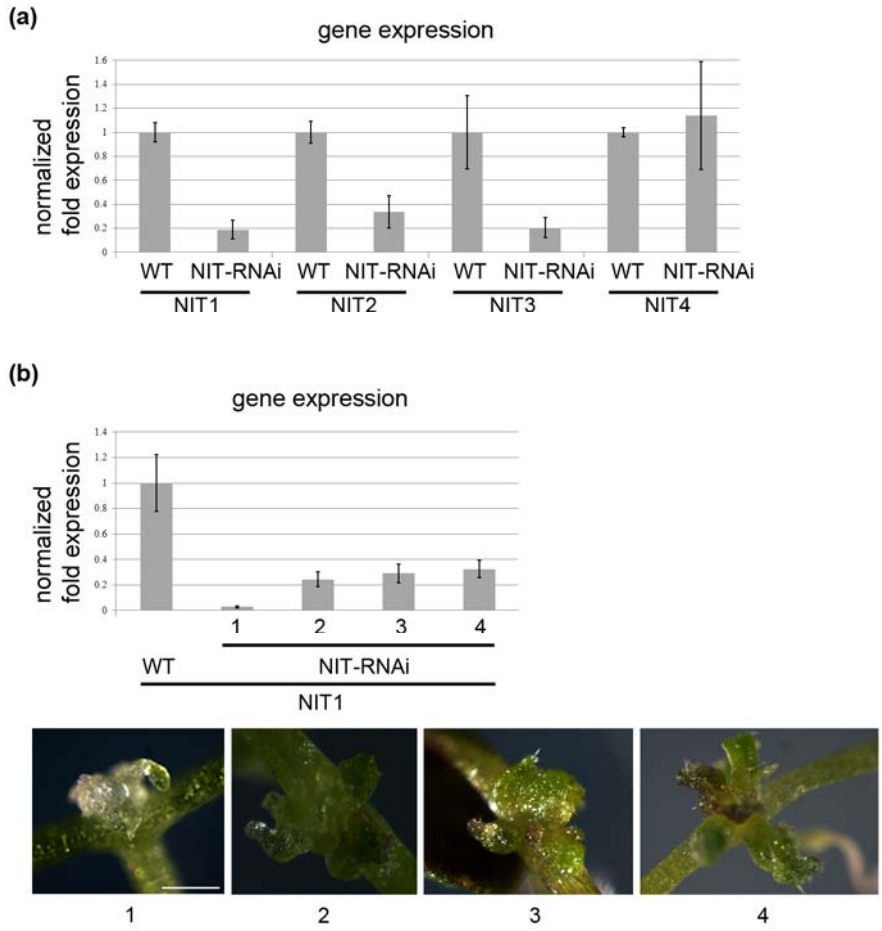

Fig. S5

(a) Q RT-PCR performed on 19-day-old WT plants and T1 transformants of NIT-RNAi plants showed that in NIT-RNAi plants the transcript level of *NIT1, 2,* and *3* was reduced compared to WT. Mean values of three repeats and standard deviation (SD) are shown. (b) Plot showing results from Q RT-PCR performed on 19-day-old WT plants and NIT-RNAi plants with stronger and milder phenotypes (NIT-RNAi columns from left to right). Mean values of three repeats are shown with SD. Representative images of NIT-RNAi plants with stronger and milder phenotypes evaluated by Q RT-PCR (1→ 4). Scale bar, 0.5 mm.

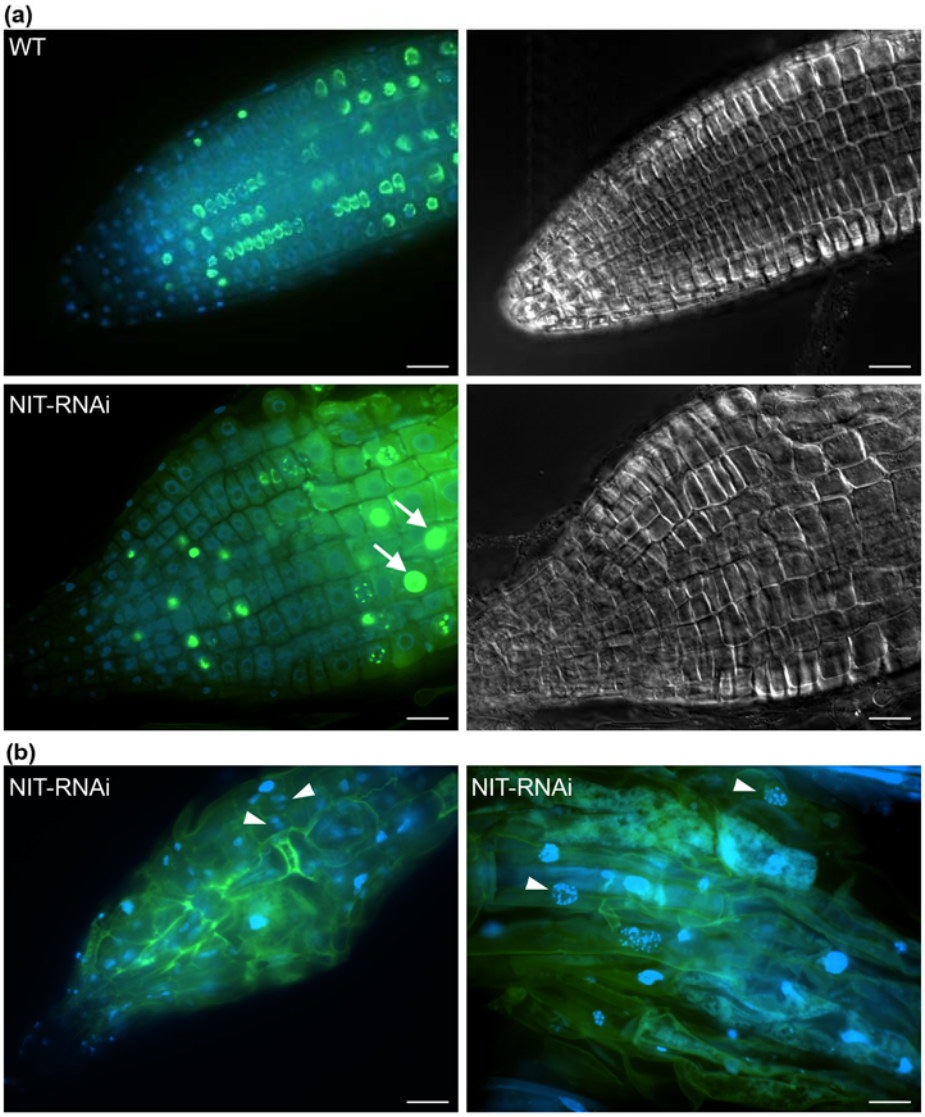

Fig. S6

Representative images of root phenotypes of T1 transformants of NIT-RNAi Columbia plants. EdU labelling three hours pulse (green). DAPI staining of chromatin (blue). (a) 7-day-old NIT-RNAi plants with remarkably shortened division zone of the main root. Enlarged nuclei of elongation zone progressed S-phase as shown by EdU labelling (arrows). (b) Stronger phenotypes of 15-day-old NIT-RNAi plants had malformated shortened root with irregular cell files, binuclear cells, and cells with enlarged nuclei (arrowheads). Bars, (a,b) 20 µm.

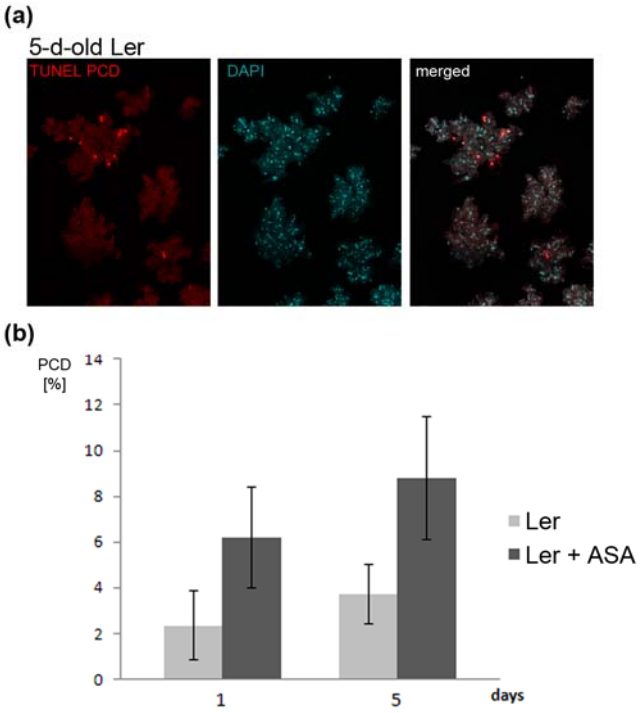

Fig. S7

Induction of programmed cell death (PCD) in *Arabidopsis* Ler cells by acetylsalicylic acid (ASA)-treatment. (a) Cultured cells were stained with TUNEL assay (red) and DAPI (blue). (b) Percentage of PCD (TUNEL-positive cells) in untreated (Ler) and ASA-treated (Ler + ASA) culture first and fifth day after subculturing. Bars represent SD.

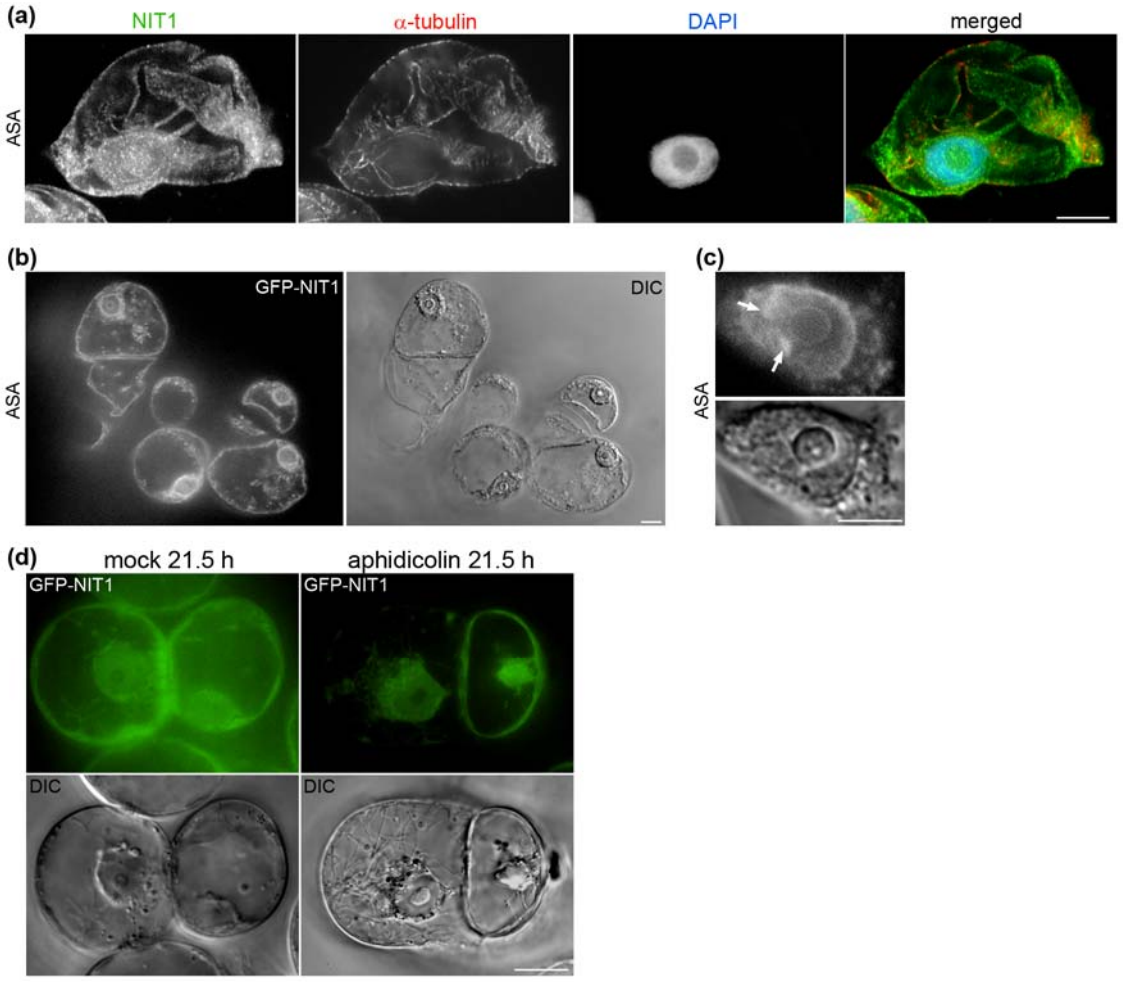

Fig. S8

NIT1 localization during induction of PCD by acetylsalicylic acid (ASA) and during replication stress. (a) Double immunofluorescence labelling of *Arabidopsis* cultured cells after ASA treatment (2 mM, 4 h). Antibodies against NIT1 (green) and α-tubulin (red) were used. DNA was stained with DAPI (blue). NIT1 accumulated around nuclear envelope and entered the nuclei. (b) The same results were obtained from live-cell imaging when cells expressing GFP-NIT1 under its own promoter were treated with ASA. GFP-NIT1 signal was observed around nuclei and also in the nuclei (c, arrows). (d) GFP-NIT1 accumulated around and in the nuclei after replication stress caused by 21.5 h aphidicolin treatment. Bars, (a,b,d) 20 μm; (c) 10 μm.

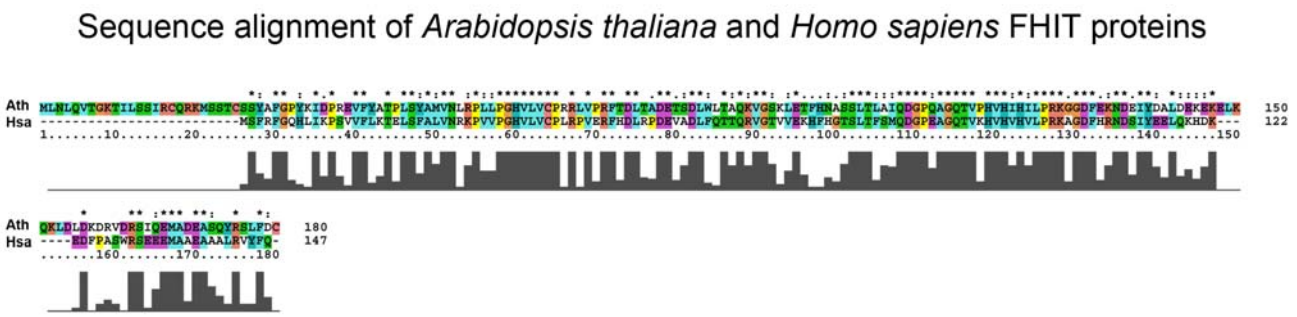

Fig. S9

Sequence alignment of FHIT proteins from *Arabidopsis thaliana* (Ath) and *Homo sapiens* (Hsa). The chemical nature of the individual amino acids is color-coded as follows: cyan, A, F, H, I, M, L, V, W, Y; orange, G; yellow, P; magenta, D, E; green, N, Q, S, T; red, K, R; pink, C. Identical amino acids are marked with asterisk, conserved substitutions are marked with colon, and semi-conserved substitutions are marked with dot.

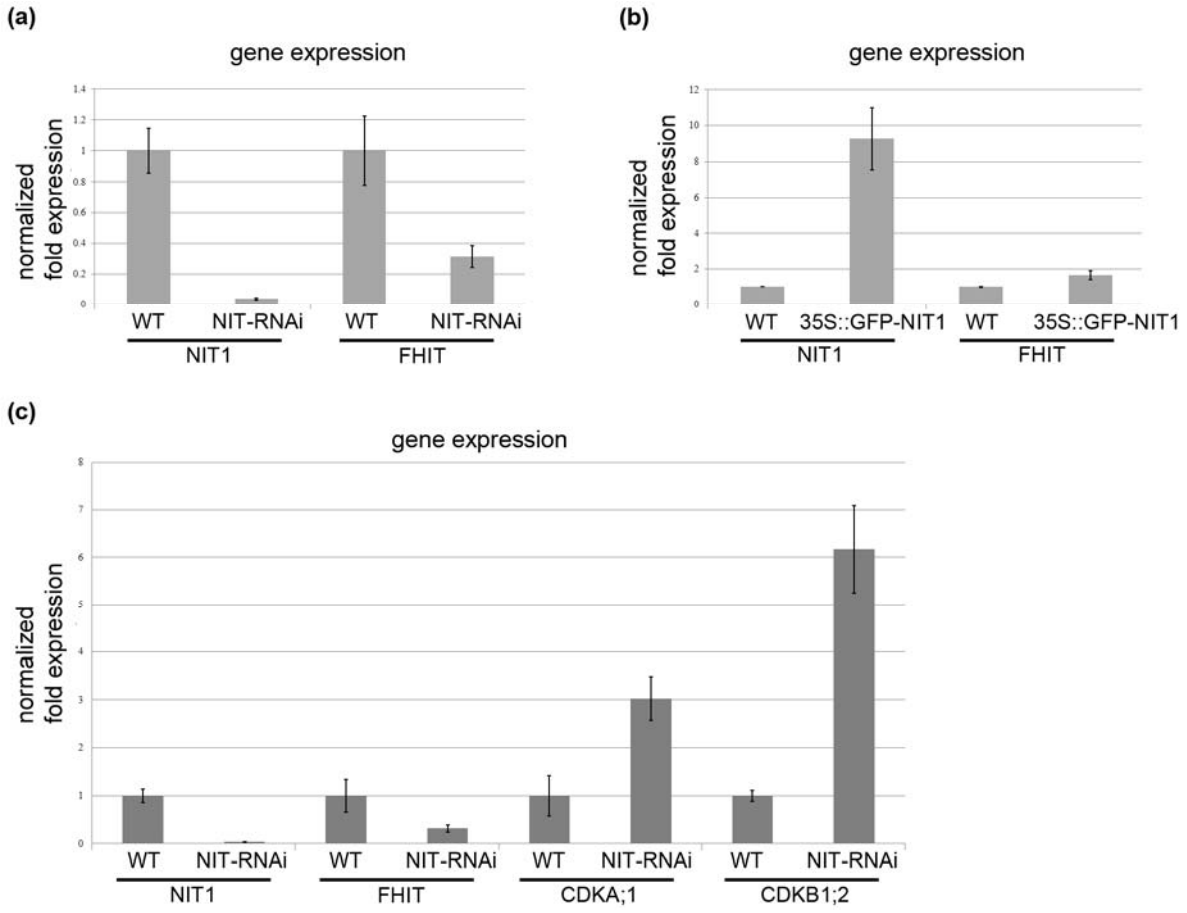

Fig. S10

Co-expression of *NIT1* and *FHIT*. (a) Q RT-PCR analysis of *NIT1* and *FHIT* expression in 19-day-old WT and T1 NIT-RNAi plant transformants. (b) Q RT-PCR analysis of *NIT1* and *FHIT* expression in cultured cells over-expressing GFP-NIT1 and in WT cells. (c) Expression of *NIT1*, *FHIT*, *CDKA;1* and *CDKB1;2*. Q RT-PCR analysis of *NIT1*, *FHIT*, *CDKA;1* and *CDKB1;2* expression in 19-day-old WT and T1 NIT-RNAi plant transformants. (a-c) Mean values of three repeats are shown with SD.

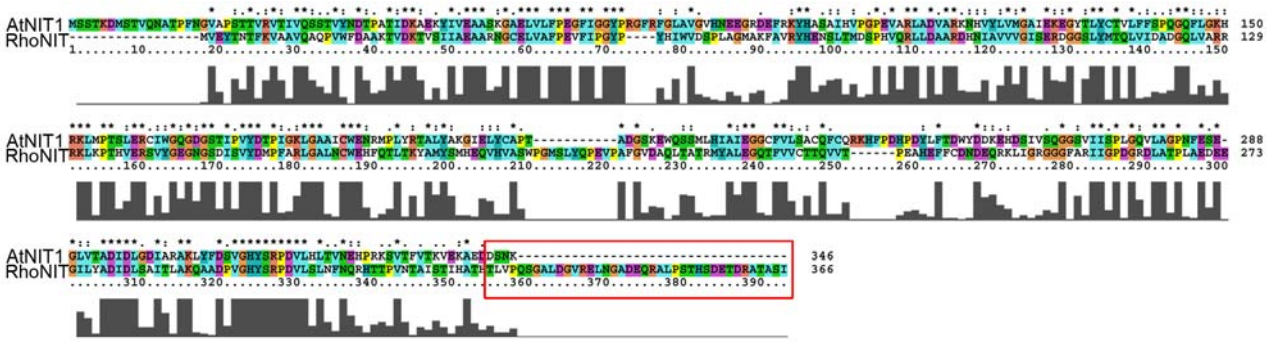

Fig. S11

Sequence alignment of *Rhodococcus rhodochrous* J1 (RhoNIT) nitrilase and *Arabidopsis thaliana* NIT1 (AtNIT1). Rectangle marks the C-terminal extra part of *Rhodococcus* nitrilase molecule which has to be cleaved prior filament formation. The chemical nature of the individual amino acids is color-coded as follows: cyan, A, F, H, I, M, L, V, W, Y; orange, G; yellow, P; magenta, D, E; green, N, Q, S, T; red, K, R; pink, C. Identical amino acids are marked with asterisk, conserved substitutions are marked with colon, and semi-conserved substitutions are marked with dot.

Video S1 Mitosis in *Arabidopsis* cultured cell expressing GFP-NIT1 under 35S CaMV promoter.
(http://onlinelibrary.wiley.com/doi/10.1111/nph.12185/suppinfo)

Video S2 Cytokinesis in *Arabidopsis* cultured cell expressing GFP-NIT1 under 35S CaMV promoter.
(http://onlinelibrary.wiley.com/doi/10.1111/nph.12185/suppinfo)

7.3

Petrovská, B.[#], Jeřábková, H.[#], Kohoutová, L.[#], Cenklová, V., Pochylová Z., Gelová, Z., Kočárová, G., Váchová, L., Kurejová, M., Tomaštíková, E., and Binarová, P.; (2013) Overexpressed TPX2 causes ectopic formation of microtubular arrays in the nuclei of acentrosomal plant cells. J Exp Bot, 64(14):4575-87

[#]These authors contributed equally to this article.

Journal of Experimental Botany, Vol. 64, No. 14, pp. 4575–4587, 2013
doi:10.1093/jxb/ert271 Advance Access publication 4 September, 2013
This paper is available online free of all access charges (see http://jxb.oxfordjournals.org/open_access.html for further details)

Journal of Experimental Botany
www.jxb.oxfordjournals.org

RESEARCH PAPER

Overexpressed TPX2 causes ectopic formation of microtubular arrays in the nuclei of acentrosomal plant cells

Beáta Petrovská[1,*], Hana Jeřábková[1,*], Lucie Kohoutová[2,*], Věra Cenklová[3], Žaneta Pochylová[3], Zuzana Gelová[3], Gabriela Kočárová[2], Lenka Váchová[3], Michaela Kurejová[1], Eva Tomaštíková[1], and Pavla Binarová[2,†]

[1] Centre of the Region Haná for Biotechnological and Agricultural Research, Institute of Experimental Botany, AS CR, v.v.i., Šlechtitelů 31, Olomouc 783 71, Czech Republic
[2] Institute of Microbiology, AS CR, v.v.i., Vídeňská 1083, 142 20 Prague 4, Czech Republic
[3] Institute of Experimental Botany, AS CR, v.v.i., Sokolovská 6, 772 00 Olomouc, Czech Republic

* These authors contributed equally to this manuscript.
† To whom correspondence should be addressed. E-mail: binarova@biomed.cas.cz

Received 26 June 2013; Revised 17 July 2013; Accepted 19 July 2013

Abstract

TPX2 performs multiple roles in microtubule organization. Previously, it was shown that plant AtTPX2 binds AtAurora1 kinase and colocalizes with microtubules in a cell cycle-specific manner. To elucidate the function of TPX2 further, this work analysed *Arabidopsis* cells overexpressing AtTPX2-GFP. Distinct arrays of bundled microtubules, decorated with AtTPX2-GFP, were formed in the vicinity of the nuclear envelope and in the nuclei of overexpressing cells. The microtubular arrays showed reduced sensitivity to anti-microtubular drugs. TPX2-mediated formation of nuclear/perinuclear microtubular arrays was not specific for the transition to mitosis and occurred independently of Aurora kinase. The fibres were not observed in cells with detectable programmed cell death and, in this respect, they differed from TPX2-dependent microtubular assemblies functioning in mammalian apoptosis. Colocalization and co-purification data confirmed the interaction of importin with AtTPX2-GFP. In cells with nuclear foci of overexpressed AtTPX2-GFP, strong nuclear signals for Ran and importin diminished when microtubular arrays were assembled. This observation suggests that TPX2-mediated microtubule formation might be triggered by a Ran cycle. Collectively, the data suggest that in the acentrosomal plant cell, in conjunction with importin, overexpressed AtTPX2 reinforces microtubule formation in the vicinity of chromatin and the nuclear envelope.

Key words: *Arabidopsis thaliana*, AtTPX2, Aurora kinase, fibres, γ-tubulin, importin, microtubules, nuclei, Ran.

Introduction

The targeting protein for Xklp2 (TPX2), is a microtubule-associated protein with multiple functions. Originally, it was identified as a protein required for targeting kinesin-12 (Xklp2) to the spindle pole in *Xenopus* egg extracts (Wittmann *et al.*, 1998). TPX2 and NuMA have been identified as potential downstream effectors of RanGTP in microtubule assembly in *Xenopus* egg extracts and both proteins are the targets of importin blocking activity; they are found in complexes with importin α and β (Gruss *et al.*, 2001; Nachury *et al.*, 2001; Wiese *et al.*, 2001). TPX2 and NuMA proteins colocalize to the interphase nucleus, probably with Ran and importin α and β. This nuclear localization prevents them from acting on microtubules in the cytoplasm until the nuclear envelope breaks down at the beginning of mitosis or meiosis (Kahana and Cleveland, 2001). In the initial phase of mitosis, RanGTP releases TPX2 from its interphase binding partner, importin β, and thus activates TPX2 for bipolar spindle assembly.

TPX2 is also a well-characterized upstream regulator of Aurora A kinase (Kufer *et al.*, 2002; Eyers *et al.*, 2003; Marumoto *et al.*, 2005) and TPX2-activated Aurora A kinase was shown to be essential for Ran-stimulated spindle assembly in the presence/absence of centrosomes (Tsai and Zheng, 2005). TPX2 is an important protein in centrosomal and acentrosomal microtubule nucleation in chromatin and its role with γ-tubulin in chromatin-driven mitotic spindle nucleation in animal cells is well characterized (Wilde and Zheng, 1999; Groen *et al.*, 2004). Recently, TPX2 was identified as a new scaffolding protein and a co-activator of Aurora B in the chromosomal passenger complex (Iyer and Tsai, 2012). Proteomic analysis of human metaphase chromosomes has shown that TPX2 is a nuclear protein belonging to the group of chromosomal fibrous proteins (Uchiyama *et al.*, 2005). However, of the 18 different proteins in this group (e.g. β-actin, vimentin, tubulin), the contribution of TPX2 is unknown (Pederson and Aebi, 2002).

Plant TPX2 contains all of the functional domains of its vertebrate counterpart, but the TPX2 signature motif is present only once in vertebrate sequences compared to twice in plants (Vos *et al.*, 2008; Evrard *et al.*, 2009) where its coiled-coil signature is poorly understood. In *Arabidopsis*, two copies of the TPX2 gene are expressed per genome (Vos *et al.*, 2008), where it is predominantly nuclear during interphase but is actively exported before nuclear envelope breakdown. AtTPX2 is essential for nuclear envelope breakdown and initiation of prospindle assembly (Vos *et al.*, 2008; Evrard *et al.*, 2009). Plant microtubule-associated proteins sharing the same microtubule binding domain as TPX2 play important roles in the organization of microtubular arrays, cell growth, and regulation of cell division (for reviews see Hamada, 2007; Sedbrook and Kaloriti, 2008). Recently, Panteris and Adamakis (2012) speculated about the possible role of fern TPX2 in cortical microtubule assembly.

In 2012, this study group reported that AtAurora1 kinase and AtTPX2 colocalize in plant microtubules in a cell cycle-specific manner, from preprophase to early telophase (Petrovská *et al.*, 2012). In addition, *Arabidopsis* TPX2 protein is intranuclear, and although important mitotic functions for the protein have already been well documented (Vos *et al.*, 2008; Petrovská *et al.*, 2012), any functional role for its accumulation in interphase nuclei is far from being understood.

This study presents data on specific arrays of microtubules decorated with AtTPX2 formed in nuclei and in the vicinity of the nuclear envelope of cells overexpressing AtTPX2-GFP. The formation of nuclear and perinuclear microtubules occurred without participation of Aurora kinase 1 and mitotic signalling. Microtubular arrays heavily decorated with AtTPX2 were not specific to programmed cell death as was described in mammalian cells (Moss *et al.*, 2009). These data on the functions of AtTPX2 in the formation of specific nuclear/perinuclear microtubular arrays and the interaction of importin with AtTPX2 bring further insight to the poorly understood molecular mechanisms of acentrosomal plant microtubule organization.

Materials and methods

Molecular cloning of AtTPX2 *and* AtAurora1

Molecular cloning of *AtTPX2* (At1g03780) and *AtAurora1* (At4g32830) for N- and C-terminal fusions was performed according to Petrovská *et al.* (2012). Gateway binary vectors pK7WGF2,0 for N-terminal GFP fusion, pH7WGR2,0 for N-terminal RFP fusion (Karimi *et al.*, 2002), pMDC43 for C-terminal GFP fusion (Curtis and Grossniklaus, 2003), and pB7RWG2,0 for C-terminal RFP fusion (Karimi *et al.*, 2002) for *AtTPX2* cloning were used, and pGEM T-Easy P2R-P3 (Invitrogen), pGEM T-Easy P4-P1R (Invitrogen), pGEM T-Easy 221 (Invitrogen), and pK7m34GW (purchased from Ghent University, Ghent, Belgium) for *AtAurora1* cloning were used.

Stable transformation of cell suspension cultures and plants

Suspension cultures of *Arabidopsis thaliana* cv. Columbia and cv. Lansberg erecta (Ler) with stable expression of AtTPX2-GFP or/and AtAurora1-RFP were derived as described in Petrovská *et al.* (2012), using the techniques of Mathur *et al.* (1998) and Koroleva *et al.* (2005). *Arabidopsis* Columbia plants were transformed with AtTPX2-GFP using the floral-dip method (Clough and Bent, 1998) as described in Petrovská *et al.* (2012).

Quantitative real-time PCR analysis

Quantitative real-time PCR (qPCR) was performed following MIQE recommendations (Bustin *et al.*, 2009). Total RNA was isolated from *A. thaliana* control and AtTPX2-overexpressed suspension cultures using the Plant RNeasy Extraction Kit (Qiagen). Digestion of DNA during RNA purification was performed using the RNase-Free DNase Set (Qiagen). Purified RNA (100 ng) was reverse transcribed using the Transcriptor High Fidelity cDNA Synthesis Kit (Roche) with an anchored-oligo $(dT)_{18}$ primer according to the Roche instructions. *QPDR* using SYBR Green I Dye (Top-Bio, Czech Republic) was performed using the CFX96 Real-Time PCR Detection System (Bio-Rad). Three replicate PCR amplifications were performed for each sample. The PDF2 gene (Czechowski *et al.*, 2005) was used as a reference. Quantification of transcripts of each gene, normalized to the internal reference PDF2 gene (At1g13320), was determined using CFX Manager Software (Bio-Rad). The transcript level of each target gene of control cells or the reference gene in controls or overexpressed AtTPX2 cells, was designated as 1.0. The primers used for real-time PCR were: PDF2For 5′-TAACGTGGCCAAAATGATGC-3′, PDF2Rev 5′-GTTCTCCACAACCGCTTGGT-3′, *AtTPX2*For 5′-AAGCTCGACCTGTGAACAAGA-3′, and *AtTPX2*Rev 5′-CTGGCAGATGTGGTGTACTTCT-3′. To ensure specificity of primers, primer pairs were designed to span across two neighbouring exons and were detected as a single peak in dissociation curve analysis.

Drug treatment

Amiprophos methyl (APM; Duchefa) at a concentration of 5 μM was used for microtubule depolymerization as described Weingartner *et al.* (2001); taxol (Sigma-Aldrich) was used at a concentration 5 μM. Inhibition of Cdk and Aurora kinase activity was done adding 100 μM roscovitine (a gift from Miroslav Strnad, Olomouc, Czech Republic) as described by Planchais *et al.* (1997) and Binarová *et al.* (1998) and 2 μM Aurora kinase inhibitor ZM447439 (Tocris Bioscience) as described by Ditchfield *et al.* (2003).

Co-immunoprecipitation

Co-immunoprecipitations were performed using GFP-Trap A and RFP-Trap A (ChromoTek, Planegg-Martinsried, Germany) according to the manufacturer's instructions using the modified protocol

described in Petrovská *et al*. (2012). The extract from the *A. thaliana* cell culture expressing AtTPX2-GFP or co-expressing AtAurora1-RFP and AtTPX2-GFP (protein concentration 3–4 mg ml^{-1}) after centrifugation at 10,000 *g* for 10 min were used directly or solubilized by 1% NP-40 for 1 h at 4 °C. The extracts were supplemented with double concentration of inhibitors of proteases, with inhibitors of phosphatases and 50 µM MG132 (Sigma) and incubated with GFP-Trap or RFP-Trap beads for 1.5 h at 4 °C. As a negative control, GFP immunoprecipitate from wild-type Ler *Arabidopsis* culture was used. The immunoprecipitated proteins were released by elution with glycine (pH 2.5). Proteins in the eluates were resolved by SDS-PAGE and analysed for importin, γ-tubulin, and AtAurora1 by immunoblotting with rabbit polyclonal anti-importin antibody 1:3000 (Secant Chemicals), affinity-purified rabbit polyclonal antibody AthTU 1:2,500 (Dryková *et al.*, 2003), anti-actin 1:1000 (Affinity BioReagents), anti-GFP and anti-RFP 1:2000 (Abcam and ChromoTek) antibodies, and anti-Ran antibody 1:200 (Transduction Laboratories). Secondary antibodies anti-rabbit and anti-mouse IgG HRP Conjugates (Promega or Amersham-GE Healthcare) were used; Super Signal West Pico Chemiluminiscent Substrate (Thermo Scientific) was used according to the manufacturer's instructions.

Immunofluorescence

Arabidopsis thaliana suspension cultures were fixed for 1 h using 3.7% paraformaldehyde and processed for immunofluorescence as described in Binarová *et al*. (1993). Primary antibodies, anti-α-tubulin monoclonal antibody DM1A (Sigma) at a dilution of 1:500, monoclonal anti-γ-tubulin TU-32 (kindly provided by Pavel Dráber from IMG, Prague, Czech Republic) diluted 1:10, affinity purified rabbit polyclonal antibody AthTU 1:1000 (Dryková *et al.*, 2003), anti-GFP antibody (Abcam) at a dilution 1:1000, anti-actin (Affinity BioReagents) at a dilution 1:1000, anti-phospho-histone H3 (Ser10) antibody (Cell Signaling Technology) at a dilution 1:2000, monoclonal mouse anti-importin antibody (Secant Chemicals, Winchendon, MA) at a a dilution 1:2000, rabbit polyclonal anti-importin antibody (Secant Chemicals) at a dilution 1:3000, and anti-Ran antibody (Transduction Laboratories) at a dilution 1:200 were used with anti-mouse and anti-rabbit conjugated antibodies to FITC, DyLight 488, Cy3, DyLight 550, or Alexa Fluor 647 (Jackson ImmunoResearch Laboratories). DNA was stained with DAPI.

In situ *detection of fragmented DNA*

The *In Situ* Cell Death Detection Kit (Roche) was used for the TUNEL (TdT-mediated dUTP nick-end labelling) test according to the manufacturer's instructions. Besides the TUNEL test, the viability assay (on the basis of its penetration into non-viable cells) was determined by 10 min incubation of cell suspension with 0.1% of Evans blue dye.

Microscopy

Microscopy was performed using an IX81 motorized inverted research microscope CellR (Olympus) equipped with disk scanning unit and digital monochrome CCD camera CCD-ORCA/ER, and using an Olympus IX-81 FV-1000 confocal microscope. To avoid filter crosstalk, fluorescence was detected using HQ 480/40 exciter and HQ 510/560 emitter filter cubes for FITC and HQ 545/30 exciter and HQ 610/75 emitter filter cubes for Cy3 (both AHF Analysen Technique). Images were processed and analysed using CellR Software and Quick Photo Camera Software version 2.3 (Olympus). Images from confocal laser scanning microscopy were taken with PLAPO objective 100×/1.45 using the sequential multitrack mode to avoid bleed-through; excitation and emission wavelengths were 405 and 425–460 nm for DAPI, 473 and 485–545 nm for FITC or DyLight 488, 559 and 575–620 nm for Cy3 or DyLight 550, and 635 and 655–755 nm for Alexa Fluor 647. Green fluorescent protein was excited by 473 nm and emission was detected from 485 to 545 nm. Whenever needed, z-stacks were taken with 0.2 µm z-step. Images were analysed using FV10-ASW (Olympus); 3-D reconstruction and animation from z-stacks, and sectioning of gained 3D objects was performed using Imaris software (Bitplane) in the section and animation mode.

Figures were prepared using Adobe Photoshop 7.0. The quantitative colocalization analyses were performed using ImageJ software with JACoP (Just Another Co-localization Plug-in) plugin (Bolte and Cordeliéres, 2006) based on Pearson's coefficient, overlap coefficient, and Manders' coefficient (colocalization coefficient for channel M1, M2). Costes' approach was expressed with a plot of the distribution of the Pearson's coefficient of randomized images (curve) and of the green channel image (red line) and showed a probability of colocalization. Another development based on Pearson's coefficient used for confirmation of a degree of colocalization was Van Steensel's approach. Li's approach were presented as a set of two graphs, each showing the normalized intensities (from 0 to 1) as a function of the product $(A_i - a)(B_i - b)$ for each channel. Observed positive product $(A_i - a)(B_i - b)$ and dot cloud concentrated on the right side of the $x = 0$ line (although adopting a C-shape) indicated high colocalization.

Results

In silico *analyses suggested nuclear localization as well as nuclear function of AtTPX2.*

The AtTPX2 protein is composed of two domains: TPX2_importin (pfam: PF12214) and TPX2 domain (pfam: PF06886) (Fig. 1A) (Punta *et al.*, 2012). *Arabidopsis* TPX2 has two nuclear localization signals andm unlike other TPX2s, AtTPX2 has a signal for nuclear export (Vos *et al.*, 2008). AtTPX2 also possesses two domains that can mediate its localization to microtubules (Vos *et al.*, 2008; Petrovská *et al.*, 2012). The AtTPX2 protein also contains a short region (amino acids 588–619) that shows significant probability for coiled coil formation, as confirmed using several algorithms: Coils (Lupas *et al.*, 1991), Paircoil (Berger *et al.*, 1995), MultiCoil (Wolf *et al.*, 1997), and ELM (Dinkel *et al.*, 2012). The coiled coil region was found in plant proteins that contain TPX2_importin and TPX2 motifs across various plant species (Fig. 1B); most of them belonged to as-yet uncharacterized or hypothetical plant proteins.

Deeper analysis of *Arabidopsis* TPX2 amino acid sequence (Dinkel *et al.*, 2012) revealed the following: the presence of an HP1 ligand (interacts with chromoshadow domain of heterochromatin-binding protein 1, amino acids 95–99), KEN box (148–152, 275–279, and 667–671), D box (327–645), three cyclin recognition sites (305–309, 332–336, 516–519), several FHA phosphopeptide ligands (predominant in nuclear proteins that are involved in cell cycle checkpoint, DNA repair and transcriptional regulation), mitotic spindle checkpoint protein MAD2 binding motif (361–369), mitogen-activated protein kinase, docking motifs (41–47, 492–502, 538–549, 723–731), sumoylation sites (68–71, 208–211, 529–532, 575–578), and several phosphorylation sites (i.e. PIKK, glycogen synthase kinase 3, PKA; Supplementary Table S1, available at *JXB* online). Localization of proteins with these motifs or interaction sites is typically nuclear. Plant TPX2 is localized in nuclei (Vos *et al.*, 2008; Petrovská *et al.*, 2012). In addition, using Nuc-PLoc (Hong-Bin and Kuo-Chen, 2007) and

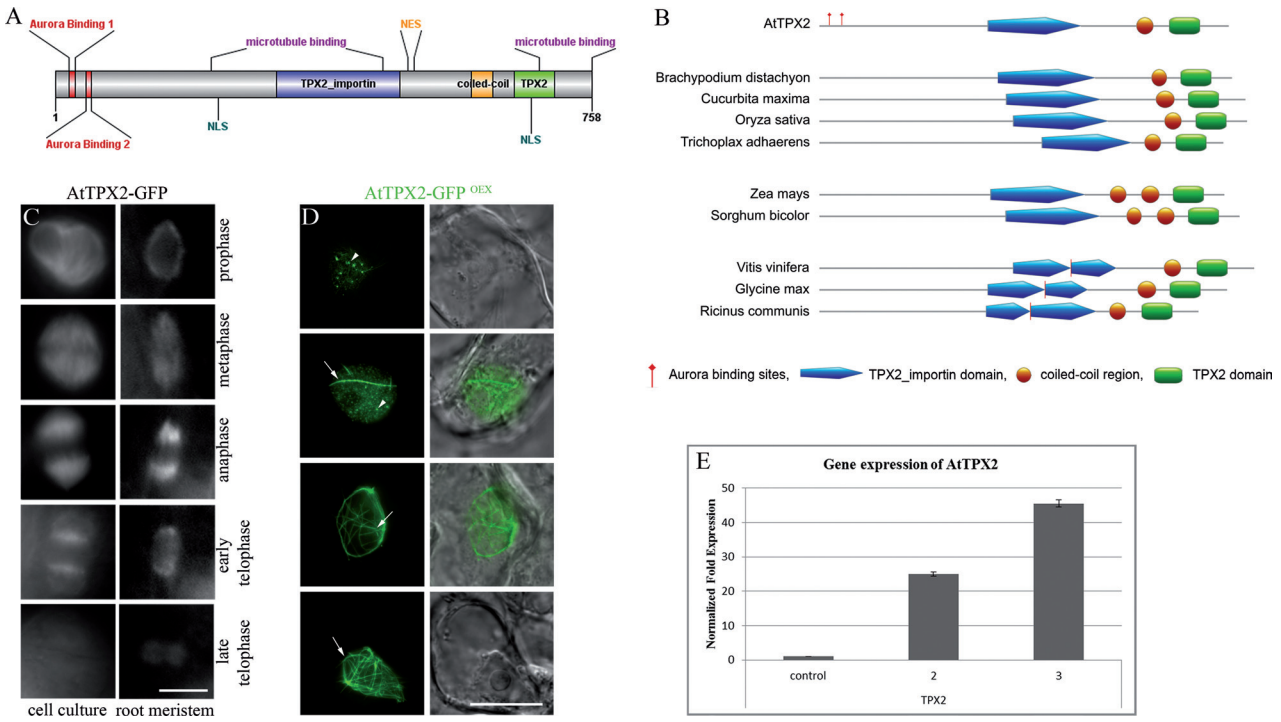

Fig. 1. Localization of AtTPX2 protein in *Arabidopsis* cells overexpressing AtTPX2. (A) Domains, putative interaction sites, and binding motifs in the amino acid sequence of *Arabidopsis* TPX2 protein. For putative interaction sites, binding motifs as well as domain graph, ELM (Dinkel *et al.*, 2012), and SUMOsp 2.0 (Ren *et al.*, 2009) databases were used. Schematic drawing was prepared in DOG (Domain Graph; Xao and Xue, 2009). (B) Domain organization of *Arabidopsis* TPX2 protein and its plant homologues: AtTPX2–targeting protein for Xklp2–TPX2 (*Arabidopsis thaliana*, AGI no. At1g03780), *Brachypodium distachyon* uncharacterized protein LOC100842911 (acc. no. XP_003560168), *Cucurbita maxima* hypothetical protein (AEK84224), *Oryza sativa* hypothetical protein OsJ_24381 *Oryza sativa Japonica Group* (EEE67237), *Trichoplax adhaerens* hypothetical protein TRIADDRAFT_55817 (XP_002112111), *Zea mays* uncharacterized protein LOC100383389 (NP_001169515), *Sorghum bicolour* hypothetical protein SORBIDRAFT_02g034250 (XP_002462908), *Vitis vinifera* uncharacterized protein LOC100262517 (XP_002274918), *Glycine max* uncharacterized protein LOC100801192 (XP_003526269), *Ricinus communis* protein with unknown function (XP_002517880). Schematic drawing of proteins was prepared in MyDomains (Prosite, http://prosite.expasy.org/cgi-bin/prosite/mydomains/). (C) Localization of AtTPX2-GFP in dividing cell in cell culture with stable expression and in root meristematic zone of *A. thaliana*. AtTPX2-GFP was localized with mitotic microtubular arrays from prophase until early telophase. Bar, 10 μm. (D) Localization of AtTPX2-GFP in *Arabidopsis* cell suspension culture overexpressing AtTPX2-GFP. AtTPX2-GFP was predominantly localized with 'dots' or 'seeds' (arrowheads), later elongated into bundled fibres around (cage-like structures) and inside the nuclei (arrows). Frequency of overexpressing cells ranged between 10–40% depending on the transformation event, bar, 10 μm. (E) Relative expression of AtTPX2 in two representative samples of dividing *Arabidopsis* suspension cultures overexpressing AtTPX2 (samples 2, 3) showed a significant increase (25-fold, 45-fold, respectively) in transcript level compared to the control cells.

Subnuclear Compartments Prediction System 2.0 (Lei and Dai, 2005, 2006), the subnuclear localization of *Arabidopsis* TPX2 protein was predicted to be nuclear speckle and nuclear lamina, respectively.

Fibres heavily decorated with TPX2 are formed in the vicinity of the nuclear envelope and in the nuclei of cells overexpressing AtTPX2

Cultured cells and seedlings of *A. thaliana* were transformed with plasmids containing full-length C- and N- terminal AtTPX2 protein fusions with GFP, under the control of the cauliflower mosaic virus (CaMV) 35S constitutive promoter. After selection, stable cell lines were derived (Petrovská *et al.*, 2012). Both C- and N- terminal AtTPX2-GFP fusion proteins showed similar localizations. The AtTPX2-GFP was observed in nuclei, the perinuclear region and, in a cell cycle-specific manner, with mitotic microtubular arrays. The localization of AtTPX2-GFP fusion protein was similar for dividing cultured cells and cells of *Arabidopsis* seedlings (Fig. 1C). The AtTPX2-GFP signal was present with perinuclear microtubules in preprophase, with kinetochore microtubular fibres in metaphase and anaphase, and with early phragmoplast in cytokinesis. It was previously found that the cell cycle-specific microtubular localization of AtTPX2-GFP requires Aurora binding (Petrovská *et al.*, 2012). TPX2 knockout in *Arabidopsis* is lethal and only heterozygous plants could be obtained for the T-DNA inserts (Vos *et al.*, 2008; data not shown). Therefore, the current study was not able to test functionality of the AtTPX2-GFP protein under

the most stringent conditions by complementation of null mutants. However, the localization data and interaction of AtTPX2-GFP with Aurora kinase (Petrovská *et al.*, 2012) suggest that the AtTPX2-GFP fusion protein is functional.

As early as 48 h after transformation, expressed fusion protein showed diffused distribution in cytoplasm with accumulation in nuclei; a later AtTPX2 signal was predominantly associated with dots and patches in nuclei and as fibrillar structures located inside the nuclei and in the perinuclear area (Fig. 1D). The effects of overproduction of AtTPX2 N- and C-terminal GFP fusion proteins were similar, suggesting that the GFP moiety did not interfere with the function of AtTPX2 in fibre formation. Overexpression of AtTPX2-GFP was confirmed by real-time qPCR (Fig. 1E). Microscopic analysis of AtTPX2-overexpressing cells showed that the dots of AtTPX2-GFP in interphase nuclei (Fig. 1D, arrowheads) were formed within a period of 3 d from transformation. AtTPX2-GFP dots and patches were gradually built into thick fibrillar structures (Fig. 1D, arrows). The AtTPX2-GFP signal was attached to filamentous structures reminiscent of microtubules that were arranged into cage-like structures surrounding the nuclei (Fig. 1D, arrows).

To prove whether AtTPX2-decorated fibres in AtTPX2-overexpressing cells represent cytoskeletal polymers, this study performed a series of double immunofluorescence experiments. Fibres were positive for α-tubulin (Fig. 2A, B), but they were not recognized by anti-actin antibody (Supplementary Fig. S1). The signal for α-tubulin localized with the AtTPX2 foci in nuclei (Fig. 2A, arrow), and with forming fibres (Fig. 2A, arrowheads). In AtTPX2-overexpressing cells containing more prominent fibrillar arrays, α-tubulin was associated with thinner AtTPX2-positive fibres along their entire length (Fig. 2B, arrow). Thicker bundles, heavily labelled with AtTPX2-GFP, showed a weaker signal for α-tubulin (Fig. 2A, arrowheads), probably due to the lower accessibility of the epitope to the anti-α-tubulin antibody.

Treatment of cells overexpressing AtTPX2 with the microtubule-depolymerizing drug APM showed that the nuclear and perinuclear microtubular bundles were resistant to drug-induced depolymerization. As shown in Fig. 2C, the microtubular arrays persisted in 98% of 5 µM APM- treated cells (n = 112), showing overexpression of AtTPX2-GFP. Microtubules were largely depolymerized by the same dose of APM in cells with stable expression of AtTPX2-GFP (Fig. 2C, inset I) and only remnants of kinetochore microtubules decorated with AtTPX2-GFP were observed (Fig. 2C, inset II). Taxol treatment did not result in further bundling or stabilization of ectopic microtubules in AtTPX2-GFP-overexpressing cells (Supplementary Fig. S2).

Serial sections of nuclei and 3-D reconstructions showed a network of microtubules decorated with AtTPX2 inside the nuclei and in the area adjacent to the nuclei (Fig. 3A). Thick intertwined bundles of microtubules were present around the nuclei (Fig. 3A, arrow) and anchored to the nucleus at the cell periphery (Fig. 3A, arrowheads). More detailed analyses using Imaris sectioning of nuclei of AtTPX2-GFP-overexpressing cells confirmed the formation of fibrillar structures inside the nuclei, in the vicinity of chromatin (Fig. 3B, cross I) and also inside the nucleoli (Fig. 3B, cross II). To prove nuclear location of ectopic arrays, cells overexpressing AtTPX2-GFP *in vivo* were analysed. As shown in Fig. 3C, fibres decorated with AtTPX2-GFP were observed, together with intranuclear foci of overexpressed TPX2.

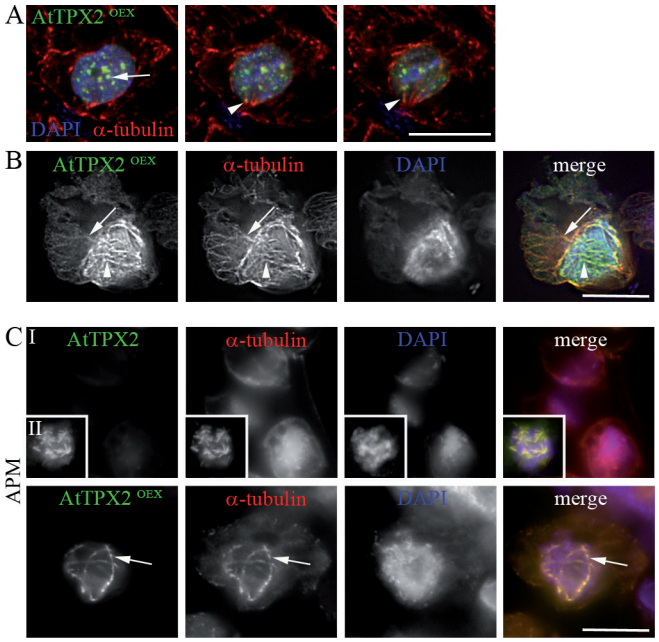

Fig. 2. AtTPX2 localization with ectopic perinuclear and nuclear microtubules in *Arabidopsis* cells overexpressing AtTPX2-GFP. (A) AtTPX2-GFP foci localized with α-tubulin in the nucleus (arrow) and AtTPX2-GFP partially loaded on α-tubulin fibres (arrowheads) in cells with foci of overexpressed AtTPX2-GFP. Serial sections (0.4 µm z-steps) of the cell immunostained by anti-GFP antibody (green) and anti-α-tubulin antibody (red) with chromatin stained by DAPI (blue) are shown. (B) α-Tubulin signal with thinner AtTPX2-GFP-decorated fibres (arrow) was stronger compared to the signal with thick bundles (arrowhead); 99% of analysed cells showed the corresponding pattern (194 analysed cells). (C) While microtubules were depolymerized, with exception of kinetochore stubs, in cells expressing AtTPX2-GPF after the treatment with 5 µM APM for 2.5 h, microtubular arrays in cell overexpressing AtTPX2-GFP (AtTPX2^{OEX}) were stable after the same treatment. Bars, 10 µm.

These data showed that overexpressed AtTPX2-GFP protein was initially present in nuclear foci and patches, and later, fibrillar microtubular arrays were formed in nuclei and the perinuclear area. The ectopic microtubular fibres, heavily decorated with AtTPX2-GFP, were resistant to microtubular drugs.

Interaction of importin with AtTPX2-GFP suggests involvement of the Ran cycle in TPX2-mediated formation of microtubular arrays.

Importin binds TPX2 protein and imports it into the nucleus, and RanGTPase sequesters the TPX2 nuclear pool before breakdown of the nuclear envelope (Gruss *et al.*, 2001). Binding of animal importin to recombinantly expressed plant TPX2 protein in a RanGTPase-dependent manner was

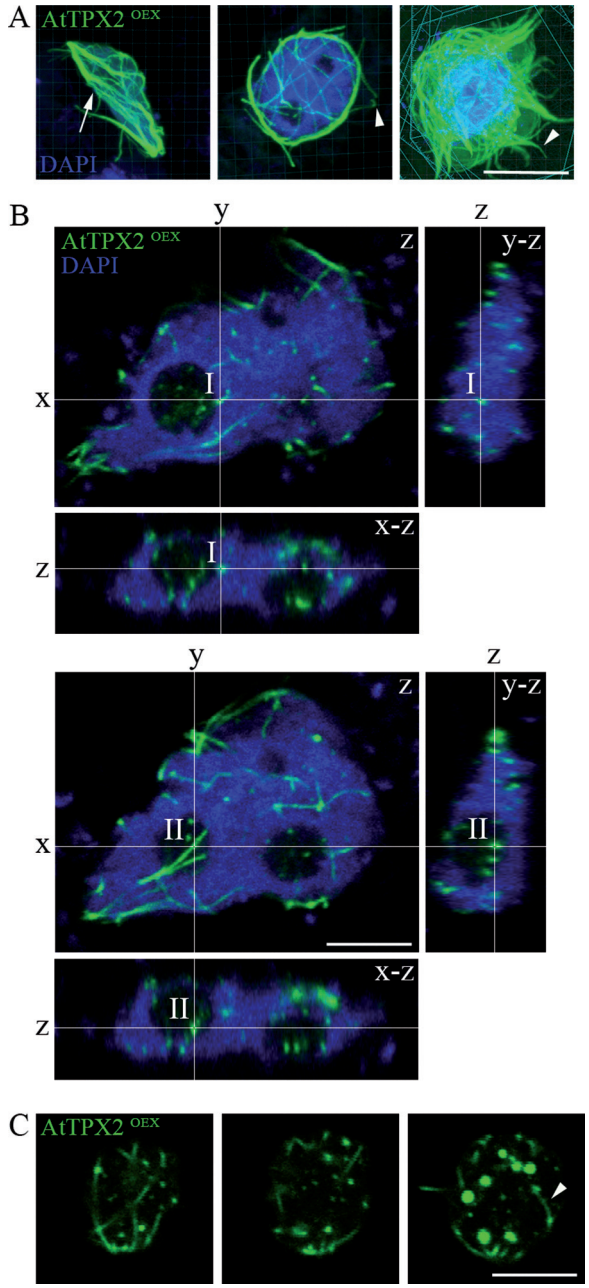

Fig. 3. Three-dimensional reconstruction and analysis of microtubular arrays in *Arabidopsis* cells overexpressing AtTPX2-GFP. (A) Representative images from 3D reconstruction of cells with AtTPX2-decorated fibres around and inside nuclei; Microtubular fibres in the perinuclear area are twisted (arrow), the microtubular fibres anchored nuclei to cell periphery (arrowheads); bar, 10 µm. (B) Two Imaris sections of the nucleus with AtTPX2-decorated fibres; AtTPX2-decorated fibres were present inside the nucleus (cross I) and the nucleolus (cross II) overexpressing AtTPX2; main panel *z* shows a single z-stack of the nucleus; right panel *y-z* shows cross-section by *y* plane perpendicular to *z* plane in the main panel; lower panel *x-z* shows cross-section by *x* plane perpendicular to *z* plane in the main panel; bar, 5 µm. (C) Serial z-stacks of nucleus of cell overexpressing AtTPX2-GFP analysed *in vivo*. Sections from nuclear surface to the centre (left to right) showed perinuclear fibres and intranuclear foci and fibres decorated by AtTPX2 (arrowhead); bar, 5 µm.

shown *in vitro* by Vos *et al.* (2008). To determine whether the RanGTPase pathway is involved in the process of AtTPX2-mediated formation of microtubular arrays, the current work analysed the immunolocalization of importin and Ran in AtTPX2-GFP-overproducing cells (Fig. 4 and Supplementary Fig. S3). The signal for importin was observed in nuclei, associated with the nuclear envelope, and with intranuclear and perinuclear microtubular fibres (Fig. 3). Quantitative co-localization analyses of AtTPX2 and importin were performed using the ImageJ plugin, JACoP (Bolte and Cordeliéres, 2006). The analyses showed high degrees of co-localization of AtTPX2-GFP, with patchy patterns of importin on perinuclear fibres (Fig. 4A, arrowhead), and with microtubular fibres extending from the perinuclear area to the periphery (Fig. 4B, arrow). All coefficients correctly reported a strong overlap between the two channels (Supplementary Fig. S5).

Previous experiments used GFP co-immunoprecipitation to show an interaction of AtAurora1-RFP with AtTPX2-GFP (Petrovská *et al.*, 2012). The current work performed GFP co-immunoprecipitation to provide evidence for an interaction between AtTPX2-GFP and importin. As shown in Fig. 4C, importin was co-purified with AtTPX2-GFP from low-speed supernatants. Negative controls as well as probing of purified TPX2 complexes with the relevant anti-actin antibody confirmed that interaction of importin with AtTPX2 was specific (Fig. 4C, Supplementary Fig. S4). It is known that AtTPX2 protein is highly unstable in plant cell extracts or under conditions of electrophoretic protein separation, and this makes detection by Western blotting difficult (Vos *et al.*, 2008; Petrovská *et al.*, 2012). In agreement with data shown by Vos *et al.* (2008) and Petrovská *et al.* (2012), several bands for the AtTPX2-GFP protein and its degradation products were detected with anti-GFP antibody in a sample of immunopurified AtTPX2-GFP (Fig. 4C).

Next, Ran protein was immunolocalized in AtTPX2-overexpressing cells. The signal for Ran was stronger in nuclei with AtTPX2-GFP nuclear dots and patches, where 83% of nuclei (n = 132) showed higher levels of the Ran signal compared to the untransformed controls (Supplementary Fig. S3). On the other hand, only 23% of nuclei (n = 94) showed any signal above that of control untransformed nuclei in cells with nuclear/perinuclear microtubular arrays (Fig. 4E). This finding suggests that the Ran nuclear signal was weakening during microtubular array assembly. Multiple labelling showed that, similarly to Ran, the importin signal was enriched in nuclei of overexpressing cells where it co-localized with some of the AtTPX2-GFP foci and accumulated around NE (Fig. 4D, arrow and arrowhead). In cells with assembled fibres, diminution of the nuclear signal for importin was even more pronounced compared to that observed for Ran (Fig. 4D, E). A smaller proportion of the importin signal was observed associated with the AtTPX2-GFP-decorated microtubular arrays.

Plant γ-tubulin is associated with microtubular arrays, around the nuclear envelope, and in nuclei (Dryková *et al.*, 2003). Petrovská *et al.* (2012) showed that γ-tubulin is localized with AtTPX2 and AtAurora1 on mitotic microtubular arrays. Therefore, this work analysed the localization of γ-tubulin in cells overexpressing AtTPX2-GFP. Signals for γ-tubulin were

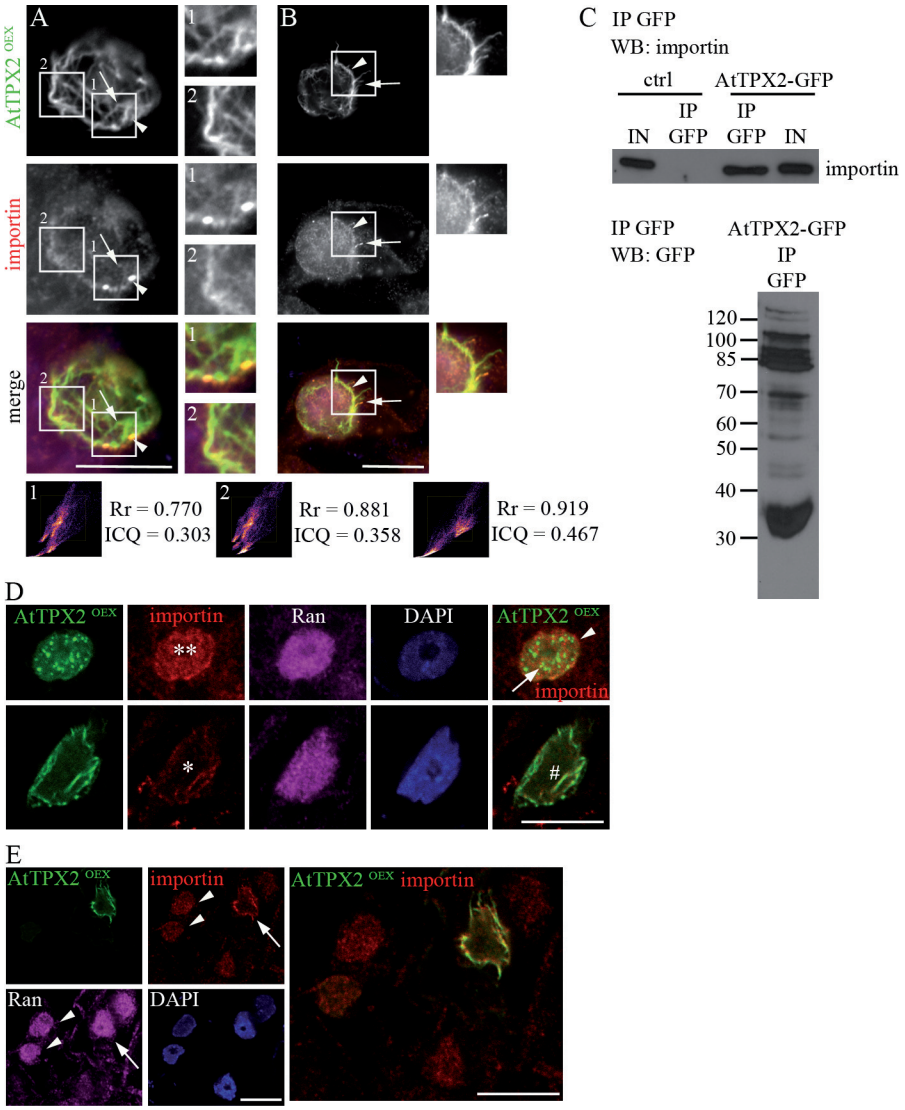

Fig. 4. Immunolocalization of importin and Ran in AtTPX2-GFP-overproducing cells. (A, B) AtTPX2 and importin colocalized in the vicinity of the nuclei (B, arrowhead), with the AtTPX2-decorated microtubular fibres (A, B, arrows), and in intranuclear foci (A, arrowhead). Colocalization was analysed by ImageJ software with JACoP plugin (Bolte and Cordeliéres, 2006). The similar labelling pattern was observed in 97% of analysed overexpressing cells (n = 112). (C) Importin was copurified with AtTPX2-GFP by GFP trap (AtTPX2-GFP IP GFP) from extracts of *Arabidopsis* cells. GFP immunoprecipitate from wild-type Ler *Arabidopsis* culture was used as a negative control (ctrl IP GFP). Immunoblotting of GFP immunoprecipitate from AtTPX2-GFP expressing cell culture with anti-GFP antibody showed several bands corresponding to the full-length molecule of AtTPX2-GFP above 100 kDa and several degradation products. (D, E) Representative images of immunofluorescence labelling of the cells overexpressing AtTPX2-GFP (green), immunostained with anti-importin (red), with anti-Ran (magenta); chromatin stained by DAPI (blue). (D) Importin signal was nuclear (two asterisks), localized around nuclei (arrowhead) and colocalized with some of the AtTPX2 foci (arrow) in overexpressing cells with AtTPX2-GFP foci and patches. Nuclear signal for importin was reduced (asterisk) in cells where AtTPX2-GFP fibres were formed and it localized with the fibres around nuclei and in the nuclei (hash mark). (E) Signal for Ran in the nuclei of cells with AtTPX2 perinuclear fibres was not above the level of signal found in untransformed cells (arrowheads). Importin nuclear signal declined in the cells with AtTPX2-GFP fibres (arrow) while a portion of signal for importin localized with AtTPX2 perinuclear fibres. Bars, 10 μm.

observed in a patchy pattern with microtubular bundles formed in the vicinity of the nuclei and extending to the cell periphery (Fig. 5A). Quantitative co-localization analyses of γ-tubulin and AtTPX2, using the ImageJ plugin JACoP, showed co-localization of γ-tubulin with AtTPX2-GFP-decorated microtubular arrays (Fig. 5B1, 2). However, the association of γ-tubulin with immunopurified AtTPX2-GFP could not be demonstrated.

Together, the immunolocalization and immunopurification data suggest a function for importin with plant AtTPX2. The accumulation of importin and Ran in the nuclei of overexpressing cells indicates a nuclear import of overexpressed AtTPX2-GFP. Diminution of the nuclear signal for importin, as observed in cells with microtubular arrays, indicates that microtubule formation was triggered by sequestered AtTPX2, possibly

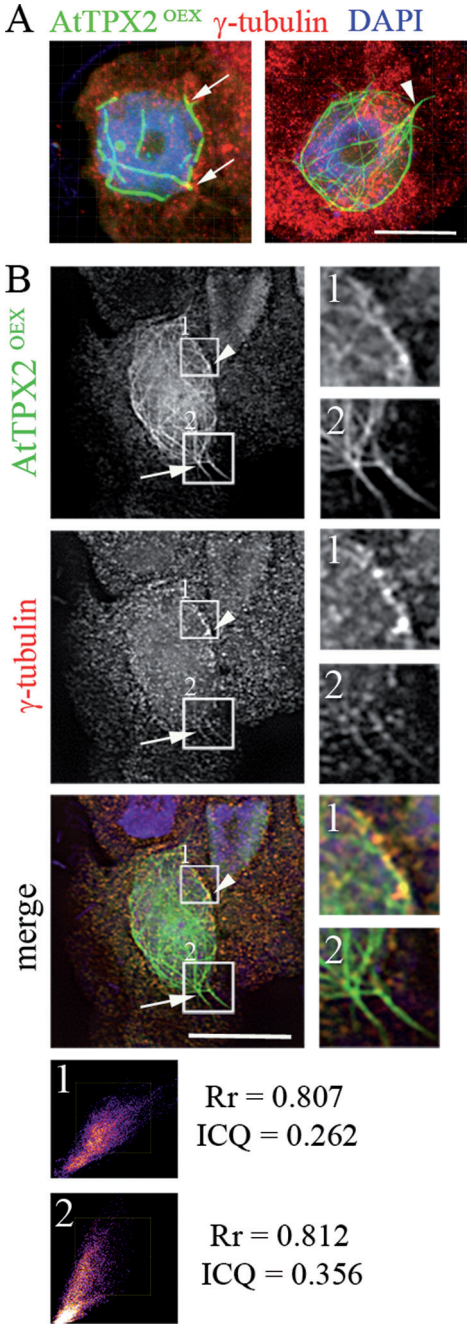

Fig. 5. Colocalization of AtTPX2 and γ-tubulin in *Arabidopsis* AtTPX2-GFP-overproducing cells. (A, B) γ-Tubulin localized together with AtTPX-GFP. (A) 3D analysis of cells overexpressing AtTPX2-GFP stained with anti-γ-tubulin antibody (red), DAPI (blue) obtained by laser scanning microscopy and 3D-reconstructed (Imaris, Bitplane). Still images from 3D reconstruction animation show γ-tubulin localized with AtTPX2-GFP-decorated fibres in vicinity of nuclear envelope (A, arrows), with intranuclear microtubules, and in patchy pattern on microtubular bundles extending from perinuclear area (arrowhead). (B) γ-Tubulin colocalized with AtTPX2 on microtubular fibres extending from perinuclear area to the cytoplasm and membranes (arrow) and on the nuclear envelope (arrowhead). Colocalization was analysed by ImageJ software with JACoP plugin (Bolte and Cordeliéres, 2006). The similar labelling pattern was observed in 93% of analysed overexpressing cells (n = 128). Bars, 10 μm.

Ran cycle-dependent. The presence of an importin signal with AtTPX2 on ectopic microtubular fibres suggests that an excess of the overexpressed AtTPX2 may still be bound to importin.

Formation of AtTPX2-decorated microtubular fibres was neither dependent on association of Aurora kinase with TPX2 nor on mitotic status of the chromatin.

Previous data showed that AtAurora1 binds to AtTPX2 and that binding is required for cell cycle-specific localization of TPX2 on mitotic microtubular arrays (Petrovská *et al.*, 2012). In cells with stable expression of AtTPX2-GFP and AtAurora1-RFP, both proteins colocalized with microtubular arrays from preprophase to early telophase (Fig. 6A) and were co-purified (Supplementary Fig. S6). However, only a weak AtAurora1 signal was found on bundled AtTPX2-decorated microtubules in overexpressing cells (Fig. 6B). To determine whether binding of Aurora kinase was required for TPX2-mediated formation of ectopic microtubular arrays, this work overexpressed a truncated version of AtTPX2 that lacked two conserved Aurora kinase binding sites (ΔN-AtTPX2; Petrovská *et al.*, 2012). Microtubular arrays were formed in the vicinity of and in the nuclei, and were associated with ΔN-AtTPX2 (Supplementary Fig. S7). This work analysed the effect of the Aurora kinase inhibitor, ZM447439 (Ditchfield *et al.*, 2003) that affected microtubular mitotic arrays in wild-type *Arabidopsis* cells (Supplementary Fig. S8). Contrary to the wild-type cells, ZM447439 treatment had no visible effect on the formation, stability, and arrangement of nuclear and perinuclear microtubular bundles in cells overexpressing AtTPX2 (Fig. 6C). These data suggest that binding of Aurora kinase with AtTPX2, which is required for localization of TPX2 on mitotic microtubules, is dispensable for the formation and organization of the ectopic peri/intranuclear microtubules in AtTPX2-overexpressing cells.

To understand whether the formation of ectopic microtubules was cell cycle specific, anti-phosphohistone H3 (Ser10) antibody was used to monitor the mitotic status of the chromatin, from pre-prophase to metaphase (Fig. 7A). Cells (n > 100) with AtTPX2-decorated fibres did not show phosphohistone staining (Fig. 7B). Further proof that fibres were not formed in preparation for mitosis was provided by DAPI staining that showed diffuse interphase chromatin but not pre-mitotic condensed chromatin in cells with the TPX2-decorated microtubular arrays. The formation and arrangement of ectopic microtubular bundles was not affected by treatment with the mitotic kinase inhibitor roscovitine (Supplementary Fig. S9), which previously showed a severe effect on microtubular arrays (Binarová *et al.*, 1998). These findings suggest that ectopic nuclear and perinuclear microtubules were not formed specifically during the transition from interphase to mitosis.

AtTPX2-stabilized microtubules are not found in cells with programmed cell death.

A type of AtTPX2-stabilized microtubular array similar to that observed in these experiments is formed in mammalian

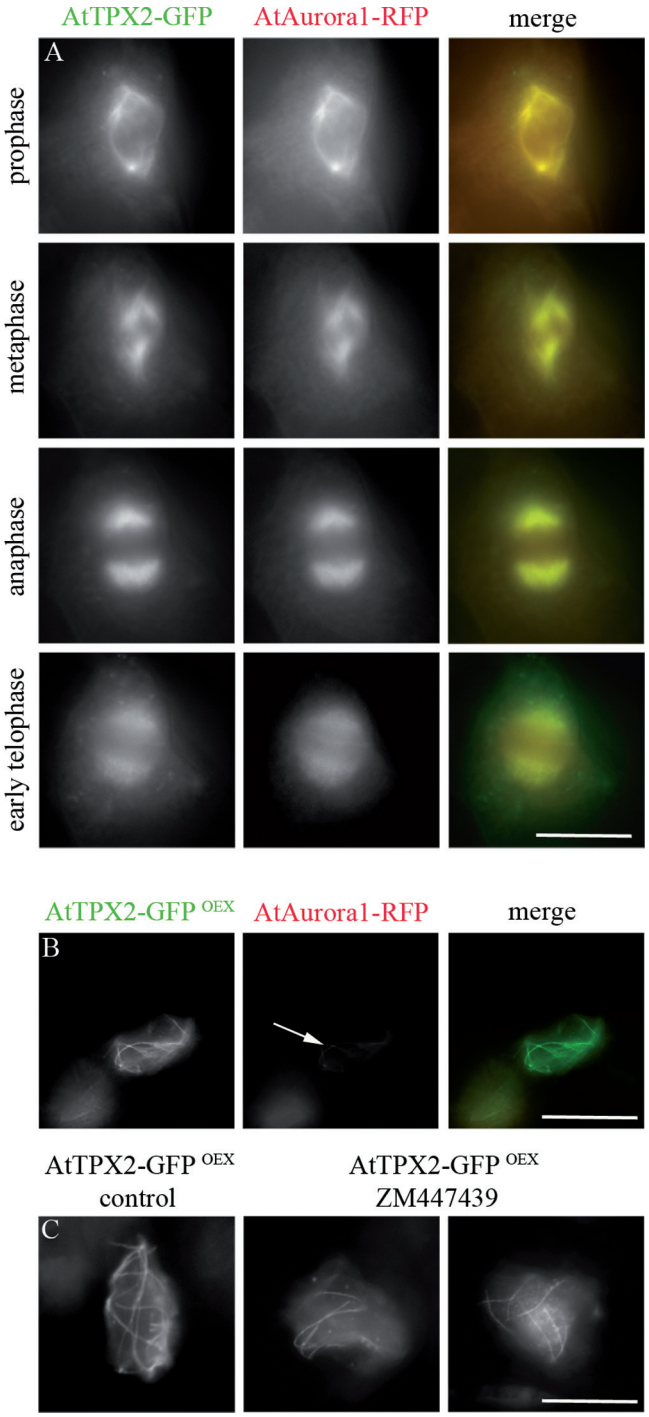

Fig. 6. Localization of AtTPX2 and AtAurora1 in control and ZM447439-treated cells overproducing AtTPX2. (A) Localization of AtTPX2-GFP and AtAurora1-RFP from the prophase until the early telophase in *Arabidopsis* cells. (B) Weak signal of AtAurora1 with AtTPX2 (arrow) in the nuclei of *Arabidopsis*. (C) AtTPX2 fibres in TPX2-overproducing cells were resistant to Aurora kinase inhibitor ZM447439 (100% of analysed cells showed resistance to ZM447439, $n = 96$). Bars, 10 µm.

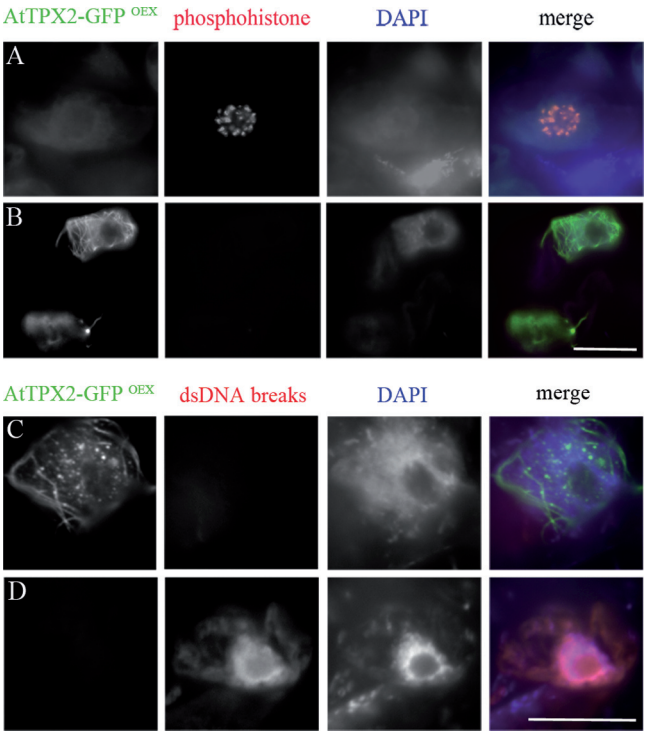

Fig. 7. Formation of AtTPX2 fibrillar structures was not dependent on mitotic status of the chromatin or connected with programmed cell death. (A, B) Immunolabelling of AtTPX2 (green) and phosphohistone (red) in prophase (A) and interphase (B) cells overexpressing AtTPX2. AtTPX2-decorated ectopic microtubules were not formed in nuclei with mitotic chromatin. (C, D) Ectopic AtTPX2-decorated microtubular arrays were not observed in cells entering programmed cell death that were positive with TUNEL labelling (red). Bars, 10 µm.

cells where it functions during apoptosis (Moss *et al.*, 2009). The current examined whether the TPX2-induced microtubules were involved in apoptosis in *Arabidopsis*. *In situ* detection of dsDNA breaks (TUNEL test) was used. The proportion of cells with TUNEL-stained nuclei was 8% in both wild-type ($n = 234$) and AtTPX2-overexpressing cells ($n = 217$). Neither AtTPX2 dots nor ectopic perinuclear or nuclear microtubules were observed in cells with TUNEL-detectable dsDNA breaks (Fig. 7C, D). To provide further evidence of programmed cell death, cell viability was analysed using Evans blue staining, which does not discriminate between apoptosis and necrosis (Danon *et al.*, 2000); however, changes in the plasma membrane recognized by Evans blue might be an early indicator of cells undergoing DNA fragmentation prior to TUNEL-detectable DNA breakage. Overexpressing cells with AtTPX2-GFP-labelled fibres were not stained with Evans blue (Supplementary Fig. S10). The formation of AtTPX2-decorated ectopic microtubules was therefore not associated with programmed cell death.

Discussion

Previous studies showed that AtTPX2 was associated with spindle microtubules and suggested a microtubular function (Vos *et al.* 2008; Petrovská *et al.*, 2012). Analysis of cells overexpressing AtTPX2 protein allowed the identification of stable microtubular arrays ectopically nucleated in the nuclei and

their periphery. Signals for overexpressed AtTPX2-GFP were initially observed in nuclear dots and patches, from which microtubules could grow and organize. Intranuclear and perinuclear AtTPX2-decorated fibrillar arrays were assembled later and formed a cage enveloping the nucleus and extending to the cell periphery.

Ran GTPase influences microtubule dynamics in mitosis by releasing spindle assembly factors from importins in the vicinity of chromatin (Joseph, 2006). There are several lines of evidence suggesting that TPX2-mediated microtubule formation observed under conditions of overproduction of AtTPX-GFP was triggered by a Ran nucleo-cytoplasmic gradient: (i) colocalization and co-immunopurification of importin with AtTPX2; (ii) accumulation of Ran and importin in the nuclei with overexpressed AtTPX2-GFP; and (iii) reduction of nuclear signals for Ran and importin that occurred simultaneously with assembly of nuclear/perinuclear microtubular arrays. Dynamic release of TPX2 from importin by Ran is active in organization of microtubules during mitosis in animals (Gruss *et al.*, 2001; Kufer *et al.*, 2002). The current data are in agreement with those on Ran GTP-dependent interaction of animal importin with recombinantly expressed plant TPX2 *in vitro* and on nucleo-cytoplasmic shuttling of the AtTPX2-GFP (Vos *et al.*, 2008). In addition to prominent nuclear and perinuclear signals for importin, the current work immunolocalized importin with TPX2-decorated ectopic microtubular arrays. While the ability of TPX2 to nucleate microtubules is abolished by binding of importin, the binding does not prevent TPX2 interaction with tubulin or with microtubules (Schatz *et al.*, 2003). The current work suggests that the importin associated with TPX2-decorated microtubules might represent the proportion of overexpressed AtTPX2 protein that was not sequestered from importin.

These data contribute to the understanding of TPX2-mediated microtubule formation in plants and suggest that the process is regulated by the Ran cycle. Most components of the Ran cycle were identified in plants and the regulatory role of Ran in cell division is, at least partially, conserved (Pay *et al.*, 2002; Jeong *et al.*, 2005). Direct visualization of the RanGTP gradient in living cells (Kalab *et al.*, 2006) has not been performed in plants. Ran FRET sensors, together with *in vivo* analysis of importin/TPX2 shuttling, are required to understand the function of the Ran cycle in microtubule formation and cell division in plants.

Microtubular nucleation in acentrosomal plants occurs from dispersed γ-tubulin-positive sites located on the nuclear envelope, in nuclei, and on pre-existing microtubules (Binarová *et al.*, 2000, 2006; Murata *et al.*, 2005; Nakamura *et al.*, 2010). The current data indicate that rearrangement from the 'seeds' through the bundled fibres might be caused by co-assembly of AtTPX2-GFP with endogenous microtubule-nucleating units, comprising γ-tubulin and TPX2 protein. A possible role of AtTPX2 with plant microtubules was indicated by previous data on colocalization of γ-tubulin with active AtAurora1/AtTPX2 on mitotic microtubular arrays (Petrovská *et al.*, 2012). Recently, it has been shown *in vitro* in *Xenopus* extracts that nucleation of branched microtubules from pre-existing microtubules requires γ-tubulin, TPX2, and augmins (Petry *et al.*, 2013). Colocalization of γ-tubulin with overexpressed AtTPX2 observed in the current work, indicating that a similar mechanism functions in TPX2-mediated formation of microtubular arrays. However, no association of γ-tubulin with immunopurified AtTPX2-GFP could be demonstrated. The low stability of plant TPX2 in extracts (Vos *et al.*, 2008; Petrovská *et al.*, 2012) might also influence the efficiency of immunopurification protocols. Furthermore, as was shown by co-immunoprecipitation by Petry *et al.* (2013), γ-tubulin is only a minor interactor with TPX2 protein. Further experiments are needed to demonstrate γ-tubulin interaction with TPX2 and to show how TPX2 cooperates with nucleation machinery in plant cells.

Similarly to animal homologues, plant TPX2 belongs to the group of cell cycle-regulated molecules that accumulate in the nuclei at the G2 phase of the cell cycle and are degraded at anaphase-telophase (Vos *et al.*, 2008). The current work found that AtTPX2-mediated microtubule formation did not require a mitotic status of chromatin, and thus is not reminiscence of Ran GTPase-dependent chromatin-mediated spindle formation in *Xenopus* extracts (Heald *et al.*, 1996). Furthermore, formation of TPX2-mediated fibres was not dependent on the binding of Aurora kinase to AtTPX2 and correspondingly was not sensitive to Aurora kinase inhibition. These data suggest that the tight tuning that depends on the cell cycle and Aurora kinase signalling to TPX2 is missing during formation of the ectopic microtubular arrays and is overdominated by AtTPX2 in microtubule nucleation and stabilization.

The TPX2-mediated microtubule nucleation pathway, regulated by Ran, is responsible for the assembly of specific acentrosomal microtubular arrays in apoptotic HeLa cells (Moss *et al.*, 2009). The TPX2-stabilized microtubular arrays functioning in apoptosis strongly resemble the stable AtTPX2-mediated microtubular arrays that was observed in plants. However, the arrays were not found in cells undergoing programmed cell death (TUNEL-positive cells) or in Evans blue-stained cells. As shown by Moss *et al.* (2009), TPX2-dependent microtubular arrays function in fragmentation of the HeLa cells nuclei during late apoptosis. While the molecular mechanisms of early apoptosis in plant and animal cells are more similar than was previously thought, the execution phase of the process differs. Electron microscopy of root initials in *Arabidopsis* showed that death of the stem cells did not show apoptotic features such as peripheral chromatin condensation and nuclear fragmentation (Fulcher and Sablowski, 2009). The TPX2-mediated formation of microtubular arrays is exploited by animal and plant cells alike, but the function of these acentrosomal microtubular arrays may reflect specific needs of the organism and cell type.

The *in silico* analysis of AtTPX2 showed the presence of a coiled-coil domain, specific motifs, interaction sites, and predicted subnuclear localization. In metazoans, coiled-coil proteins group as various cytoskeletal networks comprising intermediate filament proteins, actin-binding proteins, and microtubule-associated proteins (Burkhard *et al.*, 2001; Korolev *et al.*, 2005). Albeit several proteins closely related to the intermediate filament protein were identified *in silico* (Gardiner *et al.*, 2011), knowledge of plant coiled-coil

proteins is limited. The current work found that overproduced AtTPX2 accumulated in interphase nuclei and observed TPX2-dependent fibrillar arrays interconnecting nuclei with the nuclear periphery. A role for RanGTP in forming a lamin B spindle matrix has been reported (Tsai *et al.*, 2006) and TPX2 was shown to be required for post-mitotic nuclear envelope assembly (O'Brien and Wiese, 2006). The current study can only speculate as to whether AtTPX2 connects as-yet undefined plant cell lamina with the cytoskeleton and plays a role during interphase as a component of a plant alternative to the LINC (linker of nucleoskeleton and cytoskeleton) complex (Crisp *et al.*, 2006; Tzur *et al.*, 2006).

In summary, the overexpression of AtTPX2-GFP resulted in the formation of chromatin- and nuclei-associated microtubular arrays. The assembly of TPX2-decorated fibres was dependent on neither the mitotic status of chromatin nor the binding of Aurora kinase. The arrays were not specific to apoptotic cells. This study suggests that AtTPX2 overexpression amplified an ability of the nuclear envelope and chromatin to promote microtubule nucleation that is typical for acentrosomal plant cells. Furthermore, these findings indicate an involvement of the Ran pathway in modulation of the process.

Supplementary material

Supplementary data are available at *JXB* online.

Supplementary Table S1. *In silico* analyses of AtTPX2 protein.

Supplementary Fig. S1. Immunolocalization of AtTPX2 and actin in cell cultures of *Arabidopsis thaliana.*

Supplementary Fig. S2. AtTPX2-decorated fibres are resistant to taxol in cell cultures of *Arabidopsis thaliana.*

Supplementary Fig. S3. Immunofluorescence localization of Ran in AtTPX2-GFP-overproducing cells.

Supplementary Fig. S4. Importin copurified with AtTPX2-GFP from *Arabidopsis* cultured cells.

Supplementary Fig. S5. Colocalization analyses of AtTPX2 and importin in *Arabidopsis* cultured cells.

Supplementary Fig. S6. AtAurora1-RFP copurifies with AtTPX2-GFP from *Arabidopsis* cultured cells.

Supplementary Fig. S7. Overexpression of AtTPX2 and ΔN-AtTPX2 in *Arabidopsis* nuclei.

Supplementary Fig. S8. Treatment of mitotic microtubules with Aurora kinase inhibitor ZM447439 in cell cultures of *Arabidopsis thaliana.*

Supplementary Fig. S9. Ectopic nuclear microtubular bundles were not affected by roscovitine treatment in cell cultures of *Arabidopsis thaliana.*

Supplementary Fig. S10. Evans blue viability test in *Arabidopsis* cell cultures with overproduced AtTPX2.

Acknowledgements

This work was supported by the Grant Agency of the Czech Republic (P501/12/2333, P501/12/G090, 204/09/P155, 204/07/1169), the Centre of the Region Haná for Biotechnological and Agricultural Research (CZ.1.05/2.1.00/01.0007 to BP, HJ, MK, and ET), the Operational Program Education for Competitiveness—European Social Fund (CZ.1.07/2.3.00/20.0165 to BP), and the Internal Grant Agency UP (Prf/2013/003 to HJ and ET). The authors thank Dr Roger Y. Tsien (Howard Hughes Medical Institute and Department of Pharmacology, San Diego, CA, USA) for mRFP.

References

Berger B, Wilson DB, Wolf E, Tonchev T, Milla M, Kim PS. 1995. Predicting coiled coils by use of pairwise residue correlations. *Proceedings of the National Academy of Sciences, USA* **92,** 8259–8263.

Binarová P, Cenklová V, Hause B, Kubátová E, Lysák M, Doležel J, Bögre L, Dráber, P. 2000. Nuclear gamma-tubulin during acentriolar plant mitosis. *The Plant Cell* **12,** 433–442.

Binarová P, Cenklová V, Procházkova J, Doskočilová A, Volc J, Vrlík M, Bögre L. 2006. γ-Tubulin is essential for acentrosomal microtubule nucleation and coordination of late mitotic events in *Arabidopsis*. *The Plant Cell* **18,** 1199–1212.

Binarová P, Číhalíková J, Doležel J. 1993. Localization of MPM-2 recognized phosphoproteins and tubulin during cell cycle progression in synchronized *Vicia faba* root meristem cells. *Cell Biology International* **17,** 847–856.

Binarová P, Doležel J, Dráber P, Heberle-Bors E, Strnad M, Bögre L. 1998. Treatment of *Vicia faba* root tip cells with specific inhibitors to cyclin-dependent kinases leads to abnormal spindle formation. *The Plant Journal* **16,** 697–707.

Bolte S, Cordeliéres FP. 2006. A guided tour into subcellular colocalization analysis in light microscopy. *Journal of Microscopy* **224,** 213–232.

Burkhard P, Stetefeld J, Strelkov SV. 2001. Coiled coils: a highly versatile protein folding motif. *Trends in Cell Biology* **11,** 82–88.

Bustin SA, Benes V, Garson JA *et al.* 2009. The MIQE Guidelines: minimum information for publication of quantitative real-time PCR experiments. *Clinical Chemistry* **55,** 611–622.

Clough SJ, Bent AF. 1998. Floral-dip: a simplified method for *Agrobacterium*-mediated transformation of *Arabidopsis thaliana*. *The Plant Journal* **16,** 735–743.

Crisp M, Liu Q, Roux K, Rattner JB, Shanahan C, Burke B, Stahl PD, Hodzic D. 2006. Coupling of the nucleus and cytoplasm: role of the LINC complex. *Journal of Cell Biology* **172,** 41–53.

Curtis M, Grossniklaus U. 2003. A Gateway cloning vector set for high throughput functional analysis of genes in plants. *Plant Physiology* **133,** 462–469.

Czechowski T, Stitt M, Altmann T, Udvardi MK, Scheible WR. 2005. Genome wide identification and testing of superior reference genes for transcript normalization in *Arabidopsis*. *Plant Physiology* **139,** 5–17.

Danon A, Delorme V, Mailhac N, Gallois P. 2000. Plant programmed cell death: a common way to die. *Plant Physiology and Biochemistry* **38,** 647–655.

Ditchfield C, Johnson VL, Tighe A, Ellston R, Haworth C, Johnson T, Mortlock A, Keen N, Taylor SS. 2003. Aurora B

couples chromosome alignment with anaphase by targeting BubR1, Mad2, and CENP-E to kinetochores. *Journal of Cell Biology* **161,** 267–280.

Dinkel H, Michael S, Weatheritt RJ, *et al.* 2012. ELM—the database of eukaryotic linear motifs. *Nucleic Acids Research* **40,** 242–251.

Dryková D, Cenklová V, Sulimenko V, Volc J, Dráber P, Binarová P. 2003. Plant γ-tubulin interacts with αβ-tubulin dimers and forms membrane associated complexes. *The Plant Cell* **15,** 465–480.

Evrard JL, Pieuchot L, Vos JW, Vernos I, Schmit AC. 2009. Plant TPX2 and related proteins. *Plant Signaling and Behavior* **4,** 69–72.

Eyers PA, Erikson E, Chen LG, Maller JL. 2003. A novel mechanism for activation of the protein kinase Aurora A. *Current Biology* **13,** 691–697.

Fulcher N, Sablowski R. 2009. Hypersensitivity to DNA damage in plant stem cell niches. *PNAS* **106,** 20984–20988.

Gardiner J, Overall R, Marc J. 2011. Putative *Arabidopsis* homologues of metazoan coiled-coil cytoskeletal proteins. *Cell Biology International* **35,** 767–774.

Groen AC, Cameron LA, Coughlin M, Miyamoto DT, Mitchison TJ, Ohi R. 2004. XRHAMM functions in Ran-dependent microtubule nucleation and pole formation during anastral spindle assembly. *Current Biology* **14,** 1801–1811.

Gruss OJ, Carazo-Salas RE, Schatz CA, Guarguaglini G, Kast J, Wilm M, Le Bot N, Vernos I, Karsenti E, Mattaj IW. 2001. Ran induces spindle assembly by reversing the inhibitory effect of importin α on TPX2 activity. *Cell* **104,** 83–93.

Hamada T. 2007. Microtubule-associated proteins in higher plants. *Journal of Plant Research* **120,** 79–98.

Heald R, Tournebize R, Blank T, Sandaltzopoulos R, Becker P, Hyman A, Karsenti E. 1996. Self-organization of microtubules into bipolar spindles around artificial chromosomes in *Xenopus* egg extracts. *Nature* **382,** 420–425.

Hong-Bin S, Kuo-Chen C. 2007. Nuc-PLoc: a new web-server for predicting protein subnuclear localization by fusing PseAA composition and PsePSSM. *Protein Engineering, Design, and Selection* **20,** 561–567.

Iyer J, Tsai MY. 2012. A novel role for TPX2 as a scaffold and co-activator protein of the chromosomal passenger complex. *Cellular Signalling* **24,** 1677–1689.

Jeong SY, Rose A, Joseph J, Dasso M, Meier I. 2005. Plant-specific mitotic targeting of RanGAP requires a functional WPP domain. *The Plant Journal* **42,** 270–282.

Joseph, J. 2006. Ran at a glance. *Journal of Cell Science* **119,** 3481–3484.

Kahana JA, Cleveland DW. 2001. Some importin news about spindle assembly. *Science* **291,** 1718–1719.

Kalab P, Pralle A, Isacoff EY, Heald R, Weis K. 2006. Analysis of a RanGTP-regulated gradient in mitotic somatic cells. *Nature* **440,** 697–701.

Karimi M, Inze D, Depicker A. 2002. GATEWAY vectors for *Agrobacterium* mediated plant transformation. *Trends in Plant Science* **7,** 193–195.

Korolev AV, Chan J, Naldrett MJ, Doonan JH, Lloyd CW. 2005. Identification of a novel family of 70 kDa microtubule-associated proteins in *Arabidopsis* cells. *The Plant Journal* **42,** 547–555.

Koroleva OA, Tomlinson ML, Leader D, Shaw P, Doonan JH. 2005. High-throughput protein localization in *Arabidopsis* using *Agrobacterium*-mediated transient expression of GFP-ORF fusions. *The Plant Journal* **41,** 162–74.

Kufer TA, Silljé HHW, Körner R, Gruss OJ, Meraldi P, Nigg EA. 2002. Human TPX2 is required for targeting Aurora-A kinase to the spindle. *Journal of Cell Biology* **158,** 617–623.

Lei Z, Dai Y. 2005. An SVM-based system for predicting protein subnuclear localizations. *BMC Bioinformatics* **6,** 291.

Lei Z, Dai Y. 2006. Assessing protein similarity with Gene Ontology and its use in subnuclear localization prediction. *BMC Bioinformatics* **7,** 491.

Lupas A, Van Dyke M, Stock J. 1991. Predicting coiled coils from protein sequences. *Science* **252,** 1162–1164.

Marumoto T, Zhang D, Saya H. 2005. Aurora-A: a guardian of poles. *Nature Reviews Cancer* **5,** 42–50.

Mathur J, Szabados L, Schaefer S, Grunenberg B, Lossow A, Jonas-Straube E, Schell J, Koncz C, Koncz-Kálmán Z. 1998. Gene identification with sequenced T-DNA tags generated by transformation of *Arabidopsis* cell suspension. *The Plant Journal* **13,** 707–716.

Moss DK, Wilde A, Lane JD. 2009. Dynamic release of nuclear RanGTP triggers TPX2-dependent microtubule assembly during the apoptotic execution phase. *Journal of Cell Science* **122,** 644–655.

Murata T, Sonobe S, Baskin TI, Hyodo S, Hasezawa S, Nagata T, Horio T, Hasebe M. 2005. Microtubule-dependent microtubule nucleation based on recruitment of gamma-tubulin in higher plants. *Nature Cell Biology* **7,** 961–968.

Nachury MV, Maresca TJ, Salmon WC, Waterman-Storer CM, Heald R, Weis K. 2001. Importin beta is a mitotic target of the small GTPase Ran in spindle assembly. *Cell* **104,** 95–106.

Nakamura M, Ehrhardt DW, Hashimoto T. 2010. Microtubule and katanin-dependent dynamics of microtubule nucleation complexes in the acentrosomal *Arabidopsis* cortical array. *Nature Cell Biology* **12,** 1064–1070.

O'Brien LL, Wiese C. 2006. TPX2 is required for post-mitotic nuclear assembly in cell-free *Xenopus laevis* egg extract. *Journal of Cell Biology* **173,** 685–694.

Panteris E, Adamakis IDS. 2012. Aberrant microtubule organization in dividing root cells of p60-katanin mutants. *Plant Signaling and Behavior* **7,** 1–3.

Pay A, Resch K, Frohnmeyer H, Fejes E, Nagy F, Nick P. 2002. Plant RanGAPs are localized at the nuclear envelope in interphase and associated with microtubules in mitotic cells. *The Plant Journal* **30,** 699–709.

Pederson T, Aebi U. 2002. Actin in the nucleus: what form and what for? *Journal of Structural Biology* **140,** 3–9.

Petrovská B, Cenklová V, Pochylová Ž, Kourová H, Doskočilová A, Plíhal O, Binarová L, Binarová P. 2012. Plant Aurora kinases play a role in maintenance of primary meristems and control of endoreduplication. *New Phytologist* **193,** 590–604.

Petry S, Groen AC, Ishihara K, Mitchison TJ, Vale RD. 2013. Branching microtubule nucleation in *Xenopus* egg extracts mediated by Augmin and TPX2. *Cell* **152,** 768–777.

Planchais S, Glab N, Tréhin C, Perennes C, Bureau JM, Meijer L, Bergounioux C. 1997. Roscovitine, a novel cyclin-dependent kinase inhibitor, characterizes restriction point and G2/M transition in tobacco BY-2 cell suspension. *The Plant Journal* **12,** 191–202.

Punta M, Coggill PC, Eberhardt RY, *et al.* 2012. The Pfam protein families database. *Nucleic Acids Research* **40,** D290–D301.

Ren J, Gao X, Jin C, Zhu M, Wang X, Shaw A, Wen L, Yao X, Xue Y. 2009. Systematic study of protein sumoylation: development of a site-specific predictor of SUMOsp 2.0. *Proteomics* **9,** 3409–3412.

Schatz CA, Santarella R, Hoenger A, Karsenti E, Mattaj IW, Gruss OJ, Carazo-Salas RE. 2003. Importin α-regulated nucleation of microtubules by TPX2. *The EMBO Journal* **22,** 2060–2070.

Sedbrook JC, Kaloriti D. 2008. Microtubules, MAPs and plant directional cell expansion. *Trends in Plant Science* **13,** 303–310.

Tsai M-Y, Wang S, Heidinger JM, Shumaker DK, Adam SA, Goldman RD, Zheng X. 2006. A mitotic lamin B matrix induced by RanGTP required for spindle assembly. *Science* **311,** 1887–1893.

Tsai MY, Zheng Y. 2005. Aurora A kinase-coated beads function as microtubule-organizing centers and enhance RanGTP-induced spindle assembly. *Current Biology* **15,** 2156–2163.

Tzur YB, Wilson KL, Gruenbaum Y. 2006. SUN-domain proteins: 'Velcro' that links the nucleoskeleton to the cytoskeleton. *Nature Reviews Molecular Cell Biology* **7,** 782–788.

Uchiyama S, Kobayashi S, Takata H, *et al.* 2005. Proteome analysis of human metaphase chromosomes. *The Journal of Biological Chemistry* **280,** 16994–17004.

Vos JW, Pieuchot L, Evrard JL, Janski N, Bergdoll M, De Ronde D, Perez LH, Sardon T, Vernos I, Schmit AC. 2008. The plant TPX2 protein regulates prospindle assembly before nuclear envelope breakdown. *The Plant Cell* **20,** 2783–2797.

Weingartner M, Binarová P, Dryková D, Schweighofer A, David JP, Heberle-Bors E, Doonan J, Bögre L. 2001. Dynamic recruitment of Cdc2 to specific microtubule structures during mitosis. *The Plant Cell* **13,** 1929–1943.

Wiese C, Wilde A, Moore MS, Adam SA, Merdes A, Zheng Y. 2001. Role of importin-β in coupling Ran to downstream targets in microtubule assembly. *Science* **291,** 653–656.

Wilde A, Zheng Y. 1999. Stimulation of microtubule aster formation and spindle assembly by the small GTPase Ran. *Science* **284,** 1359–1362.

Wittmann T, Boleti H, Antony C, Karsenti E, Vernos I. 1998. Localization of the kinesin-like protein Xklp2 to spindle poles requires a leucine zipper, a microtubule-associated protein, and dynein. *Journal of Cell Biology* **143,** 673–685.

Wolf E, Kim PS, Berger B. 1997. MultiCoil: a program for predicting two and three-stranded coiled coils. *Protein Science* **6,** 1179–1189.

Xao X, Xue Y. 2009. DOG 1.0: illustrator of protein domain structures. *Cell Research* **19,** 271–273.

7.3.1 Supplementary data

Petrovská, B.[#], Jeřábková, H.[#], Kohoutová, L.[#], Cenklová, V., Pochylová Z., Gelová, Z., Kočárová, G., Váchová, L., Kurejová, M., Tomaštíková, E., and Binarová, P.; (2013) Overexpressed TPX2 causes ectopic formation of microtubular arrays in the nuclei of acentrosomal plant cells. J Exp Bot, 64(14):4575-87

[#]These authors contributed equally to this article.

Journal of Experimental Botany

Overexpressed TPX2 causes ectopic formation of microtubular arrays in the nuclei of acentrosomal plant cells.

Beáta Petrovská, Hana Jeřábková, Lucie Kohoutová, Věra Cenklová, Žaneta Pochylová, Zuzana Gelová, Gabriela Kočárová, Lenka Váchová, Michaela Kurejová, Eva Tomaštíková, and Pavla Binarová

Supplementary Table S1. *In silico* analyses of AtTPX2 protein.

Name	Positions (aa)	Description
Domains:		
TPX2_importin	313-487	domain pfam: PF12214
TPX2	649-705	domain pfam: PF06886
Coiled-coil	588-619	domain
Motifs:		
Aurora	20-29, 43-51	Aurora binding sites
MTs	220-463, 684-758	Microtubule binding sites
NES	499-507	nuclear export signal
NLS	228-236, 610-758	nuclear localization signals
KEN box	148-152, 275-279, 667-671	APCC binding destruction motifs
D box	327-645	APCC binding destruction motif
Cyclin	305-309, 332-336, 516-519	cyclin recognition sites
FHA	12-18,141-147, 218-224, 291-297, 373-379, 396-402, 437-443, 581-587	FHA phosphopeptide ligands
MAD2	361-369	binding motif
MAPK	41-47, 492-502, 538-546, 723-731	MAPK (Mitogen-activated protein kinase) docking motifs
ProDKin	53-59, 154-160, 271-277, 372-378, 419-425, 723-729	MAPK phosphorylation sites
TRFH	264-268	TRFH docking motif
USP7	5-9, 55-59, 95-99, 200-204, 289-293, 371-375, 396-400, 714-718, 748-752	USP7 binding motifs (deubiquitinating enzyme)
HP1	95-99	HP1 ligand (interact with the chromoshadow domain of Heterochromatin-binding protein 1)
WW_Pin1	53-58, 154-259, 271-276, 372-377, 723-728	WW domain ligands
14-3-3	180-186, 312-318, 395-400	14-3-3 ligands (interacts with specific phosphoserine and phosphothreonine containing motifs)
COP1	628-635	COP1 binding motif (Constitutive photomorphogenesis protein)
EH1	524-528	EH ligand (endocytotic processes)
IQ	294-312	Calmodulin binding IQ motif

Name	Positions (aa)	Description
Motifs:		
SUMO	68-71, 94-98, 208-211, 497-502, 529-532, 575-578	SUMO binding sites
TRAF2	4-7, 79-82	TRAF2 binding sites
CK1	8-14, 49-55, 98-107, 139-145, 400-406, 507-513, 747-753	CK1 phosphorylation sites (for Ser/Thr phosphorylation)
CK2	1-7, 33-39, 271-277, 289-295, 335-341, 435-441, 462-468, 491-497, 509-515, 580-586	CK2 phosphorylation sites (for Ser/Thr phosphorylation)
GSK3	1-8, 7-14, 8-15, 33-40, 49-56, 111-118, 115-122, 119-126, 132-139, 136-143, 200-207, 396-403, 395-404, 415-422, 431-438, 491-498, 714-721, 719-726, 732-739, 744-751	GSK3 phosphorylation recognition sites (for Ser/Thr phosphorylation)
N-GLC	132-137, 195-200	N-glycosylation sites
PIKK	98-104, 101-107, 195-201, 325-331, 580-586	PIKK phosphorylation sites
PKA	64-70, 122-128, 431-437, 491-497, 519-525, 694-700, 736-742, 742-748	PKA phosphorylation sites
PKB	674-682	PKB phosphorylation site
PLK	1-7, 5-11, 80-86	Site phosphorylated by the Polo-like-kinase
ENDOCYTIC	21-24, 543-546, 548-551, 570-573	Y-based sorting signals
ER	330-333, 429-432, 430-433	For ER localization

To predict putative interaction sites and binding motifs Pfam (Punta *et al*., 2012), ELM (Dinkel *et al*., 2012) and SUMOsp 2.0 (Ren et al., 2009) databases were used.

Supplementary Figure S1. Immunolocalization of AtTPX2 and actin in cell cultures of *Arabidopsis thaliana*

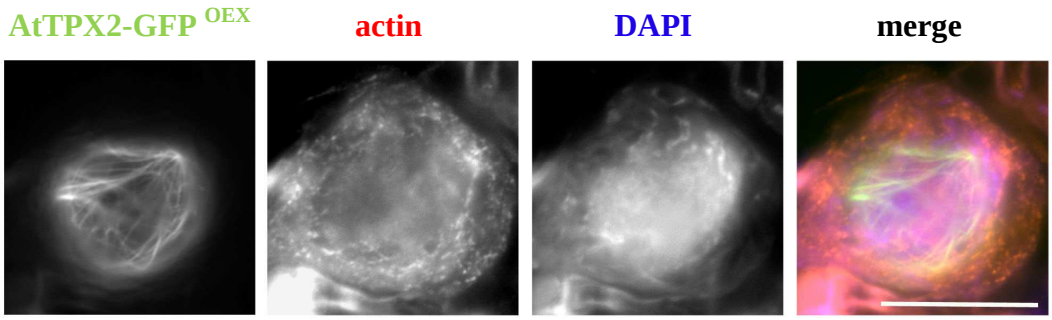

AtTPX2 fibres were not positive for actin immunolabelling. Bar: 10 µm.

Supplementary Figure S2. AtTPX2 decorated fibres were resistant to taxol in cell cultures of *Arabidopsis thaliana*

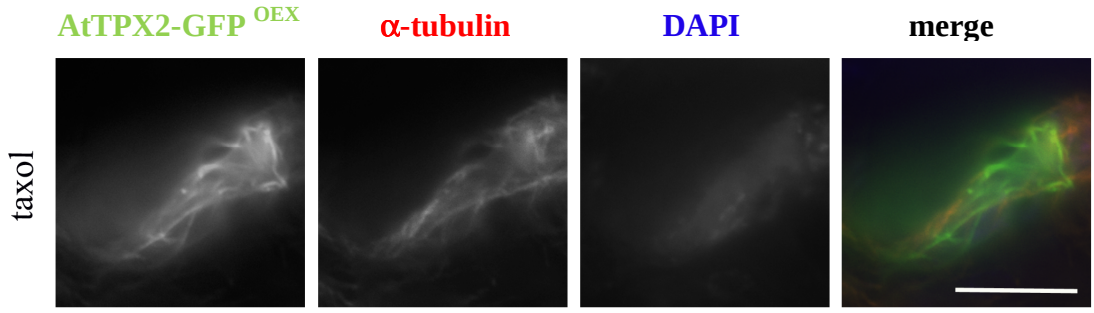

Further bundling of AtTPX2 decorated microtubules was not observed after treatment with 5 µM taxol for 3 hours. Bar: 10 µm.

Supplementary Figure S3. Immunofluorescence localization of Ran in AtTPX2-GFP overproducing cells.

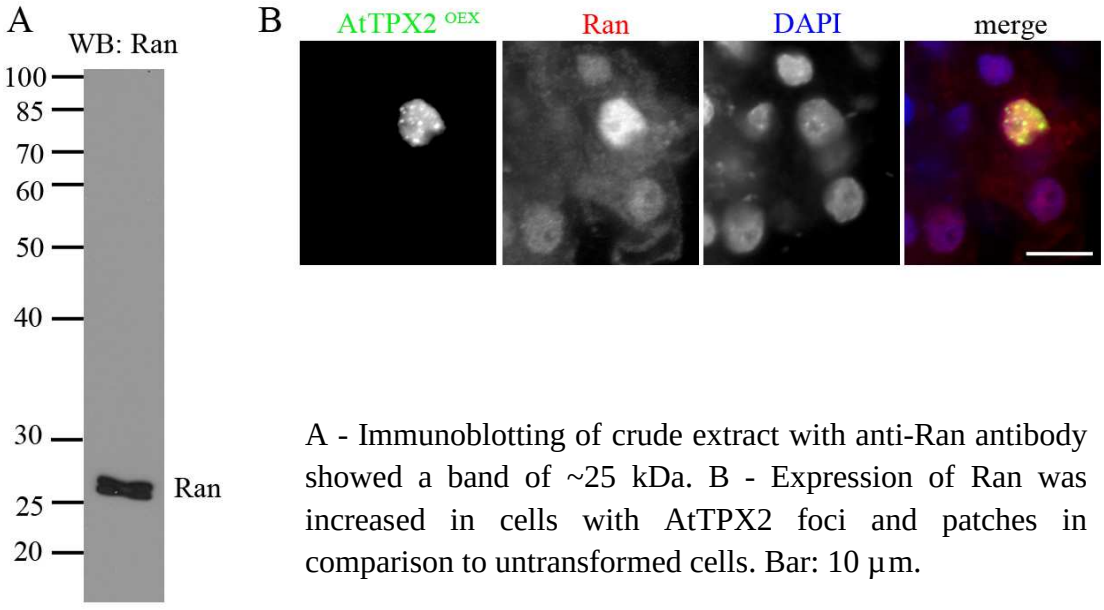

A - Immunoblotting of crude extract with anti-Ran antibody showed a band of ~25 kDa. B - Expression of Ran was increased in cells with AtTPX2 foci and patches in comparison to untransformed cells. Bar: 10 µm.

Supplementary Figure S4. Importin copurified with AtTPX2-GFP from *Arabidopsis* cultured cells.

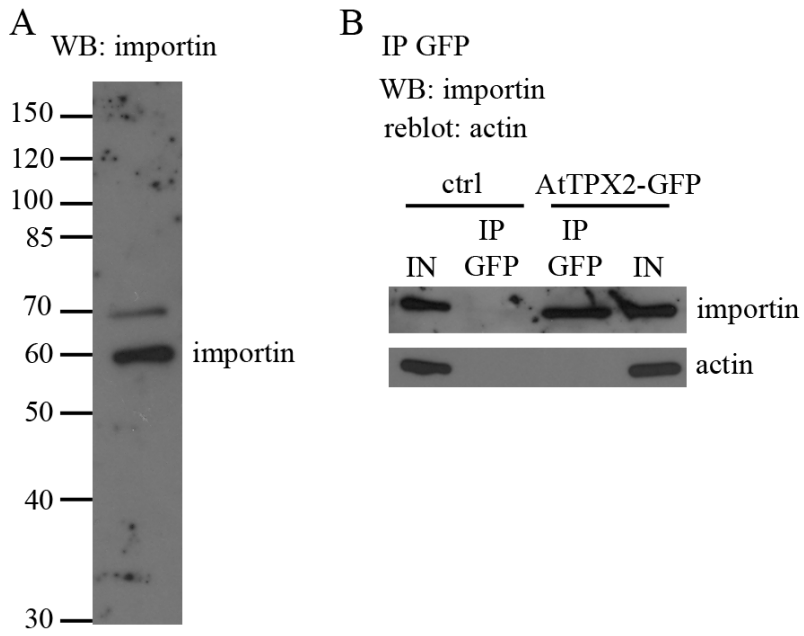

A - Immunoblotting of crude extract with anti-importin antibody showed a band of ~60 kDa. B - Immunoblotting with anti-importin antibody showed that importin was copurified with AtTPX2-GFP using GFP trap (IP GFP) from extract prepared from cell culture expressing AtTPX2-GFP. Untransformed wild type cell culture Ler was used as a negative control for GFP immunopurification. Immunoblotting with irrelevant antibody anti-actin was used as a second negative control.

Supplementary Figure S5. Colocalization analyses of AtTPX2 and importin in *Arabidopsis* cultured cells.

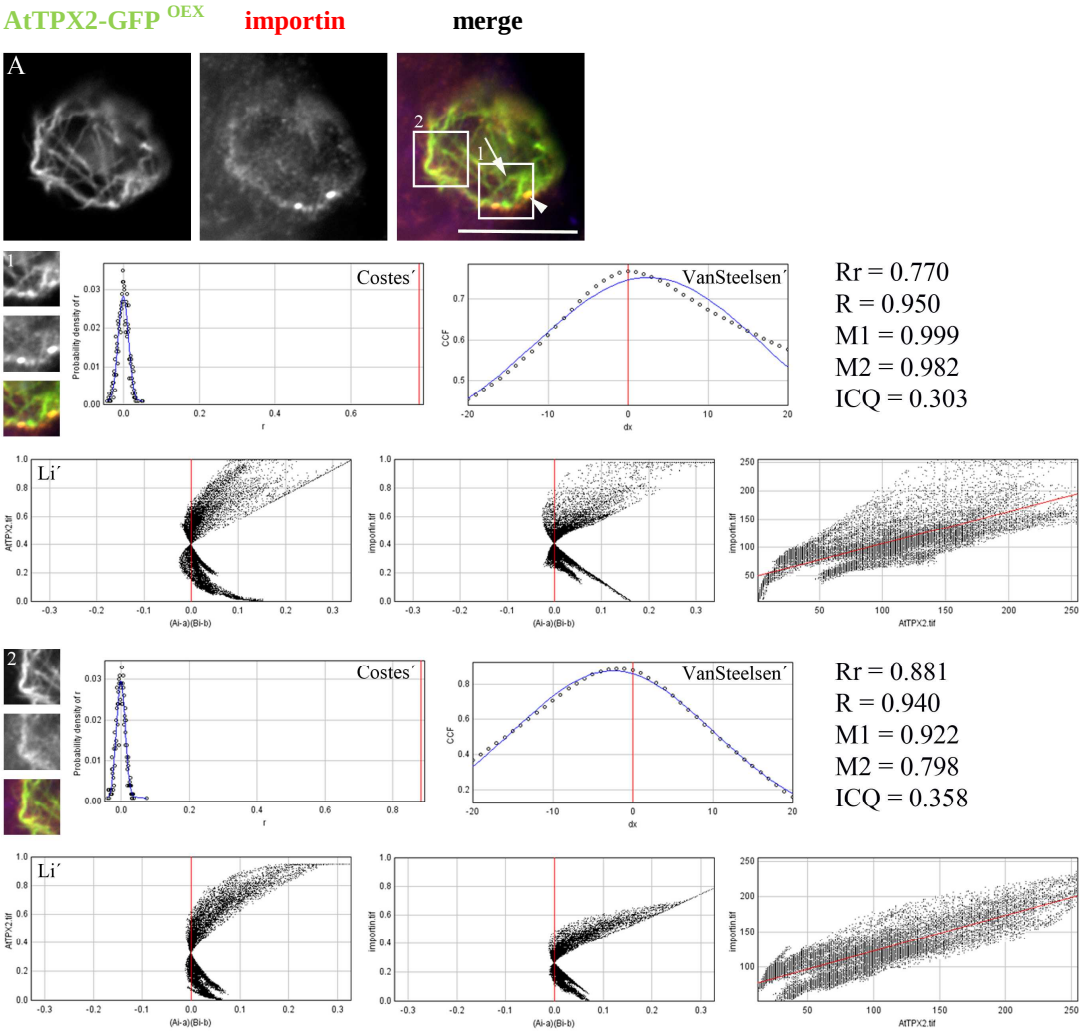

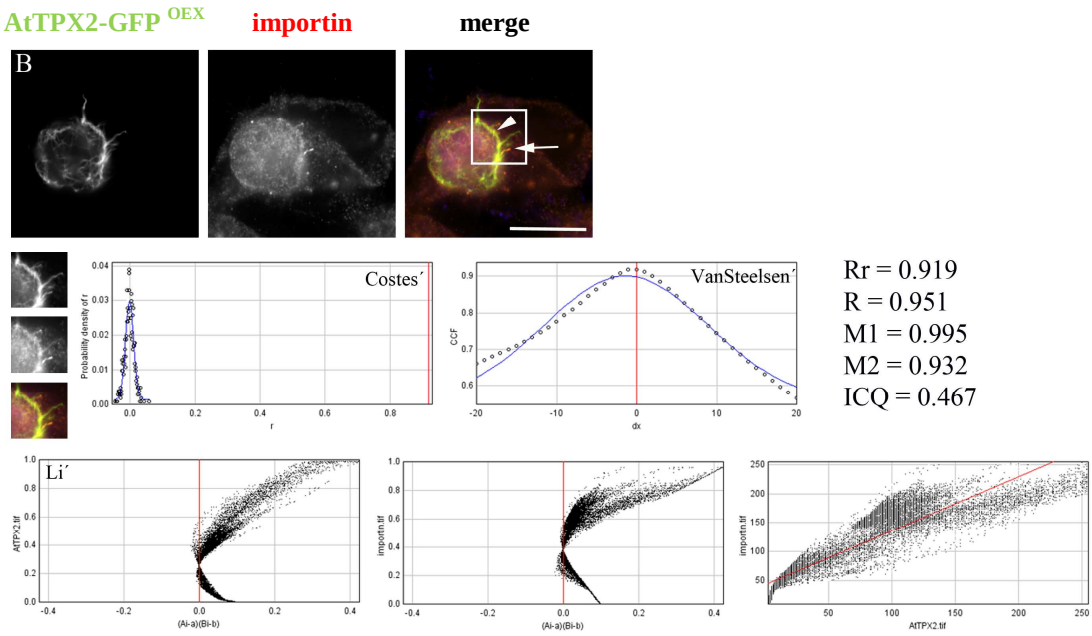

AtTPX2-GFP decorated fibres were present in close vicinity to the importin decorated nuclear envelope (A, B, arrowhead). Importin was present with AtTPX2 in dots on the nuclear envelope (A, B, arrowhead) and in the fibres (A, B, arrows). Pearson´s correlation coefficients (Rr) in Figure S8A (insets 1, 2) and S8B (0.770, 0.881, and 0.919, respectively) demonstrated colocalization of AtTPX2 and importin on the nuclear envelope and in the fibres in plant nuclei. However, Pearson´s coefficient in Figure S8A, inset 1 seemed to be complete colocalization with different intensities. The results of the Pearson´s correlation coefficient were confirmed with Manders´ coefficient (M1, M2). Figure S8 showed the completely colocalizing structure peak at the dx = 0 and bell-shaped curve. However, a difference in fluorescence intensity led to the reduction of the height of the bell-shaped curve, whereas the peak was still at dx = 0 (B). Non-colocalizing pixels in the Li´s approach are shown on the left side of the plots. The quantitative colocalization analyses of AtTPX2 and importin showed high degree of colocalization especially on the nuclear envelope. Colocalization analyses of AtTPX2 and importin was performed with ImageJ plugin JACoP (Bolte and Cordeliéres, 2006). Bars: 10 µm.

Supplementary Figure S6. AtAurora1-RFP copurified with AtTPX2-GFP from *Arabidopsis* cultured cells.

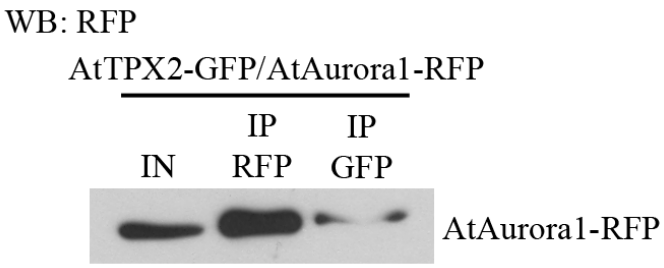

Immunoblotting with anti-RFP antibody showed that AtAurora1-RFP was copurified with AtTPX2-GFP using GFP trap (IP GFP) from extract prepared from cell culture co-expressing AtAurora1-RFP and AtTPX2-GFP. AtAurora1-RFP was purified by RFP trap (IP RFP).

Supplementary Figure S7. Overexpression of AtTPX2 and ΔN-AtTPX2 in *Arabidopsis* nuclei

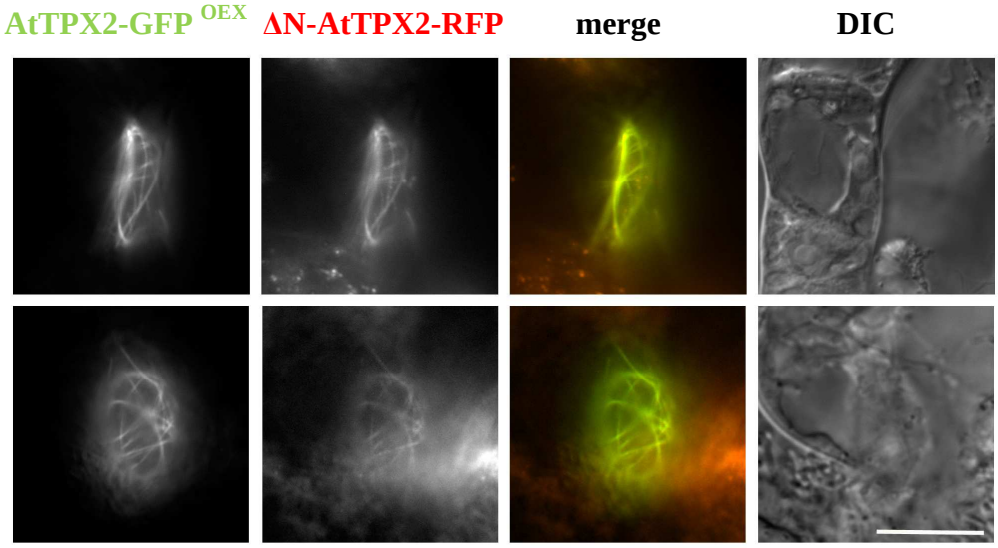

AtTPX2-GFP and its truncated version ΔN-AtTPX2-RFP localized together on microtubular array in the *Arabidopsis* nuclei. Bar: 10 µm.

Supplementary Figure S8. Treatment of mitotic microtubules with Aurora kinase inhibitor ZM447439 in cell cultures of *Arabidopsis thaliana*

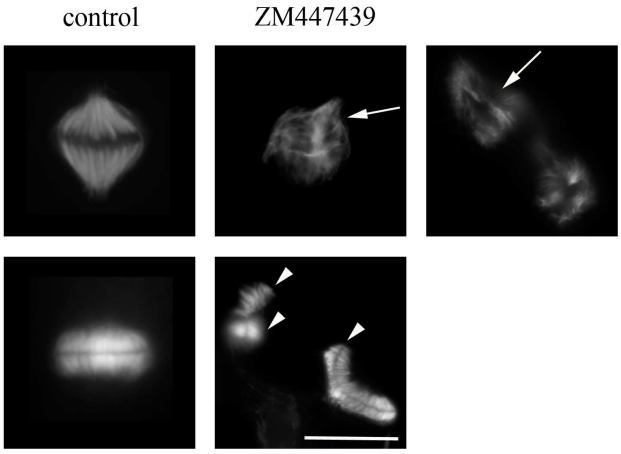

Microtubular arrays in the control (wild type) cells were affected after to the Aurora kinase inhibitor ZM447439 treatment. Multipolar mitotic spindle (arrows), fragmented phragmoplast (arrowheads) were often observed. Bar: 10 µm.

Supplementary Figure S9. Ectopic nuclear microtubular bundles were not affected by Roscovitine treatment in cell cultures of *Arabidopsis thaliana*

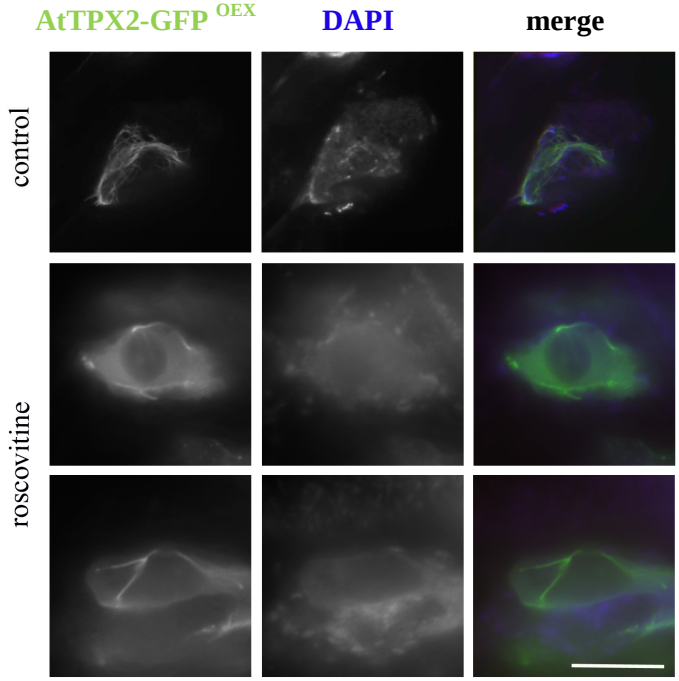

Formation of AtTPX2 decorated microtubular fibres was not affected with 100 µM Roscovitine, a cyclin dependent kinases inhibitor for 2.5 hours. Bar = 10 µm.

Supplementary Figure S10. Evans Blue viability test in *Arabidopsis* cell cultures with overproduced AtTPX2.

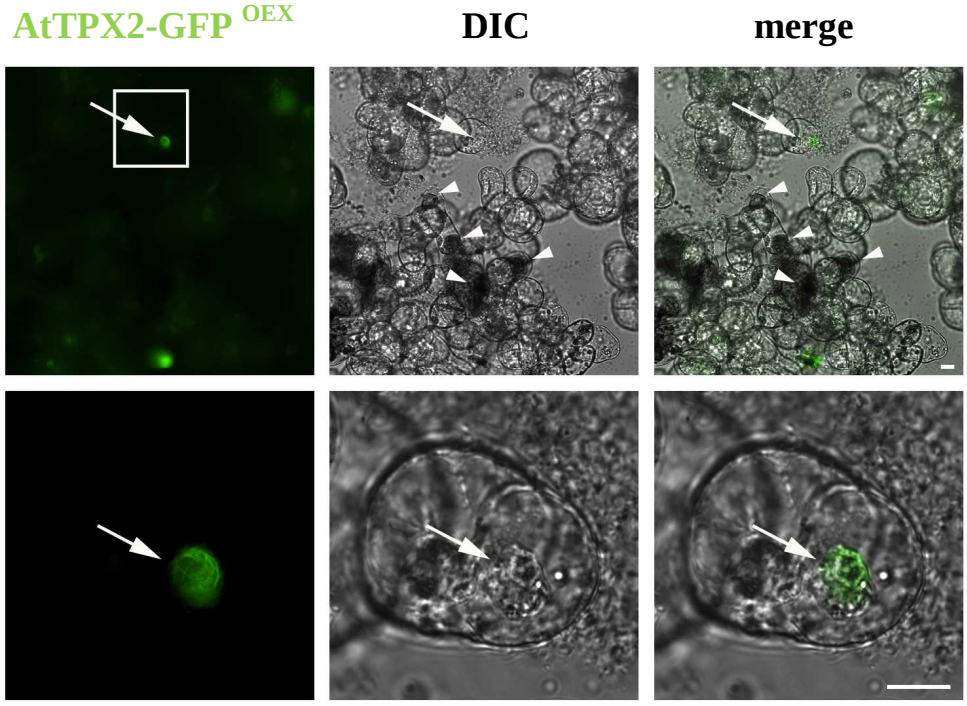

Evans Blue did not stain viable *Arabidopsis* cells with AtTPX2-GFP decorated fibres (arrows; n=68). Arrowheads showed death cells (dark grey colour). n = total number of AtTPX2-GFP analysed cells. Bars = 10 µm.

7.4

Kohoutová, L., Kourová, H., Nagy, S., Volc, J., Halada, P., Mészáros, T., Meskiene, I., Bögre, L., and Binarová, P.; (submitted 2014) The Arabidopsis mitogen-activated protein kinase 6 is associated with γ-tubulin on microtubules, phosphorylates EB1c and maintains spindle orientation under nitric oxide stress. New Phytol

The Arabidopsis mitogen-activated protein kinase 6 is associated with γ-tubulin on microtubules, phosphorylates EB1c and maintains spindle orientation under nitric oxide stress

Kohoutová, L.[1], Kourová, H.[1], Nagy, S.[2], Volc, J.[1], Halada, P.[1], Mészáros, T.[2], Meskiene, I.[3], Bögre, L.[4], and Binarová, P.[1#]

[1] Institute of Microbiology AS CR, v. v. i., Vídeňská 1083, 142 20 Prague 4, Czech Republic
[2] Semmelweis University, Department of Medical Chemistry, Molecular Biology and Pathobiochemistry, Tűzoltó u. 37-47, H-1094 Budapest, Hungary
[3] Max F. Perutz Laboratories, Vienna Biocenter, University of Vienna, Vienna, Austria
[4] Royal Holloway, University of London, School of Biological Sciences, Centre for Systems and Synthetic Biology, Plant Molecular Sciences, Egham, Surrey, TW20 0EX, United Kingdom

Running title: MPK6 interacts with γ-tubulin and EB1 and maintains spindle orientation under NO stress

[#]Author for correspondence:
Pavla Binarová
Telephone: +42 0296442 130
e-mail: binarova@biomed.cas.cz

Summary

• Developmental cues and environmental conditions have continuous impacts on the spatial and temporal regulation of cell division. The stress activated MAP kinase pathways could play a role in maintaining correct cell divisions through the regulation of cytoskeleton, but little is known about interactors or substrates of MAP kinases with cytoskeletal elements.

• We used protein interaction and phosphorylation experiments with cytoskeletal proteins, mass spectrometry based identification of MPK6 complexes, immunofluorescence analyses of microtubular cytoskeleton of dividing root cells of WT and *mpk6-2* mutants upon nitric oxide stress.

• We showed that MPK6 is associated with γ-tubulin on microtubules. The active MAPK is enriched on microtubules and follows the dynamic localization of γ-tubulin from poles to midzone during anaphase/telophase transition. We found a novel mitotic MPK6 substrate, the microtubule plus end protein, EB1c. Compared to WT *mpk6-2* mutants were more sensitive to nitrosative stress in respect to microtubular and cell division defects. Inactivation of MAPKs by the overexpression of AP2C3 phosphatase also showed frequent mitotic abnormalities and oblique cell division planes.

• Our data suggest that active MAPK and γ-tubulin interact with specific subset of mitotic microtubules in late mitosis. MPK6 phosphorylates EB1c and has a role to maintain regular cell division in stress conditions.

Introduction

Mitogen-activated protein kinases (MAPK) are involved in biotic and abiotic stress signalling and have physiological functions in regulating plant growth and differentiation in response to external signals and developmental cues (Mishra *et al.*, 2006). It is becoming evident that regulation by MAPK signalling cascade is not restricted to the transcriptional level but is more complex.

MAP kinase signalling cascade plays role in plant morphogenesis by regulation of NACK-PQR pathway in cytokinesis (Calderini *et al.*, 1998; Bogre *et al.*, 1999; Calderini *et al.*, 2001; Sasabe & Machida, 2012). MPK3, MPK4, and MPK6 are the most extensively studied MAPKs in *Arabidopsis* (Andreasson & Ellis, 2010). MPK3/MPK6 signalling module is involved in photomorphogenesis (Sethi *et al.*, 2014); it is required for specification of cell fate during development of stomata (Wang *et al.*, 2007), and for development of anthers and ovule cells (Hord *et al.*, 2008; Wang *et al.*, 2008). Data obtained on YODA mutants suggested

function of MPK6 kinase with microtubules and in cytokinesis (Smekalova *et al.*, 2014). MPK6 also functions in ROS and NO signalling during root development in *Arabidopsis* (Wang *et al.*, 2010).

MAPK signalling can crosstalk with cytoskeletal proteins either directly through their phosphorylation as substrates or via interactions with scaffold proteins that brought MAPK together with their activators or members of other pathways (Meister *et al.*, 2013). Broad range of interaction of MAP kinases with microtubular proteins in response to stress or developmental cues was reported in eukaryotic cells. For example MAP kinases regulate microtubular dynamics during osmotic stress in yeast cells (Hagan, 2008). Role of MAPK in microtubule formation and spindle organization through its interaction with γ-tubulin functions was shown in pig oocytes (Sun *et al.*, 2001). ERK signalling is involved in regulation of function of microtubule plus end protein EB1, an interaction of STIM1 with EB1 is regulated through ERK phosphorylation (Pozo-Guisado *et al.*, 2013).

Despite of the extensive studies of plant MAPK and their physiological functions in development only few substrates have been identified among microtubular proteins reviewed in (Komis *et al.*, 2011; Sasabe & Machida, 2012). The experimental data are limited to microtubule associated protein MAP65-1 and MAP65-2 that were shown to be regulated by MAPK signalling in dividing plant cells (Smertenko *et al.*, 2006; Sasabe *et al.*, 2011).

Our biochemical and microscopic data showed that *Arabidopsis* MPK6 interacts with γ-tubulin and EB1 proteins; microtubule plus end protein EB1c was indicated as a target of MPK6 phosphorylation. Findings of novel interactions of MAP kinase MPK6 with microtubular proteins together with functional studies on MPK6 mutants help to get insight into molecular mechanisms of execution of MPK6 functions in plant cell division under physiological and stress conditions.

Results

MPK6 is associated with γ-tubulin on microtubules in proliferating cells

To investigate MPK6 protein complexes, we performed immunopurification from extracts of proliferating cells in culture with anti-MPK6 antibody and specifically eluted the MPK6 complexes with the immunogenic peptide. As a control we used pre-immune serum. We identified the proteins by LC-MALDI-TOF mass spectrometry. In several independent experiments we reproducibly identified γ-tubulin among the proteins in the MPK6 immunoprecipitate, but not with preimmune serum (Fig. S1). To validate the association of γ-tubulin with MPK6, we performed Western blots and specifically detected γ-tubulin only

with MPK6 immunoprecipitate but not with preimmune serum (Fig. 1a). To confirm the interaction of γ-tubulin with MPK6, we performed reciprocal immunopurification experiments. We found that MPK6 was associated with immunopurified γ-tubulin from extracts of *Arabidopsis* cultured cells using a peptide-purified plant specific γ-tubulin antibody (Fig. 1b).

To investigate whether MPK6 associates with γ-tubulin on microtubules, we polymerized plant microtubules with taxol from extracts of cultured cells and performed spin down assays that we have previously established to show association of γ-tubulin with microtubules (Drykova *et al.*, 2003). The high speed supernatant S70 of soluble cytoplasmic extract was used for taxol driven polymerization of microtubules (Fig. 1c). α-Tubulin together with microtubule associated protein, MAP65-1, as well as the microtubule plus end proteins EB1s were detected in microtubular pellets but these proteins were undetectable in the negative control where taxol was omitted. As we published before (Drykova *et al.*, 2003), γ-tubulin was also present with taxol-polymerized microtubules. In accordance, γ-tubulin complex protein, GCP4 was also detected in microtubular pellets (Fig. 1c). The presence of microtubule nucleator γ-tubulin and GCP4, plus end proteins EB1s and micortubule-associated proteins MAP65 show the efficient polymerization of plant microtubules *in vitro*.

The same microtubular fractions were then used to test the association of MPK6 with plant microtubules. As shown in Fig. 1c, a portion of soluble pool of MPK6 was sedimented with taxol-polymerized microtubules. To address whether active MAPKs are present with micortubules, we used a commercially available antibody directed against phosphorylated and active ERK1, named p-ERK that was shown to recognize the conserved phosphoepitope on the activation loop of plant MAPKs (Umbrasaite *et al.*, 2010). We found a large enrichment of phosphorylated MPKs in microtubular pellets (Fig. 1c).

To find out whether the microtubule bound γ-tubulin or γ-tubulin complexes interact with MPK6, we released γ-tubulin complex by depolymerization of pelleted microtubules and performed immunopurification with peptide-purified antibody against plant γ-tubulin. As shown in Fig. 1d, MPK6 was detected with γ-tubulin immunoprecipitated from the microtubular fraction. We conclude that MPK6 associates with γ-tubulin present with polymerized plant microtubules.

MPK6 kinase is localized with mitotic microtubules

To get further insights into the association of MPK6 with microtubules within dividing cells, we analyzed localization of MPK6 and p-ERK in *Arabidopsis* root meristems. Double

immunofluorescence labelling showed that signal for MPK6 was present in the area of pre-prophase band (PPB; Fig. 2a, arrows), with the metaphase spindle (Fig. 2a, arrowheads), and with the phragmoplast (Fig. 2a, asterisk). Signal for p-ERK was not observed with PPBs (Fig. 2b, arrows), but was present with spindle (Fig. 2b, arrowhead) and phragmoplast (Fig. 2b, asterisk). In anaphase, MPK6 was present both with shortening kinetochore microtubular fibres (Fig. 2c, arrowheads) and with the midzone of anaphase spindle (Fig. 2c, arrow). In contrast, p-ERK labelling was largely associated with shortening kinetochore microtubular fibres on poles of anaphase spindle (Fig. 2d, arrowheads). These immunolocalization data suggested that active MPKs were associated with specific subsets of mitotic and cytokinetic microtubules. To test whether p-ERK detects MPK6, we performed Western blotting and found specific labelling corresponding to the molecular mass of MPK6 in wild type but not in *mpk6-2* knockout mutant (Fig. S2a). To see whether MPK6 labelling on mitotic microtubules are specific, we also localized two other abundant MAPKs; MPK3 was largely diffused while MPK4 was detected mainly in the midzone of anaphase spindle as was previously shown (Kosetsu *et al.*, 2010; Beck *et al.*, 2011) (Fig. S2b).

To ascertain that MPK6 and p-ERK is associated with microtubules, we treated cells with microtubule stabilizing drug taxol and depolymerization drug amiprophos methyl (APM). We found that both MPK6 and p-ERK signals were enriched with dense microtubular arrays in taxol-treated cells (Fig. S3a, b) and became dispersed when microtubules were depolymerized by APM (Fig. S3c, d). P-ERK was also accumulated in the vicinity of persistent kinetochore stubs after APM treatment (Fig. S3d) that was also decorated with γ-tubulin as we described previously (Fig. S3e) (Binarova *et al.*, 2000).

p-ERK is dynamically co-localised with γ-tubulin on kinetochore fibers and in midzone during anaphase to telophase transition

In animal cells, γ-tubulin is centrosomal while we showed that in acentrosomal plant cells it associates with mitotic microtubules with specific patterns during the progression through the cell division (Drykova *et al.*, 2003). Because MPK6 associated with γ-tubulin and p-ERK labelling showed some resembles with it, we performed double immunofluorescence labelling with MPK6 and p-ERK with γ-tubulin in dividing cells of *Arabidopsis* roots (Fig. 2e-g). Labelling for p-ERK was present together with γ-tubulin labelling on shortening polar kinetochore microtubular fibres during anaphase and with phragmoplast in telophase (Fig. 2e-g).

To analyze the co-localization of MPK6 and p-ERK with γ-tubulin, we analysed mitotic figures in more details and derived intensity profiles during late anaphase to telophase transition. γ-Tubulin predominantly localized with shortening anaphase kinetochore fibres on poles of anaphase spindle, and became gradually more abundant in the vicinity of separated chromatin facing the midzone where phragmoplast microtubules are known to be nucleated (Binarova *et al.*, 2000). P-ERK followed the γ-tubulin signal with some delay which was substantiated by the intensity profiles (Fig. 3a-d). In contrast to p-ERK, MPK6 signal was present in the entire midzone during anaphase and cytokinesis (Fig. 3e, f). Thus, the active form of MAPK is specifically enriched with polymerized microtubules, and localized with γ-tubulin on shortening anaphase kinetochore fibres on poles of acentrosomal spindle and at the vicinity of chromatin during phragmoplast formation.

MPK6 interacts with and phosphorylates microtubule plus end protein EB1c

Because of the close association of γ-tubulin with MPK6 and p-ERK, we set out to test whether γ-tubulin can be phosphorylated by MPK6. γ-Tubulin was *in vitro* translated and *in vitro* kinase assay was carried out with MKK4-activated MPK6, but no γ-tubulin phosphorylation could be detected (Fig. 4a). We showed that EB1s associate with polymerized microtubules of cell extracts from proliferating cells (Fig. 1c). EB1c is the predominant mitotic plus end microtubular protein and have predicted MAP kinase phosphosites and docking motifs (http://elm.eu.org, http://gps.biocuckoo.org). We also tested whether EB1c is a substrate of MPK6 and showed that contrary to γ-tubulin, EB1c protein was phosphorylated by MPK6 (Fig. 4a). In agreement, we showed by reciprocal immunoprecipitations that EB1c interacts with MPK6 (Fig. 4b, c). Immunocolocalization of EB1c with MPK6 and pERK showed a partial overlap on mitotic microtubule structures, anaphase spindle and phragmoplast (Fig. S4). γ-Tubulin might serve as a scaffold for recruitment of active MPK6 to microtubules, while EB1c could be directly regulated through phosphorylation by MPK6.

MPK6 regulates the alignment of cell division upon nitric oxide stress

On one hand, reactive oxygen species (ROS) are known to induce rapid activation of MPK6 that activates nitrate reductase 2 (NIA2) leading to increased nitric oxide (NO) production (Wang *et al.*, 2010). Consequently, *mpk6-2* mutant was shown to have increased sensitivity to external NO donor or to H_2O_2 treatment. On the other hand, NO was found to disrupt tyrosination/detyrosination cycle of plant microtubules needed for regular association and function of MAPs and molecular motors (Blume *et al.*, 2013) and consequently it was

shown that NO nitrosylation of α-tubulin affects cortical microtubular arrangement and cell plane alignment and therefore affects root development (Lipka & Muller, 2014). To investigate the connection between NO and MPK6 function in the regulation of mitotic microtubule organization, we treated WT and *mpk6-2* seedlings with the NO donor, NO_2-Tyr. Treatment of wild type Columbia seedlings with NO_2-Tyr resulted in shortened roots (Fig. 5a) as was shown before by (Lipka & Muller, 2014); *mpk6-2* was supersensitive to the treatment (Fig. 5a), in agreement what was found by (Wang *et al.*, 2010). Immunofluorescence analyses of whole mount α-tubulin-labelled roots upon nitrosative stress led to rare oblique alignment of spindles in wild type Columbia (Fig. 5c). While we could not detect any mitotic abnormalities in the *mpk6-2* mutant grown under normal conditions (Fig. 5d), upon nitrosative stress the effect on mitotic cytoskeleton and spindle orientation was largely enhanced (Fig. 5e). We observed enlarged cells of irregular shapes, misaligned spindles, aberrant mitosis and consequent disrupted cell files, suggesting cell division defects (Fig. 5e).

Inactivation of MAPKs MPK3, MPK4, and MPK6 through the overexpression of AP2C3 phosphatase also resulted in largely disturbed root development (Fig. 6) as well as in published cell division defects in the stomata lineage (Umbrasaite *et al.*, 2010). We looked for cell division defects in the root of AP2C3 oe. Instead of regular cell files typical for meristematic and transition zone of the WT roots, cell files of AP2C3 oe roots were disrupted, cells were of various size and shape, often isodiametric and swollen (Fig. 6a). Closer inspection revealed mitotic defects in AP2C3 oe. Chromosomes were not congressed in metaphase plate (Fig. 6b), there were lagging chromosomes in anaphase (Fig. 6c, arrowhead), and cells in stage corresponding to telophase with chromatids remained condensed formed round-shaped masses; microtubules instead of being organized in phragmoplast were randomly arranged in the vicinity of chromatin and labelling of cytokinetic syntaxin KNOLLE showed complete failure of the cell plate formation (Fig. 6c, arrow). Both spindle poles (Fig. 6d, arrow) and cell division sites were misaligned in AP2C3 oe roots (Fig. 6e, arrows).

Altogether these our data suggested that while requirement for MPK6 kinase function with microtubules and in the cell division was evident under nitrosative stress in *mpk6-2* mutants, inactivation of MPK6, MPK3, and MPK4 in AP2C3 oe was needed to induce severe mitotic defects under control conditions.

Discussion

Plant microtubules build several plant specific mitotic and cytokinetic arrays and their continuous rearrangement needs to be precisely regulated to ensure correct cell division in

absence of centrosomes and presence of rigid cells wall. Developmental or stress response signalling regulates dynamics of plant microtubules either directly through phosphorylation of microtubules or through phosphorylation of microtubule-associated proteins. Recently atypical kinase was shown to phophorylate plant α-tubulin (Fujita *et al.*, 2013). Plant MAP kinases are important for stress signalling as well as for regulation of development and their role with microtubules is suggested. However, until now only plant microtubule-associated proteins MAP65-1 and MAP65-2 were uncovered as a targets of MAP kinases signaling (Smertenko *et al.*, 2006; Sasabe *et al.*, 2011).

Our *in vitro* and *in situ* data showed that MPK6 is present with microtubules and active kinase associates with specific subset of mitotic and cytokinetic microtubules. We further demonstrated a link of MPK6 to microtubule bound fraction of γ-tubulin and to microtubule plus end protein EB1c that was shown to be a target of MPK6 phoshorylation *in vitro*. EB1c is plant specific EB1 protein with NLS sequences on its C-terminal. Search of publically available co-expression databases revealed strong correlation of EB1c expression with expression of checkpoint proteins Mad2 and Bub3. These data together with cellular localization of EB1c in nuclei and with cytokinetic sites (Van Damme *et al.*, 2004) suggests function of EB1c in the cell division. Mutant analyses indeed showed EB1c function in proper spindle positioning, chromosome congression, and genome stability (Komaki *et al.*, 2010). Interestingly, cell division defects observed by us in root cells with reduced levels of MPK3, MPK4, and MPK6 show strong analogy to phenotype of EB1c mutant reported by Komaki et al. (Komaki *et al.*, 2010). Defects of spindle polarity and uncompleted chromosome congression and separation observed in our experiments in roots with reduced MPKs levels might be a consequence of defective kinetochore microtubules attachment. This type of defects results from impaired activity of the kinetochore-associated factors that regulate dynamics of microtubules. It was shown that depletion of EB1 in animal cells results in defective spindle and problems with metaphase chromosome congression and high incidence of lagging chromosomes, similar aberrant mitotic phenotype was observed in cells overproducing EB1 (Rogers *et al.*, 2002). Mutation of plant EB1c resulted in similar mitotic problems (Komaki *et al.*, 2010). We observed lagging chromosomes and aberrant mitosis in *Arabidopsis* cells overproducing EB1c under constitutive 35S promoter (our unpublished data). Our finding of EB1c being a target and a substrate of MPK6 phoshorylation contributed to growing body of evidence that function of EB1 proteins is regulated by phosphorylation and proper regulation is essential for regulation of mitotic cytoskeleton (Tamura & Draviam, 2012).

γ-Tubulin is highly conserved eukaryotic protein with functions in microtubule nucleation but it has also other cellular roles. γ-Tubulin participates in coordination with plus end proteins or molecular motors in organization of microtubular cytoskeleton during mitosis (Bouissou *et al.*, 2014; Olmsted *et al.*, 2014). We showed that kinetochore localized γ-tubulin is important for plant spindle organization (Binarova *et al.*, 2000). Later kinetochore function of γ-tubulin was confirmed also in animal cells (Mishra *et al.*, 2010). Regulatory function of MPK6 signalling to γ-tubulin positive nucleation sites is not completely unexpected. Mitotic defects were observed in mouse oocytes with depleted p38 MAPK (Ou *et al.*, 2010) and p38 was suggested to be an important component of microtubule organizing centres. Targeting of γ-tubulin to centrosomes and nucleation activity of centrosomes were reduced in cells with inhibited MAP kinase (Colello *et al.*, 2012). In spite of that we demonstrated interaction of MPK6 with γ-tubulin we could not demonstrate phosphorylation of γ-tubulin by MAP kinases *in vitro*. We suggest that MPK6 may regulate function of γ-tubulin probably through phosphorylation of GCPs or other γ-tubulin interacting partners. Among them AtGCP4 is potential targets for MAP kinase phosphorylation as there is a docking motif for MAPK as well as phosphorylation site at its N-terminus (http://elm.eu.org). Crystalographic study showed that C-terminus of GCP4 is responsible for interaction with γ-tubulin leaving accessible the MAPK site (Guillet *et al.*, 2011). Function of GCP4 with γ-tubulin in microtubule organization in *Arabidopsis* was indicated by amiRNA depletion of GCP4 in *Arabidopsis* (Kong *et al.*, 2010). We found GCP4 in complex with plant γ-tubulin (Fig. S5) and the complex is pulled down with microtubules *in vitro*. GCP4 is downregulated in YODA mutants and it is co-expressed with MPK6 (Smekalova *et al.*, 2014). Our LC-MALDI MS/MS analysis identified 14-3-3ω protein as an interactor of MPK6 in dividing *Arabidopsis* cells, interaction was validated by Western blot (Fig. S6). Interestingly, proteomics studies of interactom of *Arabidopsis* 14-3-3 proteins showed that GCP4 is among clients of 14-3-3ω (Chang *et al.*, 2009). As 14-3-3 proteins are important for interactions of phosphorylated proteins we can hypothesize that putative interaction of active MPK6 with γ-tubulin/GCP4 complex might be possible through 14-3-3ω.

MAP kinase signaling to cytokinesis is well defined for NACK MPK4 pathway with MAP65 proteins as a target (Calderini *et al.*, 2001; Sasabe *et al.*, 2011). Involvement of other MAP kinases and other microtubule associated targets is expected (Sasabe & Machida, 2012). MAP kinase regulatory signalling to γ-tubulin complexes might be behind function of γ-tubulin in late mitotic events that we described previously using RNAi approach (Binarova *et al.*, 2006) but that is still now fully understood. We found that elimination of MPK6 was not

affecting root development under normal conditions while constitutive expression of phosphatase AP2C3 that inactivates MPK6 and also targets MPK3 and MPK4 led to very strong cell division defects. Reduction of MAP kinase activity strongly affected cell division and defects of spindle positioning, chromosome congression and separation, and misalignment of cell division sites were observed. This fact shows that MPK6 function in development/cell cycle control of cytoskeleton can be compensated by MPK3 or MPK4. During inactivation of more kinases by the phosphatase there is no compensation and strong phenotype/defects appear in normal growth conditions.

However, under stress (NO_2-Tyr and ROS) MPK6 became essential for correct development and the cell divisions. ROS activated MPK6 phosphorylates NIA2 that leads to increase of NO production (Wang *et al.*, 2010). Plant microtubule organization is affected under nitrosative stress (Lipka & Muller, 2014), tyrosine nitration of α-tubulin may function in regulation of microtubule organization through kinesin interaction or through interaction of microtubules with other microtubule-associated proteins (Blume *et al.*, 2013). NIA2, a target of MAP6 kinase signalling under ROS stress was shown to interact with 14-3-3ω in proteomic studies (Chang *et al.*, 2009) and by Y2H (Kanamaru *et al.*, 1999). Now we demonstrated interaction of 14-3-3ω with MPK6. Other experiments are needed to elucidate wheather MPK6 might function with microtubules via NIA2 phosphorylation. However, it is tempting to speculate that tubulin modification with an impact to MAPs and molecular motors function might be one of microtubule related pathways targeted by MPK6 signalling cascade.

Our data showed that γ-tubulin complexes and EB1c protein present novel interactions and targets for MPK6 signalling. Identification of novel interactors or substrates of MAP kinases signalling cascade with cytoskeletal elements help understanding of MPKs in processes such as cell cycle progression, proliferation and differentiation. Furthermore, a function of MPK6 in physiological processes protecting microtubular cytoskeleton under ROS and NO stress response was suggested.

Material and Methods

Plant material and cultured cells

Cell suspension cultures of *Arabidopsis thaliana*, Columbia (Col), Landsberg erecta (Ler), and EB1c-GFP were grown under continuous darkness at 25 °C as described previously (Drykova *et al.*, 2003). After sterilization, seedlings of *Arabidopsis thaliana* (L.) Heynh. ecotype Columbia, *mpk6-2* (Liu & Zhang, 2004), and AP2C3 oe (Umbrasaite *et al.*, 2010) were grown

on half-strength MS with 0.25 mM MES, 1% (w/v) agar and 0.5 % sucrose under 16 h of light and 8 h of dark.

Molecular methods

Arabidopsis EB1c coding sequence without stop codon was purchased in pDONR207 from GeneScript. C-terminal GFP fusion of EB1c was prepared by Gateway cloning of EB1c to pK7FWG2 vector (Karimi *et al.*, 2002). The construct was transformed to cell culture Ler through *Agrobacterium tumefaciens* GV3101 strain.

Plasmid construction, *in vitro* transcription and *in vitro* translation

Coding regions of MPK6, γ-tubulin and EB1c were amplified from cDNA library by PCR and transferred into pEU3-NII-HLICNot and pEU3-NII-GLICNot vectors by ligation independent cloning. myc-AtMKK4-GOF was inserted into pEU3-NII-gateway vector by gateway cloning (Nagy & Meszaros, 2014). Plasmids purified from ampicillin-resistant colony were sequenced to confirm the PCR accuracy.

The *in vitro* mRNA synthesis was accomplished by addition 1 μg of purified, NotI linearized vector following the provided manual of the kit (TrascriptAid T7 High Yield Transcription Kit, Thermo Scientific). The reaction was incubated for 2 h at 37°C, precipitated by ammonium acetate/ethanol mixture, dissolved in 1x SUB-AMIX and stored at -80 °C. Quality and quantity of mRNAs was verified on agarose gel electrophoresis. Cell-free translation (van den Berg *et al.*, 2006) was carried out in 20.6 μl final volume by addition of 5 μL (15 μg) mRNA, 10 μL WEPRO® (Cell Free Sciences) solution, 0.8 μL creatine kinase (1 mg/mL) and 5 μL 1x SUB-AMIX. Additional 0.5 μl of myc-AtMKK4GOF mRNA was added to the translation mixture where His6-AtMPK6.was to be activated. The translation solution was underlayed to 206 μL SUB-AMIX in a sterile 96-well plate and the reaction was incubated for 20 hours at 20°C (Nagy & Meszaros, 2014).

Protein purification, phosphatase treatment, TEV protease cleavage

In vitro translated His6-AtMPK6 proteins were purified by affinity chromatography on 10 μl TALON® Magnetic Beads (Clontech). 50 mM sodium phosphate buffer completed with 10 mM imidazole, 300 mM NaCl, 0.1% Triton-X was used as wash and binding buffer. The resin was washed three times after 1 h incubation with total translation mixture at room temperature. TEV protease was affinity purified after bacterial protein expression using pTH24_TEV construct (van den Berg *et al.*, 2006). TEV protease cleavage was performed overnight and at

4 °C with addition of 2.5 µl 20X TEV Buffer (1 M Tris-HCl, pH 8.0, 10 mM EDTA), 0.5 µl 0.1 M DTT, 10 µl TEV protease to affinity purified proteins. Protein concentration was measured by Bradford reagent. *In vitro* translated GST-tubulin and GST-EB1c were purified by affinity chromatography on 25 µl Glutathione Magnetic Beads (Thermo Scientific). 125 mM Tris, 150 mM NaCl, pH 8.0 was used as wash and binding buffer. The resin was washed three times after 1 h incubation with total translation mixture at room temperature. Phosphatase treatment was carried out with λ Protein Phosphatase (New England Biolabs) for 30 minutes at 30°C, then washed three times with PBS, pH 7.4.

In vitro kinase assays

For kinase assays 300 and 100 ng *in vitro* translated, affinity purified substrate and kinase was used, respecitively. The assay was carried out in 20 mM Hepes, pH 7.5, 100 µM ATP, 1 mM DTT, 15 mM $MgCl_2$, 5 mM EGTA, 5 µCi [γ-32P]ATP with bead bound GST-tubulin and GST-AtEB1c as substrates in 16 µl final volume for 30 minutes at room temperature, then stopped by addition of 5× Laemmli SDS buffer. Samples were fractionated on a 10% SDS-PAGE gel. The gel was fixed, stained with Coomassie Blue, dried and analyzed by autoradiography.

Protein extracts preparations

Protein extracts were prepared from *Arabidopsis* cultured cells as described before (Tomastikova *et al.*, 2012), buffer supplemented with 5 mM p-nitrophenylphosphate for p-ERK was used. Extracts S20 or P100 were solubilized with 1% Nonidet P40 (Roche Diagnostics).

Immunopurifications

Immunoprecipitations were performed from solubilized protein extracts (~ 3 $mg.mL^{-1}$). Extracts were incubated with primary antibody at 4°C, then A-Agarose beads (Roche Diagnostics) were added and incubated for other 2 hours. After washing, elution was done either by 0.1% immunogenic peptide or by boiling with sample buffer (Laemmli, 1970). Co-immunoprecipitation using GFP-Trap_A (ChromoTek, Planegg-Martinsried, Germany) were done according to the manufacturer's instructions.

The microtubule spin-down experiments were performed as described previously (Binarova *et al.*, 2006).

Gel permeation chromatography was done from solubilized microsomal pellet P100 on

Superose 6 10/300 GL column (GE Healthcare Bio-Sciences, Uppsala, Sweden) according to (Doskocilova *et al.*, 2011).

Proteins were separated on 8%, 10% or 12% SDS-PAGE and wet blotted to PVDF or nitrocelulose membrane.

Three independent experiments were performed; representative Western blots are shown.

Custom polyclonal rabbit antibody affinity-purified on immunogenic peptide (GenScript) was raised against the C-terminal sequence LIYREALAFNPEYQQ (aa 381-395) of MPK6 molecule and used for immunoprecipitations. Antibodies for Western blots were used in following dilutions: anti-AtMPK6 (Sigma) 1:4,000, and antibody against phosphorylated forms of MPKs Phospho-p44/42 MAPK (Erk1/2) (Thr202/Tyr204) (D13.14.4E) XP here called p-ERK (Cell Signaling) 1:2,000, antibody 4B9 (kindly provided by Dr. Ferl) 1:2,400, anti-MAP65-1 (kindly provided by P. Hussey) 1:2,000, anti-EB1 (Abcam, AtEB1b) 1:2,000, DM1A (Sigma) 1:1,000, anti-GCP4 (custom polyclonal rabbit antibody affinity-purified on immunogenic peptide from GenScript) 1:50 – 1:200, anti-GFP (Abcam) 1:4,000. γ-Tubulin was detected as described (Doskocilova *et al.*, 2011). Secondary horseradish peroxidase conjugated antibodies; anti-mouse and anti-rabbit were diluted 1:7,500 and 1:10,000 (Amersham-GE Healthcare, Promega, Cell Signaling).

Protein digestion and LC MALDI-TOF mass spectrometry

Protein samples were dissolved in 50 μl of 8M urea and denatured in ultrasonic bath for 30 min. After addition of 50 μl of 0.1 M 4-ethylmorpholine acetate (pH 8.1) the samples were sonicated for next 30 min. The digestion was started by addition of 3 μl of trypsin (20 ng/μl; Promega, Madison, WI) and carried out overnight at 37°C. The resulting peptides were acidified by 100 μl of 0.8% TFA and desalted on a macrotrap packed with polymeric RP-material (Michrom BioResources, Auburn, CA) according to manufacturer's protocol. The purified peptides were separated using Ultimate LC Packings HPLC system (LC Packings, Amsterdam, The Netherlands) on a Magic C18AQ column (0.2 x 150 mm, 5 μm, 200 Å). The eluent from the column was spotted directly onto MALDI PAC384 target using a ProteineerFC spotting device (Bruker Daltonics, Bremen, Germany). Automatic MALDI MS/MS analyses were performed under the control of Compass 1.3 and WarpLC 1.2 software on a Ultraflex III TOF/TOF (Bruker Daltonics). Proteins were identified by searching MS/MS spectra against *A. thaliana* subset of SwissProt or NCBInr database using in-house MASCOT program (Matrixscience) with the following search settings: enzyme: trypsin, variable

modifications: acetyl (Protein N-term), carbamidomethyl (C), oxidation (M), MS mass tolerance: 50 ppm, MS/MS mass tolerance: 0.7 Da, max. missed cleavage: 2.

Microscopy

Immunofluorescence labelling was performed as described (Drykova *et al.*, 2003). Whole-mounts were performed as described (Sauer *et al.*, 2006). Dilution of antibodies: anti-AtMPK6 (1:1,000-1:2,000), DM1A (1:2,000), anti-γ-tubulin TU-32 antibody (kindly provided by P. Dráber) (1:6), p-ERK (1:500), anti-AtMPK3 (Sigma) 1:1000, anti-AtMPK4 (Sigma) 1:2,000, anti-GFP (Roche) 1:1,000, anti-KNOLLE 1:6,000. Alexa Fluor 488, Alexa Fluor 594, DyLight 647-conjugated anti-mouse and anti-rabbit antibodies (Jackson ImmunoResearch Laboratories) diluted 1:600, 1:800, 1:700, respectively.

Drugs were used in working concentrations of: 10 μM APM (amiprophos methyl, Duchefa A0185) in DMSO, 10 μM taxol (Paclitaxel, Sigma T7402) in DMSO, 0.5 μM NO_2-Tyr (3-nitro-L-tyrosine, Sigma N7389) in 0.5 μM HCl. APM and Taxol were applied for 2 h, NO_2-Tyr was added to half strenght MS medium for plant growth.

For fluorescence microscopy Olympus IX-81 FV-1000 confocal imaging system with oil immersion objectives 100x/1.45 and 60x/1.35 was used; DAPI ex 405 nm, em 425-460 nm; Alexa488 ex 473 nm, em 485-545 nm; Alexa 594 ex 559 nm, em 575-640 nm; Alexa 647 ex 635 nm, em 655-755 nm. Laser scanning was performed using the sequential multitrack mode to avoid bleed-through. Images were analysed by FV10 ASW2.0 and prepared in Adobe Photoshop CS4 and Adobe Illustrator CS4. For macroscopic images magnifying microscope Leica MZ16F with DFC 320R2 camera and DFC Twain 7.5.0 SW (Leica) was used.

Acknowledgement

The work was supported by Grant from Grant Agency of the Czech Republic P501-12-2333 to PB, Grant MSMT Kontakt 7AMB13AT013 to PB and IM, and Grant OTKA NN111085 to TM. We thank to Dr. Ferl for 4B9 antibody. We also thank to Gabriela Kočárová for technical assistance.

References

Andreasson E, Ellis B. 2010. Convergence and specificity in the Arabidopsis MAPK nexus. *Trends in plant science* **15**(2): 106-113.

Beck M, Komis G, Ziemann A, Menzel D, Samaj J. 2011. Mitogen-activated protein kinase 4 is involved in the regulation of mitotic and cytokinetic microtubule transitions in Arabidopsis thaliana. *The New phytologist* **189**(4): 1069-1083.

Binarova P, Cenklova V, Hause B, Kubatova E, Lysak M, Dolezel J, Bogre L, Draber P. 2000. Nuclear gamma-tubulin during acentriolar plant mitosis. *Plant Cell* **12**(3): 433-442.

Binarova P, Cenklova V, Prochazkova J, Doskocilova A, Volc J, Vrlik M, Bogre L. 2006. Gamma-tubulin is essential for acentrosomal microtubule nucleation and coordination of late mitotic events in Arabidopsis. *Plant Cell* **18**(5): 1199-1212.

Blume YB, Krasylenko YA, Demchuk OM, Yemets AI. 2013. Tubulin tyrosine nitration regulates microtubule organization in plant cells. *Frontiers in plant science* **4**: 530.

Bogre L, Calderini O, Binarova P, Mattauch M, Till S, Kiegerl S, Jonak C, Pollaschek C, Barker P, Huskisson NS, et al. 1999. A MAP kinase is activated late in plant mitosis and becomes localized to the plane of cell division. *Plant Cell* **11**(1): 101-113.

Bouissou A, Verollet C, de Forges H, Haren L, Bellaiche Y, Perez F, Merdes A, Raynaud-Messina B. 2014. gamma-Tubulin Ring Complexes and EB1 play antagonistic roles in microtubule dynamics and spindle positioning. *The EMBO journal* **33**(2): 114-128.

Calderini O, Bogre L, Vicente O, Binarova P, Heberle-Bors E, Wilson C. 1998. A cell cycle regulated MAP kinase with a possible role in cytokinesis in tobacco cells. *J Cell Sci* **111**(Pt 20): 3091-3100.

Calderini O, Glab N, Bergounioux C, Heberle-Bors E, Wilson C. 2001. A novel tobacco mitogen-activated protein (MAP) kinase kinase, NtMEK1, activates the cell cycle-regulated p43Ntf6 MAP kinase. *The Journal of biological chemistry* **276**(21): 18139-18145.

Colello D, Mathew S, Ward R, Pumiglia K, LaFlamme SE. 2012. Integrins regulate microtubule nucleating activity of centrosome through mitogen-activated protein kinase/extracellular signal-regulated kinase kinase/extracellular signal-regulated kinase (MEK/ERK) signaling. *The Journal of biological chemistry* **287**(4): 2520-2530.

Doskocilova A, Plihal O, Volc J, Chumova J, Kourova H, Halada P, Petrovska B, Binarova P. 2011. A nodulin/glutamine synthetase-like fusion protein is implicated in the regulation of root morphogenesis and in signalling triggered by flagellin. *Planta* **234**(3): 459-476.

Drykova D, Cenklova V, Sulimenko V, Volc J, Draber P, Binarova P. 2003. Plant gamma-tubulin interacts with alphabeta-tubulin dimers and forms membrane-associated complexes. *Plant Cell* **15**(2): 465-480.

Fujita S, Pytela J, Hotta T, Kato T, Hamada T, Akamatsu R, Ishida Y, Kutsuna N, Hasezawa S, Nomura Y, et al. 2013. An atypical tubulin kinase mediates stress-induced microtubule depolymerization in Arabidopsis. *Current biology : CB* **23**(20): 1969-1978.

Guillet V, Knibiehler M, Gregory-Pauron L, Remy MH, Chemin C, Raynaud-Messina B, Bon C, Kollman JM, Agard DA, Merdes A, et al. 2011. Crystal structure of gamma-tubulin complex protein GCP4 provides insight into microtubule nucleation. *Nat Struct Mol Biol* **18**(8): 915-919.

Hagan IM. 2008. The spindle pole body plays a key role in controlling mitotic commitment in the fission yeast Schizosaccharomyces pombe. *Biochemical Society transactions* **36**(Pt 5): 1097-1101.

Hord CL, Sun YJ, Pillitteri LJ, Torii KU, Wang H, Zhang S, Ma H. 2008. Regulation of Arabidopsis early anther development by the mitogen-activated protein kinases, MPK3 and MPK6, and the ERECTA and related receptor-like kinases. *Molecular plant* **1**(4): 645-658.

Chang IF, Curran A, Woolsey R, Quilici D, Cushman JC, Mittler R, Harmon A, Harper JF. 2009. Proteomic profiling of tandem affinity purified 14-3-3 protein complexes in Arabidopsis thaliana. *Proteomics* **9**(11): 2967-2985.

Kanamaru K, Wang R, Su W, Crawford NM. 1999. Ser-534 in the hinge 1 region of Arabidopsis nitrate reductase is conditionally required for binding of 14-3-3 proteins and in vitro inhibition. *The Journal of biological chemistry* **274**(7): 4160-4165.

Karimi M, Inze D, Depicker A. 2002. GATEWAY vectors for Agrobacterium-mediated plant transformation. *Trends in plant science* **7**(5): 193-195.

Komaki S, Abe T, Coutuer S, Inze D, Russinova E, Hashimoto T. 2010. Nuclear-localized subtype of end-binding 1 protein regulates spindle organization in Arabidopsis. *J Cell Sci* **123**(Pt 3): 451-459.

Komis G, Illes P, Beck M, Samaj J. 2011. Microtubules and mitogen-activated protein kinase signalling. *Current opinion in plant biology* **14**(6): 650-657.

Kong Z, Hotta T, Lee YR, Horio T, Liu B. 2010. The {gamma}-tubulin complex protein GCP4 is required for organizing functional microtubule arrays in Arabidopsis thaliana. *Plant Cell* **22**(1): 191-204.

Kosetsu K, Matsunaga S, Nakagami H, Colcombet J, Sasabe M, Soyano T, Takahashi Y, Hirt H, Machida Y. 2010. The MAP kinase MPK4 is required for cytokinesis in Arabidopsis thaliana. *The Plant cell* **22**(11): 3778-3790.

Lipka E, Muller S. 2014. Nitrosative stress triggers microtubule reorganization in Arabidopsis thaliana. *Journal of experimental botany* **65**(15): 4177-4189.

Liu Y, Zhang S. 2004. Phosphorylation of 1-aminocyclopropane-1-carboxylic acid synthase by MPK6, a stress-responsive mitogen-activated protein kinase, induces ethylene biosynthesis in Arabidopsis. *The Plant cell* **16**(12): 3386-3399.

Meister M, Tomasovic A, Banning A, Tikkanen R. 2013. Mitogen-Activated Protein (MAP) Kinase Scaffolding Proteins: A Recount. *International journal of molecular sciences* **14**(3): 4854-4884.

Mishra NS, Tuteja R, Tuteja N. 2006. Signaling through MAP kinase networks in plants. *Archives of biochemistry and biophysics* **452**(1): 55-68.

Mishra RK, Chakraborty P, Arnaoutov A, Fontoura BM, Dasso M. 2010. The Nup107-160 complex and gamma-TuRC regulate microtubule polymerization at kinetochores. *Nat Cell Biol* **12**(2): 164-169.

Nagy SK, Meszaros T. 2014. In vitro translation-based protein kinase substrate identification. *Methods in molecular biology* **1118**: 231-243.

Olmsted ZT, Colliver AG, Riehlman TD, Paluh JL. 2014. Kinesin-14 and kinesin-5 antagonistically regulate microtubule nucleation by gamma-TuRC in yeast and human cells. *Nature communications* **5**: 5339.

Ou XH, Li S, Xu BZ, Wang ZB, Quan S, Li M, Zhang QH, Ouyang YC, Schatten H, Xing FQ, et al. 2010. p38alpha MAPK is a MTOC-associated protein regulating spindle assembly, spindle length and accurate chromosome segregation during mouse oocyte meiotic maturation. *Cell Cycle* **9**(20): 4130-4143.

Pozo-Guisado E, Casas-Rua V, Tomas-Martin P, Lopez-Guerrero AM, Alvarez-Barrientos A, Martin-Romero FJ. 2013. Phosphorylation of STIM1 at ERK1/2 target sites regulates interaction with the microtubule plus-end binding protein EB1. *Journal of cell science* **126**(Pt 14): 3170-3180.

Rogers SL, Rogers GC, Sharp DJ, Vale RD. 2002. Drosophila EB1 is important for proper assembly, dynamics, and positioning of the mitotic spindle. *J Cell Biol* **158**(5): 873-884.

Sasabe M, Kosetsu K, Hidaka M, Murase A, Machida Y. 2011. Arabidopsis thaliana MAP65-1 and MAP65-2 function redundantly with MAP65-3/PLEIADE in cytokinesis downstream of MPK4. *Plant signaling & behavior* **6**(5): 743-747.

Sasabe M, Machida Y. 2012. Regulation of organization and function of microtubules by the mitogen-activated protein kinase cascade during plant cytokinesis. *Cytoskeleton* **69**(11): 913-918.

Sauer M, Paciorek T, Benkova E, Friml J. 2006. Immunocytochemical techniques for whole-mount in situ protein localization in plants. *Nature protocols* **1**(1): 98-103.

Sethi V, Raghuram B, Sinha AK, Chattopadhyay S. 2014. A Mitogen-Activated Protein Kinase Cascade Module, MKK3-MPK6 and MYC2, Is Involved in Blue Light-Mediated Seedling Development in Arabidopsis. *The Plant cell* **26**(8): 3343-3357.

Smekalova V, Luptovciak I, Komis G, Samajova O, Ovecka M, Doskocilova A, Takac T, Vadovic P, Novak O, Pechan T, et al. 2014. Involvement of YODA and mitogen activated protein kinase 6 in Arabidopsis post-embryogenic root development through auxin up-regulation and cell division plane orientation. *The New phytologist* **203**(4): 1175-1193.

Smertenko AP, Chang HY, Sonobe S, Fenyk SI, Weingartner M, Bogre L, Hussey PJ. 2006. Control of the AtMAP65-1 interaction with microtubules through the cell cycle. *Journal of cell science* **119**(Pt 15): 3227-3237.

Sun QY, Lai L, Wu GM, Park KW, Day BN, Prather RS, Schatten H. 2001. Microtubule assembly after treatment of pig oocytes with taxol: correlation with chromosomes, gamma-tubulin, and MAP kinase. *Mol Reprod Dev* **60**(4): 481-490.

Tamura N, Draviam VM. 2012. Microtubule plus-ends within a mitotic cell are 'moving platforms' with anchoring, signalling and force-coupling roles. *Open biology* **2**(11): 120132.

Tomastikova E, Cenklova V, Kohoutova L, Petrovska B, Vachova L, Halada P, Kocarova G, Binarova P. 2012. Interactions of an Arabidopsis RanBPM homologue with LisH-CTLH domain proteins revealed high conservation of CTLH complexes in eukaryotes. *BMC plant biology* **12**: 83.

Umbrasaite J, Schweighofer A, Kazanaviciute V, Magyar Z, Ayatollahi Z, Unterwurzacher V, Choopayak C, Boniecka J, Murray JA, Bogre L, et al. 2010. MAPK phosphatase AP2C3 induces ectopic proliferation of epidermal cells leading to stomata development in Arabidopsis. *PLoS ONE* **5**(12): e15357.

Van Damme D, Bouget FY, Van Poucke K, Inze D, Geelen D. 2004. Molecular dissection of plant cytokinesis and phragmoplast structure: a survey of GFP-tagged proteins. *Plant J* **40**(3): 386-398.

van den Berg S, Lofdahl PA, Hard T, Berglund H. 2006. Improved solubility of TEV protease by directed evolution. *Journal of biotechnology* **121**(3): 291-298.

Wang H, Liu Y, Bruffett K, Lee J, Hause G, Walker JC, Zhang S. 2008. Haplo-insufficiency of MPK3 in MPK6 mutant background uncovers a novel function of these two MAPKs in Arabidopsis ovule development. *The Plant cell* **20**(3): 602-613.

Wang H, Ngwenyama N, Liu Y, Walker JC, Zhang S. 2007. Stomatal development and patterning are regulated by environmentally responsive mitogen-activated protein kinases in Arabidopsis. *The Plant cell* **19**(1): 63-73.

Wang P, Du Y, Li Y, Ren D, Song CP. 2010. Hydrogen peroxide-mediated activation of MAP kinase 6 modulates nitric oxide biosynthesis and signal transduction in Arabidopsis. *The Plant cell* **22**(9): 2981-2998.

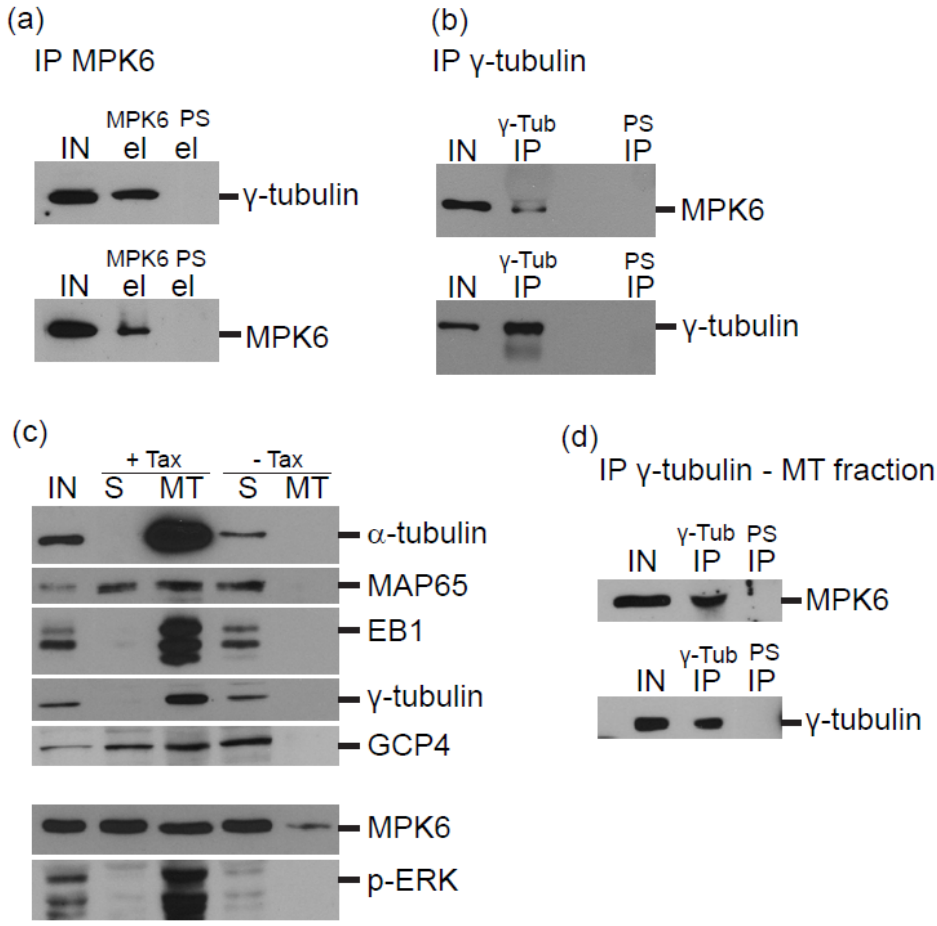

Fig. 1 MPK6 is present with microtubules and associated with γ-tubulin

(a) γ-Tubulin co-purified with MPK6. MPK6 el – eluate after immunoprecipitation with anti-MPK6 antibody, PS el – control eluate using preimmune serum, IN – crude extract S20; (b) MPK6 co-purified with γ-tubulin. γ-Tub IP – immunoprecipitate using anti-γ-tubulin antibody; PS IP – control immunoprecipitate using preimmune serum, IN – crude extract S20; (a, b) Western blots probed with anti-γ-tubulin and anti-MPK6 antibody. (c) MPK6 and p-ERK were pulled down with *in vitro* taxol-polymerized plant microtubules. Plant microtubules were polymerized from high speed supernatant S70 (IN) by taxol-driven polymerization and analyzed by antibodies against α-tubulin, MAP65-1, EB1, γ-tubulin, GCP4 protein, MPK6, and p-ERK. S/MT + Tax: supernatant/microtubular pellet after taxol treatment and without supplementing the assay with taxol (S/MT –Tax). (d) MPK6 co-purified with γ-tubulin when proteins pulled down with plant microtubules were used as an input (IN = MT + Tax). Immunoprecipitate using anti-γ-tubulin antibody (γ-Tub IP) and control immunoprecipitate using preimmune serum (PS IP) were probed with anti-MPK6 and anti-γ-tubulin antibody.

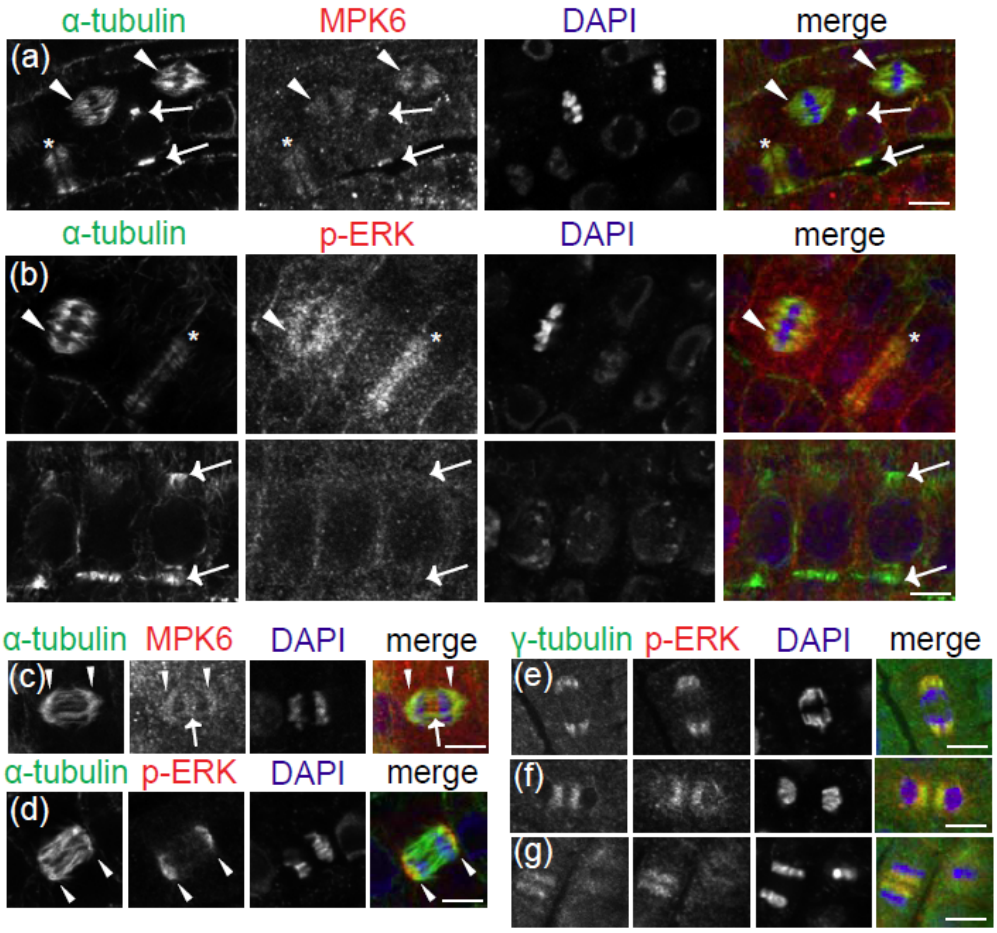

Fig. 2 MPK6 and γ-tubulin localized with specific subset of mitotic microtubules

(a) MPK6 signal on pre-prophase band (arrows), with metaphase spindles (arrowheads), and with phragmoplast area (asterisk). (b) Signal for p-ERK with metaphase spindles (arrowheads) and with phragmoplast area (asterisk), but hardly with pre-prophase bands (arrows). (c) While MPK6 besides its kinetochore fibres localization (arrowheads) was also in midzone (arrow), (d) signal for p-ERK in anaphase was mainly on shortening kinetochore fibres (arrowheads). (e) Signal for p-ERK localized on shortening kinetochore fibres with γ-tubulin in anaphase. (f) In telophase, both p-ERK signal and γ-tubulin were present on the remnants of kinetochore microtubules and with early phragmoplast. (g) Later in cytokinesis, p-ERK signal was in the phragmoplast area. Bars (a-g), 5 μm.

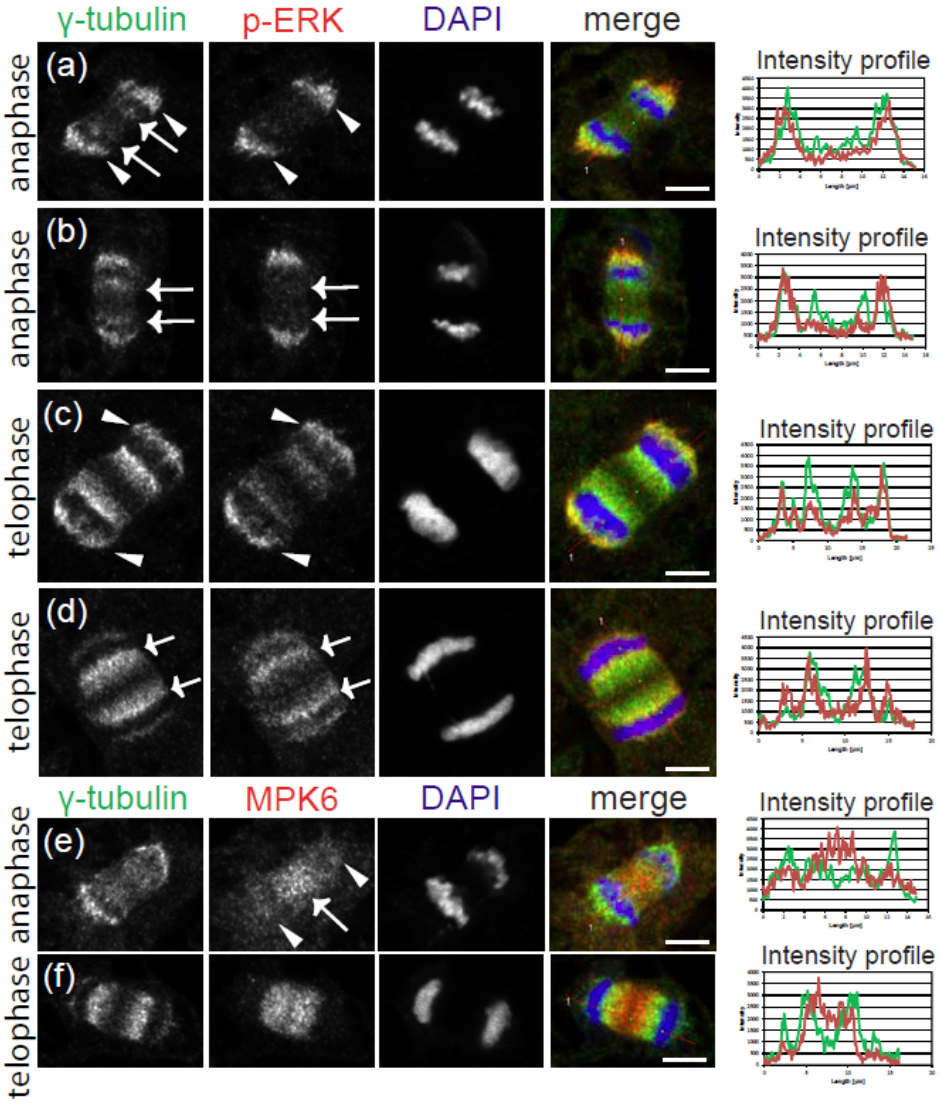

Fig. 3 Signal for p-ERK followed dynamic localization of γ-tubulin in anaphase/telophase transition

(a) In anaphase, p-ERK signal localized with γ-tubulin on shortening kinetochore fibres (arrowheads), while γ-tubulin was also partially on newly forming phragmoplast microtubules (arrows). (b) In later anaphase, p-ERK signal translocate to γ-tubulin positive area on newly forming phragmoplast (arrows) but compared to γ-tubulin the signal for p-ERK was less intense (intensity profile). (c) In telophase, both p-ERK signal and γ-tubulin were present on the remnants of kinetochore microtubules (arrowheads) and stained early phragmoplast but p-ERK signal delayed behind γ-tubulin signal in newly formed phragmoplast as shown by intensity profile. (d) Later in telophase, both p-ERK signal and γ-tubulin on the remnants of kinetochore microtubules gradually diminished and both proteins were located with early phragmoplast (arrows) as shown by intensity profile. (e) In anaphase, MPK6 signal strong in midzone (arrow), weaker signal with shortening kinetochore fibres (arrowheads) (f) In

telophase, MPK6 signal was present mainly in midzone in phragmoplast area. Double immunofluorescence labelling showing localization of MPK6 and p-ERK signal in Arabidopsis cells: p-ERK (red), MPK6 (red), γ-tubulin (green), DNA stained by DAPI (blue). Intensity profiles: x axis shows length in μm (number 1 indicates start of the line used for measurement corresponding to point 0); y axis shows relative intensity; red line for p-ERK or MPK6, respectively, green line for γ-tubulin. Bars (a-f), 5 μm.

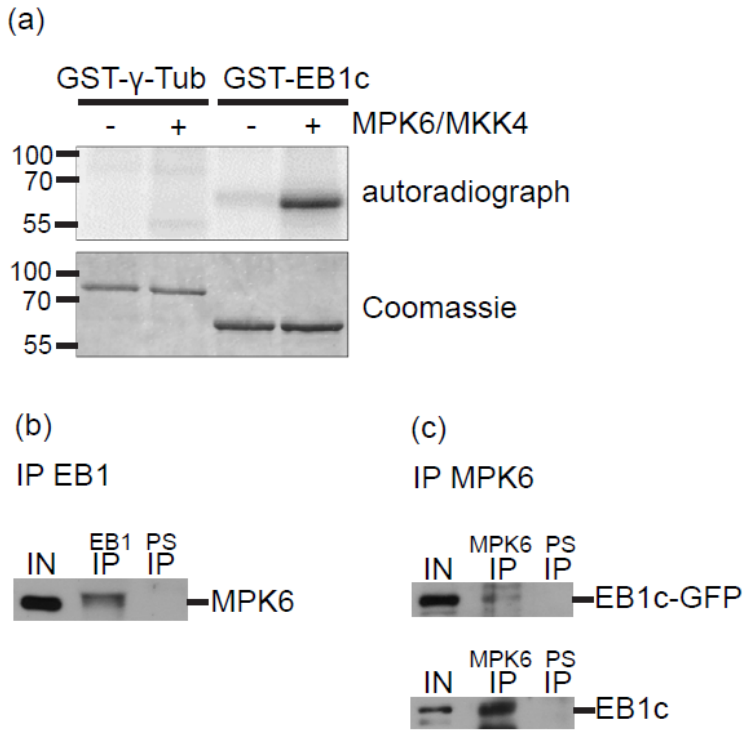

Fig. 4 Microtubule plus end protein EB1c is a target of MPK6

(a) Phosphorylation of EB1c *in vitro* by active MPK6. Unlike EB1c, γ-Tubulin was not phosphorylated by active MPK6 *in vitro*. (b) MPK6 co-purified with endogenous EB1c. EB1 IP – immunoprecipitate using anti-EB1 antibody, PS – control immunoprecipitate using preimmune serum, IN – crude extract S20; Western blot probed with anti-MPK6 antibody. (c) EB1c-GFP and endogenous EB1c co-purified with MPK6. MPK6 IP – eluate after immunoprecipitation with anti-MPK6 antibody from EB1c-GFP culture; PS IP – control eluate using preimmune serum, IN – crude extract S20; Western blots probed with anti-EB1 and anti-GFP antibody.

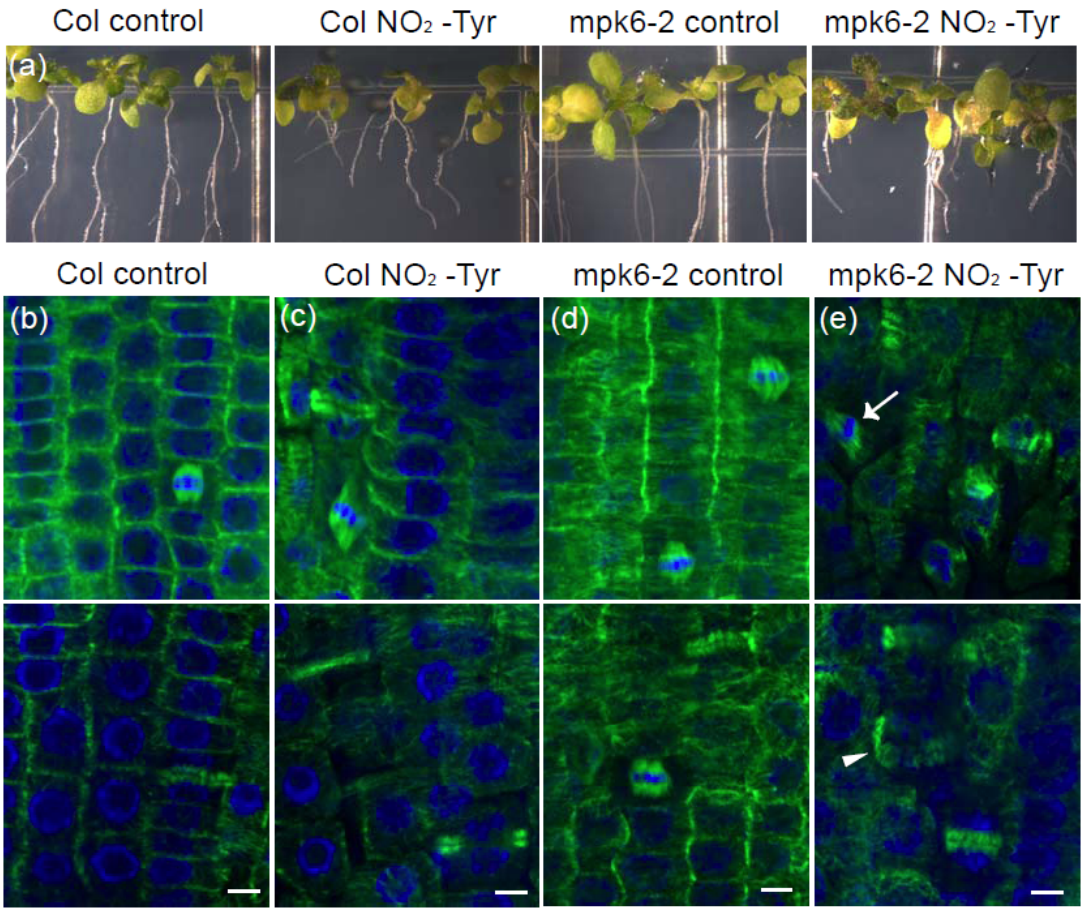

Fig. 5 A root development is strongly affected in *mpk6-2* mutants in response to NO_2-Tyr treatment compared to milder effect in WT plants

(a) Representative figures of 11-d-old WT Col and *mpk6-2* grown on control medium or on 0.5 µM NO_2-Tyr supplemented medium. NO_2-Tyr treatment affected root development: WT Col NO_2-Tyr treated roots were shortened, primary roots growth was severely retarded in *mpk6-2* mutants under NO_2-Tyr treatment. (b-e) Whole mount immunofluorescence labelling: α-tubulin (green), DAPI (blue) of control WT and *mpk6-2* seedlings and NO_2-Tyr treated WT and *mpk6-2* seedlings. (b) Regular files and spindle and phragmoplast in WT Col control. (c) Obliqued mitotic spindle in WT Col grown on NO_2-Tyr. (d) Regular files and regular spindles and phragmoplast in *mpk6-2* grown under control condition. (e) Irregular cells, misaligned spindle (arrow) and phragmoplast (arrowhead) in *mpk6-2* seedlings grown under NO_2-Tyr. Bars (b-e), 5 µm.

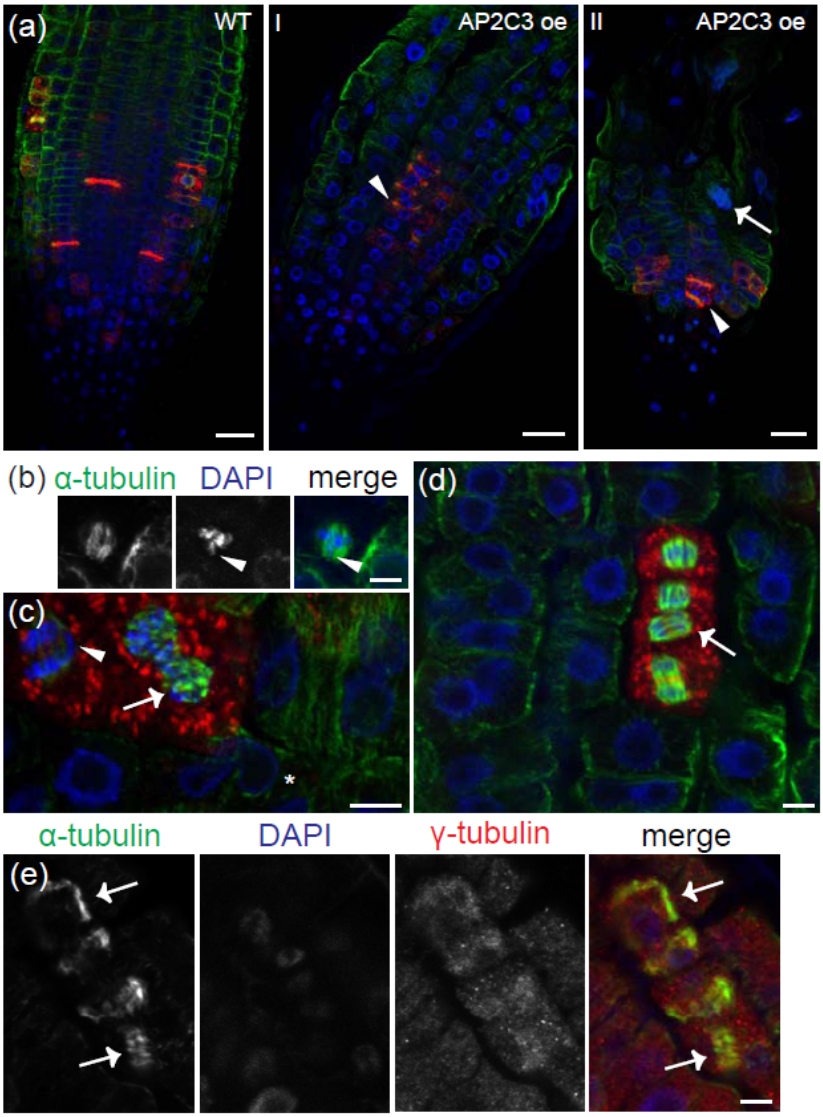

Fig. 6 Roots of AP2C3 oe Arabidopsis plants showed severe defects

(a-e) Whole mount immunofluorescence labelling of 7-d-old plants. (a) Main root of WT with regular cell files and cell plates. Typical examples of AP2C3 oe root with clusters of dividing cells with misaligned cell plates (arrowheads), irregular cell files, and multinuclear cell (arrow). α-tubulin (green), KNOLLE (red), chromatin stained by DAPI (blue). (b-e) Mitotic and cytokinetic defects in dividing cells of AP2C3 oe plants. (b) Impaired chromosome congression in metaphase (arrowhead). α-tubulin (green), chromosomes stained by DAPI (blue). (c) Anaphase with lagging chromosome (arrowhead), aberrant telophase with two clusters of condensed chromosomes surrounded by microtubules (arrow), nucleus of irregular shape (asterisk). α-tubulin (green), KNOLLE (red), DAPI (blue). (d) Misaligned anaphase spindle (arrow). α-tubulin (green), KNOLLE (red), DAPI (blue). (e) Misaligned

phragmoplasts with signal of γ-tubulin (arrows). α-tubulin (green), γ-tubulin (red). Bars (a), 20 μm; (b-e), 5 μm.

7.4.1 Supplementary data

Kohoutová, L., Kourová, H., Nagy, S., Volc, J., Halada, P., Mészáros, T., Meskiene, I., Bögre, L., and Binarová, P.; (submitted 2014) The Arabidopsis mitogen-activated protein kinase 6 is associated with γ-tubulin on microtubules, phosphorylates EB1c and maintains spindle orientation under nitric oxide stress. New Phytol

Figure S1

Protein name	DTB No.	TAIR No.	MW [kDa]	MASCOT score	No. peptides	SC [%]
Uncharacterized protein	18423534	At5g53620	76	2360	32	39
14-3-3-like protein GF14 omega	Q01525	At1g78300	29	918	15	38
Chaperonin 60 subunit alpha 1, chloroplastic	P21238	At2g28000	62	493	7	17
Adenylosuccinate lyase-like protein	Q9C8F5	At4g18440	58	373	9	16
Isoaspartyl peptidase/L-asparaginase	P50287	At5g08100	33	382	4	22
Polyribonucleotide nucleotidyltransferase 2	Q9S7G6	At5g14580	108	256	8	8
Alkaline/neutral invertase	Q9LQF2	At1g35580	63	226	6	14
Chaperonin 60 subunit beta 1, chloroplastic	P21240	At1g55490	64	235	5	11
Tubulin beta-4 chain	P29515	At2g29550	51	207	6	11
Single-stranded DNA-binding protein WHY3	Q66GR6	At2g02740	30	196	3	17
Chaperonin CPN60, mitochondrial	P29197	At3g23990	61	103	4	9
Mitogen-activated protein kinase 6	Q39026	At2g43790	45	98	2*	4
Tubulin gamma-1 chain	P38557	At3g61650	53	48	2*	6
Uncharacterized protein	186510047	At3g14172	141	52	2*	2
Putative T-complex protein 1, theta subunit	Q9SQR6	At3g03960	57	39	1*	3
T-complex protein 1 subunit gamma	Q84WV1	At5g26360	61	33	1*	1

* identity of the protein was verified using MALDI FTICR mass spectrometry with the peptide mass accuracy below 2 ppm.

Fig. S1

Identification of proteins co-purified with MPK6 from *Arabidopsis* proliferating cultured cells by LC-MALDI-TOF mass spectrometry

The table includes protein name, UniProt or NCBI database number, TAIR number, protein molecular weight, total MASCOT score of all peptides matched to the identified protein, and corresponding sequence coverage value.

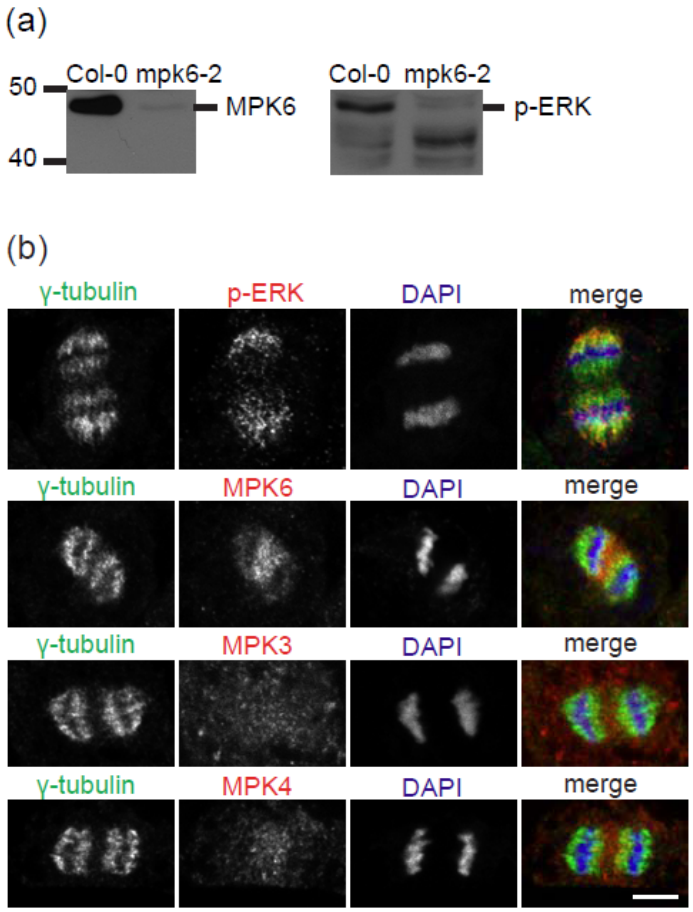

Fig. S2

p-ERK antibody recognized predominantly MPK6 on Western blots and in Arabidopsis cells

(a) In MPK6 KO mutants *mpk6-2*, expression of MPK6 was strongly reduced compared to WT Col-0 and accordingly p-ERK signal was almost missing. (b) Signals for MPKs in Arabidopsis cultured cells in late anaphase. Signal for p-ERK was mainly with shortening kinetochore fibres. MPK6 localized mainly in midzone and also stained shortening kinetochore fibres. MPK3 had diffused signal in the cell. MPK4 localized mainly in midzone. Double immunofluorescence labelling p-ERK (red), MPK6 (red), MPK3 (red), MPK4 (red), γ-tubulin (green), DNA stained by DAPI (blue). Bar, 5 μm.

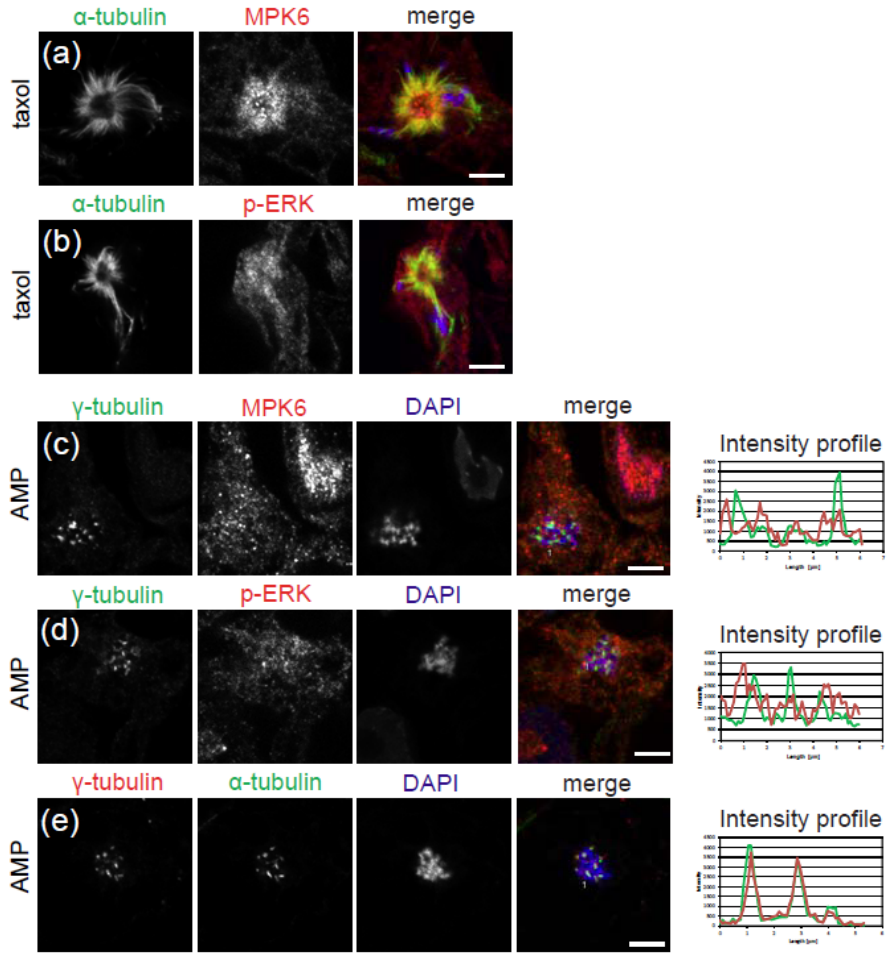

Fig. S3

MPK6 and p-ERK labelling in Taxol and APM treated cells

(a, b) Double immunofluorescence labelling of Arabidopsis cultured cells with taxol stabilized microtubules. (a) MPK6 (red) enriched on microtubules (green) after taxol treatment and in the centre of taxol star. Chromatin stained by DAPI (blue). (b) Signal for p-ERK (red) enriched on dense microtubules (green) after taxol treatment and in the centre of taxol induced microtubular asters. DAPI (blue). (c-e) Double immunofluorescence labelling of Arabidopsis cultured cells after microtubule depolymerization by APM. (c) Difused MPK6 labelling (red) is present in the area of stubs decorated with γ-tubulin (green). (d) Signal for p-ERK (red) enriched in the area of kinetochore stubs. DAPI (blue). (e) Microtubule stubs (green) decorated with γ-tubulin (red). Intensity profiles: x axis shows length in μm (number 1 indicates start of the line used for measurement corresponding to point 0); y axis shows relative intensity; red line for MPK6 or p-ERK respectively, green line for γ-tubulin. Bars (a-e), 5 μm.

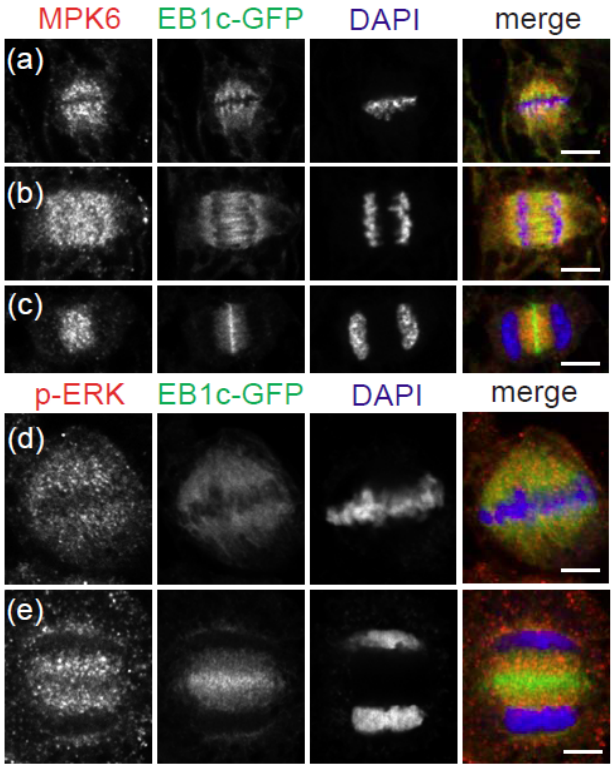

Fig. S4

MPK6 and p-ERK labelling with EB1c-GFP in Arabidopsis cultured cells

(a, b, c) Double immunofluorescence labelling: MPK6 (red), EB1c-GFP (green), DAPI (blue). MPK6 (red) and EB1c-GFP (green) localized together in metaphase spindle (a), in midzone and on shortening kinetochore fibres during anaphase (b), and in midzone in telophase (c). (d, e) Double immunofluorescence labelling: p-ERK (red), EB1c-GFP (green), DAPI (blue). Signal for p-ERK (red) localized with EB1c-GFP in metaphase spindle (d) and in telophase on remnants of kinetochore microtubules and in midzone (e). Bars (a-e), 5 µm.

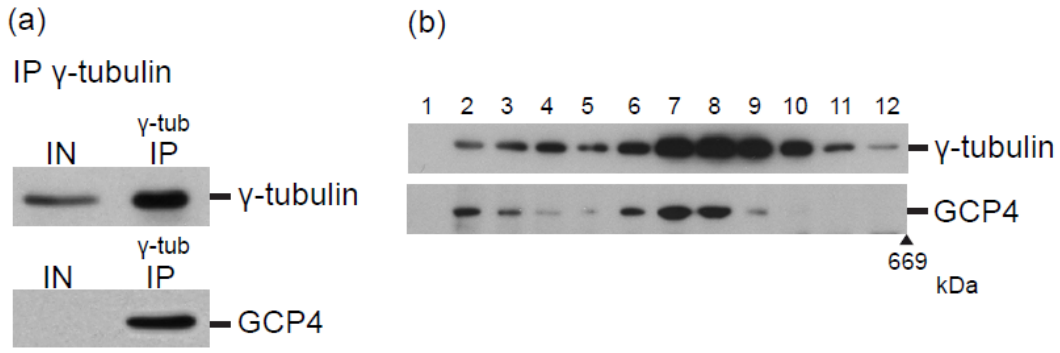

Fig. S5

GCP4 forms complexes with γ-tubulin in Arabidopsis

(a) GCP4 co-purified with γ-tubulin. IN – solubilized microsomal fraction, γ-tub IP – immunoprecipitate using anti-γ-tubulin. Western blots probed with anti-γ-tubulin antibody and anti-GCP4 antibody

(b) γ-Tubulin co-eluted with GCP4 in fractions from gel permeation chromatography corresponding to large complexes. Solubilized microsomal fraction was resolved. Thyroglobulin as a marker. (a, b) Western blots probed with anti-γ-tubulin and anti-GCP4 antibody.

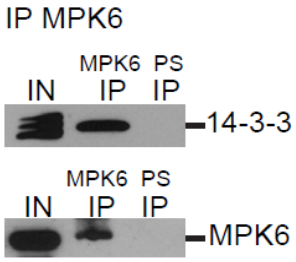

Fig. S6

14-3-3 co-purified with MPK6

IN – crude extract S20, MPK6 IP – eluate using anti-MPK6 antibody, PS IP – control eluate using preimmune serum. Western blots probed with anti-14-3-3 antibody and anti-MPK6 antibody.